frontiers | Research Topics

Deciphering antimicrobial resistance: genetic insights and perspectives

Edited by
Massimiliano Lucidi, Valerio Baldelli, Mattia Pirolo and Daniela Visaggio

Published in
Frontiers in Cellular and Infection Microbiology

ISSN 1664-8714
ISBN 978-2-8325-7098-2
DOI 10.3389/978-2-8325-7098-2

Generative AI statement
Any alternative text (Alt text) provided alongside figures in the articles in this ebook has been generated by Frontiers with the support of artificial intelligence and reasonable efforts have been made to ensure accuracy, including review by the authors wherever possible. If you identify any issues, please contact us.

About Frontiers

Frontiers is more than just an open access publisher of scholarly articles: it is a pioneering approach to the world of academia, radically improving the way scholarly research is managed. The grand vision of Frontiers is a world where all people have an equal opportunity to seek, share and generate knowledge. Frontiers provides immediate and permanent online open access to all its publications, but this alone is not enough to realize our grand goals.

Frontiers journal series

The Frontiers journal series is a multi-tier and interdisciplinary set of open-access, online journals, promising a paradigm shift from the current review, selection and dissemination processes in academic publishing. All Frontiers journals are driven by researchers for researchers; therefore, they constitute a service to the scholarly community. At the same time, the *Frontiers journal series* operates on a revolutionary invention, the tiered publishing system, initially addressing specific communities of scholars, and gradually climbing up to broader public understanding, thus serving the interests of the lay society, too.

Dedication to quality

Each Frontiers article is a landmark of the highest quality, thanks to genuinely collaborative interactions between authors and review editors, who include some of the world's best academicians. Research must be certified by peers before entering a stream of knowledge that may eventually reach the public - and shape society; therefore, Frontiers only applies the most rigorous and unbiased reviews. Frontiers revolutionizes research publishing by freely delivering the most outstanding research, evaluated with no bias from both the academic and social point of view. By applying the most advanced information technologies, Frontiers is catapulting scholarly publishing into a new generation.

What are Frontiers Research Topics?

Frontiers Research Topics are very popular trademarks of the *Frontiers journals series*: they are collections of at least ten articles, all centered on a particular subject. With their unique mix of varied contributions from Original Research to Review Articles, Frontiers Research Topics unify the most influential researchers, the latest key findings and historical advances in a hot research area.

Find out more on how to host your own Frontiers Research Topic or contribute to one as an author by contacting the Frontiers editorial office: frontiersin.org/about/contact

Deciphering antimicrobial resistance: genetic insights and perspectives

Topic editors

Massimiliano Lucidi — Roma Tre University, Italy
Valerio Baldelli — University of Milan, Italy
Mattia Pirolo — University of Copenhagen, Denmark
Daniela Visaggio — Roma Tre University, Italy

Citation

Lucidi, M., Baldelli, V., Pirolo, M., Visaggio, D., eds. (2025). *Deciphering antimicrobial resistance: genetic insights and perspectives*. Lausanne: Frontiers Media SA.
doi: 10.3389/978-2-8325-7098-2

Table of contents

05 Editorial: Deciphering antimicrobial resistance: genetic insights and perspectives
Massimiliano Lucidi, Mattia Pirolo, Valerio Baldelli and Daniela Visaggio

08 *aac(6')-Iaq*, a novel aminoglycoside acetyltransferase gene identified from an animal isolate *Brucella intermedia* DW0551
Naru Lin, Wanna Xu, Dawei Huang, Chaoqun Liu, Junwan Lu, Mei Zhu, Qiyu Bao and Wei Pan

21 Emergence and evolution of rare ST592 bla_{NDM-1}-positive carbapenem-resistant hypervirulent *Klebsiella pneumoniae* in China
Huan Zhang, Su Dong, Caiping Mao, Yuejuan Fang and Junjie Ying

30 Resistance phenotypes and genomic features of *Mycobacterium seoulense* isolates
Jin Zhao, Xinli Shen, Lulu Jin, Songjun Ji and Xinling Pan

41 Evaluation of multidrug-resistant bacteria and their molecular mechanisms found in small animal veterinary practices in Portugal
Joana Moreira da Silva, Juliana Menezes, Laura Fernandes, Cátia Marques, Sofia Santos Costa, Dorina Timofte, Andreia J. Amaral and Constança Pomba

53 Deciphering tuberculosis: lysosome-centric insights into pathogenesis and therapies
Cui Bao, Yuanyuan Zhang, Jiao Feng, Xiuwen Hong, Nan Gao and Ganzhu Feng

66 Evolution of ceftazidime-avibactam resistance driven by variation in bla_{KPC-2} to $bla_{KPC-190}$ during treatment of ST11-K64 hypervirulent *Klebsiella pneumoniae*
Zeshi Liu, Jing Lei, Xue Zhang, Jian Yin, Yanping Zhang, Ke Lei, Yan Geng, Lingjuan Huang, Qiang Han and Aili He

76 *TrexAB*, a novel tetracycline resistance determinant in *Streptococcus dysgalactiae*
Marte Glambek, Morten Kjos, Marita T. Mårli, Zhian Salehian, Steinar Skrede, Audun Sivertsen, Bård R. Kittang and Oddvar Oppegaard

85 Genomic features and fitness cost of co-existence of bla_{KPC-2} and bla_{VIM-2} plasmids in ICU-derived pan-drug resistant *Pseudomonas aeruginosa*
Lin Zheng, Zixian Wang, Xin Zhang, Gejin Lu, Jie Jing, Shiwen Sun, Yang Sun, Xue Ji, Bowen Jiang, Lingwei Zhu and Xuejun Guo

96 Caspofungin paradoxical growth in *Candida albicans* requires stress pathway activation and promotes unstable echinocandin resistance mediated by aneuploidy
Ying Wei, Jing Wang, Nan Tang, Ziwei Lin, Wenhui Li, Yi Xu and Liangsheng Guo

109 Prevalence, antimicrobial resistance, and distribution of toxin genes in methicillin-resistant *Staphylococcus aureus* from retail meat and fruit and vegetable cuts in the United Arab Emirates
Ihab Habib, Mohamed-Yousif Ibrahim Mohamed, Glindya Bhagya Lakshmi, Febin Anes, Richard Goering, Mushtaq Khan and Abiola Senok

121 Community gut colonization by *tet*(X4)-positive multidrug-resistant *Escherichia coli* in healthy individuals from urban residents in Shenzhen, China
Ruoyan Peng, Pei Liang, Wenxiao Jiang, Zhaodong Li, Li Wang, Yi Huang, Xianfang Zhang, Yijia Guo, Ying Wang, Jing Wang, Jiubiao Guo, Feifei Yin and Dachuan Lin

132 Genomic diversity, antimicrobial resistance and dissemination of *Serratia marcescens complex* in patients admitted to ICUs
Wentao Zhu, Xi Chen, Hong Shen, Ming Wei, Chunxia Yang and Li Gu

frontiers | Frontiers in Cellular and Infection Microbiology

TYPE Editorial
PUBLISHED 22 October 2025
DOI 10.3389/fcimb.2025.1720241

OPEN ACCESS

EDITED AND REVIEWED BY
Vincent Cattoir,
University of Rennes, France

*CORRESPONDENCE
Massimiliano Lucidi
massimiliano.lucidi@uniroma3.it

RECEIVED 07 October 2025
ACCEPTED 16 October 2025
PUBLISHED 22 October 2025

CITATION
Lucidi M, Pirolo M, Baldelli V and Visaggio D (2025) Editorial: Deciphering antimicrobial resistance: genetic insights and perspectives. *Front. Cell. Infect. Microbiol.* 15:1720241. doi: 10.3389/fcimb.2025.1720241

Editorial: Deciphering antimicrobial resistance: genetic insights and perspectives

Massimiliano Lucidi[1]*, Mattia Pirolo[2], Valerio Baldelli[3] and Daniela Visaggio[1]

[1]Department of Science, Roma Tre University, Rome, Italy, [2]Department of Veterinary and Animal Sciences, University of Copenhagen, Frederiksberg C, Denmark, [3]Department of Biosciences, University of Milan, Milan, Lombardy, Italy

KEYWORDS

antibiotic resistance genes (ARGs), infectious disease epidemiology, mobile genetic elements (MBEs), plasmids, phages, regulatory perspectives, resistance mechanisms, surveillance

Editorial on the Research Topic
Deciphering antimicrobial resistance: genetic insights and perspectives

Antimicrobial agents have propelled medicine into the era of modern healthcare. However, the efficacy of antimicrobial therapies is progressively weakening as antimicrobial resistance (AMR) escalates, representing a profound threat to global health that transcends human, veterinary, and environmental boundaries. The development of AMR arises from multiple drivers, including *i*) antimicrobial overuse and misuse, *ii*) insufficient diagnostic practices, and *iii*) the intrinsic adaptability of microbial genomes. As AMR continues to spread, our ability to combat common infections and undertake routine medical interventions safely is increasingly compromised (Antimicrobial Resistance Collaborators, 2022). Addressing this challenge requires comprehensive research into the genetic basis of resistance mechanisms, surveillance of microbial communities across multiple reservoirs, and the development of novel strategies to counteract AMR (Jauneikaite et al., 2023).

The Research Topic presented in *Frontiers in Cellular and Infection Microbiology* provides a comprehensive view of the genetic determinants, epidemiology, and functional consequences of AMR across clinical, veterinary, and environmental settings. These studies highlight the need for One Health strategies, integrating surveillance and interventions across humans, animals, and the environment to curb the global spread of AMR.

In veterinary settings, the study of AMR reveals both environmental and human-mediated pathways for the dissemination of resistant organisms. Moreira da Silva et al. demonstrated that small animal veterinary practices in Portugal are contaminated by multidrug-resistant (MDR) microorganisms, including carbapenem- and methicillin-resistant strains, emphasizing the urgent need for robust infection prevention and control measures. Concerning resistant pathogens, Glambek et al. identified a novel *trexAB* operon in *Streptococcus dysgalactiae*, elucidating the genetic basis of low-grade tetracycline resistance and revealing previously unrecognized mechanisms of AMR in both clinical and veterinary settings. The relevance of veterinary reservoirs extends into food production, as illustrated by Habib et al., who reported widespread MDR and toxigenic methicillin-resistant *Staphylococcus aureus* (MRSA) strains in retail meat and produce in

the United Arab Emirates, emphasizing the One Health implications of AMR and the potential for community exposure.

Mechanistic insights into novel resistance determinants further broaden our understanding of AMR evolution and its dissemination across microbial species. Lin et al. characterized *aac(6')-Iaq*, a new aminoglycoside acetyltransferase from *Brucella intermedia*, which confers resistance to multiple aminoglycosides. At the community level, Peng et al. identified silent intestinal colonization by *tet(X4)*-positive, tigecycline-resistant MDR *Escherichia coli* in healthy people, highlighting hidden reservoirs of last-resort antibiotic resistance beyond clinical settings.

Concerning the hospital settings, clinical isolates continue to offer critical insights into AMR dynamics. Liu et al. described the evolution of ceftazidime-avibactam resistance in hypervirulent ST11-K64 *Klebsiella pneumoniae*, driven by the $bla_{KPC-190}$ variant that simultaneously confers resistance and partially restores carbapenem susceptibility. Zhang et al. traced the emergence of NDM-1-positive ST592 *K. pneumoniae*, illustrating plasmid-mediated evolution toward carbapenem-resistant hypervirulence. Similarly, Zheng et al. examined the coexistence of bla_{KPC-2} and bla_{VIM-2} plasmids in intensive care unit (ICU)-derived pandrug-resistant *Pseudomonas aeruginosa* strains, pointing out their stability and minimal fitness cost, which facilitate dissemination within healthcare environments. Expanding the scope to non-tuberculous mycobacteria, Zhao et al. demonstrated that *Mycobacterium seoulense* isolates exhibit variable susceptibility and genomic diversity, reinforcing the importance of targeted susceptibility testing. In the fungal realm, Wei et al. reported that *Candida albicans* can exhibit paradoxical growth under caspofungin exposure, a phenomenon in which fungal cells resume growth at drug concentrations above the minimum inhibitory concentration. This response is driven by activation of stress-response pathways coupled with segmental aneuploidy, which together confer reversible echinocandin resistance, illustrating how dynamically fungi can adapt their genomes under antimicrobial pressure. Intracellular lifestyle is one strategy some microbes use to evade antimicrobials. In this context, Bao et al. offered a lysosome-centered view of *Mycobacterium tuberculosis* pathogenesis, revealing intracellular survival strategies that indirectly influence therapeutic efficacy and potentially contribute to resistance development.

Finally, longitudinal studies, such as that from Zhu et al., can provide an essential perspective to enhance our understanding of AMR evolution and population dynamics. Indeed, this study analysed the *Serratia marcescens* complex in ICU patients over 11 years, identifying inter-ICU transmission and the accumulation of β-lactamase and carbapenemase genes, highlighting the importance of continuous genomic surveillance

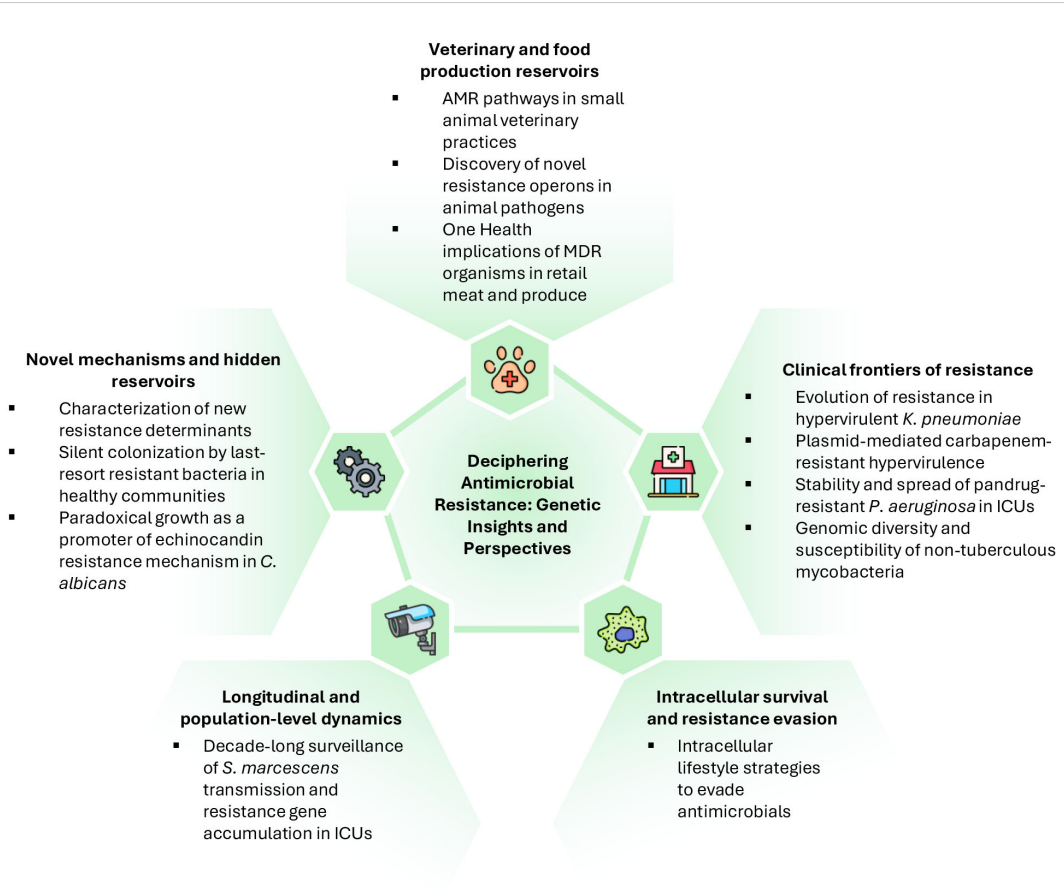

FIGURE 1
Scientific contributions to this Research Topic.

Figure 1 highlights the valuable scientific contributions of this Research Topic, exemplifying the breadth and depth of current AMR research. The studies demonstrate that resistance emerges through adaptation to intracellular lifestyle and diverse genetic mechanisms, including plasmid-mediated gene acquisition, point mutations, efflux operons, and genome-scale rearrangements. Surveillance across clinical, community, veterinary, and environmental reservoirs is indispensable to identify emerging threats, while mechanistic studies guide the development of targeted interventions. Additionally, the works highlight the importance of combining genomic, phenotypic, and epidemiological approaches to fully understand the evolution and fitness costs associated with resistance.

Altogether, this Research Topic underscores the urgent need for One Health approaches to combat AMR. It advocates investment in diagnostics, genomic surveillance, and strategies to limit its spread, as deepening our understanding of AMR sharpens surveillance and therapeutic precision while informing policies that bridge human, animal, and environmental health. By fostering interdisciplinary and mechanistic research, the field moves closer to preserving the effectiveness of antimicrobials that underpin modern medicine.

Author contributions

ML: Writing – review & editing, Writing – original draft. MP: Writing – review & editing. VB: Writing – review & editing. DV: Writing – review & editing.

Conflict of interest

The authors declare that the research was conducted in the absence of any commercial or financial relationships that could be construed as a potential conflict of interest.

The author(s) declared that they were an editorial board member of Frontiers, at the time of submission. This had no impact on the peer review process and the final decision.

Generative AI statement

The author(s) declare that no Generative AI was used in the creation of this manuscript.

Any alternative text (alt text) provided alongside figures in this article has been generated by Frontiers with the support of artificial intelligence and reasonable efforts have been made to ensure accuracy, including review by the authors wherever possible. If you identify any issues, please contact us.

Publisher's note

References

Antimicrobial Resistance Collaborators (2022). Global burden of bacterial antimicrobial resistance in 2019: a systematic analysis. *Lancet* 399, 629–655. doi: 10.1016/S0140-6736(21)02724-0

Jauneikaite, E., Baker, K. S., Nunn, J. G., Midega, J. T., Hsu, L. Y., Singh, S. R., et al. (2023). Genomics for antimicrobial resistance surveillance to support infection prevention and control in health-care facilities. *Lancet Microbe* 4, e1040–e1046. doi: 10.1016/S2666-5247(23)00282-3

frontiers | Frontiers in Cellular and Infection Microbiology

TYPE Original Research
PUBLISHED 11 March 2025
DOI 10.3389/fcimb.2025.1551240

OPEN ACCESS

EDITED BY
Massimiliano Lucidi,
Roma Tre University, Italy

REVIEWED BY
Peibo Yuan,
Southern Medical University, China
Angela Gioffrè,
National Institute for Insurance against Accidents at Work (INAIL), Italy

*CORRESPONDENCE
Mei Zhu
zhumei_d@163.com
Qiyu Bao
baoqy@genomics.cn
Wei Pan
25658507@qq.com

RECEIVED 25 December 2024
ACCEPTED 18 February 2025
PUBLISHED 11 March 2025

CITATION
Lin N, Xu W, Huang D, Liu C, Lu J, Zhu M, Bao Q and Pan W (2025) *aac(6')-Iaq*, a novel aminoglycoside acetyltransferase gene identified from an animal isolate *Brucella intermedia* DW0551. *Front. Cell. Infect. Microbiol.* 15:1551240. doi: 10.3389/fcimb.2025.1551240

aac(6')-Iaq, a novel aminoglycoside acetyltransferase gene identified from an animal isolate *Brucella intermedia* DW0551

Naru Lin[1,2], Wanna Xu[3], Dawei Huang[4], Chaoqun Liu[5], Junwan Lu[5], Mei Zhu[6]*, Qiyu Bao[2,5]* and Wei Pan[4]*

[1]Division of Tuberculosis Control and Prevention, Fujian Provincial Center for Disease Control and Prevention, Fuzhou, China, [2]Key Laboratory of Medical Genetics of Zhejiang Province, Key Laboratory of Laboratory Medicine, Ministry of Education, School of Laboratory Medicine and Life Sciences, Wenzhou Medical University, Wenzhou, China, [3]Department of Rehabilitation Medicine, Army 73rd Group Military Hospital, Xiamen, China, [4]Department of Clinical Laboratory, the People's Hospital of Yuhuan, Taizhou, Zhejiang, China, [5]Medical Molecular Biology Laboratory, School of Medicine, Jinhua Polytechnic, Jinhua, China, [6]Department of Clinical Laboratory, Zhejiang Hospital, Hangzhou, China

Background: Bacterial resistance to aminoglycoside antimicrobials is becoming increasingly severe due to their use as commonly prescribed antibiotics. The discovery of new molecular mechanisms of aminoglycoside resistance is critical for the effective treatment of bacterial infections.

Methods: Bacteria in goose feces were isolated by plate streaking. The identification and characterization of a novel resistance gene from the bacterial genome involved various techniques, including molecular cloning, drug susceptibility testing, protein expression and purification, and enzyme kinetic analysis. Additionally, whole-genome sequencing and phylogenetic studies were performed.

Results: *Brucella intermedia* DW0551, isolated from goose feces, was resistant to 35 antibiotics, and the minimum inhibitory concentration (MIC) was particularly high for most aminoglycoside antibiotics. The novel aminoglycoside resistance gene *aac(6')-Iaq* encoded by *B. intermedia* DW0551 conferred resistance to netilmicin, sisomicin, amikacin, kanamycin, gentamicin, tobramycin, and ribostamycin. The amino acid sequence of AAC(6')-Iaq shared the highest identity (52.63%) with the functionally characterized aminoglycoside acetyltransferase AAC(6')-If. AAC(6')-Iaq contained all the conserved sites of the acetyltransferase family NAT_SF. The enzyme exhibited strong affinity and catalytic activity toward netilmicin and sisomicin. The mobile genetic element (MGE) was not found in the flanking regions of the *aac(6')-Iaq* and *aac(6')-Iaq*-like genes.

Conclusion: In this work, a novel aminoglycoside acetyltransferase gene, designated *aac(6')-Iaq*, which conferred resistance to a variety of

aminoglycoside antimicrobials, was identified in an animal *Brucella intermedia* isolate. Identification of new antibiotic resistance mechanisms in bacteria isolated from animals could aid in the treatment of animal and human infectious diseases caused by related bacterial species.

KEYWORDS

***Brucella intermedia*, resistance mechanism, aminoglycoside acetyltransferase, *aac(6')-Iaq*, kinetic parameter**

Introduction

Aminoglycosides are antimicrobial molecules that are widely used in clinical practice and are usually used in combination with β-lactam drugs for the treatment of infections caused by Gram-positive and Gram-negative bacteria (Abdul-Aziz et al., 2020). Aminoglycoside resistance genes confer drug resistance to bacteria, encoding mainly aminoglycoside resistance proteins, namely, aminoglycoside acetyltransferases (AACs), aminoglycoside nucleotidyltransferases (ANTs) and aminoglycoside phosphotransferases (APHs), which acetylate, adenylate and phosphorylate drugs at specific sites, respectively (Ramirez and Tolmasky, 2010). The AAC(6') enzyme, the most common aminoglycoside N-acetyltransferase, which modifies the 6' site of aminoglycosides, such as kanamycin, tobramycin, gentamicin and amikacin, and usually confers resistance to these drugs (Ramirez and Tolmasky, 2010).

To date, 68 genes of the *aac(6')* gene family have been included in the Comprehensive Antibiotic Resistance Database (CARD) (Alcock et al., 2023). These genes are located on chromosomal and plasmid DNA and are generally related to mobile genetic elements (MGEs), such as transposons and integrons (Alcock et al., 2023). Proteins encoded by the *aac(6')* genes usually exhibit resistance to more than one aminoglycoside antibiotic. For example, AAC(6')-Ia shows resistance to tobramycin, gentamicin, amikacin, isepamicin and netilmicin (Shaw et al., 1992), while AAC(6')-Iy shows resistance to tobramycin, amikacin and netilmicin (Magnet et al., 1999).

Brucella intermedia (formerly known as *Ochrobactrum intermedium*, type strain LMG 3301 = NCTC 12171 = CNS 2-75) was first isolated from human blood in 1988 (Holmes et al., 1988) and was first described and named in 1998 (Velasco et al., 1998). These bacteria are Gram-negative facultative coccobacilli and are usually present as circular, low-convexity and smooth colonies approximately 1 mm in diameter. These bacteria generally have two chromosomes, with the larger one being responsible for activities related to functions of bacterial life and the smaller one encoding genes related to virulence. *Brucella* spp. were once thought to cause disease only in immunosuppressed populations, but more recent studies have indicated their role as opportunistic pathogens causing a wide range of diseases (Ryan and Pembroke, 2020). For example, they can lead to bacteremia in individuals with malignant tumors (Apisarnthanarak et al., 2005; Kassab et al., 2021), inflammation of the respiratory and cardiovascular systems (Hirai et al., 2016; Bharucha et al., 2017), and endophthalmitis in otherwise healthy individuals (Jacobs et al., 2013). These infections have also been reported to be associated with outbreaks of nosocomial *P. aeruginosa* infections (Sekiguchi et al., 2007). The emergence of multidrug-resistant *B. intermedia* has attracted increasing attention in recent years due to the increase in its pathogenicity (Ryan and Pembroke, 2020; Sheng et al., 2023). However, the mechanism underlying the resistance to aminoglycosides has rarely been reported (Lu et al., 2021).

In one of our recent projects, to investigate the antimicrobial resistance mechanisms of animal, human and environmental bacteria, we isolated hundreds of bacteria from fecal samples. The antimicrobial resistance profiles of these strains were examined, and their genomes were sequenced. In this work, the resistance phenotype and genotype of a microbe, designated *B. intermedia* DW0551 isolated from a goose, were characterized, and a novel chromosomal aminoglycoside resistance gene designated *aac(6')-Iaq* was identified from this bacterium.

Materials and methods

Bacterial strains and plasmids

A total of 576 strains of bacteria were isolated from samples collected from sewage and domestic fowl and livestock in animal farms in Wenzhou, Zhejiang Province, China. For all of them, the minimum inhibitory concentrations (MICs) of numerous antimicrobial agents were tested, and the genomes were sequenced. The isolates were initially identified at the species level using 16S rRNA gene homology and average nucleotide identity (ANI) analyses (Konstantinidis and Tiedje, 2005). One of them, designated *B. intermedia* DW0551 herein, was isolated from goose feces. Table 1 lists the strains and plasmids used in this study.

Drug susceptibility testing

According to the M100 performance standards for antimicrobial susceptibility testing by the Clinical and Laboratory Standards Institute (CLSI) (Lewis, 2022), the MICs were determined by the agar dilution method using Mueller–Hinton (MH) agar plates with twofold serial dilutions of antibiotics (Crump et al., 2015). After 16-20 h of incubation at 37°C, the MIC results were interpreted according to M100 performance standards and the guidelines of the European Committee on Antimicrobial Susceptibility Testing (v12.0) (EUCAST, 2022). A total of 43 antimicrobial molecules were tested (Table 2), all of which were purchased from hospitals or pharmaceutical companies. *Pseudomonas aeruginosa* ATCC27853, also a Gram-negative bacillus as *B. intermedia* DW0551, was used for quality control. The MIC results of the quality control strain remained within the predetermined limits, indicating the credible test results.

Genome sequencing, assembly, annotation, and bioinformatics analysis

The genomic DNA of the bacterium was extracted using the Universal Genomic DNA Purification Mini Spin Kit (Beyotime Biotechnology Co., Ltd., Shanghai, China). For analysis of the resistance genes in 576 bacteria, the genome of each bacterium was sequenced on the Illumina NovaSeq 6000 platform (Shanghai Personal Biotechnology Co., Ltd., Shanghai, China). The Illumina short reads of all 576 bacterial genomes were pooled together and assembled by SKESA v2.4.0 (Souvorov et al., 2018). The antibiotic resistance-related genes were annotated by Prokka (v.1.14.6) (Seemann, 2014) against the CARD (Alcock et al., 2020) and ResFinder database (Bortolaia et al., 2020). For whole-genome sequencing of *Brucella intermedia* DW0551, the PacBio Sequel II (Shanghai Personal Biotechnology Co., Ltd., Shanghai, China) sequencing platform was subsequently used. The long reads from PacBio Sequel II and the short reads from Illumina NovaSeq 6000 were hybrid assembled in a short-read-first manner using Unicycler (v0.4.8) (Wick et al., 2017) and then polished by Pilon (v 1.23) (Walker et al., 2014). The optimization of the assembly results was performed using Racon (v1.4.13) (Huang et al., 2022) and Pilon (v1.23) (Walker et al., 2014) and was assessed using QUAST (v5.0.2-fb0b821) (Gurevich et al., 2013). Putative proteins were annotated against the NCBI nonredundant protein database using DIAMOND (v2.0.14) (Buchfink et al., 2021). The average nucleotide identity (ANI) was calculated with FastANI (Zong, 2020). Multiple sequence alignment was performed with MAFFT (v7.407) (Katoh and Standley, 2013). IQ-TREE v2.2.2.3 was used to select the model that minimized the BIC score to construct a phylogenetic tree using the log-likelihood method with the Bayesian information criterion (BIC) (Lorah and Womack, 2019). The protein domains of AAC(6')-Iaq were predicted using CD-search (Marchler-Bauer and Bryant, 2004). Genetic context analysis of *aac(6')-Iaq* and other related sequences was carried out using clinker (v.0.0.25) (Gilchrist and Chooi, 2021).

Cloning of the *aac(6')-Iaq* gene

The ORF of *aac(6')-Iaq* (447 bp) with its upstream promoter region predicted by BPROM (www.softberry.com) (Supplementary Figure S1) was amplified by PCR with primers designed by SnapGene v6.0 (www.snapgene.com) (Supplementary Table S1). The PCR products (575 bp) were subsequently ligated into the T-Vector pMD^{TM}19 using T4 ligase (Takara Biomedical Technology Co., Ltd.). The recombinant plasmid pMD19-T-*aac(6')-Iaq* was subsequently transformed into competent *E. coli* DH5α cells, after which the recombinant strain DH5α(pMD19-T-*aac(6')-Iaq*) was

TABLE 1 Strains and plasmids used in this work.

Strains or plasmids	Functions	Reference
Strains		
DW0551	The wild-type strain of *Brucella intermedia* DW0551	This study
DH5α	*E. coli* DH5α was used as the host bacterium for cloning of the *aac(6')-Iaq* gene with its upstream promoter region	CGMCC*
ATCC 27853	*Pseudomonas aeruginosa* ATCC 27853 was used as a quality control strain for antimicrobial susceptibility testing	CGMCC*
DH5α(pMD19-T-*aac (6')-Iaq*)	*E. coli* DH5α carrying the recombinant plasmid pMD19-T-*aac(6')-Iaq*	This study
DH5α(pMD19-T)	*E. coli* DH5α carrying the pMD19-T vector was used as a control strain for the recombinant strain in the drug susceptibility testing	CGMCC*
BL21(pCold I-*aac(6')-Iaq*)	*E.coli* BL21 carrying the recombinant plasmid pCold I -*aac(6')-Iaq*	This study
Plasmids		
pMD19-T vector	T-Vector pMD^{TM}19 (Simple) was used as a vector for cloning of the *aac(6')-Iaq* gene with its upstream promoter region, AMP^r	CGMCC*
pCold I	pCold I was used as a vector for expression of the ORF of the *aac(6')-IVa* gene, AMP^r	CGMCC*

CGMCC, China General Microbiological Culture Collection Center.

10.3389/fcimb.2025.1551240

TABLE 2 Antibiotic resistance of the strains used in this study (MIC, μg/mL).

Class	Antibiotic	DW0551	DH5α(pMD19-T-*aac(6')-Iaq*)	DH5α(pMD19-T)	DH5α	ATCC27853
Aminoglycosides	streptomycin	1,024	2	2	2	4
	ribostamycin	4,096	256	2	≤ 1	1024
	gentamicin	≥ 512	2	0.25	0.25	0.5
	tobramycin	≥ 512	16	0.5	0.5	1
	kanamycin	≥ 4,096	8	1	1	512
	sisomicin	≥ 512	8	0.125	0.25	0.0625
	amikacin	512	8	1	1	2
	netilmicin	≥ 64	4	0.0625	0.0625	1
	paromomycin	128	4	8	4	512
	neomycin	16	2	8	16	8
Aminocyclitols	spectinomycin	512	8	8	8	64
β-Lactams	amoxicillin	256	/	/	/	1,024
	piracillin	≥ 256	≥ 256	≥ 256	8	8
	penicillin G	≥ 4,096	/	/	/	2,048
	ampicillin	1,024	/	/	/	512
	cefthiophene	1,024	/	/	/	≥ 2,048
	cefuroxime	512	/	/	/	512
	cefazolin	256	/	/	/	≥ 2,048
	ceftriaxone	≥ 256	0.0625	0.125	0.0625	32
	cefepime	≥ 32	0.0625	0.0625	0.016	0.5
	cefoxitin	256	/	/	/	≥ 1,024
	cefotaxime	256	/	/	/	8
	ceftazidime	≥ 2,048	/	/	/	1
	aztreonam	≥ 1,024	/	/	/	2
	imipenem	1	/	/	/	2
	meropenem	2	/	/	/	0.5
Quinolones	enrofloxacin	≤ 1	/	/	/	/
	levofloxacin	0.5	≤ 0.025	≤ 0.025	≤ 0.0125	0.5
	nalidixic acid	128	/	/	/	128
Tetracycline	tetracycline	16	/	/	/	4
	doxycycline	≥ 128	/	/	/	/
	tigecycline	0.5	/	/	/	0.5
	oxytetracycline	64	/	/	/	/
Chloramphenicol	chloramphenicol	128	16	16	16	128
	florfenicol	128	/	/	/	64
Macrolides	avermectin	128	/	/	/	/
	tylosin	≥ 2,048	/	/	/	/
	acetylmequine	≥ 2,048	/	/	/	/

(Continued)

TABLE 2 Continued

Class	Antibiotic	DW0551	DH5α(pMD19-T-*aac(6')-Iaq*)	DH5α(pMD19-T)	DH5α	ATCC27853
	azithromycin	≤ 0.5	≤ 0.5	≤ 0.5	≤ 0.5	16
	erythromycin	8	/	/	/	128
Lincosamide	lincomycin	≥ 2,048	/	/	/	/
Sulfanilamide	8	/	/	/	/	
fosfomycin		≥ 512	/	/	/	8

"/" the test was not performed.

selected on LB agar plates supplemented with 100 μg/mL ampicillin. Finally, the cloned fragment [*aac(6')-Iaq* with its upstream promoter region] was verified by Sanger sequencing (Shanghai Sunny Biotechnology Co., Ltd., Shanghai, China).

Expression and purification of *aac(6')-Iaq*

The PCR-amplified ORF of the *aac(6')-Iaq* gene was inserted into the pCold I vector (Table 1 and Supplementary Table S1), and the recombinant plasmid pCold I-*aac(6')-Iaq* was subsequently transformed into *E. coli* BL21. The recombinant BL21(pColdI-*aac(6')-Iaq*) was cultured in 100 mL of LB to an OD_{600} of 0.6 in a shaker at a constant temperature of 37°C. After cooling, 1 mM isopropyl-β-D-thiogalactopyranoside was added, and the mixture was shaken at a constant temperature of 16°C for 18 h. Bacteria were then collected by centrifugation at 10,000 × g for 10 min at 4°C and lysed with 4 mL of nondenaturing lysis solution. Subsequently, the lysed bacteria were subjected to 10 min of ultrasonic lysis. After 30 min of centrifugation (10,000 × g) at 4°C, the supernatant containing the recombinant protein was obtained, and the protein was purified using the Beyotime His-tag Protein Purification Kit (Beyotime Biotechnology Co., Ltd., Shanghai, China). The His tag of the recombinant protein was excised using Thrombin (Beijing Solarbio Science & Technology Co., Ltd., Beijing, China) at 4°C for 72 h. The AAC(6')-Iaq protein was then concentrated using an Amicon Ultra15 centrifugal filter equipped with an Ultracel-10 membrane (Casanovas et al., 2017) and stored at -20°C with 50% glycerol.

Enzyme kinetic analysis

The kinetic parameters of AAC(6')-Iaq were measured as reported previously with slight modifications (Vetting et al., 2008). The AAC(6')-Iaq activity was determined by measuring the NTB ions produced from the interaction of the acetylation reaction product CoA-SH (containing sulfhydryl groups) with DTNB (CoA-SH + DTNB → TNB^-). The total reaction volume was 200 μL, and the pH ranged from 7-7.5. The mixture contained 2 mM DTNB, 1 mM EDTA, 100 mM CoA-SH, 25 mM MES, 5-500 μg/mL aminoglycoside substrate dissolved using sterile double-distilled water and 2 μg of purified AAC(6')-Iaq protein (Magnet et al., 2001). The reaction was monitored at 412 nm using Synergy Neo2 (BioTek Instruments Inc., VT, United States) at a constant temperature of 37°C for 10 min at 4-second intervals. The AAC(6')-Iaq protein in the reaction system was replaced with an equal volume of double distilled water as a control for each assay, and the experiments were repeated three times for each aminoglycoside substrate. The steady-state kinetic parameters (k_{cat} and K_m) were determined by nonlinear regression of the initial reaction rates with the Michaelis-Menten equation in Prism (v9.4.0) software (GraphPad Software, CA, United States). Another AAC(6') variant [AAC(6')-Va] was analyzed together as a positive control (Zhang et al., 2023).

Gene expression analysis by RT-qPCR

Reverse transcription quantitative PCR (RT-qPCR) was performed according to previous methods with slight changes (Rocha et al., 2020). Bacteria were cultured in LB broth until the OD_{600} reached 0.5, and for the experimental group, 1/4 MIC ribostamycin (1,024 μg/mL) was then added. The bacteria were further incubated for 2, 4, or 8 h, followed by RNA extraction with RNAprep Pure Cell/Bacteria Kit (Tiangen, Beijing, China) and quantification with a DS-11+ Spectrophotometer (DeNovix, Delaware, United States). The DNA-free RNA extract was verified by PCR of the *Brucella intermedia* 16S rRNA gene. cDNA was synthesized for each sample using HiScript III RT SuperMix for qPCR (Vazyme Biotech, Nanjing, China). RT-qPCR was performed on a CFX96™ Touch Real-Time PCR Detection System (Bio-Rad Laboratories, Hercules, CA, United States), and the increase in real-time fluorescence was monitored by using SYBR qPCR Master Mix (Vazyme Biotech, Nanjing, China). The housekeeping 16S rRNA gene was utilized as a reference gene for relevant quantification via the CT method (Schmittgen and Livak, 2008). Comparisons of expression levels were performed using a *t*-test to evaluate the effects of aminoglycosides, and $p \leq 0.05$ was considered to indicate statistical significance.

Data availability

The nucleotide sequences of the *B. intermedia* DW0551 genome have been submitted to GenBank under accession number CP131474 for chromosome_1, CP131475 for chromosome_2, CP131476 for pDW0551, and OR395485 for the *aac(6')-Iaq* gene.

Results and discussion

Screening the candidate novel resistance genes

As mentioned above, to explore the resistance mechanisms of the bacteria against antimicrobial molecules, we sequenced 576 bacteria isolated from sewage, domestic fowl and livestock feces. Annotation of the pooled genomic sequences of these bacteria via Illumina sequencing demonstrated that they encoded putative resistance genes against various classes of antimicrobial agents, including resistance genes for aminoglycosides, β-lactams, fluoroquinolones, tetracyclines, phenicols, and glycopeptides. In this work, we focused on identifying new resistance mechanisms for aminoglycosides. Of the potential aminoglycoside antibiotic resistance genes annotated from the pooled genomic sequences of 576 bacteria, ten [*aph(3')-Ia-*, *ant(9)-Ia-*, *aadA5-*, *aph(6)-Ic-*, *aph(6)-Ic-*, *aac(3)-IIIb-*, *aac(6')-If-*, *aac(6')-Iaa-*, *aph(6)-Id-*, and *aac(2')-IIb-*like genes sharing < 80% amino acid sequence identity with the functionally characterized aminoglycoside resistance genes] were cloned, and their resistance functions were determined by MIC tests of several aminoglycoside antimicrobials. Finally, we found that one of these genes, an *aac(6')-If* homolog [eventually designated *aac(6')-Iaq* in this work] carried by the isolate DW0551 isolated from a goose, conferred resistance to several aminoglycosides.

General features of the DW0551 genome and resistance characteristics of DW0551

To analyze the structure of the novel resistance gene-related sequence, the whole genome of DW0551, which consists of two chromosomes and one plasmid (designated pDW0551), was sequenced. The larger chromosome (chromosome_1) is approximately 2.67 Mb in size, encoding 2,787 open reading frames (ORFs) with an average length of 847 bp, and the other (chromosome_2) is approximately 1.97 Mb in length, encoding 2,034 ORFs with an average length of 871 bp (Figure 1). The plasmid is 221.64 kb in size and encodes 250 ORFs (Table 3). Species identification analysis of DW0551 revealed that it shared the highest genome-wide ANI (97.83%) with the type strain *Brucella intermedia* 34576_H01 (GenBank assembly accession: GCA_900454225.1) in the NCBI nucleotide database, and 16S rRNA gene homology analysis revealed that the 16S rRNA gene of DW0551 shared the highest similarity (99.66%) with that of *Brucella intermedia* O. intermedium_CIP_105838 (GCA_012103055.1). According to the criteria for classifying a bacterium as a certain species (a threshold of ≥ 95% ANI was set to classify a bacterium as a certain species) (Richter and Rosselló-Móra, 2009), the isolate DW0551 belonged to the species *Brucella intermedia* and was thus designated *Brucella intermedia* DW0551.

A total of 59 *Brucella intermedia* genomes were present in the NCBI genome database, the genome sizes of which ranged from 3.94 Mb (GCA_001637305.1) to 5.39 Mb (GCA_028621395.1).

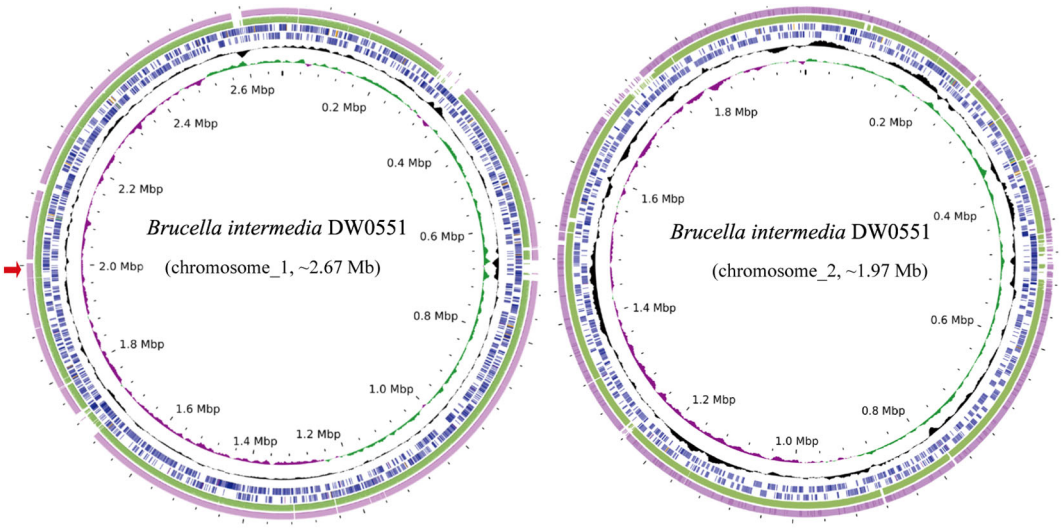

FIGURE 1
Genome maps of *B intermedia* DW0551 and its closest relatives. The circles, from inside to outside, represent the GC skew, GC content, and genes encoded in the forward and reverse strands of chromosome_1 (chromosome_2) of *B intermedia* DW0551, *B intermedia* ZJ499 chromosome 1 (chromosome 2) (CP061039.1), and *B intermedia* SG. G2 chromosome 1 (chromosome 2) (CP106662.1). The red arrow on the left represents the location of the novel resistance gene *aac(6')-Iaq*.

TABLE 3 General features of the DW0551 genome.

	Chromosome_1	Chromosome_2	pDW0551
Size (bp)	2,670,871	1,968,216	221,642
GC content (%)	58.18	57.24	53.46
ORFs	2,787	2,034	250
Known proteins	2,084 (76.79%)	1,450 (72.54%)	117 (46.80%)
Hypothetical proteins	630 (23.21%)	549 (27.46%)	133 (53.20%)
Protein coding (%)	97.38	98.28	96.15
Average ORF length (bp)	847	871	829.8
Average protein length (aa)	286.8	297.1	265.3
tRNA	40	17	0
rRNA	(16S-23S-5S) × 1	(16S-23S-5S) × 2	0

Only four strains had complete genomes, namely, *B. intermedia* ZJ499 (GCA_014495725.1), *B. intermedia* SG. G2 (GCA_025490555.1), *B. intermedia* ZL (GCA_029834515.1) and *B. intermedia* TSBOI (GCA_029855085.1). The remaining genomes were incomplete draft genomes. The four complete genomes each contained two chromosomes, and only *B. intermedia* SG. G2 had a plasmid, which was 176.21 kb in length, approximately 45 kb smaller than the plasmid pDW0551 in this study. When searching for similar plasmid sequences in the NCBI nucleotide database, no sequence that shared an identity of more than 10% with pDW0551 was found.

The results of antibiotic susceptibility testing revealed that DW0551 had high MIC levels of ≥ 16 μg/mL to 81.40% (35/43) of the antimicrobial agents tested. The MICs for aminoglycosides were especially high. Among the 10 aminoglycosides tested, except for a relatively low MIC value of 16 μg/mL for neomycin, DW0551 exhibited high MICs for the other 9 antimicrobial agents, with MIC ≥ 512 μg/mL for sisomicin and ≥ 64 μg/mL for netilmicin (Table 2). Compared to the recombinant carrying *aac(6')-Iaq* DH5α (pMD19-T-*aac(6')-Iaq*), the wild strain DW0551 showed higher MIC levels to aminoglycosides tested. This variation may be due to the presence of other resistance mechanisms, such as efflux pumps, modifying enzymes, target bypass, different intrinsic resistance mechanisms between different bacterial species and so on.

Considering the resistance genotype of the genome, a total of 106 drug resistance-related genes that shared amino acid identities ≥ 30% with functionally characterized resistance genes were predicted (Supplementary Table S2). Among them, 8 were putative aminoglycoside resistance genes encoding aminoglycoside-modifying enzymes, of which both *aac(6')-Il* (Bunny et al., 1995) and *ant(2")-Ia* (Cox et al., 2015) shared amino acid identities of 100% with the functionally characterized resistance genes, while the remaining six (including the novel resistance gene *aac(6')-Iaq* of this work) shared amino acid identities ranging from 44.1% to 73.2% with the functionally characterized genes.

Functional determination and molecular characterization of the novel aminoglycoside acetyltransferase gene *aac(6')-Iaq*

To determine the drug resistance function of the *aac(6')-Iaq* gene, the ORF of the *aac(6')-Iaq* gene with its promoter region was cloned (the *aac(6')-Iaq* gene and its flanking regions, including the proposed -10 and -35 regions of the promoter, are shown in Supplementary Figure S1), and the recombinant strain DH5α(pMD19-T-*aac(6')-Iaq*) exhibited resistance to numerous aminoglycosides, including ribostamycin, netilmicin, sisomicin, tobramycin, gentamicin, kanamycin, and amikacin, with 128-, 64-, 64-, 32-, 8-, 8-, and 8-fold higher MIC levels, respectively, than that of the control strain DH5α(pMD19-T) (Table 2). However, the MICs of spectinomycin and streptomycin did not vary.

The *aac(6')-Iaq* gene encoded in the chromosome 1 (Figure 1) is 447 bp in length and encodes a protein of 148 amino acids with a theoretical pI value of 4.64. To investigate the possible induction of *aac(6')-Iaq* expression by antibiotics, we performed RT-qPCR experiments to compare the relative expression levels of the genes in the presence and absence of antibiotics. After induction by ribostamycin for 8 h, the expression of the *aac(6')-Iaq* gene in the ribostamycin-treated group increased approximately 3-fold in comparison to that in the control group ($P < 0.05$) (Figure 2). When analyzing the relationship of *aac(6')-Iaq* with functionally characterized proteins, a total of 4 functionally characterized resistance genes (all *aac(6')-I* genes) with aa identities greater than 50% were found in the public antibiotic resistance gene database CARD. These genes were *aac(6')-If* (Ploy et al., 1994), *aac(6')-Iaa* (Salipante and Hall, 2003), *aac(6')-Iy* (Magnet et al., 1999) and *aac(6')-Ic* (Shaw et al., 1992), and the proteins they encoded shared amino acid identities of 52.63%, 52.05%, 51.37% and 50.74%, respectively, with that encoded by *aac(6')-Iaq*. Evolutionary analysis of all the members of the functionally characterized AAC(6') family revealed that they were roughly clustered into 4 clusters (C1-C4) (Figure 3;

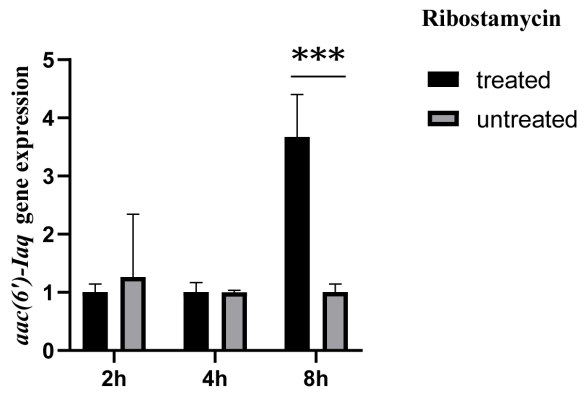

FIGURE 2
Comparison of the expression levels of the *aac(6')-Iaq* gene in the recombinant strains treated with or without 1024 μg/mL ribostamycin. The bars indicate the means ± standard errors, and the experiments were conducted in triplicate. A statistically significant difference was observed between the treated and untreated groups at 8 h. "***": Significant difference, $P < 0.05$.

Supplementary Table S3). The AAC(6') genes that shared higher identities with *aac(6')-Iaq* were clustered together.

To compare the resistance spectra of strains harboring different *aac(6')* genes, the resistance phenotypes of 13 *aac(6')* genes from different evolutionary clusters were analyzed; four of these genes were most closely related to *aac(6')-Iaq* (no resistance profile was available for *aac(6')-If*) in cluster 1, and the remaining 9 *aac(6')* genes were randomly selected from the other 3 clusters (Supplementary Table S4). The novel aminoglycoside resistance gene *aac(6')-Iaq* conferred resistance to all seven aminoglycosides detected; however, for the other 13 *aac(6')* genes, among the 4 to 7 antimicrobial agents tested, each showed susceptibility to 1 or 2 antirobial agents. Among the three antimicrobial agents tested, all the genes conferred resistance to tobramycin, and most (12/14) conferred resistance to amikacin; however, only a small portion (4/14) of the genes conferred resistance to gentamicin. All of the genes tested conferred resistance to the antimicrobial molecules tested, except for *aac(6')-Iaf* (Kitao et al., 2009) and *aac(6')-Isa* (Hamano et al., 2004), both of which showed susceptibility to sisomicin. The *aac(6')* genes exhibited different resistance spectra even though they were phylogenetically closely related.

When analyzing the essential functional residues of the protein, multiple sequence alignment of AAC(6')-Iaq with the functionally characterized proteins of the AAC(6')-I proteins was performed (Marchler-Bauer et al., 2017). The coenzyme A chemical binding pocket of the conserved protein domain family NAT_SF (PSSM-Id: 173926), consisting of 5 residues (I84, Y85, V86, A96 and R97) (Rojas et al., 1999), was present in AAC(6')-Iaq (I^{84}-Y^{85}-V^{86}-X-X-X-X-X-X-X-X-X-A^{96}-R^{97}) (Figure 4). The conserved protein domain family NAT_SF belongs to the cl17182 superfamily

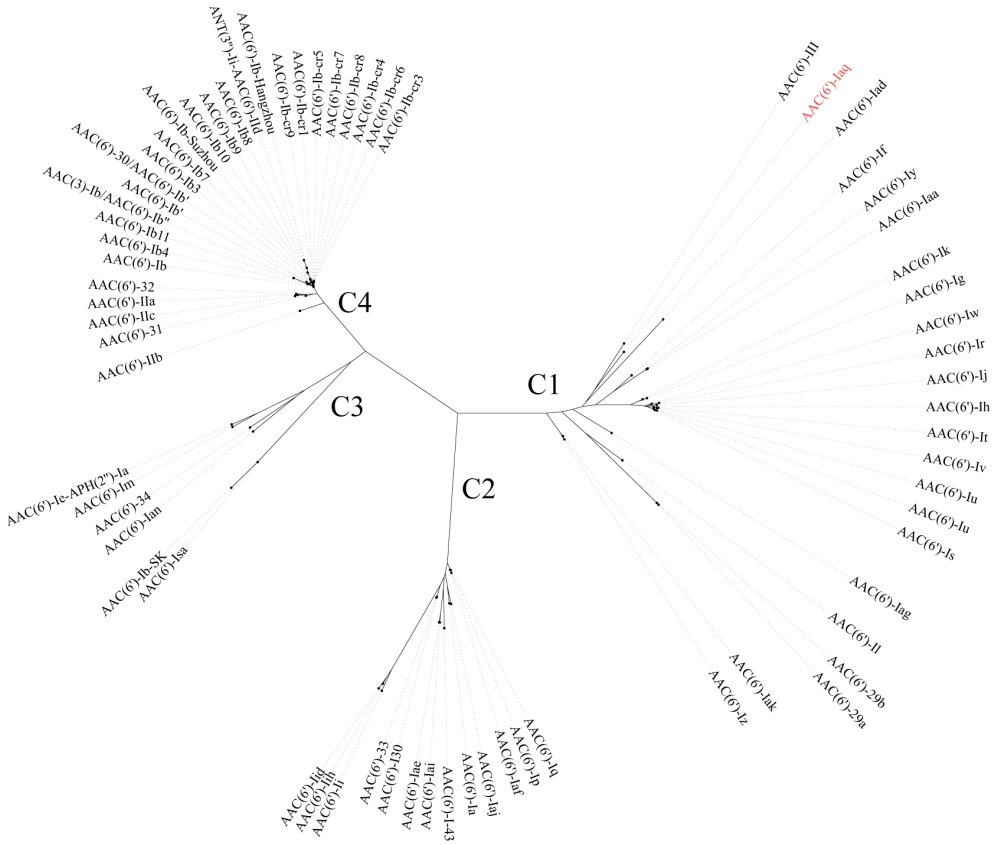

FIGURE 3
A phylogenetic tree showing the relationship of AAC(6')-Iaq with other functionally characterized AAC(6')s; C1-C4 refer to clusters 1-4. AAC(6')-Iaq is highlighted in red. The accession numbers of these genes are listed in Supplementary Table S3.

(domain architecture ID 10456837, a family of proteins containing various enzymes with catalytic acyl-transfer substrates) (Wybenga-Groot et al., 1999).

aac(6')-Iaq showed higher affinity and catalytic efficiency for netilmicin than the other related proteins

The results of the acetyltransferase activity and enzyme kinetic parameter analyses of AAC(6')-Iaq demonstrated that, consistent with the MIC results, AAC(6')-Iaq was able to acetylate ribostamycin, netilmicin, sisomicin, kanamycin and amikacin. No acetyltransferase activity could be detected for streptomycin. According to the Michaelis-Menten constant, this enzyme had the highest affinities and catalytic efficiencies for netilmicin [K_m of 3.83 ± 0.34 μM and k_{cat}/K_m of (9.08 ± 1.83) × 10^4 M^{-1}/s^{-1}] and sisomicin [K_m of 4.33 ± 1.32 μM and k_{cat}/K_m of (6.13 ± 2.26) × 10^4 M^{-1}/s^{-1}] (Table 4).

In addition to streptomycin, which has a hydroxyl group at the 6'-position, AAC(6')-Iaq exhibited acetyltransferase activity toward five other aminoglycosides harboring an amino group at the 6' position, and this regiospecific acetyltransferase transfer is consistent with previous findings (Magnet et al., 2001). Among these aminoglycoside substrates, amikacin and kanamycin were poor substrates, exhibiting lower affinities (with K_m values of 14.08 ± 0.76 μM and 13.34 ± 9.07 μM, respectively); this difference is thought to be related to the fact that the substituent at position 1 of ring I of amikacin and kanamycin is a hydroxyl group rather than an amino group (Tada et al., 2016).

AAC(6')-Iaq exhibits a higher affinity and a higher catalytic efficiency for netilmicin than several other AAC(6') enzymes reported previously. The K_m values for netilmicin of AAC(6')-Ial, AAC(6)-Iy, and AAC(6')-Ic were 23 ± 6, 8 ± 1 and 20 ± 5 μM, respectively (Magnet et al., 2001; Tada et al., 2016), while the k_{cat}/K_m values for netilmicin of AAC(6')-Ial, AAC(6')-Iap and AAC(6')-III [AAC(6')-Ic] were 4.1×10^4 M^{-1}/s^{-1}, 2.2 × 10^4 M^{-1}/s^{-1}, and 2.9×10^4 M^{-1}/s^{-1}, respectively (Kim et al., 2007; Tada et al., 2016); however, AAC(6')-Ib (Vetting et al., 2008) had a much greater catalytic efficiency for netilmicin than the other AAC (6')-I proteins, showing a k_{cat}/K_m value of (2.0 ± 0.5) × 10^6 M^{-1}/s^{-1}.

The *aac(6')-Iaq* gene related sequences conserved in *Brucella* species

To analyze the genetic context of the *aac(6')-Iaq*-encoding region, a sequence approximately 20 kb in length with *aac(6')-Iaq* at the center was used as a query to search the nonredundant nucleotide database of the NCBI. A total of 18 sequences with > 80% nucleotide identity were retrieved, and all of them were from the genus *Brucella*/*Ochrobactrum*. Of these 18 sequences, the four sequences with the highest identities (> 96.0%) were from *Brucella intermedia* (CP123056.1, identity 98.29%, CP061039.1, identity 97.20%, CP122438.1, identity 97.04%, and CP106662.1, identity 96.98%), and all of them contained an *aac(6')-Iaq*-like gene (an *aac(6')-Iaq*-like gene is a gene other than *aac(6')-Iaq* according to the public database and the protein it encoded shares aa identity of ≥ 80% with AAC(6')-Iaq). The remaining 14 sequences showed identities ranging from 82.24% to 85.64% and were all free of an *aac*

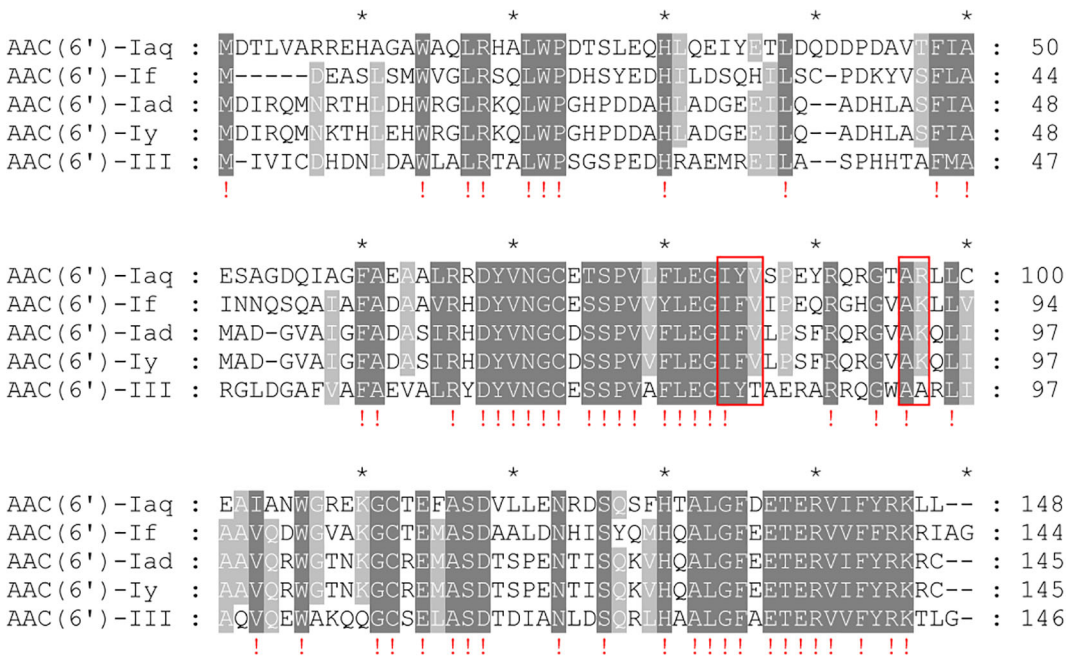

FIGURE 4
Multiple sequence alignment of AAC(6')-Iaq with other close relatives of the C1 cluster. The numbers on the right represent the corresponding amino acid sequence length. Exclamation marks indicate fully conserved residues; gaps are represented using hyphens. The red frames represent the residues of the conserved protein domain family NAT_SF. "*" is a location marker. Dark gray indicates conserved sites, and light gray indicates relatively conserved sites.

TABLE 4 Kinetic parameters of AAC(6')-Iaq.

Substrate	K_{cat} (s^{-1})	K_m (μM)	k_{cat}/K_m (M^{-1}/s^{-1})
sisomicin	0.25 ± 0.03	4.33 ± 1.32	(6.13 ± 2.26) × 10^4
ribostamycin	0.17 ± 0.004	10.05 ± 2.45	(1.83 ± 0.45) × 10^4
netilmicin	0.34 ± 0.04	3.83 ± 0.34	(9.08 ± 1.83) × 10^4
kanamycin	0.49 ± 0.08	13.34 ± 9.07	(4.64 ± 2.25) × 10^4
amikacin	0.46 ± 0.08	14.08 ± 0.76	(3.26 ± 0.72) × 10^4
streptomycin	NA[a]	NA[a]	NA[a]

[a]NA, no activity observed.

(6')-Iaq-like gene. Comparative structural analysis of 10 sequences, including four sequences that shared identities higher than 96.0% and five sequences that shared lower identities with the sequence of interest in this work, was performed, and the results revealed that they had similar genetic contexts in terms of gene content and gene order. Except for the *aac(6')-Iaq*-like gene, at most one or two predicted ORFs (such as *vapC*, *mazE*, *fbcH*, *rnaseL*, *yijF*, *rpmH* or a hypothetical protein-encoding gene) differed between them (Figure 5). No MGE was found within the 20 kb sequences. However, the mechanism underlying its appearance in *Brucella intermedia* chromosomes remains to be further studied.

To analyze the distribution of the *aac(6')-Iaq*(-like) genes, the aa sequence of AAC(6')-Iaq was used as a query to search the NCBI nonredundant nucleotide database, and approximately one hundred sequences with amino acid similarities greater than 50.0% were retrieved. Of these sequences, only four (mentioned above) had similarities > 95.0% and they were from the same species as AAC(6')-Iaq, *Brucella intermedia*. As mentioned above, there are four complete *Brucella intermedia* genomes in the NCBI genome database, and the sequences carrying the AAC(6')-Iaq(-like) proteins are from them, respectively: CP106662.1 (identity 97.3% chromosome of SG.G2), isolated from houseplant; CP122438.1 (identity 96.62%, chromosome of ZL), isolated from environment; CP061039.1 (identity 96.62%, chromosome of ZJ499), isolated from human sputum; CP123056.1 (identity 95.95%, chromosome of TSBOI), isolated from soil, and all the others had similarities < 60% with AAC(6')-Iaq; these similar sequences were from bacteria of different families, such as one (CP120373.1, identity 54.60%) from *Ensifer garamanticus* LMG 24692, or from different classes, such as one (CP116005.1, identity 59.59%) from *Sphingosinicella microcystinivorans* DMF-3. The genetic context of these sequences was entirely different from that of the sequence in this work (*Brucella intermedia* DW0551). To analyze the evolutionary relationships between these genes, additional *aac(6')-Iaq*-like genes with higher identities would be included.

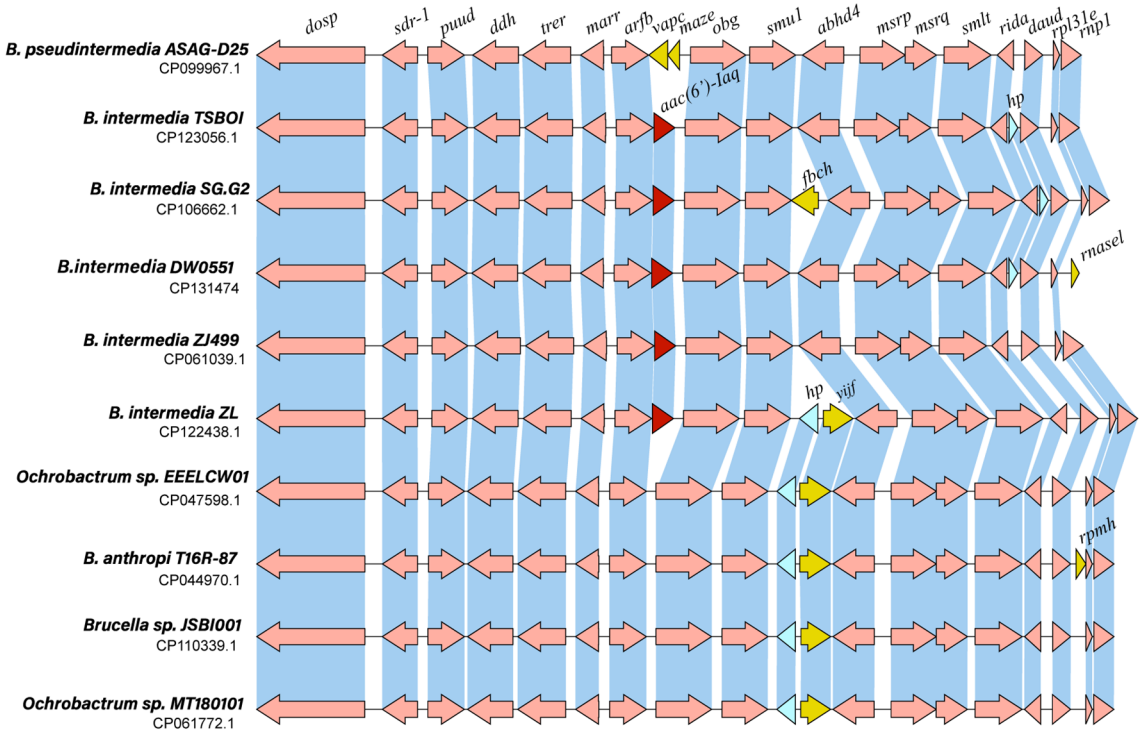

FIGURE 5
Genetic context of *aac(6')-Iaq* and other related sequences. Regions with ≥ 80% amino acid identity are in blue. hp: hypothetical protein. The *aac (6')-Iaq* and *aac(6')-Iaq*-like genes (similarity > 95.0%) are shown in red. The genes specific to each sequence are shown in yellow, and the hypothetical protein-encoding genes are shown in blue.

Conclusion

In this study, a novel aminoglycoside resistance gene, designated *aac(6')-Iaq*, encoded on the chromosome of a *Brucella intermedia* isolate from goose feces, was identified. AAC(6')-Iaq shares < 60% amino acid identity with all functionally characterized aminoglycoside resistance gene encoded proteins and shows resistance to several aminoglycosides including ribostamycin, netilmicin, sisomicin, tobramycin, gentamicin, kanamycin, and amikacin. AAC(6')-Iaq exhibited acetylation activity toward the aminoglycoside substrates analyzed. The discovery of novel resistance mechanisms in animal bacteria might also aid in the treatment of microbial infections in animals and humans.

Data availability statement

The datasets presented in this study can be found in online repositories. The names of the repository/repositories and accession number(s) can be found in the article/Supplementary Material.

Ethics statement

This study used strains isolated from animals in animal farms in Wenzhou, China. The owners of the farms were informed in writing of the study and provided approval for the sampling of animals. The studies involving human participants and animals were reviewed and approved by the Animal Welfare and Ethics Committee of Wenzhou Medical University, Zhejiang Province, China (protocol number: wydw2021-0323).

Author contributions

NL: Formal Analysis, Investigation, Methodology, Software, Writing – original draft. WX: Data curation, Formal Analysis, Investigation, Writing – original draft. DH: Conceptualization, Project administration, Supervision, Writing – original draft. CL: Formal Analysis, Investigation, Resources, Writing – original draft. JL: Conceptualization, Data curation, Validation, Writing – original draft. MZ: Data curation, Methodology, Resources, Writing – review & editing. QB: Conceptualization, Data curation, Formal Analysis, Funding acquisition, Investigation, Methodology, Project administration, Resources, Software, Supervision, Validation, Visualization, Writing – original draft, Writing – review & editing. WP: Funding acquisition, Resources, Writing – review & editing.

Funding

The author(s) declare that financial support was received for the research, authorship, and/or publication of this article. This study was supported by Zhejiang Provincial Natural Science Foundation of China (QN25H190009), the Science & Technology Project of Jinhua City, China (2024-4-030, 2022-2-013), the Science & Technology Project of Taizhou City, China (21ywb126), and the Science & Technology Project of Wenzhou City, China (N20210001).

Acknowledgments

The authors would like to acknowledge the teachers and scientists of the Science and Technology Platforms of Wenzhou Medical University who helped with the analysis of the enzyme kinetic parameters.

Conflict of interest

The authors declare that the research was conducted in the absence of any commercial or financial relationships that could be construed as a potential conflict of interest.

Generative AI statement

The author(s) declare that no Generative AI was used in the creation of this manuscript.

Publisher's note

Supplementary material

The Supplementary Material for this article can be found online at: https://www.frontiersin.org/articles/10.3389/fcimb.2025.1551240/full#supplementary-material

SUPPLEMENTARY FIGURE 1
The *aac(6')-Iaq* gene and its flanking regions. The underlined regions are the -10 and -35 regions of the proposed promoter. The *aac(6')-Iaq* gene is shaded gray.

SUPPLEMENTARY TABLE 1
Primers used in this study.

SUPPLEMENTARY TABLE 2
106 resistance genes predicted from the DW0551 genome.

SUPPLEMENTARY TABLE 3
Sequences used to reconstruct the phylogenetic tree.

SUPPLEMENTARY TABLE 4
Resistance phenotypes conferred by *aac(6')* genes belonging to different phylogenetic clusters.

References

Abdul-Aziz, M. H., Alffenaar, J. C., Bassetti, M., Bracht, H., Dimopoulos, G., Marriott, D., et al. (2020). Antimicrobial therapeutic drug monitoring in critically ill adult patients: a Position Paper(). *Intensive Care Med.* 46, 1127–1153. doi: 10.1007/s00134-020-06050-1

Alcock, B. P., Huynh, W., Chalil, R., Smith, K. W., Raphenya, A. R., Wlodarski, M. A., et al. (2023). CARD 2023: expanded curation, support for machine learning, and resistome prediction at the Comprehensive Antibiotic Resistance Database. *Nucleic Acids Res.* 51, D690–d699. doi: 10.1093/nar/gkac920

Alcock, B. P., Raphenya, A. R., Lau, T. T. Y., Tsang, K. K., Bouchard, M., Edalatmand, A., et al. (2020). CARD 2020: antibiotic resistome surveillance with the comprehensive antibiotic resistance database. *Nucleic Acids Res.* 48, D517–D525. doi: 10.1093/nar/gkz935

Apisarnthanarak, A., Kiratisin, P., and Mundy, L. M. (2005). Evaluation of Ochrobactrum intermedium bacteremia in a patient with bladder cancer. *Diagn. Microbiol. Infect. Dis.* 53, 153–155. doi: 10.1016/j.diagmicrobio.2005.05.014

Bharucha, T., Sharma, D., Sharma, H., Kandil, H., and Collier, S. (2017). Ochromobactrum intermedium: an emerging opportunistic pathogen-case of recurrent bacteraemia associated with infective endocarditis in a haemodialysis patient. *New Microbes New Infections* 15, 14–15. doi: 10.1016/j.nmni.2016.09.016

Bortolaia, V., Kaas, R. S., Ruppe, E., Roberts, M. C., Schwarz, S., Cattoir, V., et al. (2020). ResFinder 4.0 for predictions of phenotypes from genotypes. *J. Antimicrobial Chemotherapy* 75, 3491–3500. doi: 10.1093/jac/dkaa345

Buchfink, B., Reuter, K., and Drost, H.-G. (2021). Sensitive protein alignments at tree-of-life scale using DIAMOND. *Nat. Methods* 18, 366–368. doi: 10.1038/s41592-021-01101-x

Bunny, K. L., Hall, R. M., and Stokes, H. W. (1995). New mobile gene cassettes containing an aminoglycoside resistance gene, aacA7, and a chloramphenicol resistance gene, catB3, in an integron in pBWH301. *Antimicrobial Agents Chemotherapy* 39, 686–693. doi: 10.1128/AAC.39.3.686

Casanovas, A., Pinto-Llorente, R., Carrascal, M., and Abian, J. (2017). Large-scale filter-aided sample preparation method for the analysis of the ubiquitinome. *Analytical Chem.* 89, 3840–3846. doi: 10.1021/acs.analchem.6b04804

Cox, G., Stogios, P. J., Savchenko, A., and Wright, G. D. (2015). Structural and molecular basis for resistance to aminoglycoside antibiotics by the adenylyltransferase ANT(2″)-Ia. *MBio* 6, e02180–14. doi: 10.1128/mBio.02180-14

Crump, J. A., Sjölund-Karlsson, M., Gordon, M. A., and Parry, C. M. (2015). Epidemiology, clinical presentation, laboratory diagnosis, antimicrobial resistance, and antimicrobial management of invasive salmonella infections. *Clin. Microbiol. Rev.* 28, 901–937. doi: 10.1128/CMR.00002-15

EUCAST (2022). Breakpoint tables for interpretation of MICs and zone diameters. Version 12.0. Available online at: http://www.eucast.org (Accessed October 25, 2022).

Gilchrist, C. L. M., and Chooi, Y.-H. (2021). clinker & clustermap.js: automatic generation of gene cluster comparison figures. *Bioinf. (Oxford England)* 37, 2473–2475. doi: 10.1093/bioinformatics/btab007

Gurevich, A., Saveliev, V., Vyahhi, N., and Tesler, G. (2013). QUAST: quality assessment tool for genome assemblies. *Bioinf. (Oxford England)* 29, 1072–1075. doi: 10.1093/bioinformatics/btt086

Hamano, Y., Hoshino, Y., Nakamori, S., and Takagi, H. (2004). Overexpression and characterization of an aminoglycoside 6'-N-acetyltransferase with broad specificity from an epsilon-poly-L-lysine producer, Streptomyces albulus IFO14147. *J. Biochem.* 136, 517–524. doi: 10.1093/jb/mvh146

Hirai, J., Yamagishi, Y., Sakanashi, D., Koizumi, Y., Suematsu, H., and Mikamo, H. (2016). A case of bacteremia caused by ochrobacterium intermedium]. Kansenshogaku zasshi. *J. Japanese Assoc. For Infect. Dis.* 90, 129–133. doi: 10.11150/kansenshogakuzasshi.90.129

Holmes, B., Popoff, M., Kiredjian, M., and Kersters, K. (1988). Ochrobactrum anthropi gen. nov., sp. nov. from Human Clinical Specimens and Previously Known as Group Vd. *Int. J. Syst. Evol. Microbiol.* 38, 406–416. doi: 10.1099/00207713-38-4-406

Huang, N., Nie, F., Ni, P., Gao, X., Luo, F., and Wang, J. (2022). BlockPolish: accurate polishing of long-read assembly via block divide-and-conquer. *Briefings In Bioinf.* 23, bbab406. doi: 10.1093/bib/bbab405

Jacobs, D. J., Grube, T. J., Flynn, H. W., Greven, C. M., Pathengay, A., Miller, D., et al. (2013). Intravitreal moxifloxacin in the management of Ochrobactrum intermedium endophthalmitis due to metallic intraocular foreign body. *Clin. Ophthalmol. (Auckland N.Z.)* 7, 1727–1730. doi: 10.2147/OPTH.S44212

Kassab, I., Sarsam, N., Affas, S., Ayas, M., and Baang, J. H. (2021). A case of ochrobactrum intermedium bacteremia secondary to cholangitis with a literature review. *Cureus* 13, e14648. doi: 10.7759/cureus.14648

Katoh, K., and Standley, D. M. (2013). MAFFT multiple sequence alignment software version 7: improvements in performance and usability. *Mol. Biol. Evol.* 30, 772–780. doi: 10.1093/molbev/mst010

Kim, C., Villegas-Estrada, A., Hesek, D., and Mobashery, S. (2007). Mechanistic characterization of the bifunctional aminoglycoside-modifying enzyme AAC(3)-Ib/AAC(6')-Ib' from Pseudomonas aeruginosa. *Biochemistry* 46, 5270–5282. doi: 10.1021/bi700111z

Kitao, T., Miyoshi-Akiyama, T., and Kirikae, T. (2009). AAC(6')-Iaf, a novel aminoglycoside 6'-N-acetyltransferase from multidrug-resistant Pseudomonas aeruginosa clinical isolates. *Antimicrobial Agents Chemotherapy* 53, 2327–2334. doi: 10.1128/AAC.01360-08

Konstantinidis, K. T., and Tiedje, J. M. (2005). Genomic insights that advance the species definition for prokaryotes. *Proc. Natl. Acad. Sci. United States America* 102, 2567–2572.

Lewis, J. S. II (2022). *M100 performance standards for antimicrobial susceptibility testing* (West Valley Road, Suite 2500 Wayne, PA 19087, USA: Clinical and Laboratory Standards Institute), 402. P., FIDSA.

Lorah, J., and Womack, A. (2019). Value of sample size for computation of the Bayesian information criterion (BIC) in multilevel modeling. *Behav. Res. Methods* 51, 440–450. doi: 10.3758/s13428-018-1188-3

Lu, W., Li, K., Huang, J., Sun, Z., Li, A., Liu, H., et al. (2021). Identification and characteristics of a novel aminoglycoside phosphotransferase, APH(3')-IId, from an MDR clinical isolate of Brucella intermedia. *J. Antimicrobial Chemotherapy* 76, 2787–2794. doi: 10.1093/jac/dkab272

Magnet, S., Courvalin, P., and Lambert, T. (1999). Activation of the cryptic aac(6')-Iy aminoglycoside resistance gene of Salmonella by a chromosomal deletion generating a transcriptional fusion. *J. Bacteriol* 181, 6650–6655. doi: 10.1128/jb.181.21.6650-6655.1999

Magnet, S., Lambert, T., Courvalin, P., and Blanchard, J. S. (2001). Kinetic and mutagenic characterization of the chromosomally encoded Salmonella enterica AAC (6')-Iy aminoglycoside N-acetyltransferase. *Biochemistry* 40, 3700–3709. doi: 10.1021/bi002736e

Marchler-Bauer, A., Bo, Y., Han, L., He, J., Lanczycki, C. J., Lu, S., et al. (2017). CDD/SPARCLE: functional classification of proteins via subfamily domain architectures. *Nucleic Acids Res.* 45, D200–D203. doi: 10.1093/nar/gkw1129

Marchler-Bauer, A., and Bryant, S. H. (2004). CD-Search: protein domain annotations on the fly. *Nucleic Acids Res.* 32, W327–W331. doi: 10.1093/nar/gkh454

Ploy, M. C., Giamarellou, H., Bourlioux, P., Courvalin, P., and Lambert, T. (1994). Detection of aac(6')-I genes in amikacin-resistant Acinetobacter spp. by PCR. *Antimicrobial Agents Chemotherapy* 38, 2925–2928. doi: 10.1128/AAC.38.12.2925

Ramirez, M. S., and Tolmasky, M. E. (2010). Aminoglycoside modifying enzymes. *Drug Resist. Update* 13, 151–171. doi: 10.1016/j.drup.2010.08.003

Richter, M., and Rosselló-Móra, R. (2009). Shifting the genomic gold standard for the prokaryotic species definition. *Proc. Natl. Acad. Sci. United States America* 106, 19126–19131. doi: 10.1073/pnas.0906412106

Rocha, D. J. P. G., Castro, T. L. P., Aguiar, E. R. G. R., and Pacheco, L. G. C. (2020). Gene expression analysis in bacteria by RT-qPCR. *Methods In Mol. Biol. (Clifton N.J.)* 2065, 119–137. doi: 10.1007/978-1-4939-9833-3_10

Rojas, J. R., Trievel, R. C., Zhou, J., Mo, Y., Li, X., Berger, S. L., et al. (1999). Structure of Tetrahymena GCN5 bound to coenzyme A and a histone H3 peptide. *Nature* 401, 93–98. doi: 10.1038/43487

Ryan, M. P., and Pembroke, J. T. (2020). The genus ochrobactrum as major opportunistic pathogens. *Microorganisms* 8, 1797. doi: 10.3390/microorganisms8111797

Salipante, S. J., and Hall, B. G. (2003). Determining the limits of the evolutionary potential of an antibiotic resistance gene. *Mol. Biol. Evol.* 20, 653–659. doi: 10.1093/molbev/msg074

Schmittgen, T. D., and Livak, K. J. (2008). Analyzing real-time PCR data by the comparative C(T) method. *Nat. Protoc.* 3, 1101–1108. doi: 10.1038/nprot.2008.73

Seemann, T. (2014). Prokka: rapid prokaryotic genome annotation. *Bioinf. (Oxford England)* 30, 2068–2069. doi: 10.1093/bioinformatics/btu153

Sekiguchi, J.-I., Asagi, T., Miyoshi-Akiyama, T., Kasai, A., Mizuguchi, Y., Araake, M., et al. (2007). Outbreaks of multidrug-resistant Pseudomonas aeruginosa in community hospitals in Japan. *J. Clin. Microbiol.* 45, 979–989. doi: 10.1128/JCM.01772-06

Shaw, K. J., Rather, P. N., Sabatelli, F. J., Mann, P., Munayyer, H., Mierzwa, R., et al. (1992). Characterization of the chromosomal aac(6')-Ic gene from Serratia marcescens. *Antimicrob. Agents Chemother.* 36, 1447–1455. doi: 10.1128/aac.36.7.1447

Sheng, X., Lu, W., Li, A., Lu, J., Song, C., Xu, J., et al. (2023). ANT(9)-ic, a novel chromosomally encoded aminoglycoside nucleotidyltransferase from brucella intermedia. *Microbiol. Spectr.* 11, e0062023. doi: 10.1128/spectrum.00620-23

Souvorov, A., Agarwala, R., and Lipman, D. J. (2018). SKESA: strategic k-mer extension for scrupulous assemblies. *Genome Biol.* 19, 153. doi: 10.1186/s13059-018-1540-z

Tada, T., Miyoshi-Akiyama, T., Shimada, K., Dahal, R. K., Mishra, S. K., Ohara, H., et al. (2016). A novel 6'-N-aminoglycoside acetyltransferase, AAC(6')-ial, from a clinical isolate of serratia marcescens. *Microbial Drug Resistance (Larchmont N.Y.)* 22, 103–108. doi: 10.1089/mdr.2015.0126

Velasco, J., Romero, C., López-Goñi, I., Leiva, J., Díaz, R., and Moriyón, I. (1998). Evaluation of the relatedness of Brucella spp. and Ochrobactrum anthropi and description of Ochrobactrum intermedium sp. nov., a new species with a closer relationship to Brucella spp. *Int. J. Systematic Bacteriology* 48 Pt 3, 759–768. doi: 10.1099/00207713-48-3-759

Vetting, M. W., Park, C. H., Hegde, S. S., Jacoby, G. A., Hooper, D. C., and Blanchard, J. S. (2008). Mechanistic and structural analysis of aminoglycoside N-acetyltransferase AAC(6')-Ib and its bifunctional, fluoroquinolone-active AAC(6')-Ib-cr variant. *Biochemistry* 47, 9825–9835. doi: 10.1021/bi800664x

Walker, B. J., Abeel, T., Shea, T., Priest, M., Abouelliel, A., Sakthikumar, S., et al. (2014). Pilon: an integrated tool for comprehensive microbial variant detection and genome assembly improvement. *PloS One* 9, e112963. doi: 10.1371/journal.pone.0112963

Wick, R. R., Judd, L. M., Gorrie, C. L., and Holt, K. E. (2017). Unicycler: Resolving bacterial genome assemblies from short and long sequencing reads. *PloS Comput. Biol.* 13, e1005595. doi: 10.1371/journal.pcbi.1005595

Wybenga-Groot, L. E., Draker, K., Wright, G. D., and Berghuis, A. M. (1999). Crystal structure of an aminoglycoside 6'-N-acetyltransferase: defining the GCN5-related N-acetyltransferase superfamily fold. *Structure (London England: 1993)* 7, 497–507. doi: 10.1016/S0969-2126(99)80066-5

Zhang, G., Zhang, L., Sha, Y., Chen, Q., Lin, N., Zhao, J., et al. (2023). Identification and characterization of a novel 6'-N-aminoglycoside acetyltransferase AAC(6')-Va from a clinical isolate of Aeromonas hydrophila. *Front. In Microbiol.* 14. doi: 10.3389/fmicb.2023.1229593

Zong, Z. (2020). Genome-based taxonomy for bacteria: A recent advance. *Trends In Microbiol.* 28, 871–874. doi: 10.1016/j.tim.2020.09.007

frontiers | Frontiers in Cellular and Infection Microbiology

TYPE Original Research
PUBLISHED 31 March 2025
DOI 10.3389/fcimb.2025.1565980

OPEN ACCESS

EDITED BY
Daniela Visaggio,
Roma Tre University, Italy

REVIEWED BY
Dao-Feng Zhang,
Hohai University, China
Fei Jiang,
The Affiliated Hospital of Xuzhou Medical University, China
Chao Liu,
Peking University Third Hospital, China
Cemal Sandalli,
University of Missouri, United States

*CORRESPONDENCE
Junjie Ying
652868133@qq.com
Yuejuan Fang
15168326714@163.com

RECEIVED 24 January 2025
ACCEPTED 06 March 2025
PUBLISHED 31 March 2025

CITATION
Zhang H, Dong S, Mao C, Fang Y and Ying J (2025) Emergence and evolution of rare ST592 *bla*$_{NDM-1}$-positive carbapenem-resistant hypervirulent *Klebsiella pneumoniae* in China. *Front. Cell. Infect. Microbiol.* 15:1565980. doi: 10.3389/fcimb.2025.1565980

Emergence and evolution of rare ST592 *bla*$_{NDM-1}$-positive carbapenem-resistant hypervirulent *Klebsiella pneumoniae* in China

Huan Zhang[1], Su Dong[2], Caiping Mao[1], Yuejuan Fang[3]* and Junjie Ying[4]*

[1]Department of Clinical Laboratory, Zhejiang Cancer Hospital, Hangzhou Institute of Medicine (HIM), Chinese Academy of Sciences, Hangzhou, Zhejiang, China, [2]Department of Clinical Laboratory, Shaoxing Hospital of Traditional Chinese Medicine Affiliated to Zhejiang Chinese Medical University, Shaoxing, Zhejiang, China, [3]Department of Pharmacy, Quzhou Maternal and Child Health Care Hospital, Quzhou, China, [4]Department of Urology, The Quzhou Affiliated Hospital of Wenzhou Medical University, Quzhou People's Hospital, Quzhou, China

Objectives: This study aimed to characterize the genomes of two rare ST592 *Klebsiella pneumoniae* isolates and to explore their evolution into carbapenem-resistant hypervirulent *K. pneumoniae* (CR-hvKp).

Methods: The minimum inhibitory concentrations (MICs) were determined using a VITEK 2 compact system. Conjugation experiments were conducted using film matings. Whole-genome sequencing (WGS) was performed using the Illumina and Nanopore platforms. The antimicrobial resistance determinants were identified using the ABRicate program in the ResFinder database. Insertion sequences were identified using ISFinder and the bacterial virulence factors identified using the Virulence Factor Database (VFDB). The K and O loci were examined using Kleborate. Multilocus sequence typing (MLST) and replicon type identification were performed by the Center for Genomic Epidemiology. Conjugation-related elements were predicted using *oriT*finder. The plasmid structure was visualized using Circos, and a possible evolutionary model was constructed using BioRender.

Results: Isolates KPZM6 and KPZM16 were identified as ST592 and KL57, respectively, and were collected from the same department. The antimicrobial susceptibility testing data revealed that KPZM16 possesses an extensively drug-resistant (XDR) profile, whereas KPZM6 is a susceptible *K. pneumoniae*. The hybrid assembly showed that both KPZM6 and KPZM16 have one pLVPK-like virulence plasmid carrying the *rmpA*, *rmpA2*, and *iucABCD-iutA* gene clusters. However, strain KPZM16 harbors one IncN plasmid carrying the carbapenem resistance genes *bla*$_{NDM-1}$, *dfrA14*, and *qnrS1*. The results of the conjugation experiments demonstrated that the plasmid could be transferred to the recipient strain. It is possible that the NDM-1-producing plasmid was transferred from KPZM6 to KPZM16 via conjugation, leading to the formation of CR-hvKp.

Conclusions: This is the first study in which complete genomic characterization of the rare NDM-1-producing ST592 *K. pneumoniae* clinical isolate was performed. This study provides a possible evolutionary hypothesis for the formation of CR-hvKp via conjugation. Early detection is recommended to avoid the extensive spread of this clone.

KEYWORDS

WGS, ST592, NDM-1, evolution, CR-hvKp

Introduction

Carbapenem-resistant Enterobacteriaceae (CRE) are known to cause serious nosocomial infections associated with high mortality rates, posing a global public health threat (Hala et al., 2019). Of great concern is carbapenem-resistant *Klebsiella pneumoniae* (CRKP), which causes untreatable or nearly untreatable infections, as determined by the US Centers for Disease Control and Prevention (CDC) (Gu et al., 2018). Importantly, the carbapenem resistance rates have increased with the incidence of CRKP in China, demonstrating that CRKP remains a significant multidrug-resistant pathogen, particularly in the case of the ST11–KL64 CRKP clone, which is associated with a highly resistant and virulent epidemic in China (Zhou et al., 2023; Wang et al., 2024a). Due to its resistance to the commonly used antimicrobial drugs in the clinic, the novel β-lactamase inhibitor avibactam has been developed for the treatment of CRKP strains and has been used in combination with ceftazidime in recent years, which has exhibited excellent *in vitro* activity against CRKP (Qiao et al., 2024; Zhang et al., 2024). However, the widespread use of ceftazidime–avibactam has led to several *K. pneumoniae* carbapenemase (KPC) variants (e.g., KPC-135, KPC-33, and KPC-84) showing ceftazidime–avibactam resistance (Gong et al., 2024; Shi et al., 2024; Zhang et al., 2024).

Apart from resistance in CRKP, virulence is another important issue that requires great attention (Chen et al., 2024). There are two possible evolution pathways to becoming hypervirulent and resistant, simultaneously. Hypervirulent *K. pneumoniae* (hvKp) strains that acquire carbapenem resistance plasmids could be recognized as carbapenem-resistant hypervirulent *K. pneumoniae* (CR-hvKp). On the other hand, CRKP strains can acquire pLVPK-like virulence plasmids and are known as hypervirulent carbapenem-resistant *K. pneumoniae* (hv-CRKP) (Xu et al., 2021; Tian et al., 2022b). However, the specific evolutionary mechanisms remain unclear.

In this study, two ST592 *K. pneumoniae* isolates were obtained from the same department of one hospital in China, and their complete genetic characteristics were studied. One ST592 *K. pneumoniae* isolate might be an hvKp that only carries virulence genes, such as *rmpA*, *rmpA2*, *iroBCDN*, *iucABCD*, and *iutA*. Interestingly, the other ST592 *K. pneumoniae* isolate is likely a CR-hvKp that had acquired the NDM-1-producing plasmid. To the best of our knowledge, this is the first report on a clinical ST592 *K. pneumoniae* isolate and its evolution. This information will help in the understanding of the rare genomic characteristics of CR-hvKp bacteria and in the prevention and control of their spread in healthcare settings.

Methods

Bacterial isolation and identification

The *K. pneumoniae* clinical isolates KPZM6 and KPZM16 were obtained from pus samples collected from the same department of a hospital in China in 2020 and 2021 (Table 1). The pus was inoculated into a blood agar plate and incubated overnight at 37° C. Bacterial morphology was observed on the second day. A clone suspected to be *K. pneumoniae* was further characterized. The isolates were further identified with matrix-assisted laser desorption ionization time-of-flight mass spectrometry (MALDI-TOF MS; Bruker Daltonics GmbH, Bremen, Germany) and sequencing.

Antimicrobial susceptibility testing

The minimum inhibitory concentrations (MICs) were measured using the VITEK 2 compact system: amikacin, aztreonam, gentamicin, cefotetan, cefotaxime, cefuroxime, cefazolin, ceftazidime, ciprofloxacin, ceftriaxone, cefepime, cefoxitin, piperacillin, ciprofloxacin, imipenem, and meropenem. *Escherichia coli* ATCC 25922 was used as a control strain. The results were interpreted according to the recommendations of the Clinical and Laboratory Standards Institute (CLSI) 2021 guidelines.

Plasmid conjugation assays via film mating

To determine the transferability of bla_{NDM-1}-positive plasmids, conjugation experiments using *E. coli* EC600 (rifampin-resistant) as the recipient strain were conducted using the film-mating method

TABLE 1 Basic information of the two patients.

Patient ID	Isolate	Collection date	Age	Department	Source	Diagnosis
A	KPZM6	16.05.20	51	Anorectal surgery	Pus	Anal fistula
B	KPZM16	19.12.21	63	Anorectal surgery	Pus	Perianal abscess

(Yang et al., 2021b; Tian et al., 2022a). Putative transconjugants were screened on Mueller–Hinton agar plates containing rifampin (150 μg/ml) and meropenem (4 μg/ml) and were further confirmed with PCR using specific primers and MALDI-TOF MS.

Whole-genome sequencing and bioinformatics analyses

Genomic DNA was extracted using a Qiagen Minikit (Qiagen, Hilden, Germany) and the Gentra® Puregene® Yeast/Bact kit (Qiagen, Germany) and further sequenced using the Illumina and Oxford Nanopore platforms. Hybrid assembly of the short and long reads was performed using Unicycler v0.4.8 (Wick et al., 2017). Genome annotation was performed using the National Center for Biotechnology Information (NCBI) Prokaryotic Genome Annotation Pipeline (PGAP) (http://www.ncbi.nlm.nih.gov/genome/annotation_prok/) (Tatusova et al., 2016) and Prokka (Seemann, 2014). Antimicrobial resistance genes were identified using ABRicate v1.0.1 and ResFinder 4.0. Virulence factors were identified using the Virulence Factor Database (VFDB; http://www.mgc.ac.cn/VFs/) (Liu et al., 2022). The capsular polysaccharide (K locus) and lipooligosaccharide (OC locus) were analyzed using Kleborate with the command line of kleborate, ASSEMBLIES-k (Lam et al., 2021, 2022). Multilocus sequence typing (MLST) was performed and the replicon types were identified using the Center for Genomic Epidemiology website (https://genomicepidemiology.org/). The conjugation transfer elements, including the origin site of DNA transfer (*oriT*), the type IV secretion system (T4SS) region, the type IV coupling protein (T4CP), and the relaxase, were predicted using *oriT*finder (Li et al., 2018). The insertion sequences (ISs) were identified using ISfinder (Siguier et al., 2006), and the plasmid structure was visualized using Circos (Krzywinski et al., 2009). The plasmids were compared using the online tool BLAST. A possible evolutionary model was constructed using BioRender. Default parameters were used for all software packages.

Phylogenetic analysis of the ST592 *K. pneumoniae* strains

The ST592 genomes of the *K. pneumoniae* in this study and other *K. pneumoniae* genomes from the BIGSdb-Pasteur (https://bigsdb.pasteur.fr/klebsiella/) and BacWGSTdb (http://bacdb.cn/BacWGSTdb/) databases were used to establish phylogenetic trees. Snippy v4.4.5 (https://github.com/tseemann/snippy) was utilized to align the Illumina reads against a reference (accession no. GCA_000693075.1) and to generate a core genome alignment (Zhang et al., 2022). Core SNP alignment was used to generate a maximum likelihood (ML) phylogenetic tree using RaxML v8.2.12, with the GTRGAMMA model. The generated tree files were visualized using iTOL software.

Results

MICs and the antimicrobial resistance gene profile

Antimicrobial susceptibility testing revealed that the clinical isolate KPZM16 possesses an extensively drug-resistant (XDR) profile: it was resistant to all of the tested cephalosporins, ciprofloxacin, imipenem, and meropenem, but remained susceptible to amikacin, aztreonam, and gentamicin. However, the strain KPZM6 was found to be carbapenem-susceptible, and the results of the assays showed that it was susceptible to all of the antimicrobial agents tested.

Analysis of the genome of KPZM16 revealed that, in addition to co-harboring chromosomal $bla_{\text{SHV-26}}$, a series of genes conferring resistance to β-lactams ($bla_{\text{NDM-1}}$), the strain also contains genes associated with trimethoprim/sulfamethoxazole (*dfrA14*) and quinolones (*qnrS1*) (Table 2). However, in the case of KPZM6, only $bla_{\text{SHV-26}}$ was detected.

Virulence factors in the two clinical strains

Numerous virulence factors were found in the clinical isolates KPZM6 and KPZM16, including the iron–enterobactin transporter-related protein gene (*fepABCDG*), the type 3 fimbriae (*mrkABCDFHIJ*), and the type 1 fimbriae (*fimABCDEFGHI*). Other important virulence factors, including *rmpA*, *rmpA2*, *iroBCDN*, *iucABCD*, and *iutA*, were further identified.

Multilocus sequence typing and the K and O loci

Based on the *K. pneumoniae* MLST scheme, KPZM6 and KPZM16 were classified as rare ST592. Moreover, *Kleborate* was used and result showed the strain contains KL57 and O3b. In addition, the results showed that Wzi, an outer membrane protein lectin, was Wzi206.

Chromosome and plasmid characterization analyses

The hybrid assembly showed that strain KPZM6 had a 5,143,477-bp circular chromosome with a GC content of 57.65% (Table 2). Moreover, a 253,679-bp pLVPK-like virulence plasmid with IncHI1B and RepB replicons was identified in strain KPZM6. In KPZM16, the plasmid pKPZM16-1, a 208,216-bp pLVPK-like virulence plasmid containing IncFIB(K)–IncHI1B replicons, was identified. In addition, three other plasmids were identified in this isolate, namely, pKPZM16-2 to pKPZM16-4, with sizes ranging from 5,905 to 111,160 bp and with GC contents ranging from 48.62% to 52.06% (Table 2). Importantly, pKPZM16-3 is an IncN plasmid that carries the carbapenem resistance genes $bla_{\text{NDM-1}}$, *dfrA14*, and *qnrS1*.

Genetic features of the virulence and resistance plasmids and evolutionary insights into the formation of the CR-hvKp strain

The basic backbones of the two pLVPK-like virulence plasmids (pKPZM6-1 and pKPZM16-1) were similar, with 77% coverage and 99.98% sequence identity. The *rmpA*, *rmpA2*, and *iucABCD-iutA* gene clusters were found in this plasmid. The plasmid structure is shown in Figures 1 and 2A. pKPZM16-3 is a $bla_{\text{NDM-1}}$-positive plasmid (Figure 2B). This plasmid is composed of several resistance genes (e.g., *dfrA14*, *qnrS1*, and $bla_{\text{NDM-1}}$), the *oriT*, the T4SS region, T4CP, a gene encoding a relaxase, and a series of various ISs, including IS*26* and IS*3000*. Downstream of $bla_{\text{NDM-1}}$ is the bleomycin resistance-related gene *ble-MBL*. However, IS*Aba125* was not found upstream of $bla_{\text{NDM-1}}$. Based on the BLASTN results using the NCBI database, the data showed similar plasmids with 100% coverage and 99.99% identity to other *K. pneumoniae* (pNDM1_LL34, accession no. CP025965.2), *Citrobacter freundii* (pNDM-Cf7308, accession no. CP092465.1), and *E. coli* (pNDM-BTR, accession no. KF534788.2) isolates. All plasmids had a size of approximately 59 kb. The results of the conjugation experiments demonstrated that it could be transferred to the recipient strain. However, both pLVPK-like virulence plasmids failed to transfer to the recipient strain.

Considering that both KPZM6 and KPZM16 were collected from the same hospital department, there may have been an evolutionary process (gene flow) between them. A diagram was drawn with regard to the possible evolutionary mechanism of CR-hvKp formation based on $bla_{\text{NDM-1}}$-harboring plasmid transfer (Figure 3). It is possible that the NDM-1-producing plasmid was transferred from KPZM6 (hvKp) to KPZM16 (CR-hvKp) through conjugation. This process may be accompanied by the co-transfer of two other plasmids (i.e., pKPZM16-2 and pKPZM16-4).

Comparative genomics analysis of the ST592 *K. pneumoniae* isolates

To analyze the genetic characteristics of the ST592 *K. pneumoniae* strains from different countries, a comparative genomics analysis was performed. The data showed that nine ST592 *K. pneumoniae* strains were isolated from Thailand, China, and the USA from 2013 to 2021 (Figure 4). There is a huge diversity among these strains. Two strains carrying $bla_{\text{OXA-232}}$, $bla_{\text{KPC-2}}$, and $bla_{\text{NDM-1}}$ were identified. Importantly, all ST592 *K. pneumoniae* strains carried several virulence-related genes: *iroBCDEN*, *iucABCD*, *iutA*, *rmpA*, *rmpA2*, *fepABCDG*, *mrkABCDFHIJ*, and *fimABCDEFGHI*.

Discussion

CRKP has attracted great attention worldwide and is increasingly considered an important nosocomial pathogen in hospitals (Jin et al., 2021). In 2020, Zhou et al. reported the emergence of *rmpA*/*rmpA2*-positive ST11-KL64 isolates, which progressively replaced ST11–KL47 to become a new hypervirulent subclone, suggesting the evolution of carbapenem-resistant and

TABLE 2 Molecular characterization of the genomes of clinical strains KPZM6 and KPZM16.

Isolate ID	Genome	Replicon	Size (bp)	Resistance gene	Accession number
KPZM6	Chromosome	–	5,143,477	$bla_{\text{SHV-26}}$	PRJNA1212823
	pKPZM6-1	IncFIB(K), IncHI1B	253,679	–	PRJNA1212823
KPZM16	Chromosome	–	5,048,454	$bla_{\text{SHV-26}}$	PRJNA1213023
	pKPZM16-1	IncFIB(K), IncHI1B	208,216	–	PRJNA1213023
	pKPZM16-2	IncFIB	111,160	–	PRJNA1213023
	pKPZM16-3	IncN	59,596	*dfrA14*, *qnrS1*, $bla_{\text{NDM-1}}$	PRJNA1213023
	pKPZM16-4	–	5,905	–	PRJNA1213023

– Not detected.

hypervirulent *K. pneumoniae* (Zhou et al., 2020). However, the global occurrence of ST592 *K. pneumoniae* remains sporadic, and no NDM-1-producing ST592 CR-hvKp has been reported to date, particularly with regard to the genetic structure and evolutionary characteristics of the ST592 *K. pneumoniae* clinical strains.

Mobile genetic elements (MGEs), including the ISs, the transposons (Tn), the integrative conjugative elements (ICEs), and the integrons (In), play key roles in the horizontal acquisition of antimicrobial resistance genes in various species or between chromosomes and plasmids (He et al., 2022). The *oriT* region, the relaxase gene, the T4CP gene, and the *tra* gene cluster for the T4SS are important for plasmid transfer. In a previous study, it was shown that pLVPK-like virulence plasmids are non-conjugative owing to the lack of a complete conjugative module comprising *tra* genes, which is consistent with our findings (Yang et al., 2021a). However, in the present study, the bla_{NDM-1}-positive plasmid was transferred to the recipient strain, as evidenced by the fact that it contains complete conjugation elements. This type of plasmid transfer contributes to the generation of CR-hvKp from hvKp, which harbors only one pLVPK-like virulence plasmid. Based on the BLASTN results from the NCBI database, the bla_{NDM-1}-positive plasmid pKPZM16-3 shares high similarity to the pNDM1_LL34 (CP025965.2), pNDM-Cf7308 (CP092465.1), and pNDM-BTR (KF534788.2) plasmids in the *K. pneumoniae*, *C. freundii*, and *E. coli* strains, respectively, suggesting the spread of the resistance plasmid in various bacterial species. This phenomenon further explains the transfer of the bla_{NDM-1}-positive plasmid to CR-hvKp in our study.

Several biomarkers have been used to identify CR-hvKp strains, including the presence of a combination of *rmpA* and/or *rmpA2* with *iucA*, *iroB*, or *peg-344* (Liu et al., 2020; Li et al., 2023). A study by Liu et al. suggested that the apparent changing epidemiology of hvKp is the result of ST11 classic *K. pneumoniae* (cKp) acquiring a virulence-like plasmid to replace the cKp among nosocomial infections (Liu et al., 2020). In China, the ST11 *K. pneumoniae* subclone KL64 is associated with a highly resistant and virulent epidemic, and the expansion of the ST11–KL64 clone is becoming increasingly concerning. This could be caused by multiple factors involved in mutations in antimicrobial resistance, virulence, and

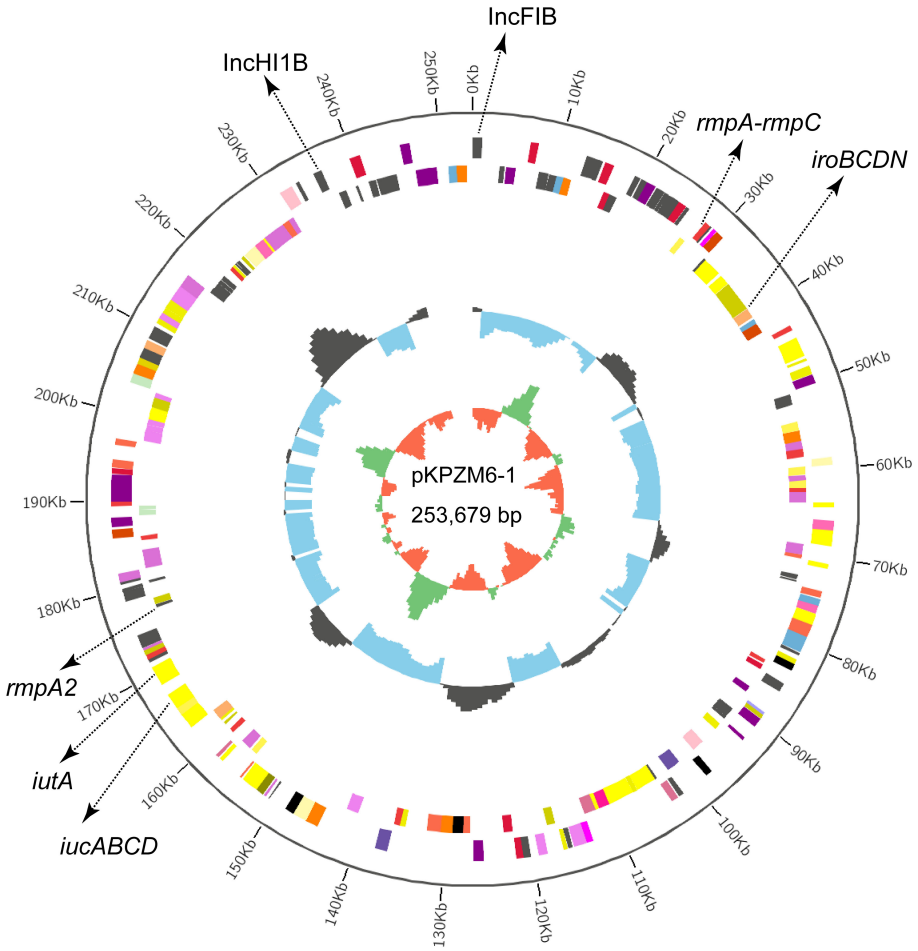

FIGURE 1
Circular map of the pLVPK-like virulence plasmid pKPZM6-1 in KPZM6. The two replicons, *rmpA*, *rmpA2*, and the *iucABCD–iutA* gene cluster are labeled.

metabolism-associated genes (Wang et al., 2024a). Importantly, researchers have shown that the virulence plasmids in the ST11–KL64 clone are derived from a sub-lineage of ST23–KL1 (Wang et al., 2024b). However, some studies have shown that another important clone, ST23, can also transform into CR-hvKp by acquiring a bla_{NDM}-harboring or a bla_{KPC-2}-positive plasmid (Yan et al., 2021; Gu et al., 2025). This would also appear to be the case with the strains analyzed in the present study.

There are some limitations to this study, including the lack of data concerning the virulence level of this strain. This could be

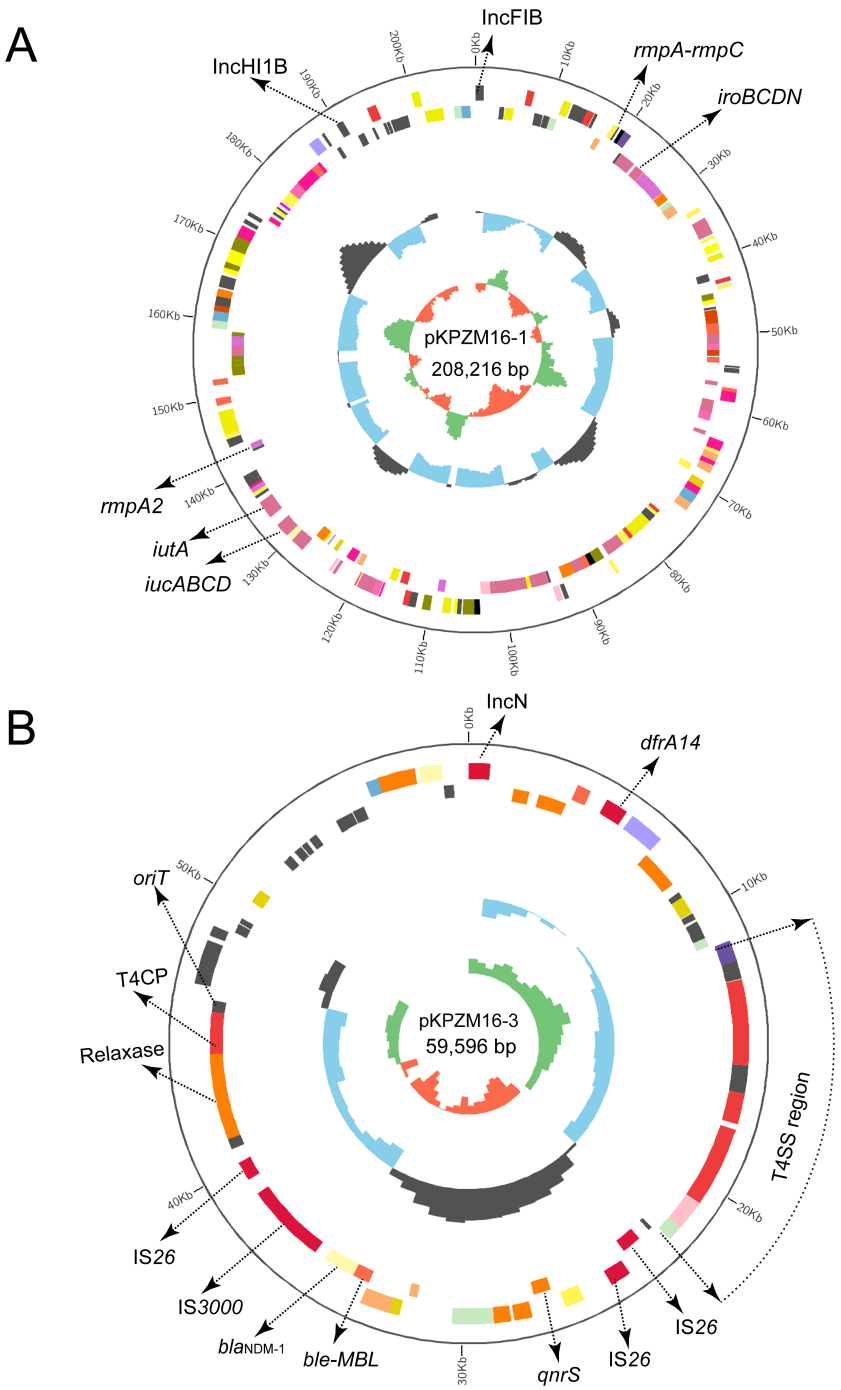

FIGURE 2
Circular map of the pLVPK-like virulence plasmid pKPZM16-1 and the bla_{NDM-1}-positive plasmid pKPZM16-3 in KPZM16. **(A)** Circular map of the pKPZM16-1 plasmid. The two replicons, *rmpA*, *rmpA2*, and the *iucABCD–iutA* gene cluster were labelled. **(B)** Structure of the resistance plasmid pKPZM16-3. The replicon, the insertion sequences (ISs), and the resistance genes are shown. The type IV secretion system (T4SS) region, *oriT*, the type IV coupling protein (T4CP), and the relaxase are further labeled.

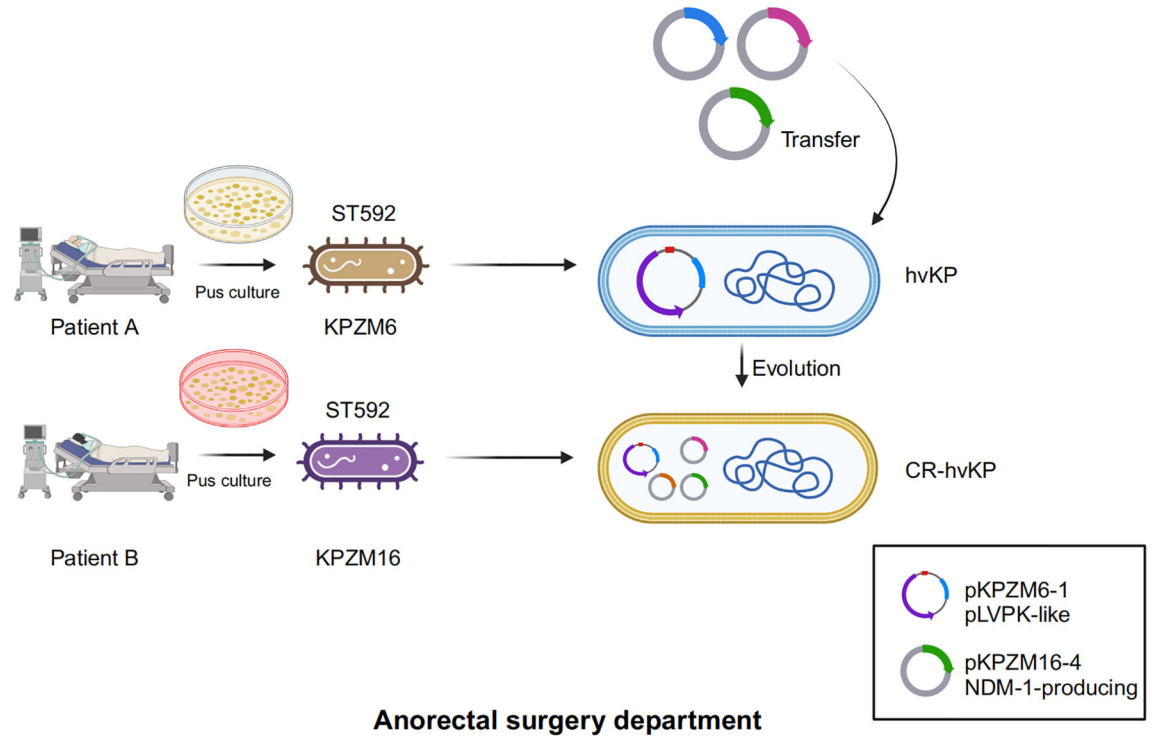

FIGURE 3
Diagram of the possible evolution mechanism of the formation of carbapenem-resistant hypervirulent *K. pneumoniae* (CR-hvKp). KPZM6 and KPZM16 were both collected from pus samples in one department. NDM-1-producing plasmid transfer from the KPZM6 (hvKp) to KPZM16 (CR-hvKp) through conjugation.

assessed using insect larval or murine models. In addition, the plasmid transfer frequency of the NDM-1-positive plasmid could be measured via conjugation. Lastly, we did not obtain direct evidence of the plasmid transfer and evolution into CR-hvKp.

Conclusion

To our knowledge, this is the first study in which the complete genomic characteristics of rare ST592 *K. pneumoniae* clinical

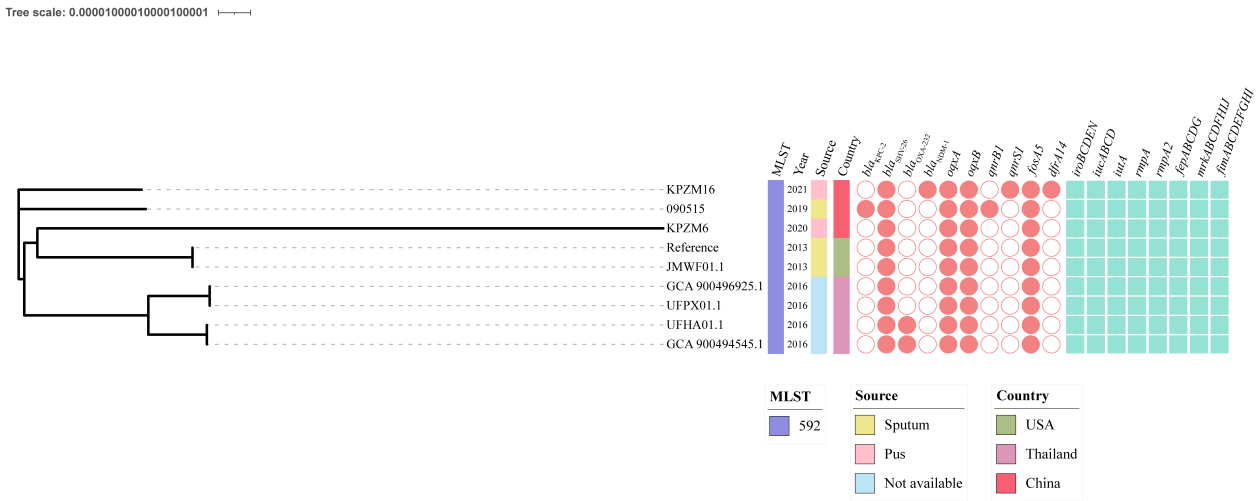

FIGURE 4
Phylogenetic analysis of ST592 *Klebsiella pneumoniae* strains. A phylogenetic tree was built using RaxML v8.2.12 under the GTRGAMMA model. The generated tree file was visualized using iTOL. The ST, sources, countries, collection year, and the resistance and virulence genes are shown.

isolates have been investigated. This study provides a possible evolutionary hypothesis for the formation of CR-hvKp via conjugation. Considering the huge threat posed by CR-hvKp bacteria, which are prevalent in the pus of patients in healthcare settings, early detection and control should be strengthened to avoid the wide dissemination of this high-risk clone.

Data availability statement

Publicly available datasets were analyzed in this study. This data can be found here: Bioproject PRJNA1212823 and PRJNA1213023.

Ethics statement

The studies involving humans were approved by local Ethics Committees of the Hospital with the approval number: IRB-2024-554 (IIT). The studies were conducted in accordance with the local legislation and institutional requirements. The participants provided their written informed consent to participate in this study.

Author contributions

HZ: Writing – original draft, Writing – review & editing. SD: Writing – review & editing. CM: Writing – review & editing. YF: Writing – review & editing. JY: Writing – review & editing.

Funding

The author(s) declare that financial support was received for the research and/or publication of this article. This work was supported by the Shaoxing Health Science and Technology Project, China (2024SKY059).

Conflict of interest

The authors declare that the research was conducted in the absence of any commercial or financial relationships that could be construed as a potential conflict of interest.

Generative AI statement

The author(s) declare that no Generative AI was used in the creation of this manuscript.

Publisher's note

References

Chen, T., Wang, Y., Chi, X., Xiong, L., Lu, P., Wang, X., et al. (2024). Genetic, virulence, and antimicrobial resistance characteristics associated with distinct morphotypes in ST11 carbapenem-resistant Klebsiella pneumoniae. *Virulence* 15, 2349768. doi: 10.1080/21505594.2024.2349768

Gong, Y., Feng, Y., Zong, Z., and Lv, X. (2024). Characterization of a KPC-84 harboring Klebsiella pneumoniae ST11 clinical isolate with ceftazidime-avibactam resistance. *Eur. J. Clin. Microbiol. Infect. Dis.* 43, 2029–2035. doi: 10.1007/s10096-024-04910-y

Gu, D., Dong, N., Zheng, Z., Lin, D., Huang, M., Wang, L., et al. (2018). A fatal outbreak of ST11 carbapenem-resistant hypervirulent Klebsiella pneumoniae in a Chinese hospital: a molecular epidemiological study. *Lancet Infect. Dis.* 18, 37–46. doi: 10.1016/S1473-3099(17)30489-9

Gu, Y., Wang, X., Zhang, W., Weng, R., Shi, Q., Hou, X., et al. (2025). Dissemination of bla(NDM)-harboring plasmids in carbapenem-resistant and hypervirulent Klebsiella pneumoniae. *Microbiol. Spectr.* 13 (3), e0196824. doi: 10.1128/spectrum.01968-24

Hala, S., Antony, C. P., Alshehri, M., Althaqafi, A. O., Alsaedi, A., Mufti, A., et al. (2019). First report of Klebsiella quasipneumoniae harboring bla(KPC-2) in Saudi Arabia. *Antimicrob. Resist. Infect. Control* 8, 203. doi: 10.1186/s13756-019-0653-9

He, J., Du, X., Zeng, X., Moran, R. A., Van Schaik, W., Zou, Q., et al. (2022). Phenotypic and genotypic characterization of a hypervirulent carbapenem-resistant klebsiella pneumoniae ST17-KL38 clinical isolate harboring the carbapenemase IMP-4. *Microbiol. Spectr.* 10, e0213421. doi: 10.1128/spectrum.02134-21

Jin, X., Chen, Q., Shen, F., Jiang, Y., Wu, X., Hua, X., et al. (2021). Resistance evolution of hypervirulent carbapenem-resistant Klebsiella pneumoniae ST11 during treatment with tigecycline and polymyxin. *Emerg. Microbes Infect.* 10, 1129–1136. doi: 10.1080/22221751.2021.1937327

Krzywinski, M., Schein, J., Birol, I., Connors, J., Gascoyne, R., Horsman, D., et al. (2009). Circos: an information aesthetic for comparative genomics. *Genome Res.* 19, 1639–1645. doi: 10.1101/gr.092759.109

Lam, M. M. C., Wick, R. R., Judd, L. M., Holt, K. E., and Wyres, K. L. (2022). Kaptive 2.0: updated capsule and lipopolysaccharide locus typing for the Klebsiella pneumoniae species complex. *Microb. Genom* 8. doi: 10.1099/mgen.0.000800

Lam, M. M. C., Wick, R. R., Watts, S. C., Cerdeira, L. T., Wyres, K. L., and Holt, K. E. (2021). A genomic surveillance framework and genotyping tool for Klebsiella pneumoniae and its related species complex. *Nat. Commun.* 12, 4188. doi: 10.1038/s41467-021-24448-3

Li, L., Li, S., Wei, X., Lu, Z., Qin, X., and Li, M. (2023). Infection with Carbapenem-resistant Hypervirulent Klebsiella Pneumoniae: clinical, virulence and molecular epidemiological characteristics. *Antimicrob. Resist. Infect. Control* 12, 124. doi: 10.1186/s13756-023-01331-y

Li, X., Xie, Y., Liu, M., Tai, C., Sun, J., Deng, Z., et al. (2018). oriTfinder: a web-based tool for the identification of origin of transfers in DNA sequences of bacterial mobile genetic elements. *Nucleic Acids Res.* 46, W229–W234. doi: 10.1093/nar/gky352

Liu, C., Du, P., Xiao, N., Ji, F., Russo, T. A., and Guo, J. (2020). Hypervirulent Klebsiella pneumoniae is emerging as an increasingly prevalent K. pneumoniae pathotype responsible for nosocomial and healthcare-associated infections in Beijing, China. *Virulence* 11, 1215–1224. doi: 10.1080/21505594.2020.1809322

Liu, B., Zheng, D., Zhou, S., Chen, L., and Yang, J. (2022). VFDB 2022: a general classification scheme for bacterial virulence factors. *Nucleic Acids Res.* 50, D912–D917. doi: 10.1093/nar/gkab1107

Qiao, S., Xin, S., Zhu, Y., Zhao, F., Wu, H., Zhang, J., et al. (2024). A large-scale surveillance revealed that KPC variants mediated ceftazidime-avibactam resistance in clinically isolated Klebsiella pneumoniae. *Microbiol. Spectr.* 12, e0025824. doi: 10.1128/spectrum.00258-24

Seemann, T. (2014). Prokka: rapid prokaryotic genome annotation. *Bioinformatics* 30, 2068–2069. doi: 10.1093/bioinformatics/btu153

Shi, Q., Shen, S., Tang, C., Ding, L., Guo, Y., Yang, Y., et al. (2024). Molecular mechanisms responsible KPC-135-mediated resistance to ceftazidime-avibactam in ST11-K47 hypervirulent Klebsiella pneumoniae. *Emerg. Microbes Infect.* 13, 2361007. doi: 10.1080/22221751.2024.2361007

Siguier, P., Perochon, J., Lestrade, L., Mahillon, J., and Chandler, M. (2006). ISfinder: the reference centre for bacterial insertion sequences. *Nucleic Acids Res.* 34, D32–D36. doi: 10.1093/nar/gkj014

Tatusova, T., Dicuccio, M., Badretdin, A., Chetvernin, V., Nawrocki, E. P., Zaslavsky, L., et al. (2016). NCBI prokaryotic genome annotation pipeline. *Nucleic Acids Res.* 44, 6614–6624. doi: 10.1093/nar/gkw569

Tian, D., Liu, X., Chen, W., Zhou, Y., Hu, D., Wang, W., et al. (2022b). Prevalence of hypervirulent and carbapenem-resistant Klebsiella pneumoniae under divergent evolutionary patterns. *Emerg. Microbes Infect.* 11, 1936–1949. doi: 10.1080/22221751.2022.2103454

Tian, C., Xing, M., Zhao, Y., Fan, X., Bai, Y., Fu, L., et al. (2022a). Whole genome sequencing of OXA-232-producing wzi93-KL112-O1 carbapenem-resistant Klebsiella pneumoniae in human bloodstream infection co-harboring chromosomal ISEcp1-based bla (CTX-M-15) and one rmpA2-associated virulence plasmid. *Front. Cell Infect. Microbiol.* 12, 984479. doi: 10.3389/fcimb.2022.984479

Wang, Q., Wang, R., Wang, S., Zhang, A., Duan, Q., Sun, S., et al. (2024a). Expansion and transmission dynamics of high risk carbapenem-resistant Klebsiella pneumoniae subclones in China: An epidemiological, spatial, genomic analysis. *Drug Resist. Update* 74, 101083. doi: 10.1016/j.drup.2024.101083

Wang, R., Zhang, A., Sun, S., Yin, G., Wu, X., Ding, Q., et al. (2024b). Increase in antioxidant capacity associated with the successful subclone of hypervirulent carbapenem-resistant Klebsiella pneumoniae ST11-KL64. *Nat. Commun.* 15, 67. doi: 10.1038/s41467-023-44351-3

Wick, R. R., Judd, L. M., Gorrie, C. L., and Holt, K. E. (2017). Unicycler: Resolving bacterial genome assemblies from short and long sequencing reads. *PloS Comput. Biol.* 13, e1005595. doi: 10.1371/journal.pcbi.1005595

Xu, Y., Zhang, J., Wang, M., Liu, M., Liu, G., Qu, H., et al. (2021). Mobilization of the nonconjugative virulence plasmid from hypervirulent Klebsiella pneumoniae. *Genome Med.* 13, 119. doi: 10.1186/s13073-021-00936-5

Yan, R., Lu, Y., Zhu, Y., Lan, P., Jiang, S., Lu, J., et al. (2021). A Sequence Type 23 Hypervirulent Klebsiella pneumoniae Strain Presenting Carbapenem Resistance by Acquiring an IncP1 bla(KPC-2) Plasmid. *Front. Cell Infect. Microbiol.* 11, 641830. doi: 10.3389/fcimb.2021.641830

Yang, X., Dong, N., Chan, E. W., Zhang, R., and Chen, S. (2021a). Carbapenem resistance-encoding and virulence-encoding conjugative plasmids in klebsiella pneumoniae. *Trends Microbiol.* 29, 65–83. doi: 10.1016/j.tim.2020.04.012

Yang, X., Dong, N., Liu, X., Yang, C., Ye, L., Chan, E. W., et al. (2021b). Co-conjugation of virulence plasmid and KPC plasmid in a clinical klebsiella pneumoniae strain. *Front. Microbiol.* 12, 739461. doi: 10.3389/fmicb.2021.739461

Zhang, X., Xie, Y., Zhang, Y., Lei, T., Zhou, L., Yao, J., et al. (2024). Evolution of ceftazidime-avibactam resistance driven by mutations in double-copy bla(KPC-2) to bla(KPC-189) during treatment of ST11 carbapenem-resistant Klebsiella pneumoniae. *mSystems* 9, e0072224. doi: 10.1128/msystems.00722-24

Zhang, D. F., Zhang, Z. F., Li, P. D., and Qu, P. H. (2022). Characterization of carbapenem-resistant Acinetobacter baumannii ST540 and Klebsiella pneumoniae ST2237 isolates in a pneumonia case from China. *J. Appl. Microbiol.* 133, 1434–1445. doi: 10.1111/jam.15648

Zhou, K., Xiao, T., David, S., Wang, Q., Zhou, Y., Guo, L., et al. (2020). Novel subclone of carbapenem-resistant klebsiella pneumoniae sequence type 11 with enhanced virulence and transmissibility, China. *Emerg. Infect. Dis.* 26, 289–297. doi: 10.3201/eid2602.190594

Zhou, K., Xue, C. X., Xu, T., Shen, P., Wei, S., Wyres, K. L., et al. (2023). A point mutation in recC associated with subclonal replacement of carbapenem-resistant Klebsiella pneumoniae ST11 in China. *Nat. Commun.* 14, 2464. doi: 10.1038/s41467-023-38061-z

frontiers | Frontiers in Cellular and Infection Microbiology

TYPE Original Research
PUBLISHED 07 April 2025
DOI 10.3389/fcimb.2025.1553591

OPEN ACCESS

EDITED BY
Mattia Pirolo,
University of Copenhagen, Denmark

REVIEWED BY
Elias Eger,
Helmholtz Institute for One Health, Germany
Stacy Julisa Carrasco Aliaga,
University of Milan, Italy

*CORRESPONDENCE
Xinling Pan
panfengyuwuzu@163.com

†These authors have contributed equally to this work

RECEIVED 31 December 2024
ACCEPTED 13 March 2025
PUBLISHED 07 April 2025

CITATION
Zhao J, Shen X, Jin L, Ji S and Pan X (2025) Resistance phenotypes and genomic features of *Mycobacterium seoulense* isolates. *Front. Cell. Infect. Microbiol.* 15:1553591. doi: 10.3389/fcimb.2025.1553591

Resistance phenotypes and genomic features of *Mycobacterium seoulense* isolates

Jin Zhao†, Xinli Shen†, Lulu Jin, Songjun Ji and Xinling Pan*

Department of Biomedical Sciences Laboratory, Affiliated Dongyang Hospital of Wenzhou Medical University, Dongyang, Zhejiang, China

Background: *Mycobacterium seoulense* (*M. seoulense*) is an emerging pathogen increasingly associated with infections; however, its resistance phenotypes and genomic characteristics remain largely unknown.

Methods: Seven *M. seoulense* isolates were collected from clinical samples. Drug susceptibility testing was conducted using Sensititre™ SLOMYCO2 susceptibility plates. Whole genome sequencing and supporting bioinformatics analyses were performed to analyze the genomic features.

Results: All *M. seoulense* isolates (n=7) exhibited growth on 7H10 agar medium containing thiophenecarboxylic acid hydrazide or p-Nitrobenzoic acid, with marked diversity in growth rates in liquid culture. All strains exhibited high minimum inhibitor concentrations (MICs) for minocycline (>8 μg/mL), doxycycline (>8 μg/mL), and amikacin (16-32 μg/mL). The MICs for linezolid, rifabutin, moxifloxacin, ciprofloxacin, streptomycin, clarithromycin, and rifampicin varied among the isolates. High levels of genomic diversity were noted among these strains concerning genome-called single nucleotide polymorphisms and average nucleotide identity. In total, 4,282 genes were shared across all genomes, while 315 unique genes were restricted to one strain. Comparative genomic analysis identified two unique virulence genes encoding a catalase enzyme and a protein involved in capsule biosynthesis and transport. Additionally, all *M. seoulense* strains demonstrated the ability to survive within macrophages.

Conclusion: The clinical *M. seoulense* isolates analyzed in this study exhibited varying levels of antibiotic susceptibility, suggesting the potential need for susceptibility testing to guide clinical treatment. Genomic features of these isolates indicated that they are likely pathogenic non-tuberculous mycobacterium, highlighting a need for closer epidemiological monitoring.

KEYWORDS

***M. seoulense*, whole genome sequencing, virulence factor, drug susceptibility, intracellular survival**

Introduction

Most non-tuberculous mycobacteria (NTM) are widely distributed in the environment, including dust and water sources. Although typically nonpathogenic, they can cause infections in immunocompetent individuals, resulting in pulmonary, soft tissue, and lymphatic infections (Nguyen et al., 2024; Sun et al., 2024). Among immunosuppressed patients, NTM can also cause disseminated infections (Kitazawa et al., 2024; Nithirungruang et al., 2024), posing an immense therapeutic challenge to those with preexisting diseases. With the rapid development of molecular detecting techniques, over 200 species of NTM have been identified to date (https://lpsn.dsmz.de/genus/mycobacterium) (Armstrong et al., 2023), many of which have been implicated in clinical infections. Several treatment guidelines have been proposed for NTM infections (Haworth et al., 2017; Kurz et al., 2020), but there remains limited evidence regarding the most appropriate therapeutic regimens when combatting infections caused by less common NTM species (Lange et al., 2022). Therefore, phenotypic and genomic investigations are warranted for those novel NTM species with rising clinical prevalence (Zhang et al., 2013).

Mycobacterium seoulense (*M. seoulense*), which was first reported in Korea in 2007 (Mun et al., 2007), has also been found to cause pulmonary infection in Japan and China (Zhao et al., 2022; Nakamoto et al., 2024). Four cases of *M. seoulense* infection were identified in our previous study through radiological examination. However, anti-mycobacterial treatment was not initiated due to limited clinical experience, a lack of public data on *M seoulense* infections, and patients' reluctance to receive antibiotic therapy. Only the case from Japan received antibiotic therapy, and had a optimal outcome. While the growth features and biochemical features of this NTM have been reported (Mun et al., 2007), the resistance phenotype for *M. seoulense* remains unknown. Like most NTM, the addition of thiophene carboxylic acid hydrazide (TCH) and p-nitrobenzoic acid (PNB) to the culture medium has no impact on the growth of *M. seoulense*, potentially providing a means of differentiating it from *M. nebraskense*, a biochemically similar species. Although two genomes for *M. seoulense* are available (https://www.ncbi.nlm.nih.gov/datasets/genome/?taxon=386911), no genomic analysis has been conducted, leaving some uncertainty regarding the relevant virulence factors and core genes for this species. Therefore, in this study, seven strains isolated from clinical samples in our hospital were sequenced, and drug susceptibility test was performed to provide clinicians with insights to help guide the management of patients infected by *M. seoulense*.

Abbreviations: MTB, Mycobacterium tuberculosis; NTM, non-tuberculous mycobacterium; MIC, minimum inhabitation concentration; SNP, single nucleotide polymorphism; CDS, coding sequence; CFU, colony forming units; TCH, thiophene carboxylic acid hydrazide; PNB, p-Nitrobenzoic acid.

Methods

Bacterial culture

Strains were recovered from -80°C by subculturing them in Middlebrook 7H9 broth medium (BD Bioscience, USA) containing 10% ADC broth enrichment medium (Shanghai Yiyan Bio-technology Co. Ltd, Shanghai, China) and 0.05% Tween-80. Isolates were incubated at 37°C until reaching an optical density at 600 nm (OD600) of 0.6-1.0 as measured with an Implen (Germany) instrument. A shaking culture was then performed at 37°C and 250 rpm, and growth curves were obtained by testing the OD600 every three days before day 21 and every six days after day 21. In addition, the medium was imaged after an 18-day incubation.

To assess the morphology of these isolates on the Middlebrook 7H10 agar medium, cultures with an OD600 between 0.6 and 1.0 were diluted to an OD600 of 0.02 using a complete 7H9 medium, and 5 µL of the culture was spotted onto a 7H10 complete agar plate supplemented with 10% glycerol. The 7H10 agar plates were supplemented with 5 µg/mL of TCH or 500 µg/mL of PNB. The plates were incubated in an incubator at 37°C and imaged until the colonies had formed after 21 days.

Drug susceptibility test

Bacterial cultures with an OD600 between 0.6 and 1.0 were obtained as described above, followed by dilution with phosphate-buffered saline (PBS) to a final OD600 of 0.2 (about 0.5 McFarland) (Penuelas-Urquides et al., 2013). The bacterial suspension was then diluted 100-fold using Mueller-Hinton medium, and 100 µL was transferred into the Sensititre™ SLOMYCO2 drug susceptibility test plates (Thermo Fisher, USA). These plates were sealed with parafilm and cultured in an incubator at 37°C. Readings were taken after 7 days, with the minimum inhibitory concentration defined as the lowest drug concentration at which no visible bacterial sediment was observed at the bottom of the well. Two replicate wells were established for this drug susceptibility assay. *M. intracellulare* ATCC 13950 was used as the reference strain.

Genomic DNA extraction and next-generation sequencing

Bacteria in the early exponential phase were harvested via centrifugation, and cell pellets were used to extract genomic DNA based on the provided instructions (Tiangen, Beijing, China). High-quality DNA was used to prepare a library with a NEXTFLEX Rapid DNA-Seq Kit (Revvity, MA, USA). Sequencing was performed on a NovaSeq™ X Plus (Illumina, CA, USA), and raw data was analyzed to remove low-quality reads using the fastp software (Chen et al., 2018). The high-quality reads were assembled with Unicycler software (Wick et al., 2017), and the sequences were uploaded to

the NCBI database (PRJNA1196008). Genes were annotated using Prokka (Seemann, 2014), and pan-genome analyses were conducted using Roary (Page et al., 2015).

Genomic analysis of the assembled sequences

M. seoulense strain JCM16018 was the reference genome (Accession No: GCA_010731595.1) for calling core single nucleotide polymorphisms (coreSNPs) of clinical isolates using the Snippy software as described previously (Seemann, 2015). Following the removal of SNPs in recombinant regions using Gubbins (Croucher et al., 2015), the coreSNP distribution matrix was used to construct a Phylogenic tree with IQ-TREE (Nguyen et al., 2015). Genomic alignment was performed via BLAST and visualized in the form of rings with BRIG (Alikhan et al., 2011). The identity percentages between any two strains were evaluated based on average nucleotide identity (ANI) (Yoon et al., 2017).

Third-generation sequencing

Genomic DNA was fragmented into sequences ~10 kb in length, after which an SMRT Bell library was constructed with an SMRT Bell Prep Kit 3.0 (Pacific Biosciences, CA). The raw data was sequenced using the PacBio Sequel IIe sequencing platform. Genomic assembly was performed with the Unicycler software, and the results were uploaded to the NCBI database (PRJNA1195676). The whole genome was aligned to the JCM16018 strain, and the arranged genomes were analyzed using Mauve (Darling et al., 2004).

Analyses of intracellular survival in macrophages

THP-1 cells were purchased from the China Center for Type Culture Collection (Shanghai, China) and cultured in RPMI 1640 medium (Gibco, USA) containing 10% fetal bovine serum (Vivacell, China). Cells were seeded into 24-well plates (1 x 10^5/well) and differentiated into macrophages via treatment for 24 h with 60 ng/mL phorbol 12-myristate 13-acetate. Bacterial cultures with an OD600 between 0.6 and 1.0 were harvested by centrifugation (2,000 rpm, 5 min). After washing thrice with PBS, the bacterial pellet was resuspended as a single-cell suspension in RPMI 1640 medium via repeated pipetting. The concentration was adjusted into an OD600 of 0.6 (equivalent to 1×10^8/mL) and co-cultured with the macrophage at a multiplicity of infection of 10. After three hours of incubation, the extracellular bacteria were washed away twice with PBS and killed by adding 30 μg/mL gentamycin for one hour. The infected cells were incubated in a complete RPMI 1640 medium supplemented with 5 μg/mL gentamycin in a 37°C 5% CO_2 incubator. After incubation for 24 h, the cells were lysed with sterile deionized water and serially diluted with PBS. The diluted lysed cell solutions were spread on the 7H10 agar medium plates with 10% glycerol. After incubation for 20 days, the colony-forming units (CFUs) on these plates were counted. The survival rate was calculated as the ratio of CFU obtained after infection for 24 h to the initial CFU obtained after infection. This experiment was repeated three times.

Statistical analysis

The survival rates of *M. seoulense* within macrophages were compared to that of *M. intracellulare* ATCC13950 strain using a *t*-test in GraphPad Prism (version 9.3.1). Statistical significance was defined as *, $P<0.05$; **, $P<0.01$.

Results

Biological features of *M. seoulense* in culture

A total of seven *M. seoulense* strains were isolated from six patients (Supplementary Table 1), including four previously described cases. The two additional cases in this study had *M. seoulense* in their bronchoalveolar lavage fluid specimens. In the 7H9 broth medium, these clinical isolates exhibited different growth rates (Figure 1A). Specifically, the 16NTM017 and 20NTM121 isolates grew more rapidly than the 23NTM055 and 21NTM074 isolates, with these four strains entering the stationary phase after about 21 days, similar to *M. intracellulare* ATCC 13950. The 20NTM058, 20NTM062, and 22NTM124 strains grew gradually and entered the stationary phase until 40 days. The color of the liquid culture medium for all *M. seoulense* isolates was brown-yellow, while that for *M. intracellular* was opalescent (Figure 1B).

On solid medium, all isolates were able to grow on the 7H10 complete medium with or without TCH or PNB (Figure 1C). However, the clones grown on PNB were white, whereas those grown on other mediums were yellow. Moreover, strains 16NTM017 and 20NTM121 exhibited a darker color compared to other strains.

Drug susceptibility test of *M. seoulense* isolates

All *M. seoulense* strains exhibited high MICs for Amikacin, ranging from 16-32 μg/mL (Table 1). For doxycycline and minocycline, all the strains exhibited MIC levels higher than the upper limit of detection. These clinical isolates presented varying levels of susceptibility to moxifloxacin, ciprofloxacin, streptomycin, and clarithromycin, as indicated by at least four MICs for these seven strains.

10.3389/fcimb.2025.1553591

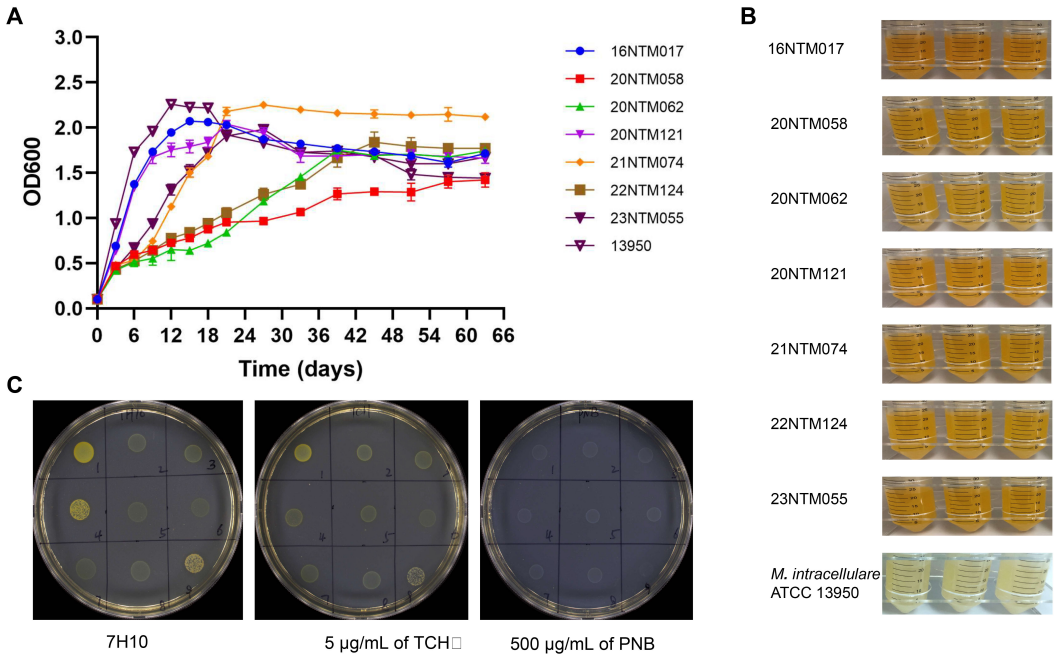

FIGURE 1
The growth features of *Mycobacterium seoulense* in culture medium. **(A)** The growth curve in the 7H9 Middlebrook medium with 10% ADC and 0.05% Tween 80; **(B)** The color of 7H9 medium liquid medium; **(C)** The morphology of *Mycobacterium seoulense* on the 7H10 agar medium with 10% glycerol. 1, 16NTM017; 2, 20NTM058; 3, 20NTM062; 4, 20NTM121; 5, 21NTM074; 6, 21NTM160 (*M. colombiense*); 7, 22NTM124; 8, 23NTM055; 9, ATCC13950.

Phylogenetic analyses of *M. seoulense* isolates

Based on the coreSNPs detected in individual strains, an established phylogenetic tree revealed the clustering of the JCM16017 and DSM 44998 strains (Figure 2A), with an average nucleotide identity of 99.99% (Supplementary Figure 1). The two strains derived from the same case (20NTM062 and 20NTM058) were also clustered with ANI of 99.98%. Two strains that were isolated from different cases were close to each other in the phylogenetic tree. The differing SNP distributions among the analyzed strains provided support for the phylogenetic tree results (Figure 2B). For the clustered strains, the strains derived from the same case exhibited eight coreSNPs that differed from one another, while those from different cases exhibited 181-1643 differing coreSNPs. In addition, 22NTM124 and 23NTM055 were distant from the other strains (Figure 2A), with approximately 50,000 coreSNPs differing from the other strains (Figure 2B). The diversity of coreSNPs was similar to the ANI distributions between any two strains (Supplementary Figure 1).

TABLE 1 Distribution of MICs for *M. seoulense* strains.

Strain name	MIC (μg/mL)										
	DOX	LZD	RFB	AMI	MXF	CFZ	CIP	STR	CLA	MIN	RIF
16NTM017	>8	4	4	16	0.25	1	1	2	0.25	>8	1
20NTM058	>8	8	0.25	16	2	0.5	>8	16	0.5	>8	2
20NTM062	>8	32	1	32	4	1	>8	>32	2	>8	4
20NTM121	>8	16	>4	16	2	1	>8	16	1	>8	0.25
21NTM074	>8	16	0.12	16	1	1	8	16	2	>8	0.25
22NTM124	>8	16	0.5	16	1	1	4	8	1	>8	2
23NTM055	>8	16	0.25	32	1	1	4	8	2	>8	2
ATCC13950	>8	8	0.25	4	1	1	2	4	1	4	0.25

DOX, doxycycline; LZD, linezolid; RFB, rifabutin; AMI, amikacin; MXF, moxifloxacin; CFZ, clofazimine; CIP, ciprofloxacin; STR, streptomycin; CLA, clarithromycin; MIN, minocycline; RIF, rifampicin.

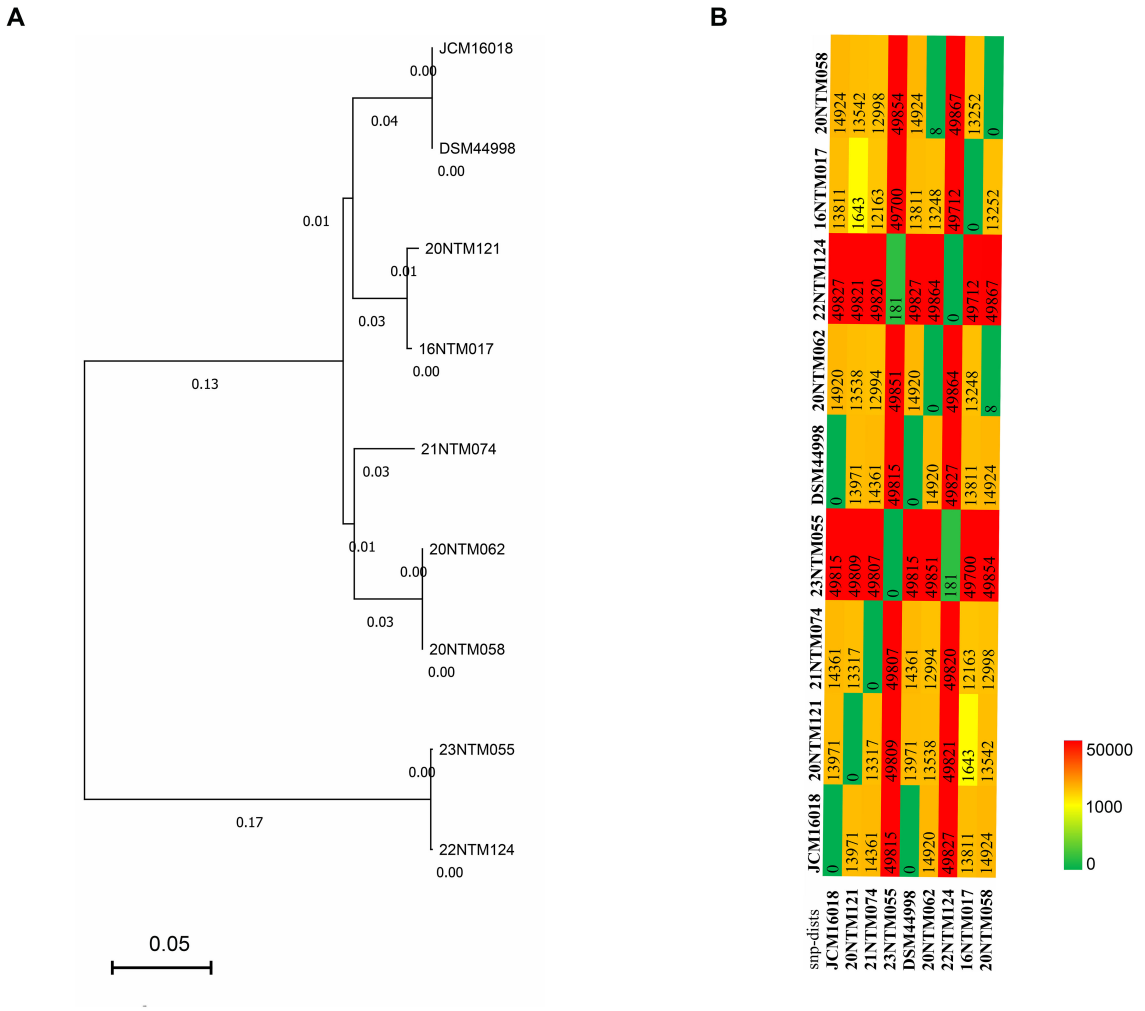

FIGURE 2
The phylogenetic analysis of *Mycobacterium seoulense* strains. **(A)** phylogenetic tree based on the coreSNPs; **(B)** distribution matrix of coreSNPs among *Mycobacterium seoulense* strains.

Pan-genome analyses of *M. seoulense* isolates

In order to establish the core genes of *M. seoulense*, nine isolates, including our clinical isolates and reference strains, were subjected to alignment and pan-genome analyses. Relative to the 16NTM017 strain, diversity hot spots were observed across the genome, including from 1965.5-2391 kb and 3600-3700 kb (Figure 3A). These regions exhibited a higher percentage of GC content than other regions. For the genes in these strains, 4,282 conserved genes were present in all genomes, while 315 unique genes were present in a single strain (Figure 3B, Supplementary Table 2). There were 552 genes associated with lipid transport and metabolism, accounting for 15.4% of the 3,595 genes with available COG annotation. This category was associated with the most diversity in terms of the number of related genes among these clinical isolates, while the numbers of genes associated with "cell motility", "extracellular structure", and "intracellular trafficking, secretion, and vesicular transport" were largely conserved (Figure 3C).

Genomic analyses of *M. seoulense*

In order to comprehensively analyze the genomic features of 16NTM017, assembled genomic data was obtained via third-generation sequencing. Relative to strain JCM16018, 16NTM017 exhibited an ANI of 99.03% (Figure 4A), with several long insertion sequences and one rearranged region in the genome (Figure 4B). The longest inserted sequence corresponded to position 1965.5 kb to 2391 kb, encoding 434 CDS.

Virulence factors in *M. seoulense*

When compared with three reference strains (*Mycobacterium tuberculosis*, *Mycobacterium bovis BCG* strain, and *Mycobacterium avium* complex (MAC)), the reference *M. seoulense* strain and our clinical isolates exhibited a range of common virulence factors (Figure 5). Specifically, the *M. seoulense* strains were found to harbor two unique genes encoding a catalase enzyme and a

10.3389/fcimb.2025.1553591

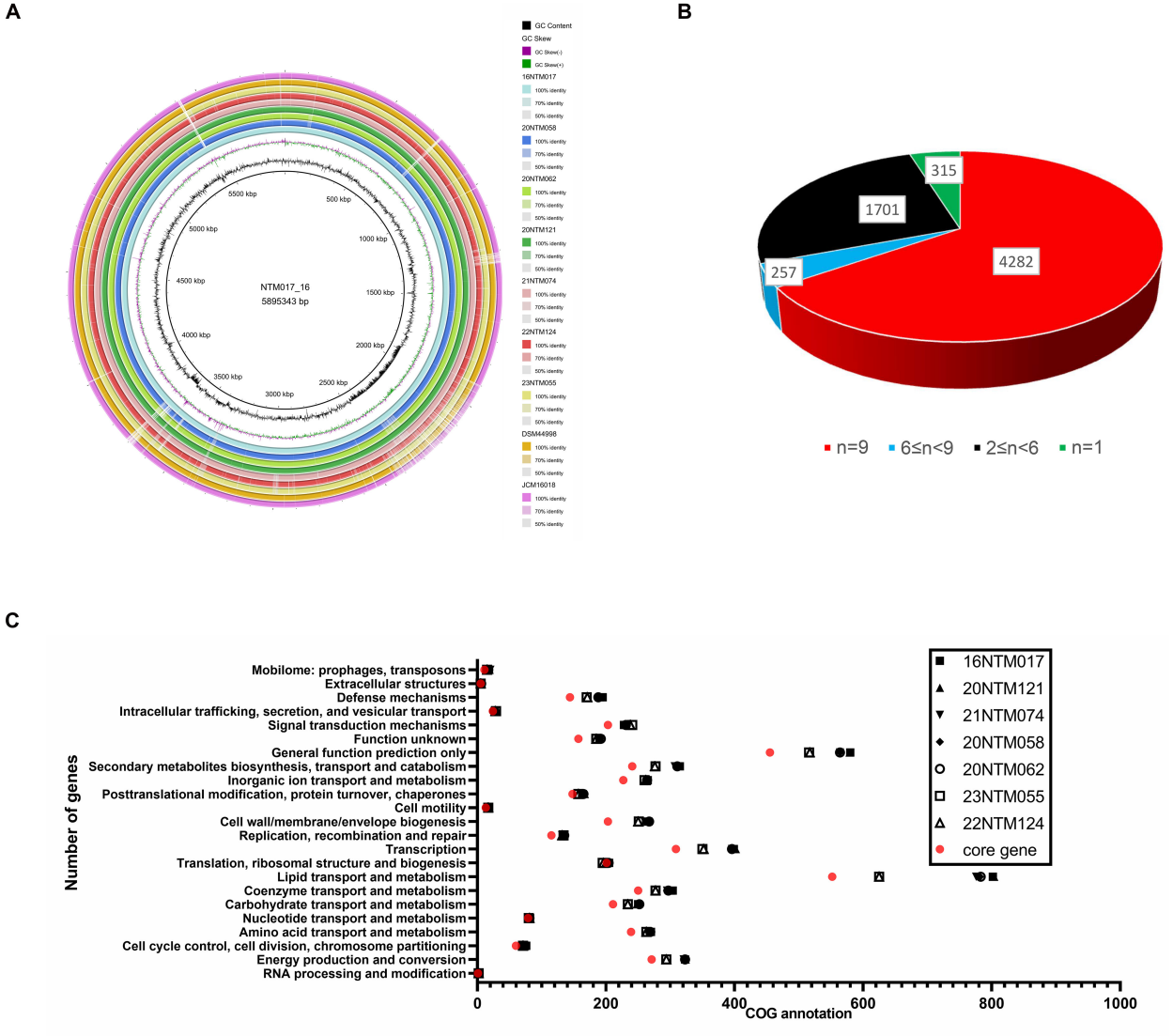

FIGURE 3
The pan-genome analysis of *Mycobacterium seoulense* strains. **(A)** Genomic alignment by circular ring; **(B)** A summary of genes in the pan-genome analysis; **(C)** The number of genes with COG annotation of genes in the pan-genome analysis.

protein involved in capsule biosynthesis and transport. In addition, the *M. seoulense* strains were found to lack *rmlA*, *mbtL*, *fad23*, and *eis*, which are associated with the GPL locus, a trehalose-recycling ABC transporter, mycobactin, and the enhanced intracellular survival protein. The distribution of several genes also varied among clinical isolates (Supplementary Table 3).

Analyses of intracellular survival in macrophages

The *M. intraellulare* reference strain ATCC13950 exhibited a survival rate of ~60% in macrophages for 24 h (Figure 6). Relative to *M. intracellulare*, the clinical *M. seoulense* isolates demonstrated enhanced intracellular survival in macrophages, albeit with variations among these strains.

Discussion

In this study, whole genome sequencing was performed to characterize this novel mycobacterial species and to identify virulence factors related to pathogenicity. These efforts provided an opportunity to analyze the genomic features of clinical *M. seoulense* isolates. Compared to the commonly isolated NTM species, such as the *Mycobacterium avium* complex, *M. seoulense* strains exhibited a yellow pigmentation in culture, indicating carotenoid production (Robledo et al., 2011; Tran et al., 2020). In mycobacteria, the carotenoid production is used mainly for taxonomic identification. However, in other bacterial species, carotenoids possess antioxidant, anti-inflammatory, anti-cancer, and antimicrobial properties (Tran et al., 2020). Although most NTM can be isolated from living environments and medical devices, *M. seoulense* has not been reported in the soil or water (Abbas et al., 2024; Zhang et al., 2024).

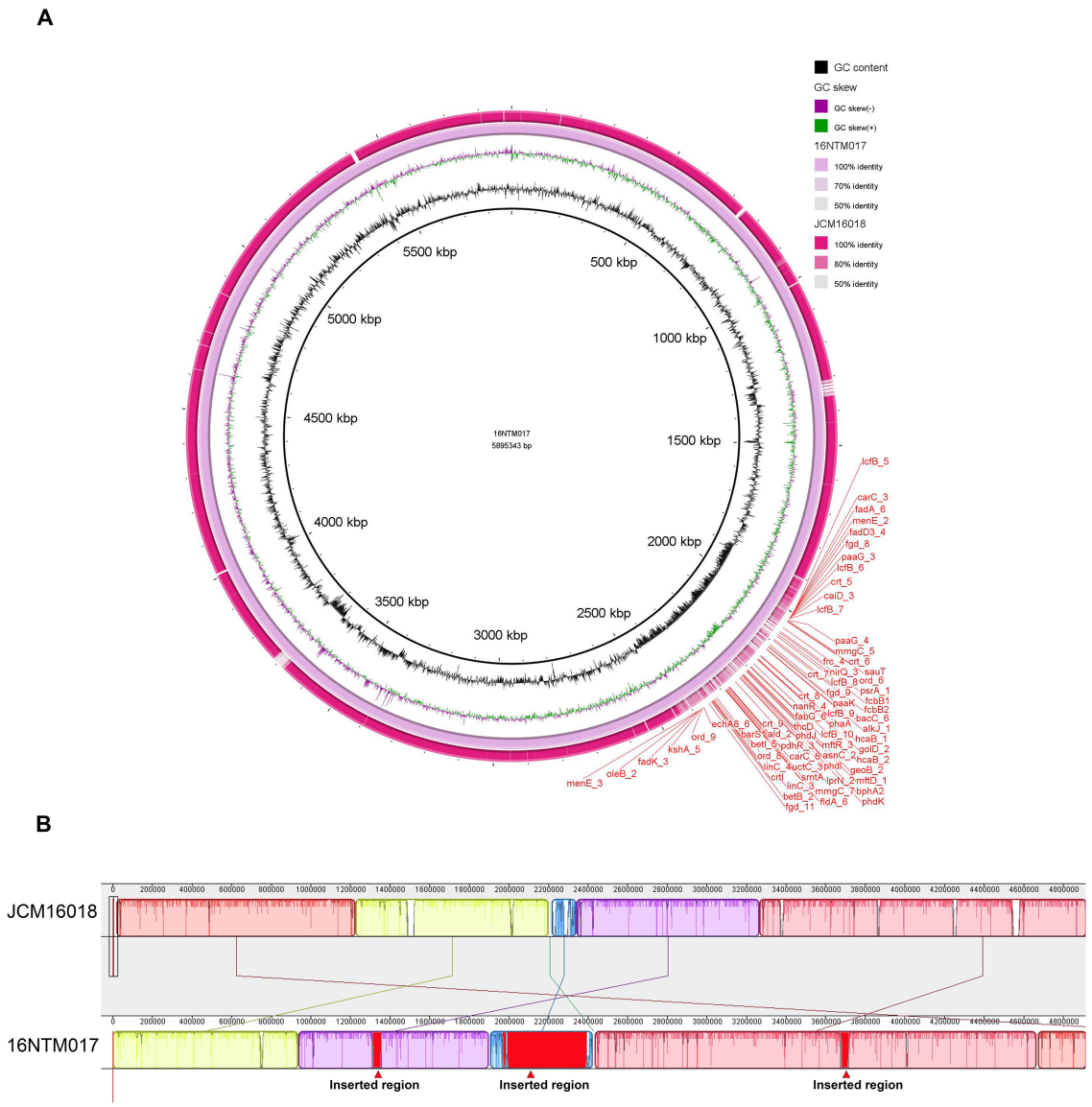

FIGURE 4
The genomic alignment of 16NTM017 and JCM16018 based on the assembled whole genome sequence. **(A)** The global view of genomic alignment; **(B)** the rearrangement of genomic regions between the aligned genomes. The red regions indicated for inserted regions in 16NTM017 comparing to JCM16018.

One explanation is that it was overlooked in epidemiological studies, as *M. seoulense* infections tend to be less common in clinical practice relative to other NTM species (Zhao et al., 2022; Nakamoto et al., 2024). Owing to the absence of data regarding the recommended threshold of SNPs in defining clonal transmission in this species, evidence of transmission between these cases could not be obtained based on the available epidemiological data. Based on the SNPs that differed between the strains isolated from the same patient (8 SNPs), the genomic diversity among clonal *M. seoulense* strains may be greater than for other species belonging to the MAC (Namkoong et al., 2021; Wetzstein et al., 2024). Different drug susceptibility phenotypes for several antibiotic agents were indicated for high heterogeneity of these two strains. Interestingly, two *M. seoulense* strains with available genomes (DSMD44998 and JCM16018) shared highly similar genomes despite their submission by different individuals. Moreover, their identity percentages were higher than those from the same case in this study, indicating the possibility of a common source. This finding warrants further study, as these microbes were isolated from different countries, potentially indicating interregional transmission. Unfortunately, the possible epidemiological connections for these two strains could not be established based on the information submitted to the database.

The MICs for *M. seoulense* were first reported in this study, but the resistance phenotypes could not be established owing to limited data on these MICs and recommended breakpoints (Brown-Elliott and Woods, 2019). Based on its growth feature, *M. seoulense* is classified as a slow NTM (Mun et al., 2007). When using the breakpoints for slow-growth NTM species other than for MAC or

10.3389/fcimb.2025.1553591

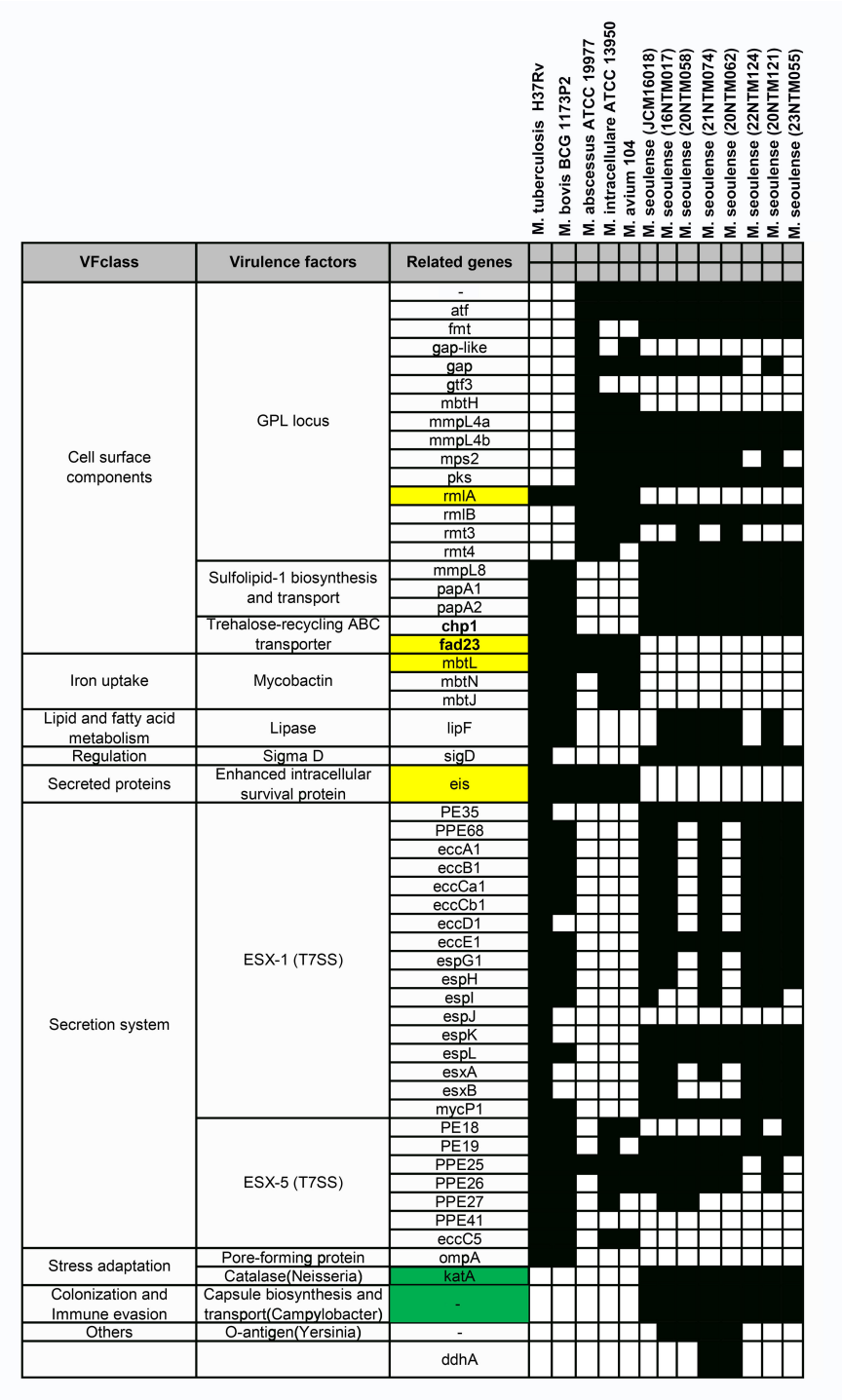

FIGURE 5
The virulence factor-related genes for *Mycobacterium seoulense*. The genes with yellow background were specifically absent in *Mycobacterium seoulense* strains comparing to other mycobacterial species; The genes with green background were uniquely present in the *Mycobacterium seoulense* strains comparing to other mycobacterial species.

M. kansasii used in a previous study (Liu et al., 2021), *M. seoulense* strains could be not efficiently inhibited by doxycycline, minocycline, or ciprofloxacin. Based on susceptibility results, a multi-drug regimen containing clofazimine or clarithromycin in combination with rifampicin and moxifloxacin may be effective for *M. seoulense* infections, offering a potential alternative drug regimen in clinical practice (Nakamoto et al., 2024). In cases of suboptimal treatment response, drug susceptibility test for rifampicin and clarithromycin may be necessary, as the MICs vary among isolates. However, further research is required to

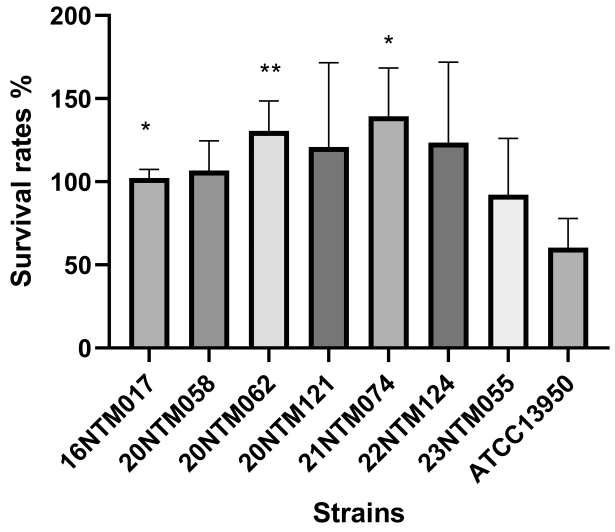

FIGURE 6
The intracellular survival of *Mycobacterium seoulense* strains within the macrophage. The survival rate was defined as the ratio of CFU after 24 hours infection to CFU at the time of infection. *, P<0.05; **, P<0.01.

establish resistance breakpoints, evaluate the efficacy of different drug regimens in clinical settings, and assess treatment outcomes for *M. seoulense* infections (Huh et al., 2019; Kwon et al., 2019).

There was substantial diversity among the analyzed *M. seoulense* genomes in this study based on identity and annotated genes. Despite two strains isolated from the same region, a higher level of diversity was noted among strains. Pan-genomic analyses allowed us to focus on conserved genes in molecular diagnosis and pathogenicity investigations while assessing accessory genes helps to study intra-species diversity (Zekic et al., 2018; Zakham et al., 2021). Further research revealed that the diversity among these clinical strains was related to the number of genes, especially for those annotated in the category "lipid transport and metabolism". Variations in lipid metabolism-related genes among clinical isolates are also observed in different lineages of *Mycobacterium tuberculosis*, contributing to differences in virulence and transmissibility (O'Neill et al., 2015; Moopanar and Mvubu, 2020). In addition, pathogenic mycobacteria exhibit a contraction in genes related to lipid and secondary metabolite biosynthesis and metabolism (Zhu et al., 2023). Given that lipids are a critical source of energy supporting bacterial survival under nutrient-limiting conditions, the diversity of lipid-related genes may play a significant role in mycobacterial virulence and could have implications for drug development (Bailo et al., 2015). The inconsistent number of transport-associated genes may have contributed to the diverse pathogenicity in the cell infection model and the varying levels of drug resistance (Samuels et al., 2022). In contrast, the genes associated with nucleotide transport and metabolism were more conserved than those related to carbohydrate, amino acid, and lipid transport and metabolism. However, further investigation will be necessary owing to the limited data on the genomic analyses of metabolic activity for NTM (Karmakar and Sur, 2024).

The distribution of virulence factor-related genes in *M. seoulense* may provide insight into the mechanisms that may be responsible for infection, helping to guide the selection of molecular targets for drug design efforts. Mycobactin is important for supporting mycobacterial survival under iron-stress conditions in host macrophages through siderophore formation (Luo et al., 2005; Shyam et al., 2021; Shankar and Akhter, 2024). There are 14 genes in the *mbt* gene clusters that are involved in the biosynthesis of mycobactin, with three of these genes (*mbtL*, *mbtN*, and *mbtJ*) being absent in the *M. seoulense* strains relative to the MTB reference strain (H37Rv). The synthesis of the core mycobactin scaffold is mediated by enzymes encoded by *mbt* A-J, while the transfer of the lipophilic aliphatic chain to the ε-amino group of the lysine fragment is facilitated by enzymes encoded by *mbt*K-N, resulting in the potential loss of function of mycobactin in *M. seoulense* (Shyam et al., 2021). In addition, *faD33* (*mbtM*) was absent in *M. seoulense*, resulting in the absence of inhibitory effects by the antituberculosis agents (C16-AMS nucleoside) targeting *mbtM* (Guillet et al., 2016; Shyam et al., 2021). Moreover, *pks2* and *fad23* were absent in *M. seoulense*, which would impair the biosynthesis of Sulfolipid-1 (Yan et al., 2023). This protein can restrict the intracellular survival of MTB in human macrophages in a species-specific manner (Gilmore et al., 2012), and it can also serve as a nociceptive molecule that activates nociceptive neurons and induces coughing in infected animal models (Ruhl et al., 2020). The *rmlA* gene, which was not detected in the genome of *M. seoulense*, has been identified as a virulence factor enhancing the intracellular growth of MTB (Sassetti et al., 2003) and may be a target for antituberculosis agents (Xiao et al., 2021). Eis, a secreted protein not present in *M. seoulense* but present in other mycobacterial species, suppresses host innate immune defenses by modulating autophagy, inflammation, and cell death in a redox-dependent manner (Shin et al., 2010). *M. seoulense* strains lacking certain genes mentioned above were able to survive within macrophages, other virulence factors may have played a compensatory role in enhancing intracellular survival, such as those associated with the ESX-1 secretion system (Guo et al., 2021; Bo et al., 2023). Notably, *katA* is uniquely present in *M. seoulense*, while *KatG* is conserved across all the mycobacterial species (Supplementary Table 3). Both *katA* and *katG* encode catalase enzymes that are essential for detoxifying antimicrobial hydrogen peroxide (Stacy et al., 2014; Santander et al., 2018), with *katG* also contributing to isoniazid resistance (Ofori-Anyinam et al., 2024).

This study has several limitations. While certain virulence factor-encoding genes were uniquely detected or absent in the genomes of these *M. seoulense* strains, their precise roles in intracellular survival and pathogenicity remain unclear. The current *in vitro* macrophage infection data serve as an initial reference, but future studies utilizing gene-editing techniques will be necessary to elucidate their functional significance. Additionally, information regarding possible interactions between cases could not be obtained owing to the prolonged period over which these clinical isolates were obtained, although their living addresses were not geographically linked. Furthermore, clinical follow-up after species identification was not conducted, resulting in missing data on patient prognosis following *M. seoulense* infection.

Conclusion

Based on the MICs measured, *M. seoulense* strains can be efficiently inhibited by rifampicin, rifabutin, linezolid, and clarithromycin but not by doxycycline, minocycline, or ciprofloxacin. Pan-genomic analyses revealed the core genes across all the strains, and the distribution of virulence factor-related genes differed from those of other common NTM species. Our findings may not only help clinicians select appropriate drug therapies for *M. seoulense*-related infections but may also provide possible targets for studies of the mechanisms underlying the pathogenicity of these mycobacteria.

Data availability statement

All the genomic sequences could be accessible from NCBI data with No. PRJNA1196008 and No. PRJNA1195676.

Ethics statement

All the enrolled cases gave written consent to provide the strains and clinical information in an anonymous format at their admission to the hospital. This study was conducted according to the guidelines of the Declaration of Helsinki and approved by the Ethics Committee and Institutional Review Board of Dongyang People's Hospital (2023-YX-272).

Author contributions

JZ: Funding acquisition, Investigation, Methodology, Writing – original draft, Writing – review & editing. XS: Data curation, Validation, Writing – original draft, Writing – review & editing. LJ: Funding acquisition, Investigation, Methodology, Software, Writing – original draft, Writing – review & editing. SJ: Data curation, Resources, Validation, Writing – original draft, Writing – review & editing. XP: Conceptualization, Funding acquisition, Investigation, Writing – original draft, Writing – review & editing.

Funding

The author(s) declare that financial support was received for the research and/or publication of this article. This study was supported by the Medical Health Science and Technology Project of Zhejiang Provincial Health Commission (2023KY386) and the Science and Technology Bureau of Jinhua (2022-3-013 and 2022-3-011).

Conflict of interest

The authors declare that the research was conducted in the absence of any commercial or financial relationships that could be construed as a potential conflict of interest.

Generative AI statement

The author(s) declare that no Generative AI was used in the creation of this manuscript.

Publisher's note

Supplementary material

The Supplementary Material for this article can be found online at: https://www.frontiersin.org/articles/10.3389/fcimb.2025.1553591/full#supplementary-material

SUPPLEMENTARY FIGURE 1
The distribution of average nucleotide identity among *Mycobacterium seoulense* strains.

References

Abbas, M., Khan, M. T., Iqbal, Z., Ali, A., Eddine, B. T., Yousaf, N., et al. (2024). Sources, transmission and hospital-associated outbreaks of nontuberculous mycobacteria: a review. *Future Microbiol.* 19, 715–740. doi: 10.2217/fmb-2023-0279

Alikhan, N. F., Petty, N. K., Ben Zakour, N. L., and Beatson, S. A. (2011). BLAST Ring Image Generator (BRIG): simple prokaryote genome comparisons. *BMC Genomics* 12, 402. doi: 10.1186/1471-2164-12-402

Armstrong, D. T., Eisemann, E., and Parrish, N. (2023). A brief update on mycobacterial taxonomy, 2020 to 2022. *J. Clin. Microbiol.* 61, e0033122. doi: 10.1128/jcm.00331-22

Bailo, R., Bhatt, A., and Ainsa, J. A. (2015). Lipid transport in Mycobacterium tuberculosis and its implications in virulence and drug development. *Biochem. Pharmacol.* 96, 159–167. doi: 10.1016/j.bcp.2015.05.001

Bo, H., Moure, U. A. E., Yang, Y., Pan, J., Li, L., Wang, M., et al. (2023). Mycobacterium tuberculosis-macrophage interaction: Molecular updates. *Front. Cell Infect. Microbiol.* 13, 1062963. doi: 10.3389/fcimb.2023.1062963

Brown-Elliott, B. A., and Woods, G. L. (2019). Antimycobacterial susceptibility testing of nontuberculous mycobacteria. *J. Clin. Microbiol.* 57, e00834-19. doi: 10.1128/JCM.00834-19

Chen, S., Zhou, Y., Chen, Y., and Gu, J. (2018). fastp: an ultra-fast all-in-one FASTQ preprocessor. *Bioinformatics* 34, i884–ii90. doi: 10.1093/bioinformatics/bty560

Croucher, N. J., Page, A. J., Connor, T. R., Delaney, A. J., Keane, J. A., Bentley, S. D., et al. (2015). Rapid phylogenetic analysis of large samples of recombinant bacterial whole genome sequences using Gubbins. *Nucleic Acids Res.* 43, e15. doi: 10.1093/nar/gku1196

Darling, A. C., Mau, B., Blattner, F. R., and Perna, N. T. (2004). Mauve: multiple alignment of conserved genomic sequence with rearrangements. *Genome Res.* 14, 1394–1403. doi: 10.1101/gr.2289704

Gilmore, S. A., Schelle, M. W., Holsclaw, C. M., Leigh, C. D., Jain, M., Cox, J. S., et al. (2012). Sulfolipid-1 biosynthesis restricts Mycobacterium tuberculosis growth in human macrophages. *ACS Chem. Biol.* 7, 863–870. doi: 10.1021/cb200311s

Guillet, V., Galandrin, S., Maveyraud, L., Ladeveze, S., Mariaule, V., Bon, C., et al. (2016). Insight into structure-function relationships and inhibition of the fatty acyl-AMP ligase (FadD32) orthologs from mycobacteria. *J. Biol. Chem.* 291, 7973–7989. doi: 10.1074/jbc.M115.712612

Guo, Q., Bi, J., Wang, H., and Zhang, X. (2021). Mycobacterium tuberculosis ESX-1-secreted substrate protein EspC promotes mycobacterial survival through endoplasmic reticulum stress-mediated apoptosis. *Emerg. Microbes Infect.* 10, 19–36. doi: 10.1080/22221751.2020.1861913

Haworth, C. S., Banks, J., Capstick, T., Fisher, A. J., Gorsuch, T., Laurenson, I. F., et al. (2017). British Thoracic Society guidelines for the management of non-tuberculous mycobacterial pulmonary disease (NTM-PD). *Thorax* 72, ii1–ii64. doi: 10.1136/thoraxjnl-2017-210929

Huh, H. J., Kim, S. Y., Jhun, B. W., Shin, S. J., and Koh, W. J. (2019). Recent advances in molecular diagnostics and understanding mechanisms of drug resistance in nontuberculous mycobacterial diseases. *Infect. Genet. Evol.* 72, 169–182. doi: 10.1016/j.meegid.2018.10.003

Karmakar, M., and Sur, S. (2024). Unlocking the Mycobacteroides abscessus pan-genome using computational tools: insights into evolutionary dynamics and lifestyle. *Antonie Van Leeuwenhoek* 118, 30. doi: 10.1007/s10482-024-02042-z

Kitazawa, T., Yamamoto, A., Nakayama, S., Kawase, K., and Wakabayashi, Y. (2024). Disseminated nontuberculous mycobacterium infection during treatment of multiple myeloma: A case report and review of the literature. *Intern. Med.* doi: 10.2169/internalmedicine.4234-24

Kurz, S. G., Zha, B. S., Herman, D. D., Holt, M. R., Daley, C. L., Ruminjo, J. K., et al. (2020). Summary for clinicians: 2020 clinical practice guideline summary for the treatment of nontuberculous mycobacterial pulmonary disease. *Ann. Am. Thorac. Soc.* 17, 1033–1039. doi: 10.1513/AnnalsATS.202003-222CME

Kwon, Y. S., Daley, C. L., and Koh, W. J. (2019). Managing antibiotic resistance in nontuberculous mycobacterial pulmonary disease: challenges and new approaches. *Expert Rev. Respir. Med.* 13, 851–861. doi: 10.1080/17476348.2019.1638765

Lange, C., Bottger, E. C., Cambau, E., Griffith, D. E., Guglielmetti, L., van Ingen, J., et al. (2022). Consensus management recommendations for less common non-tuberculous mycobacterial pulmonary diseases. *Lancet Infect. Dis.* 22, e178–ee90. doi: 10.1016/S1473-3099(21)00586-7

Liu, C. F., Song, Y. M., He, W. C., Liu, D. X., He, P., Bao, J. J., et al. (2021). Nontuberculous mycobacteria in China: incidence and antimicrobial resistance spectrum from a nationwide survey. *Infect. Dis. Poverty* 10, 59. doi: 10.1186/s40249-021-00844-1

Luo, M., Fadeev, E. A., and Groves, J. T. (2005). Mycobactin-mediated iron acquisition within macrophages. *Nat. Chem. Biol.* 1, 149–153. doi: 10.1038/nchembio717

Moopanar, K., and Mvubu, N. E. (2020). Lineage-specific differences in lipid metabolism and its impact on clinical strains of Mycobacterium tuberculosis. *Microb. Pathog.* 146, 104250. doi: 10.1016/j.micpath.2020.104250

Mun, H. S., Kim, H. J., Oh, E. J., Kim, H., Bai, G. H., Yu, H. K., et al. (2007). Mycobacterium seoulense sp. nov., a slowly growing scotochromogenic species. *Int. J. Syst. Evol. Microbiol.* 57, 594–599. doi: 10.1099/ijs.0.64744-0

Nakamoto, K., Fujiwara, K., Morimoto, K., and Ohta, K. (2024). Nontuberculous mycobacterial pulmonary disease caused by Mycobacterium seoulense. *Respirol Case Rep.* 12, e70049. doi: 10.1002/rcr2.v12.10

Namkoong, H., Omae, Y., Asakura, T., Ishii, M., Suzuki, S., Morimoto, K., et al. (2021). Genome-wide association study in patients with pulmonary Mycobacterium avium complex disease. *Eur. Respir. J.* 58, 1902269. doi: 10.1183/13993003.02269-2019

Nguyen, M. H., Haas, M. K., Kasperbauer, S. H., Calado Nogueira de Moura, V., Eddy, J. J., Mitchell, J. D., et al. (2024). Nontuberculous mycobacterial pulmonary disease: patients, principles, and prospects. *Clin. Infect. Dis.* 79, e27–e47. doi: 10.1093/cid/ciae421

Nguyen, L. T., Schmidt, H. A., von Haeseler, A., and Minh, B. Q. (2015). IQ-TREE: a fast and effective stochastic algorithm for estimating maximum-likelihood phylogenies. *Mol. Biol. Evol.* 32, 268–274. doi: 10.1093/molbev/msu300

Nithirungruang, P., Tanpowpong, P., Getsuwan, S., and Boonsathorn, S. (2024). Disseminated macrolide-resistant mycobacterium intracellulare infection in a child with autoimmune lymphoproliferative disorder: A case report and literature review. *Am. J. Trop. Med. Hyg* 111, 1051–1055. doi: 10.4269/ajtmh.24-0076

O'Neill, M. B., Mortimer, T. D., and Pepperell, C. S. (2015). Diversity of Mycobacterium tuberculosis across Evolutionary Scales. *PloS Pathog.* 11, e1005257. doi: 10.1371/journal.ppat.1005257

Ofori-Anyinam, B., Hamblin, M., Coldren, M. L., Li, B., Mereddy, G., Shaikh, M., et al. (2024). Catalase activity deficiency sensitizes multidrug-resistant Mycobacterium tuberculosis to the ATP synthase inhibitor bedaquiline. *Nat. Commun.* 15, 9792. doi: 10.1038/s41467-024-53933-8

Page, A. J., Cummins, C. A., Hunt, M., Wong, V. K., Reuter, S., Holden, M. T., et al. (2015). Roary: rapid large-scale prokaryote pan genome analysis. *Bioinformatics* 31, 3691–3693. doi: 10.1093/bioinformatics/btv421

Penuelas-Urquides, K., Villarreal-Trevino, L., Silva-Ramirez, B., Rivadeneyra-Espinoza, L., Said-Fernandez, S., and de Leon, M. B. (2013). Measuring of Mycobacterium tuberculosis growth. A correlation of the optical measurements with colony forming units. *Braz. J. Microbiol.* 44, 287–289. doi: 10.1590/S1517-83822013000100042

Robledo, J. A., Murillo, A. M., and Rouzaud, F. (2011). Physiological role and potential clinical interest of mycobacterial pigments. *IUBMB Life* 63, 71–78. doi: 10.1002/iub.v63.2

Ruhl, C. R., Pasko, B. L., Khan, H. S., Kindt, L. M., Stamm, C. E., Franco, L. H., et al. (2020). Mycobacterium tuberculosis sulfolipid-1 activates nociceptive neurons and induces cough. *Cell* 181, 293–305 e11. doi: 10.1016/j.cell.2020.02.026

Samuels, A. N., Wang, E. R., Harrison, G. A., Valenta, J. C., and Stallings, C. L. (2022). Understanding the contribution of metabolism to Mycobacterium tuberculosis drug tolerance. *Front. Cell Infect. Microbiol.* 12, 958555. doi: 10.3389/fcimb.2022.958555

Santander, R. D., Figas-Segura, A., and Biosca, E. G. (2018). Erwinia amylovora catalases KatA and KatG are virulence factors and delay the starvation-induced viable but non-culturable (VBNC) response. *Mol. Plant Pathol.* 19, 922–934. doi: 10.1111/mpp.2018.19.issue-4

Sassetti, C. M., Boyd, D. H., and Rubin, E. J. (2003). Genes required for mycobacterial growth defined by high density mutagenesis. *Mol. Microbiol.* 48, 77–84. doi: 10.1046/j.1365-2958.2003.03425.x

Seemann, T. (2014). Prokka: rapid prokaryotic genome annotation. *Bioinformatics* 30, 2068–2069. doi: 10.1093/bioinformatics/btu153

Seemann, T. (2015). "Snippy: rapid haploid variant calling and core SNP phylogeny," in *GitHub*. Available at: github.com/tseemann/snippy.

Shankar, G., and Akhter, Y. (2024). Stealing survival: Iron acquisition strategies of Mycobacteriumtuberculosis. *Biochimie.* 227, 37–60. doi: 10.1016/j.biochi.2024.06.006

Shin, D. M., Jeon, B. Y., Lee, H. M., Jin, H. S., Yuk, J. M., Song, C. H., et al. (2010). Mycobacterium tuberculosis eis regulates autophagy, inflammation, and cell death through redox-dependent signaling. *PloS Pathog.* 6, e1001230. doi: 10.1371/journal.ppat.1001230

Shyam, M., Shilkar, D., Verma, H., Dev, A., Sinha, B. N., Brucoli, F., et al. (2021). The mycobactin biosynthesis pathway: A prospective therapeutic target in the battle against tuberculosis. *J. Med. Chem.* 64, 71–100. doi: 10.1021/acs.jmedchem.0c01176

Stacy, A., Everett, J., Jorth, P., Trivedi, U., Rumbaugh, K. P., and Whiteley, M. (2014). Bacterial fight-and-flight responses enhance virulence in a polymicrobial infection. *Proc. Natl. Acad. Sci. U.S.A.* 111, 7819–7824. doi: 10.1073/pnas.1400586111

Sun, Y., Zhang, C., Lu, B., Chen, J., and Pan, X. (2024). Case report: Mycobacterium chimaera-induced lymph node infection in a patient with chronic myeloproliferative neoplasm misdiagnosed as tuberculous lymphadenitis. *Front. Public Health* 12, 1387722. doi: 10.3389/fpubh.2024.1387722

Tran, T., Dawrs, S. N., Norton, G. J., Virdi, R., and Honda, J. R. (2020). Brought to you courtesy of the red, white, and blue-pigments of nontuberculous mycobacteria. *AIMS Microbiol.* 6, 434–450. doi: 10.3934/microbiol.2020026

Wetzstein, N., Diricks, M., Anton, T. B., Andres, S., Kuhns, M., Kohl, T. A., et al. (2024). Clinical and genomic features of Mycobacterium avium complex: a multi-national European study. *Genome Med.* 16, 86. doi: 10.1186/s13073-024-01359-8

Wick, R. R., Judd, L. M., Gorrie, C. L., and Holt, K. E. (2017). Unicycler: Resolving bacterial genome assemblies from short and long sequencing reads. *PloS Comput. Biol.* 13, e1005595. doi: 10.1371/journal.pcbi.1005595

Xiao, G., Alphey, M. S., Tran, F., Pirrie, L., Milbeo, P., Zhou, Y., et al. (2021). Next generation Glucose-1-phosphate thymidylyltransferase (RmlA) inhibitors: An extended SAR study to direct future design. *Bioorg Med. Chem.* 50, 116477. doi: 10.1016/j.bmc.2021.116477

Yan, M., Cao, L., Zhao, L., Zhou, W., Liu, X., Zhang, W., et al. (2023). The key roles of mycobacterium tuberculosis fadD23 C-terminal domain in catalytic mechanisms. *Front. Microbiol.* 14, 1090534. doi: 10.3389/fmicb.2023.1090534

Yoon, S. H., Ha, S. M., Lim, J., Kwon, S., and Chun, J. (2017). A large-scale evaluation of algorithms to calculate average nucleotide identity. *Antonie Van Leeuwenhoek* 110, 1281–1286. doi: 10.1007/s10482-017-0844-4

Zakham, F., Sironen, T., Vapalahti, O., and Kant, R. (2021). Pan and Core Genome Analysis of 183 Mycobacterium tuberculosis Strains Revealed a High Inter-Species Diversity among the Human Adapted Strains. *Antibiotics (Basel)* 10, 500. doi: 10.3390/antibiotics10050500

Zekic, T., Holley, G., and Stoye, J. (2018). Pan-genome storage and analysis techniques. *Methods Mol. Biol.* 1704, 29–53. doi: 10.1007/978-1-4939-7463-4_2

Zhang, L., Lin, T. Y., Liu, W. T., and Ling, F. (2024). Toward characterizing environmental sources of non-tuberculous mycobacteria (NTM) at the species level: A tutorial review of NTM phylogeny and phylogenetic classification. *ACS Environ. Au.* 4, 127–141. doi: 10.1021/acsenvironau.3c00074

Zhang, Z. Y., Sun, Z. Q., Wang, Z. L., Hu, H. R., Wen, Z. L., Song, Y. Z., et al. (2013). Identification and pathogenicity analysis of a novel non-tuberculous mycobacterium clinical isolate with nine-antibiotic resistance. *Clin. Microbiol. Infect.* 19, 91–96. doi: 10.1111/j.1469-0691.2012.03818.x

Zhao, J., Lu, B., Zhou, Y., Wang, S., and Pan, X. (2022). Molecular identification and clinical significance of Mycobacterium seoulense strains from patients with nontuberculous mycobacterium infections. *Diagn. Microbiol. Infect. Dis.* 104, 115756. doi: 10.1016/j.diagmicrobio.2022.115756

Zhu, X., Lu, Q., Li, Y., Long, Q., Zhang, X., Long, X., et al. (2023). Contraction and expansion dynamics: deciphering genomic underpinnings of growth rate and pathogenicity in Mycobacterium. *Front. Microbiol.* 14, 1292897. doi: 10.3389/fmicb.2023.1292897

frontiers | Frontiers in Cellular and Infection Microbiology

TYPE Original Research
PUBLISHED 05 May 2025
DOI 10.3389/fcimb.2025.1582411

OPEN ACCESS

EDITED BY
Mattia Pirolo,
University of Copenhagen, Denmark

REVIEWED BY
Chamara De Silva Benthotage,
Southern Cross University, Australia
Salome N. Seiffert,
Zentrum für Labormedizin (ZLM), Switzerland

*CORRESPONDENCE
Constança Pomba
cpomba@fmv.ulisboa.pt
jcsilva@egasmoniz.edu.pt

RECEIVED 24 February 2025
ACCEPTED 10 April 2025
PUBLISHED 05 May 2025

CITATION
Moreira da Silva J, Menezes J, Fernandes L, Marques C, Costa SS, Timofte D, Amaral AJ and Pomba C (2025) Evaluation of multidrug-resistant bacteria and their molecular mechanisms found in small animal veterinary practices in Portugal.
Front. Cell. Infect. Microbiol. 15:1582411.
doi: 10.3389/fcimb.2025.1582411

Evaluation of multidrug-resistant bacteria and their molecular mechanisms found in small animal veterinary practices in Portugal

Joana Moreira da Silva[1,2], Juliana Menezes[1,2,3], Laura Fernandes[1,2], Cátia Marques[3,4,5], Sofia Santos Costa[6], Dorina Timofte[7], Andreia J. Amaral[1,2,8] and Constança Pomba[1,2,5]*

[1]CIISA - Centre for Interdisciplinary Research in Animal Health, Faculty of Veterinary Medicine, University of Lisbon, Lisbon, Portugal, [2]AL4AnimalS - Associate Laboratory for Animal and Veterinary Sciences, Lisbon, Portugal, [3]IMVET- Research in Veterinary Medicine, Faculty of Veterinary Medicine, Lusófona University- Lisbon University Centre, Lisbon, Portugal, [4]Animal and Veterinary Research Center (CECAV), Lusófona University, University Centre of Lisbon, Lisbon, Portugal, [5]Genevet™, Veterinary Molecular Diagnostic Laboratory, Carnaxide, Portugal, [6]Global Health and Tropical Medicine, GHTM, Associate Laboratory in Translation and Innovation Towards Global Health, Associated Laboratory in Translation and Innovation Towards Global Health (LA-REAL), Instituto de Higiene e Medicina Tropical, IHMT, Universidade Nova de Lisboa, Lisbon, Portugal, [7]Institute of Infection, Veterinary and Ecological Sciences, School of Veterinary Science, Department of Veterinary Anatomy, Physiology and Pathology, University of Liverpool, Leahurst, United Kingdom, [8]Science and Technology School, University of Évora, Évora, Portugal

Introduction: Intensive medical care provided in companion animal practices carries the potential risk of selecting and disseminating multidrug-resistant organisms (MDROs). However, data on infection, prevention and control standards specific to small animal veterinary practices (SAVPs) remains limited. The goal of our work was to evaluate the environmental contamination and staff carriage by MDROs in veterinary practices across Portugal.

Methods: Fourteen SAVPs were enrolled. Environmental samples were collected from critical areas such as operating room, wards and pre-operative area. Veterinary team members voluntarily gave nasal, hand and rectal swabs. All samples were screened for the presence of, including extended-spectrum β-lactamases (ESBL)- and carbapenemase-producing Gram-negative bacteria and methicillin-resistant *Staphylococcus* spp. (MRS). Whole-genome sequencing was performed for carbapenem resistant strains.

Results: Environmental evaluation by surface swabs revealed that 6.5% (n=32/490) were contaminated with multidrug-resistant Gram-negative bacteria. OXA-23-producing *Acinetobacter* spp. (n=5) and IMP-8-producing *Pseudomonas juntendi* (n=2) strains were described on different locations of different SAVPs. Moreover, *Stenotrophomonas maltophilia* (n=12) and *Pseudomonas aeruginosa* (n=3) strains were also found on multiple surfaces of different SAVPs. Three human samples (two rectal, one hand) had carbapenem-resistant *P. aeruginosa* strains by OprD mutations, while *S. maltophilia* strains were recovered from four

samples (two rectal, two hands). One nasal swab was positive for carbapenem-resistant *Klebsiella pneumoniae* ST11. Only one SAVP surface was positive for the newly typed for methicillin-resistant *Staphylococcus aureus* (MRSA) ST9220-II. MRSA nasal carriage was found in 14% of samples (n=9/64), with an equal prevalence of ST22-IV and ST8-VI. As for hand samples, MRSA was present in 10.7% (n=4/38), with a predominance of ST8-VI.

Discussion: These emerging data indicate that SAVPs may significantly contribute to the dissemination of MDROs. To address this, rigorous infection, prevention and control (IPC) measures should be implemented, alongside educational workshops directed to all veterinary staff as well as to veterinary and nursing students.

KEYWORDS

small animal veterinary practices, multidrug-resistant organisms, environmental contamination IPC, carbapenem resistance, MRSA, veterinary staff carriage

1 Introduction

In recent years, antimicrobial resistance has led to approximately 1.27 million global deaths (Murray et al., 2022). The rise in antimicrobial resistance is driven by multiple mechanisms, notably the acquisition of resistance genes, such as *mec*A or $bla_{\text{CTX-M-15}}$ and $bla_{\text{KPC-like}}$, through plasmids (Dulon et al., 2011; Mathers et al., 2015). Key culprits include *Escherichia coli*, *Staphylococcus aureus*, *Klebsiella pneumoniae*, *Acinetobacter baumannii* and *Pseudomonas aeruginosa*. These microorganisms are linked to community- and to healthcare-associated infections, posing challenges due to extended treatment periods, increased mortality and higher economic costs. The European Centre for Disease Prevention and Control (ECDC) reported that 4.3 million patients in Europe experienced at least one healthcare-associated infections in 2022-2023 (European Centre for Disease Prevention and Control, 2024). The World Health Organization updated the list of medically important antibiotics, classifying which antibiotics can be used in veterinary medicine, following the prescribing cascade. As expected, last-line antibiotics, such as carbapenems and oxazolidinones, are only to be used in human medicine (European Centre for Disease Prevention and Control, 2024), while 3rd generation cephalosporins, high-priority critically important antimicrobials, are authorized for both human and veterinary medicine (Volkov, 2024). This classification is aligned with European Medicines Agency guidelines, released in 2019 (EMA, 2019).

In the last years, the bond between humans and companion animals has significantly evolved, with animals now being regarded as integral members of the family. This shift has led to an increase not only in the number of veterinary practices, as well as in rapid advancements in small animal care and animals' lifespan, pressuring veterinarians towards higher standards of healthcare (Eurodev, 2024). Although carbapenems are not approved for veterinary use (EMA, 2019), carbapenem-resistant Enterobacterales, *Acinetobacter* spp. and *P. aeruginosa* are sporadically but consistently reported in companion animals in Europe (Gentilini et al., 2018; Moreira da Silva et al., 2024b). Furthermore, cases of multidrug-resistant organisms (MDROs) such extended-spectrum β-lactamases (ESBL) - producing Enterobacterales and methicillin-resistant *Staphylococcus* spp. (MRS) sharing between humans and companion animals have been reported (Sing et al., 2008; Nienhoff et al., 2009; Grönthal et al., 2018; Hemeg, 2021; Menezes et al., 2022; Menezes et al., 2023), showing the need for a One Health and integrative approach to mitigate the dissemination of MDROs.

The implementation of infection, prevention and control (IPC) programs has long been recognized as a cornerstone to minimize the spread of MDROs within human hospital environments. Not only do they protect hospital staff and patients, IPC also helps to minimize the spillover of resistant bacteria into the community (World Health Organization, 2023). In veterinary medicine, antimicrobial stewardship and IPC programs are rising concepts; notwithstanding, a lack of studies characterizing veterinary IPC programs or which MDROs are circulating within small animal veterinary practices (SAVP) still exists. According to ECDC (European Centre for Disease Prevention and Control, 2016), only genomic-level investigations, such as Whole Genome Sequencing (WGS), can provide the resolution needed to track the distribution of resistance genes across hosts, time, and space. In this way, this study aimed to assess the standard cleanliness of high-touch surfaces in SAVP and to characterize the environmental contamination and staff transient carriage by relevant bacterial pathogens, particularly carbapenem-resistant Gram-negative bacteria and MRS, together with determining bacterial transmission between humans, companion animals, and hospital surfaces through WGS. The outcomes of this study clarified how effective standard IPC protocols in SAVPs are, as well as elucidate on the role SAVPs have in the dissemination of MDROs within a One Health context.

2 Materials and methods

2.1 Hospitals and clinics characteristics

Fourteen SAVP were enrolled between March 2021 and November 2023, and coded from A to N. SAVP-A to SAVP-G were hospitals and SAVP-H to SAVP-N were clinics. According to the Portuguese legislation, it is mandatory for hospitals to have emergency care available 24/7, as opposed to clinics. SAVPs were located in different regions of Portugal. A previously published self-assessment form was adapted and provided to each SAVP covering different aspects of each facility's functioning characteristics and IPC practices (Schmidt et al., 2020). After the results evaluation, all SAVP received a written report of the findings and suggestions for improvement.

2.2 On-site collection

Contact plates (Plate Count Agar, 28.26 cm^2) and surface swabs (TS/5–42 with 10 mL neutralizing buffer, TSC Ltd.) were used to sample critical surfaces in the practice environment. Surface swab samples were collected from a defined area of 100 cm^2 using a sterile template frame. Both methods were applied to flat surfaces, while only surface swabs were used for irregular surfaces. Samples were taken from the locations as they were found, without any previous cleaning and disinfecting procedure. Surfaces that had been immediately used before sampling were excluded to avoid biased results.

Critical areas for sampling were defined as high-touch and high-rotation surfaces within the practice. Due to their importance for veterinary activities and potential to act as transmission hubs, three locations were always sampled: operating room, wards and pre-operative area. Other locations such as examination rooms and treatment areas were included in the study depending on availability at the time of sampling (if the areas were not in use and were cleaned) and the individual concerns pertaining to each SAVP. Supplementary Tables 1, 2 describe the sampling techniques and the surfaces considered in each SAVP.

The disinfection protocols and products in use were defined by each SAVP, and as such, these varied across practices. This information was recorded in the general SAVP self-assessment form previously mentioned.

2.3 Human sampling

Sampling was voluntary and written informed consent was obtained. Three swabs (one per nostril and one for both hands) were collected from each member of the working force per SAVP (89 veterinary doctors, 32 nurses, 35 technicians and 13 administrative staff, n=169). Rectal swabs were sampled from 30 people (17.7%, n= 30/169). To reduce potential bias, hand swabs were taken randomly during daily procedures, to avoid unusual hygiene prior to collection. All samples were carefully coded and placed in a cooler until processing. Ethical approval for the study was obtained (CEBEA011/2021) and performed in accordance to relevant guidelines.

2.4 Sample analysis

Contact plates were incubated at 37°C and colony forming units (CFU) were counted at 24 and 48 hours of incubation. Following previously established efficacy criteria for aerobic colony count (ACC), a growth >2.5 CFU/cm^2 indicated failure of the cleaning protocol (Mulvey et al., 2011).

For surface swabs, a cleaning criterion of >1 CFU/cm^2 was applied (Dancer, 2004) for direct plating growth in non-selective media Brain Heart Agar (Biokar Diagnostics, France) after 24 and 48 hours incubation at 37°C. Following an overnight enrichment step on Brain Heart Infusion broth (Biokar Diagnostics, France) at 37°C, samples were plated onto MacConkey agar supplemented with 1.5 mg/mL cefotaxime or 1.5 mg/mL of meropenem (Thermofisher Scientific, United States) (to select for ESBL-producing or carbapenem-resistant bacteria, respectively), CHROMagar™ *Acinetobacter* supplemented with CHROMagar™ MDR Selective (CR102, Chromagar, Japan), and Brilliance™ MRSA 2 agar (Thermofisher Scientific, United States).

One randomly selected nasal swab was placed overnight on buffered peptone water (Biokar Diagnostics, France) at 37°C, and then plated onto MacConkey agar plates supplemented with 1.5 mg/mL cefotaxime or 1.5 mg/mL meropenem, and on CHROMagar™ *Acinetobacter* supplemented with CHROMagar™ MDR Selective. The other nasal swab was placed overnight on sodium chloride supplemented with 13% tryptone soy broth at 37°C and then plated onto Mannitol Salt Agar (Biokar Diagnostics, France) and Brilliance™ MRSA 2 agar (Thermofisher Scientific, United States).

Rectal and hand swabs were incubated overnight at 37°C in peptone water, followed by plating onto the non-selective and selective media described above.

In all cases, up to three isolates with similar phenotypical appearance were isolated for further characterization. Microdilution antibiotic susceptibility testing was performed for Gram-negative bacteria isolated from MacConkey agar with cefotaxime and meropenem supplementation following EUCAST guidelines (European Committee on Antimicrobial Susceptibility Testing, 2024), to further confirm their resistant phenotype.

2.5 Resistance genes detection

DNA was extracted from pure cultures using a boiling extraction method (Dashti et al., 2009). Multiplex PCRs followed by Sanger sequencing were performed as previously described for the detection of β-lactamase genes in Gram-negative bacteria,

including ESBL and carbapenemase genes (Menezes et al., 2022). Gram-negative bacteria species identification was performed by sequencing 16S rRNA (Srinivasan et al., 2015).

Staphylococci species identification and *mecA* gene detection was performed as previously described (Couto et al., 2015; Rodrigues et al., 2018). MLST and SCC*mec* identification (Kondo et al., 2007) was performed for methicillin-resistant *Staphylococcus aureus* (MRSA), and one new sequence type (ST) was assigned in accordance to PubMLST (Jolley et al., 2018).

2.6 Whole-genome sequencing analysis

One representative resistant strain from each surface was selected for WGS. Genomic DNA was extracted from RNase-treated lysates via NZY Tissue gDNA Isolation kit (NZYTech, Portugal). All libraries for WGS were prepared using TruSeq DNA PCR-Free preparation kit (Illumina, United States). DNA sequencing was performed using Illumina NovaSeq platform with 2×150 bp paired-end reads. *De novo* assembled genomes were obtained using a previously described pipeline (Menezes et al., 2022). ResFinder 4.1 (available at the Centre of Genomic Epidemiology – https://www.genomicepidemiology.org/) and CARD database (available at https://card.mcmaster.ca/home (Alcock et al., 2023),) were used for the screening of the novel generated assemblies for identification of antimicrobial resistance genes. Single-nucleotide polymorphism (SNP) analysis was conducted for each bacterial species using Parsnp v1.2 for multiple sequence alignment of the generated assemblies plus a reference genome. *De novo* assemblies were submitted to NCBI under the bioprojects accession numbers PRJNA1131754 and PRJNA1000421 (OXA-23-producing *Acinetobacter* spp.). Newly identified STs were assigned and submitted to the PubMLST database.

3 Results

3.1 Surface hygiene evaluation by direct culture

According to contact plate evaluation, 28% of the flat surfaces (n=74/264) failed the cleaning efficacy assessment when interpreted with the criteria of >2.5 CFU/cm^2, in accordance to Mulvey et al., 2011 (Mulvey et al., 2011) (Supplementary File 1). On the other hand, flat and irregular surface evaluation using swabs revealed that 17.7% of surfaces (n=87/490) failed the criteria established by Dancer 2004 of >1 CFU/cm^2 (Dancer, 2004) (Supplementary File 1). Contact plates and swab results were discordant in 27.6% (n=72/264) of flat surfaces. Considering both evaluation methods, flat surfaces cleaning efficacy failure increased to 36.8% (n=96/261). All SAVP had at least one unclean surface (Supplementary File 1) with frequencies varying from 3.3% (n=1/30) in SAVP-C to 72% (n=18/25) in SAVP-G.

Surfaces that frequently failed cleaning efficacy assessment included weight scales (60.9%, n=14/23), sinks and taps (44.1%, n=15/34), animal cages (40.5%, n=17/42), shearing blades (41.7%, n=10/24) and keyboards (30.3%, n=10/33).

The average results on the self-assessment form were 37/60 points (25–51 points). The highest scoring practice was SAVP-G; yet, SAVP-G showed the highest level of environmental contamination in the different areas of the hospital, with 72% of surfaces (n=18/25) failing the cleaning efficacy assessment (Supplementary File 1).

3.2 Surface contamination with Gram-negative bacteria

Considering all surfaces, 6.5% (n=32/490) had positive growth in the selective culture media for Gram-negative bacteria, namely, *Acinetobacter* spp. (3.1%, n=15/490), *Stenotrophomonas* spp. (2.5%, n=12/490), *Pseudomonas* spp. (1.0%, n=5/490), *Enterobacter* spp. (0.4%, n=2/490), *Escherichia* spp. (0.2%, n=1/490), *Klebsiella* spp. (0.2%, n=1/490), and *Leclercia* spp. (0.2%, n=1/490). Table 1 summarizes all the different bacterial species found on each SAVP.

Carbapenem-resistant non-fermenting Gram-negative bacteria were also recovered on 58.9% (n=20/32) of contaminated surfaces. Overall, 57.1% (n=8/14) of SAVP had at least one positive surface for carbapenem-resistant Gram-negative bacteria – three hospitals and five clinics (Table 1).

Considering veterinary hospitals, *Stenotrophomonas maltophilia*, which is intrinsically resistant to multiple classes of antibiotics, including carbapenems (due to intrinsic carbapenemases L1 and L2 (Brooke, 2021)), was identified on two surfaces of the cat ward of SAVP-E, and on the tap of the washing area of SAVP-F. In SAVP-G, *P. aeruginosa* and *S. maltophilia* were present on different surfaces (Table 1). Additionally, carbapenem-resistant *Pseudomonas juntendi* was found on a plastic mat on the countertop and inside one dog cage (Table 1).

Regarding veterinary clinics, carbapenem-resistant *Acinetobacter* spp. was found on four surfaces of SAVP-H. Carbapenem-resistant *P. aeruginosa* (A6E4P2) was found on the cat examination room sink of SAVP-I. *S. maltophilia* were found on the examination room sinks of SAVP-K) and SAVPL. For SAVP-N, it was present, on the post-surgery cage the practice's mobile phone and a hand cloth (Table 1).

All *S. maltophilia* were susceptible to trimethoprim/sulfamethoxazole (MIC < 0,001 mg/L). All carbapenem-resistant isolates were characterized using WGS.

3.2.1 Whole-genome sequence analysis of carbapenem-resistant Gram-negative bacteria from surfaces

The two *S. maltophilia* isolated from SAVP-E belonged to different STs, namely, ST4 in a cat cage (HVD1E4P1), and the newly assigned ST1185 on a cage handle from the same cat ward (HVD4E4P1). The *S. maltophilia* from SAVP-F belonged to ST94 (EP3G8P3).

On SAVP-H, all the carbapenem-resistant *Acinetobacter* spp. (n=5) harbored bla_{OXA-23} carbapenemase gene in the same plasmid

10.3389/fcimb.2025.1582411

TABLE 1 Gram-negative bacteria identified upon environmental evaluation of SAVPs A-N.

SAVP	Location	Area	Identified organism	Sequence Type (ST)	NCBI strain ID	Carbapenem Resistance*	
						Imipenem	Meropenem
C	Pre-operative area	Plastic mat table 02	*Acinetobacter calcoaceticus-baumannii* complex	NA	NA	≤2 (S)	≤2 (S)
		Plastic mat table 03					
		Weight scale					
		Oxygen balloon					
		Anaesthetic device buttons					
		Tap					
	Wash room	Countertop					
	Operating room 02	Blanket					
D	Cat ward	Big cage	*Acinetobacter baumannii*	NA	NA	≤2 (S)	≤2 (S)
		Small cage		NA	NA		
E	Pre-operative area	Tap	CTX-M-15-producing *Enterobacter kobei*	NA	NA	≤2 (S)	≤2 (S)
	Cat ward	Cage	CTX-M-15-producing *Escherichia hermannii*	NA	NA	≤2 (S)	≤2 (S)
			Stenotrophomonas maltophilia	4	HVD1E4P1	NA	NA
		Cage handle	*Stenotrophomonas maltophilia*	1185 (new ST)	HVD4E4P1	NA	NA
F	Wash room	Tap	*Stenotrophomonas maltophilia*	94	EP3G8P3	NA	NA
G	Dog ward	Tap	*Pseudomonas aeruginosa*	253	ER3C4P3	>16 (R)	>32 (R)
			CTX-M-3-producing *Klebsiella pneumoniae*	11	ER3C8K2	≤2 (S)	≤2 (S)
	Dog ward	Treatment table plastic mat	IMP-8-producing *Pseudomonas juntendi*	NA	ER1C4P2	16 (R)	32 (R)
		Cage	IMP-8-producing *Pseudomonas juntendi*	NA	ER4C8A1	16 (R)	32 (R)
		Treatment table grids	GES-7-producing *Leclercia adecarboxylata*	NA	ER5C2K1	≤2 (S)	≤2 (S)
	Isolation unit	Cage	*Stenotrophomonas maltophilia*	120	ER3F8A1	NA	NA
		Plastic mat on countertop	*Stenotrophomonas maltophilia*	115	ER2F4P2		
			Pseudomonas aeruginosa	253	ER2F8P2	16 (R)	>32 (R)
	Cat ward	Tap	*Stenotrophomonas maltophilia*	120	ER3D8P2	NA	NA
			CTX-M-15- producing *Enterobacter hormaechei*	NA	ER3D2K1	≤2 (S)	≤2 (S)
H	Treatment area	Weight scale	OXA-23-producing *Acinetobacter lwoffii*	NA	B4Z4A1 B4Z8A1	8 (R)	4 (S)
	Treatment room	Stainless steel supporting tray	OXA-23-producing *Acinetobacter lwoffii*	NA	B11Z4A1	8 (R)	8 (R)
		Keyboard computer	OXA-23-producing *Acinetobacter lwoffii*	NA	B12Z8A1	4 (I)	4 (S)
	Waiting room	Weight scale	OXA-23-producing *Acinetobacter schindleri*	NA	B1E8A1	8 (R)	4 (S)

(Continued)

TABLE 1 Continued

SAVP	Location	Area	Identified organism	Sequence Type (ST)	NCBI strain ID	Carbapenem Resistance*	
						Imipenem	Meropenem
I	Cat examination room	Sink	*Pseudomonas aeruginosa*	267	A6E4P2	8 (R)	4 (I)
K	Dog examination room	Sink	*Stenotrophomonas maltophilia*	967 (new type)	C1DE4P2	NA	NA
	Cat examination room	Sink	*Stenotrophomonas maltophilia*	5	C6EE4A1	NA	NA
L	Examination room 01	Sink	*Stenotrophomonas maltophilia*	39	B4EE4A2	NA	NA
N	Recovery ward	Cage	*Stenotrophomonas maltophilia*	27	EX2C4P3	NA	NA
	Fomites	Practice's mobile phone	*Stenotrophomonas maltophilia*	115	EX3I8A1	NA	NA
		Hand cloth	*Stenotrophomonas maltophilia*	115	EX2I4A1	NA	NA

NA, Not applicable; S, Susceptible; I, Susceptible to increased exposure; R, Resistant.
*EUCAST 2024 breakpoints (European Committee on Antimicrobial Susceptibility Testing, 2024) – for Enterobacterales, breakpoints are as follows: imipenem (S ≤2; R > 4) and meropenem (S ≤2; R > 4); for *Acinetobacter* spp., imipenem (S ≤2; R > 4) and meropenem (S ≤2; R > 2); and for *Pseudomonas* spp., imipenem (S ≤0.001; R > 4) and meropenem (S ≤2; R > 8). There are no breakpoints for *S. maltophilia* due to their naturally occurring carbapenemases, making them intrinsically resistant.

across different sub-species, as previously described by our group (Moreira da Silva et al., 2024a).

The two *P. aeruginosa* strains from SAVP-G belonged to ST253 and were unrelated (single nucleotide polymorphism (SNP) difference > 14, Supplementary Table 4) (Schürch et al., 2018). Both strains were carbapenem-resistant, having the same mutations on OprD porin channel, and on *nalC* and *mexR* genes (MexAB-OprM efflux pump repressor and regulator, respectively) (Table 2). Both *P. juntendi* were IMP-8-producers (ER1C4P2 and ER4C8A1) and were considered unrelated by using the SNP relatedness cut-off of *P. aeruginosa* (SNP difference >14, Supplementary Table 5), as no cut-of has been proposed for this sub-species (Schürch et al., 2018). The $bla_{\text{IMP-8}}$ carbapenemase gene was possibly chromosomally inserted as no plasmids were detected (Aytan-Aktug et al., 2022).

Finally, one *S. maltophilia* ST115 strain (ER2F4P2) and two ST120 strains (ER3F8A1 and ER3D8P2) were identified. Interestingly, the two ST120 were closely related (5 SNP difference) showing its likely dissemination between the isolation unit and cat ward of SAVP-G (Supplementary Table 6).

SAVP-I, SAVP-K and SAVP-L are veterinary clinics from the same business group (i.e. some staff alternate between veterinary practices); however, none of the isolated strains were shared between practices. The SAVP-I carbapenem-resistant *P. aeruginosa* ST267 strain (A6E4P2) had one mutation on OprD porin channel and a wild-type MexAb-OprM efflux pump (Table 2). As for *S. maltophilia* strains, multiple STs were identified, namely ST5 (C6EE4A1) and a newly assigned ST967 (C1DE8A3) in SAVP-K; and ST39 strain (B4EE4A2) in SAVP-L.

Lastly, on SAVP-N, there was one *S. maltophilia* ST27 strain (EX2C4P3) and two ST115 strain (EX3I8A1 and EX2I4A1; 10 SNP difference).

3.3 Carbapenem-resistant Gram-negative bacteria transient carriage by veterinary staff

Diverse and normal microbial flora was observed across the 30 fecal samples available. Carbapenem-resistant non-fermenting Gram-negative bacteria were isolated from 16.7% (n=5/30) participants, including *P. aeruginosa* (n=3) and *S. maltophilia* (n=2).

The three *P. aeruginosa* strains were isolated from participants of different SAVP, namely a ST27 (HVD5R4P1) in one veterinarian from SAVP-E; a ST244 (A5R4P1) in one veterinarian from SAVP-I; and a ST274 (C8R8P1) in one nurse from SAVP-K.

P. aeruginosa ST244 strain was carbapenem-susceptible and was found to have a wild-type OprD porin channel and MexAB-OprM efflux pump. *P. aeruginosa* ST27 strain had an early stop codon on *oprD* together with mutations on *nalC* and *mexR; and P. aeruginosa* ST274 had several mutations on *oprD*, thus explaining their carbapenem-resistant phenotype (Table 2).

One *S. maltophilia* ST317 strain (B3R4P1) was detected in a nurse from SAVP-L, and one *S. maltophilia* ST84 strain (C10R8A1) in a technician from SAVP-K, both susceptible to trimethoprim/sulfamethoxazole.

Gram-negatives were rarely isolated from nasal swabs (1.2%, n=2/169) using selective media. One veterinarian from SAVP-G was positive for an imipenem-resistant CTX-M-3-producing *K. pneumoniae* ST11 (R11Np4K1; MIC= 8 mg/mL), albeit susceptible to meropenem, showing a 15% truncated Omp36K in the WGS analysis (Supplementary Figure 1). One veterinarian from SAVP-I was positive for a carbapenem-susceptible *P. aeruginosa* ST244 (A6Np4P1) that was related to the ST244 (A5R4P1, SNP difference ≤ 3, Supplementary Table 3) isolated from the rectal swab of a distinct veterinarian from the same veterinary practice.

TABLE 2 Mutations on OprD porin channel and MexAB-OprM efflux pump of *P. aeruginosa* strains (n=8).

SAVP	Type of Sample	NCBI strain ID	ST	Serotype	OprD	MexAB-OprM	Carbapenem resistance*	
							Imipenem	Meropenem
G	Environmental	ER3C4P3	253	O10	T103S; K115T; F170L; E185Q; P186G; V189T; R310E; A315G; A425G	*nalC* (G71E; A145V; S209R); *mexR* (V126E)	>16 (R)	>32 (R)
	Environmental	ER2F8P2	253	O10	T103S; K115T; F170L; E185Q; P186G; V189T; R310E; A315G; A425G	*nalC* (G71E; A145V; S209R); *mexR* (V126E)	>16 (R)	>32 (R)
I	Environmental	A6E4P2	267	O2	S278P	Wild-type	>8 (R)	4 (I)
E	Rectal swab	HVD5R4P1	27	O1	Stop Codon (TAG) at position 94	*nalC* (G71E; S209R); *mexR* (V126E; V132A)	>16 (R)	>32 (R)
I	Rectal swab	A5R4P1	244	O2	Wild-type	Wild-type	≤1 (S)	≤1 (S)
K	Rectal swab	C8R8P1	274	O3	D43N; S57E; S59R; E202Q; I210A; E230K; S240T; N262T; A267S; S278P; A281G; K296Q; Q301E; R310G; V359L; M372V; S373D; D374S; N375S; N376S; V377S; G378S; K380A; N381G; Y382L	*nalC* (S209R, G71E)	>8 (R)	8 (R)
I	Nasal swab	A6Np4P1	244	O2	Wild-type	Wild-type	≤1 (S)	≤1 (S)
K	Hand swab	C11Hp4P1	274	O3	Stop Codon (TAG) at position 378; filled with deletions	*nalC* (G71E, S209R)	>16 (R)	>32 (R)

S, Susceptible; I, Susceptible to increased exposure; R, Resistant. *EUCAST 2024 breakpoints (European Committee on Antimicrobial Susceptibility Testing, 2024) –for *Pseudomonas* spp., imipenem (S ≤0.001; R > 4) and meropenem (S ≤2; R > 8).

Only 1.8% (n=3/169) hand swabs were positive for Gram-negative bacteria. One *P. aeruginosa* ST274 strain (C11Hp4P1) was found on a technician from SAVP-K, showing an early stop codon on *oprD*, leading to failure in of the protein expression; and mutations on *nalC* (Table 2). In SAVP-N, two related *S. maltophilia* ST115 (6 SNP difference, Supplementary Table 7) were detected on the hands of a veterinarian (X4Hp4P2) and a technician (X3Hp4P1). These were closely related to the strains present in the fomites (≤ 10 SNPs difference, Supplementary Table 7), showing likely dissemination across the practice fomites and staff.

3.4 Surface contamination with methicillin-resistant *Staphylococcus* spp.

Nearly five percent (n=23/489) of surfaces were contaminated with methicillin-resistant *Staphylococcus* spp. (MRS). Two veterinary hospitals (SAVP-A; and SAVP-C) and one clinic (SAVP-N) had surfaces contaminated with MR *Staphylococcus pseudintermedius* (MRSP) (n=4) (Table 3). Overall, coagulase-negative MRS isolates predominated (78.3%, n=18/23), especially MR *Staphylococcus epidermidis* (72%, n=13/18) (Table 3). One newly typed ST9220 (clonal complex, or CC, 5) MRSA, harboring SCC*mec*II, was isolated from a cage at the cat ward of hospital SAVP-E.

3.5 Methicillin-resistant *Staphylococcus* spp. transient carriage by staff

A total of 169 nasal swabs were collected, of which 38% were positive for MRS (n=64/169). Amongst these, 14% were MRSA (n=9/64). Further characterization identified them as belonging to different CCs: ST22-IV (also known as EMRSA-15) (n=2) (SAVP-A, n=1; SAVP-B, n=1) and ST974-IV (SAVP-I, n=1) from CC22; ST8-VI (n=3) (SAVP-B, n=2; SAVP-L, n=1) from CC8; ST30-V (SAVP-C, n=1) from CC30; ST9220-II (SAVP-E, n=1) and ST125-IV (SAVP-F, n=1) from CC5. MRSP was not detected.

Considering hand swabs, 22.4% (n=38/169) were positive for MRS, and again, none was identified as MRSP. MLST and SSC*mec* cassette characterization of MRSA (10.5%, n=4/38) yielded the following classifications: ST8-VI (n=2) (SAVP-I, n=1; SAVP-L,

10.3389/fcimb.2025.1582411

TABLE 3 Methicillin resistant *Staphylococcus* spp. on environmental evaluation of SAVPs A-N.

SAVP	Location	Area	Identified organism
A	Waiting room	Weight scale	MRSP
	Operating room	Stainless steel supporting tray	MRSE
B	Treatment area	Treatment table 02	MRSE
		Computer keyboard	
	Cat ward	Cage 06 (group on the left)	MRS
	Operating room 02	Computer keyboard	MRSE
C	Pre-operative area	Tap	MRSP
		Anaesthetic device buttons	
H	Ultrasound room	Ultrasound keyboard	MRSE
J	Examination room/Treatment room	Computer keyboard	MRS
	Examination room/Treatment room	Desk	MRSE
K	Pre-operative/Treatment area	Fridge handle	MRSE
	Operating room	Anesthesia tent - Outside	MRSE
		Operating table - Head	MRSE
		Blanket	MR *Staphylococcus hominis*
	Ward	Inside knob	MRSE
		Drawer handles	
		Pink blanket	
		Tap	
		Shearing blade	*MR Staphylococcus warneri*
E	Operating room	Detergent dispenser	MRS
	Cat ward	Cage left top	MRSA
N	Others	Keyboard personal computer	MRSP

MRSA, Methicillin resistant *S. aureus*; MRSE, Methicillin resistant *S. epidermidis*; MRS, Methicillin resistant *Staphylococcus* spp.; MRSP, Methicillin resistant *S. pseudintermedius*.

n=1) from CC8, ST9220-II (SAVP-E, n=1) from CC5 and non-typable ST from CC45 (SAVP-B, n=1) – it was not possible to type this strain of MRSA, albeit it carried SCC*mec*V.

Both MRSA ST8-VI strains belong to different clinics, despite being part of the same business group, with these members rotating between the different practices.

Interestingly, the new MRSA ST9220-II was only identified on SAVP-E in one surface, one nasal swab from a nurse, and one hand swab from a technician, pointing to an ongoing dissemination within this veterinary hospital.

4 Discussion

This study depicts the environmental contamination and veterinary staff carriage by resistant bacteria towards medically important antimicrobials within veterinary clinics and hospitals in Portugal. It was found that 6.5% (n=32/490) surfaces analyzed were positive for MDROs, amongst which were detected carbapenem-resistant bacteria, namely OXA-23-producing *Acinetobacter* spp., (n=5) and IMP-8 *P. juntendi* (n=2). Veterinary carriage analysis revealed that 38% and 22.4% were positive for MRS in their nasal cavities and hand swabs, respectively. For rectal swabs, only 16.7% yielded carbapenem-resistant bacteria carriage.

Notably, carbapenem-resistant Gram-negative bacteria (*Acinetobacter* spp., *Pseudomonas* spp. and *S. maltophilia*) and MRSA, belonging to epidemiologically relevant clones such as EMRSA-15, were found in several high-touch surfaces and fomites of SAVPs. The SAVP-G is a particularly interesting case, since, despite having a high self-assessment score about ongoing IPC procedures, it showed the highest level of environmental contamination, together with the isolation of the highest diversity of resistant bacteria. These results highlight that inadequate/insufficient IPC programs or the lack of compliance to them, may facilitate environmental contamination by MDROs, increasing the chance of their dissemination within SAVP and into the environment and community (e.g., staff, tutors, animal patients).

The hygiene evaluation of high-touch surfaces was conducted by two distinct methods, using contact plates and/or surface swabs.

The observed discrepancies between results could be attributed to the design of the contact plates, which support the growth of all types of microorganisms (such as fungi and yeast), while surface swabs are loaded with a universal neutralizing liquid buffer specifically geared towards bacterial growth. Conversely, swabs can be used to evaluate irregular surfaces, supporting the use of both techniques for a more complete evaluation of environmental contamination. Considering both methods, 96 surfaces failed the cleaning efficacy assessment (Dancer, 2004). Coincidently, most of these were high-rotation surfaces such as weight scales, sinks and taps, animal cages and computer keyboards.

The worldwide ongoing rising in carbapenem-resistance is worrisome, as these are last-line antibiotics (EMA, 2019). In this study carbapenem-resistant bacteria and possible dissemination events within some SAPV were detected. On SAVP-H, OXA-23-producing *Acinetobacter* spp. strains were found on different surfaces of the same room, indicating a possible transfer (previously published (Moreira da Silva et al., 2024a)).

The detection of various clones of carbapenem-resistant *P. aeruginosa* strains on high-touch surfaces is worrisome. Between 2022-2023, 7.9% of healthcare-associated infections reported in Europe in the human healthcare setting were caused by *P. aeruginosa*, of which 29.7% were resistant to carbapenems (European Centre for Disease Prevention and Control, 2024). *P. aeruginosa* ST244, ST27 and ST253 clonal lineages are commonly associated with outbreaks and nosocomial infections in humans (del Barrio-Tofiño et al., 2020). A previous study conducted in a veterinary teaching hospital reported the presence of *P. aeruginosa* ST244 on sinks (Soonthornsit et al., 2023), while *P. aeruginosa* ST27 has higher affinity towards cystic-fibrosis patients (Weimann et al., 2024). There aren't any guidelines that support rectal sampling on healthy healthcare-workers in human medicine, as studies have shown that in low prevalence settings of MDROs, the transient carriage by healthcare-workers will also be low (Bassyouni et al., 2015; Decker et al., 2018). Since in this study's context, the reality of MDROs carriage by healthcare-workers is unknown, we decided to evaluate it. The low percentage of rectal samples positive for carbapenem-resistant bacteria (n=5/30, 16.7%) of veterinary healthcare-workers aligned with what is already known in human medicine as they work in a low-exposure setting to MDROs.

Strains reported on our study were from healthy human samples (*P. aeruginosa* ST244 from one nasal and one rectal swab from unrelated individuals; carbapenem-resistant *P. aeruginosa* ST27 from one rectal swab). Although SAVP-I and SAVP-K belong to the same business group, it was interesting to perceive that each SAVP had its own associated clone shared between staff members, namely, *P. aeruginosa* ST244 on SAVP-I, and carbapenem-resistant *P. aeruginosa* ST274 on SAVP-K (rectal swab and hand swab from unrelated individuals). Although none of these clones were recovered from the environment, their sharing among team members points to their potential for dissemination. These results highlight the importance of screening veterinary staff as part of an effective IPC protocol to identify potential carriers, thereby preventing transmission to patients, staff, and the community. Moreover, a carbapenem-resistant *P. aeruginosa* ST253 was present on a plastic mat on a countertop inside an isolation unit (SAVP-G), an area with specific cleaning and disinfection protocols (Weese, 2004), and although it is not expected for this area to be completely sterile, potentially nosocomial microorganisms should not be present.

Genetically unrelated IMP-8-producing *P. juntendi* strains were present on the inside of an empty cage and on the plastic cover of the treatment table in the dog ward of SAVP-G. To the best of our knowledge, this is the first description of IMP-8-producing *P. juntendi*. So far, only one description of carbapenem-resistant *P. juntendi*, harboring an IMP-1, has been made in a Chinese human patient (Zheng et al., 2022). This data highlights the capacity of this species to acquire and disseminate resistance genetic elements, making it a pathogen to be considered in epidemiological surveillance schemes.

S. maltophilia is an opportunistic pathogen with intrinsic resistance to many antibiotics, including carbapenem, posing major challenges in clinical settings (Mojica et al., 2022). In our study, multiple clones (including the new ST967 and ST1185) of *S. maltophilia* were described in the environment of various SAVPs, as well as colonizing staff members. These bacteria are ubiquitous in the environment, yet they have also been associated with nosocomial and community-acquired infections (Gröschel et al., 2020; Mojica et al., 2022; European Centre for Disease Prevention and Control, 2024) The relatedness between environmental and pathogenic *S. maltophilia* strains has been described, indicating that the environment may be a source of human contamination – including from sinks and taps (Mojica et al., 2022). As expected, the majority of the contaminated surfaces in our study were water-related. The spread of *S. maltophilia* through fomites ultimately causing human infection has also been described (Gideskog et al., 2020). The occurrence of *S. maltophilia* ST115 strains on the handcloth, the practice's mobile phone and on the hands of two staff members of SAVP-N demonstrate that such objects likely acted as fomite and contributed to dissemination of this clone (Gideskog et al., 2020). Yet, in veterinary medicine, reports of infections caused by this agent are rare. Nonetheless, *S. maltophilia* ST115 clonal lineage has been associated with infections in cats (Shimizu et al., 2021), underscoring its disease-causing capability and the importance of closely monitoring it.

In Europe and according to the 2022–2023 ECDC report, 23.7% of *S. aureus* causing healthcare-associated infections were MRSA, showing a 6.3% decrease from the previous report (European Centre for Disease Prevention and Control, 2024). EMRSA-15 is a major clone found in hospitals and in the community in Portugal (Tavares et al., 2013). This epidemic clone has also been described on clinical strains from pets (Couto et al., 2015; Costa et al., 2022), with studies showing that working in close contact with companion animals is a risk factor for MRSA carriage (Weiß et al., 2013; Bal et al., 2016; Feßler et al., 2018; Rodrigues et al., 2018). The newly described MRSA ST9220-II, belonging to CC5, was found on SAVP-E. The presence on a surface as well as on a nasal swab from a nurse and a hand swab from a technician suggests that this

clone might be spreading within this veterinary practice, possibly through contaminated surfaces.

A Portuguese study identified 61% of nasal carriage of MRS among veterinary professionals (Rodrigues et al., 2018), which is higher than what was found in the present study. However, this same study reported 14% carriage of MRSA, comparable to our findings, with EMRSA-15 also being the most prevalent clone (Rodrigues et al., 2018). The frequent colonization by MRS and MRSA reported in these two studies showcases that veterinary healthcare providers may contribute to the transmission cycle of these pathogens into the community. The frequency of MRSA recovered from hand swabs was lower. It is known that hand hygiene is a pivotal measure in IPC programs, with studies showing that improvements in the healthcare workers' hand hygiene protocols cause a direct decrease in the carriage of MRSA (Marimuthu et al., 2014).

Overall, the detection of MRS and carbapenem-resistant Gram-negative bacteria on high-touch surfaces in SAVPs underscores the need for strict IPC procedures. These measures are essential not only to protect patients but also to address the ongoing antimicrobial resistance crisis.

5 Conclusion

The current study depicts varying levels of environmental contamination and staff carriage of carbapenem-resistant Gram-negative and MRS strains in SAVP across Portugal. These findings question the effectiveness of ongoing IPC protocols and highlight the risk of environment/staff cross-contamination through high-touch surfaces. This data suggests that SAVP may play an active role in the spread of priority pathogens resistant to medically important antimicrobials, emphasizing the need for targeted educational workshops for veterinary healthcare students and professionals. In the long run, implementing and monitoring evidence-based IPC protocols and staff training should be mandatory to ensure strict compliance in SAVP.

Data availability statement

The datasets presented in this study can be found in online repositories. The names of the repository/repositories and accession number(s) can be found below: https://www.ncbi.nlm.nih.gov/, PRJNA1131754 https://www.ncbi.nlm.nih.gov/, PRJNA1000421.

Ethics statement

The studies involving humans were approved by the Comissão de ética e bem-estar animal (CEBEA) of Veterinary Faculty of the University of Lisbon - CEBEA011/2021. The studies were conducted in accordance with the local legislation and institutional requirements. The participants provided their written informed consent to participate in this study.

Author contributions

JMS: Conceptualization, Data curation, Investigation, Writing – original draft, Writing – review & editing. JM: Investigation, Writing – review & editing. LF: Investigation, Writing – review & editing. CM: Writing – original draft, Writing – review & editing. SC: Writing – review & editing. DT: Writing – review & editing. AA: Writing – review & editing. CP: Conceptualization, Supervision, Writing – review & editing.

Funding

The author(s) declare that financial support was received for the research and/or publication of this article. This research was funded by the Portuguese Foundation for Science and Technology (FCT), under projects UIDB/00276/2020 (CIISA) and LA/P/0059/2020 (AL4AnimalS) and GHTM through FCT (UID/04413/2020) and LA-REAL -LA/P/0117/2020. This study was funded by FCT project 2022.08669.PTDC. -VetCare. JMS, JM and LF were supported by a Fundação para a Ciência e Tecnologia (FCT) PhD fellowship (2020.06540.BD; 2020.07562.BD; UI/BD/153070/2022, respectively).

Acknowledgments

The authors would like to thank all the members of the small animal veterinary practices participating in the project.

Conflict of interest

The authors declare that the research was conducted in the absence of any commercial or financial relationships that could be construed as a potential conflict of interest.

Generative AI statement

The author(s) declare that no Generative AI was used in the creation of this manuscript.

Publisher's note

Supplementary material

The Supplementary Material for this article can be found online at: https://www.frontiersin.org/articles/10.3389/fcimb.2025.1582411/full#supplementary-material

References

Alcock, B. P., Huynh, W., Chalil, R., Smith, K. W., Raphenya, A. R., Wlodarski, M. A., et al. (2023). CARD 2023: expanded curation, support for machine learning, and resistome prediction at the Comprehensive Antibiotic Resistance Database. *Nucleic Acids Res.* 51, D690–D699. doi: 10.1093/nar/gkac920

Aytan-Aktug, D., Grigorjev, V., Szarvas, J., Clausen, P. T. L. C., Munk, P., Nguyen, M., et al. (2022). SourceFinder: a machine-learning-based tool for identification of chromosomal, plasmid, and bacteriophage sequences from assemblies. *Microbiol Spectr.* 10. doi: 10.1128/spectrum.02641-22

Bal, A. M., Coombs, G. W., Holden, M. T. G., Lindsay, J. A., Nimmo, G. R., Tattevin, P., et al. (2016). Genomic insights into the emergence and spread of international clones of healthcare-, community- and livestock-associated meticillin-resistant Staphylococcus aureus: Blurring of the traditional definitions. *J. Global Antimicrobial Resistance. Elsevier Ltd;* 6, 95–101. doi: 10.1016/j.jgar.2016.04.004

Bassyouni, R. H., Gaber, S. N., and Wegdan, A. A. (2015). Fecal carriage of extended-spectrum β-lactamase- and AmpC- producing escherichia coli among healthcare workers. *J. Infect. Dev. Ctries.* 9, 304–308. doi: 10.3855/jidc.5633

Brooke, J. S. (2021). Advances in the microbiology of stenotrophomonas maltophilia. *Clin. Microbiol. Rev.* 34. doi: 10.1128/CMR.00030-19

Costa, S. S., Ribeiro, R., Serrano, M., Oliveira, K., Ferreira, C., Leal, M., et al. (2022). Staphylococcus aureus causing skin and soft tissue infections in companion animals: antimicrobial resistance profiles and clonal lineages. *Antibiotics.* 11, 599. doi: 10.3390/antibiotics11050599

Couto, N., Belas, A., Kadlec, K., Schwarz, S., and Pomba, C. (2015). Clonal diversity, virulence patterns and antimicrobial and biocide susceptibility among human, animal and environmental MRSA in Portugal. *J. Antimicrobial Chemotherapy.* 70, 2483–2487. doi: 10.1093/jac/dkv141

Dancer, S. J. (2004). How do we assess hospital cleaning? A proposal for microbiological standards for surface hygiene in hospitals. *J. Hosp. Infection.* 56, 10–15. doi: 10.1016/j.jhin.2003.09.017

Dashti, A. A., Jadaon, M. M., Abdulsamad, A. M., and Dashti, H. M. (2009). Heat treatment of bacteria: A simple method of DNA extraction for molecular techniques. *Kuwait Med. J.* 41, 117–122. Available online at: https://applications.emro.who.int/imemrf/kmj_2009_41_2_117.pdf.

Decker, B. K., Lau, A. F., Dekker, J. P., Spalding, C. D., Sinaii, N., Conlan, S., et al. (2018). Healthcare personnel intestinal colonization with multidrug-resistant organisms. *Clin. Microbiol. Infection.* 24, 82.e1–82.e4. doi: 10.1016/j.cmi.2017.05.010

del Barrio-Tofiño, E., López-Causapé, C., and Oliver, A. (2020). Pseudomonas aeruginosa epidemic high-risk clones and their association with horizontally-acquired β-lactamases: 2020 update. *Int. J. Antimicrob Agents* 56. doi: 10.1016/j.ijantimicag.2020.106196

Dulon, M., Haamann, F., Peters, C., Schablon, A., and Nienhaus, A. (2011). Mrsa prevalence in european healthcare settings: A review. *BMC Infect. Dis.* 11. doi: 10.1186/1471-2334-11-138

EMA (2019). *Categorisation of antibiotics for use in animals for prudent and responsible use* (European Medicines Agency), 1–73. Available at: https://www.ema.europa.eu/en/documents/report/categorisation-antibiotics-european-union-answer-request-european-commission-updating-scientific_en.pdf (Accessed July 30, 2024).

Eurodev (2024). *Exploring the veterinary industry in europe*. Available online at: https://www.eurodev.com/blog/veterinary-industry-in-europe-trends (Accessed Jun 14, 2024).

European Centre for Disease Prevention and Control (2016). *Expert opinion on whole genome sequencing for public health surveillance Strategy to harness whole genome sequencing to strengthen EU outbreak investigations and public health surveillance*. Available online at: www.ecdc.europa.eu (Accessed April 12, 2025).

European Centre for Disease Prevention and Control (2024). *Point prevalence survey of healthcare-associated infections and antimicrobial use in European acute care hospitals 2022-2023*. Available online at: www.ecdc.europa.eu (Accessed July 30, 2024).

European Committee on Antimicrobial Susceptibility Testing. (2024). "The European Committee on Antimicrobial Susceptibility Testing," in *Breakpoint tables for interpretation of MICs and zone diameters. Version 14.0*, vol. 2024.

Feßler, A. T., Schuenemann, R., Kadlec, K., Hensel, V., Brombach, J., Murugaiyan, J., et al. (2018). Methicillin-resistant Staphylococcus aureus (MRSA) and methicillin-resistant Staphylococcus pseudintermedius (MRSP) among employees and in the environment of a small animal hospital. *Vet Microbiol.* 221, 153–158. doi: 10.1016/j.vetmic.2018.06.001

Gentilini, F., Turba, M. E., Pasquali, F., Mion, D., Romagnoli, N., Zambon, E., et al. (2018). Hospitalized pets as a source of carbapenem-resistance. *Front. Microbiol* 9, 1-9. doi: 10.3389/fmicb.2018.02872

Gideskog, M., Welander, J., and Melhus, Å. (2020). Cluster of S. maltophilia among patients with respiratory tract infections at an intensive care unit. *Infection Prev. Practice.* 2. doi: 10.1016/j.infpip.2020.100097

Grönthal, T., Österblad, M., Eklund, M., Jalava, J., Nykäsenoja, S., Pekkanen, K., et al. (2018). Sharing more than friendship – transmission of NDM-5 ST167 and CTX-M-9 ST69 Escherichia coli between dogs and humans in a family, Finland, 2015. *Eurosurveillance* 23. doi: 10.2807/1560-7917.ES.2018.23.27.1700497

Gröschel, M. I., Meehan, C. J., Barilar, I., Diricks, M., Gonzaga, A., Steglich, M., et al. (2020). The phylogenetic landscape and nosocomial spread of the multidrug-resistant opportunist Stenotrophomonas maltophilia. *Nat. Commun.* 11. doi: 10.1038/s41467-020-15123-0

Hemeg, H. A. (2021). Determination of phylogenetic relationships among methicillin-resistant Staphylococcus aureus recovered from infected humans and Companion Animals. *Saudi J. Biol. Sci.* 28, 2098–2101. doi: 10.1016/j.sjbs.2021.01.017

Jolley, K. A., Bray, J. E., and Maiden, M. C. J. (2018). Open-access bacterial population genomics: BIGSdb software, the PubMLST.org website and their applications. *Wellcome Open Res.* 3. doi: 10.12688/wellcomeopenres.14826.1

Kondo, Y., Ito, T., Ma, X. X., Watanabe, S., Kreiswirth, B. N., Etienne, J., et al. (2007). Combination of multiplex PCRs for staphylococcal cassette chromosome mec type assignment: Rapid identification system for mec, ccr, and major differences in junkyard regions. *Antimicrob Agents Chemother.* 51, 264–274. doi: 10.1128/AAC.00165-06

Marimuthu, K., Pittet, D., and Harbarth, S. (2014). The effect of improved hand hygiene on nosocomial MRSA control. *Antimicrobial Resistance Infection Control* 3. doi: 10.1186/2047-2994-3-34

Mathers, A. J., Peirano, G., and Pitout, J. D. D. (2015). The role of epidemic resistance plasmids and international high- risk clones in the spread of multidrug-resistant Enterobacteriaceae. *Clin. Microbiol Rev.* 28, 565–591. doi: 10.1128/CMR.00116-14

Menezes, J., Frosini, S. M., Belas, A., Marques, C., da Silva, J. M., Amaral, A. J., et al. (2023). Longitudinal study of ESBL/AmpC-producing Enterobacterales strains sharing between cohabiting healthy companion animals and humans in Portugal and in the United Kingdom. *Eur. J. Clin. Microbiol. Infect. Diseases.* 42, 1011–1024. doi: 10.1007/s10096-023-04629-2

Menezes, J., Moreira da Silva, J., Frosini, S. M., Loeffler, A., Weese, S., Perreten, V., et al. (2022). mcr-1 colistin resistance gene sharing between Escherichia coli from cohabiting dogs and humans, Lisbon, Portugal, 2018 to 2020. *Eurosurveillance* 27. doi: 10.2807/1560-7917.ES.2022.27.44.2101144

Mojica, M. F., Humphries, R., Lipuma, J. J., Mathers, A. J., Rao, G. G., Shelburne, S. A., et al. (2022). Clinical challenges treating Stenotrophomonas maltophilia infections: An update. *JAC-Antimicrobial Resistance* 4. doi: 10.1093/jacamr/dlac040

Moreira da Silva, J., Menezes, J., Fernandes, L., Marques, C., Costa, S. S., Timofte, D., et al. (2024a). Dynamics of blaOXA-23 gene transmission in Acinetobacter spp. from contaminated veterinary environmental surfaces: an emerging One Health threat? *J. Hosp. Infection.* 146, 116–124. doi: 10.1016/j.jhin.2024.02.001

Moreira da Silva, J., Menezes, J., Fernandes, L., Santos Costa, S., Amaral, A., and Pomba, C. (2024b). Carbapenemase-producing Enterobacterales strains causing infections in companion animals—Portugal. *Microbiol Spectr.*doi: 10.1128/spectrum.03416-23

Mulvey, D., Redding, P., Robertson, C., Woodall, C., Kingsmore, P., Bedwell, D., et al. (2011). Finding a benchmark for monitoring hospital cleanliness. *J. Hosp. Infection* 77, 25–30. doi: 10.1016/j.jhin.2010.08.006

Murray, C. J., Ikuta, K. S., Sharara, F., Swetschinski, L., Robles Aguilar, G., Gray, A., et al. (2022). Global burden of bacterial antimicrobial resistance in 2019: a systematic analysis. *Lancet* 399, 629–655. doi: 10.1016/S0140-6736(21)02724-0

Nienhoff, U., Kadlec, K., Chaberny, I. F., Verspohl, J., Gerlach, G. F., Schwarz, S., et al. (2009). Transmission of methicillin-resistant Staphylococcus aureus strains between humans and dogs: Two case reports. *J. Antimicrobial Chemotherapy.* 64, 660–662. doi: 10.1093/jac/dkp243

Rodrigues, A. C., Belas, A., Marques, C., Cruz, L., Gama, L. T., and Pomba, C. (2018). Risk factors for nasal colonization by methicillin-resistant staphylococci in healthy humans in professional daily contact with companion animals in Portugal. *Microb Drug Resist.* 24, 434–446. doi: 10.1089/mdr.2017.0063

Schmidt, J. S., Kuster, S. P., Nigg, A., Dazio, V., Brilhante, M., Rohrbach, H., et al. (2020). Poor infection prevention and control standards are associated with environmental contamination with carbapenemase-producing Enterobacterales and other multidrug-resistant bacteria in Swiss companion animal clinics. *Antimicrob Resist. Infect. Control.* 9, 1–13. doi: 10.1186/s13756-020-00742-5

Schürch, A. C., Arredondo-Alonso, S., Willems, R. J. L., and Goering, R. V. (2018). Whole genome sequencing options for bacterial strain typing and epidemiologic analysis based on single nucleotide polymorphism versus gene-by-gene–based approaches. *Clin. Microbiol. Infection* 24, 350–354. doi: 10.1016/j.cmi.2017.12.016

Sing, A., Tuschak, C., and Hörmansdorfer, S. (2008). Methicillin-resistant *Staphylococcus aureus* in a family and its pet cat. *N. Engl. J. Med.* 358 (11), 1200–1201. doi: 10.1056/NEJMc0706805

Shimizu, T., Tsuyuki, Y., Shimoike, K., Iyori, K., Miyamoto, T., and Harada, K. (2021). Antimicrobial resistance and multilocus sequence types of Stenotrophomonas maltophilia isolated from dogs and cats in Japan. *J. Med. Microbiol* 70. doi: 10.1099/jmm.0.001344

Soonthornsit, J., Pimwaraluck, K., Kongmuang, N., Pratya, P., and Phumthanakorn, N. (2023). Molecular epidemiology of antimicrobial-resistant Pseudomonas aeruginosa in a veterinary teaching hospital environment. *Vet Res. Commun.* 47, 73–86. doi: 10.1007/s11259-022-09929-0

Srinivasan, R., Karaoz, U., Volegova, M., MacKichan, J., Kato-Maeda, M., Miller, S., et al. (2015). Use of 16S rRNA gene for identification of a broad range of clinically relevant bacterial pathogens. *PloS One* 10, 1–22. doi: 10.1371/journal.pone.0117617

Tavares, A., Miragaia, M., Rolo, J., Coelho, C., and De Lencastre, H. (2013). High prevalence of hospital-associated methicillin-resistant Staphylococcus aureus in the community in Portugal: Evidence for the blurring of community-hospital boundaries. *Eur. J. Clin. Microbiol. Infect. Diseases.* 32, 1269–1283. doi: 10.1007/s10096-013-1872-2

Volkov, S. (2024). *WHO List of Medically Important Antimicrobials A risk management tool for mitigating antimicrobial resistance due to non-human use*. Available online at: https://iris.who.int/ (Accessed August 1, 2024).

Weese, J. S. (2004). "Barrier precautions, isolation protocols, and personal hygiene in veterinary hospitals," in *Veterinary clinics of north america - equine practice* 20 (3), 543–559. doi: 10.1016/j.cveq.2004.07.006

Weiß, S., Kadlec, K., Feßler, A. T., and Schwarz, S. (2013). Identification and characterization of methicillin-resistant Staphylococcus aureus, Staphylococcus epidermidis, Staphylococcus haemolyticus and Staphylococcus pettenkoferi from a small animal clinic. *Vet Microbiol* 167, 680–685. doi: 10.1016/j.vetmic.2013.07.036

Weimann, A., Dinan, A. M., Ruis, C., Bernut, A., Pont, S., Brown, K., et al. (2024). Evolution and host-specific adaptation of Pseudomonas aeruginosa. *Sci. (1979)* 385. doi: 10.1126/science.adi0908

World Health Organization. (2023). *Global strategy on infection prevention and control*. Geneva: World Health Organization; 2023. Licence: CC BY-NC-SA 3.0 IGO.

Zheng, L., Zhang, X., Zhu, L., Lu, G., Guan, J., Liu, M., et al. (2022). A clinical Pseudomonas juntendi strain with blaIMP–1 carried by an integrative and conjugative element in China. *Front. Microbiol*, 13. doi: 10.3389/fmicb.2022.929800/full

frontiers | Frontiers in Cellular and Infection Microbiology

TYPE Review
PUBLISHED 14 May 2025
DOI 10.3389/fcimb.2025.1582037

OPEN ACCESS

EDITED BY
Massimiliano Lucidi,
Roma Tre University, Italy

REVIEWED BY
Yafeng Dou,
Wuhan University, China
Siwei Mo,
Zunyi Medical University, China

*CORRESPONDENCE
Ganzhu Feng
fgz62691@163.com

RECEIVED 23 February 2025
ACCEPTED 17 April 2025
PUBLISHED 14 May 2025

CITATION
Bao C, Zhang Y, Feng J, Hong X, Gao N and Feng G (2025) Deciphering tuberculosis: lysosome-centric insights into pathogenesis and therapies.
Front. Cell. Infect. Microbiol. 15:1582037.
doi: 10.3389/fcimb.2025.1582037

Deciphering tuberculosis: lysosome-centric insights into pathogenesis and therapies

Cui Bao[1,2], Yuanyuan Zhang[1,2], Jiao Feng[1,2], Xiuwen Hong[1,2], Nan Gao[1,2] and Ganzhu Feng[1]*

[1]Department of Respiratory and Critical Care Medicine, The Second Affiliated Hospital of Nanjing Medical University, Nanjing, Jiangsu, China, [2]Department of Respiratory and Critical Care Medicine, The Second Clinical Medical School of Nanjing Medical University, Nanjing, Jiangsu, China

Tuberculosis is a widely spread disease caused by *Mycobacterium tuberculosis* (Mtb). The pathogenicity of the pathogen is closely associated with the immune defense mechanisms of the host cells. As key cellular degradation and metabolic centers, lysosomes critically regulate tuberculosis infection. When Mtb invades the host, it is taken up by macrophages and enters phagosomes. Subsequently, the phagosomes fuse with lysosomes and form phagolysosomes, which eliminate the pathogenic bacteria through the acidic environment and hydrolytic enzymes within lysosomes. However, Mtb can interfere with the normal functions of lysosomes through various strategies. It can secrete specific factors (such as ESAT-6, ppk-1, and AcpM) to inhibit the acidification of lysosomes, enzyme activity, and the fusion of phagosomes and lysosomes, thereby enabling Mtb proliferation within host cells. An in-depth exploration of the mechanism of the interaction between Mtb and lysosomes will both uncover bacterial immune evasion strategies and identify novel anti-tuberculosis therapeutic targets.

KEYWORDS

***Mycobacterium tuberculosis* (Mtb), lysosomes, interaction, mechanism, treatment**

1 Introduction

Tuberculosis is mainly caused by the intracellular pathogen *Mycobacterium tuberculosis* (Mtb). It most commonly infects the lungs but can also affect other organs, including the intestines and bones. It seriously threatens human health and poses a heavy burden on global health services. According to the "Global Tuberculosis Report 2024" released by the World Health Organization (WHO), it was estimated that 10.8 million people worldwide suffered from TB and approximately 400,000 had drug-resistant tuberculosis (DR-TB); additionally, the disease caused 1.25 million deaths globally (Organization, W.H, 2023). Factors such as poverty, malnutrition, HIV infection, smoking, diabetes, chemotherapy, and weakened immunity all significantly increase individuals' susceptibility to infections (Chai et al., 2018; Luies and du Preez, 2020). Fortunately, TB is a preventable and generally curable disease, and currently, the first-line

drugs for TB treatment include isoniazid, rifampicin, pyrazinamide, ethambutol, and streptomycin (Zumla et al., 2013). However, the emergence of multidrug-resistant tuberculosis (MDR-TB) has presented new challenges to the treatment of TB. Thus, in-depth study of the interaction between Mtb infection and the host is conducive to our exploration of new treatment approaches.

Lysosomes are organelles discovered by de Duve in 1955 through specific enzyme staining with the aid of light microscopes and electron microscopes (de Duve, 2005). Lysosomes are acidic organelles encapsulated by a single membrane with a pH value of approximately 4.6. The endolysosomal system in cells consists of early endosomes (EE), recycling endosomes (RE), late endosomes (LE), and lysosomes (LY), and it is crucial for a variety of cellular functions, including membrane trafficking, protein transport, autophagy, and signal transduction (Luzio et al., 2007). The lysosomes contain a variety of hydrolases, including acid phosphatase, protease, lipase, and glycosidase, and the acidic interior optimally activates these hydrolases and facilitates the breakdown of intracellular waste and exogenous pathogens (Appelqvist et al., 2013). In addition, lysosomes can also eliminate pathogens through various pathways such as forming phagolysosomes by fusing with phagosomes, autophagy, and so on (Levine and Kroemer, 2008). As an organelle widely existing in eukaryotic cells, lysosomes not only degrade and recycle intracellular waste, organelles, and exogenous substances, but also regulate cell metabolism, mediate signal transduction, and participate in immune responses (Saftig and Klumperman, 2009).

When Mtb invades the body, macrophages serve as the first line of defense against its infection, swiftly recognizing and phagocytosing this pathogen (Russell, 2011). Meanwhile, lysosomes, as extremely crucial degradative organelles within cells, undertake the vital task of degrading pathogens within macrophages, playing a pivotal role in defending against Mtb infections (Armstrong and Hart, 1971). This review aims to delve deeply into the interaction between lysosome function and Mtb (show in Figure 1). Through in-depth exploration on the key role of lysosomes in Mtb, we deeply expect to provide a meaningful scientific theory for guiding anti-TB research, and thereby providing corresponding strategies for the treatment of TB.

2 The effect of Mtb infection on lysosomes

The Esx-1 secretion system (ESX-1), a specialized type VII secretion system (T7SS) unique to pathogenic mycobacteria including Mtb, is encoded by the genomic region of difference 1 (RD1) locus (Cole et al., 1998; Behr et al., 1999). On the one hand, ESX-1 secretes effector proteins, such as ESAT-6 and CFP-10. Both are immunodominant antigens and major virulence factors of Mtb, which disrupt the host cell membrane's integrity to assist Mtb to more easily invade cells (Simeone et al., 2009). On the other hand, it can assist Mtb in surviving within cells by damaging phagosome membranes, preventing the fusion of autophagosomes with lysosomes and so on (Simeone et al., 2012) (Lienard et al., 2023). Transcriptomic and functional studies revealed that CD11c low monocyte-derived cells (MNC1) display compromised lysosomal activity (reduced TFEB expression, acidification, and proteolysis) relative to alveolar macrophages (AMs) and CD11c high counterparts (MNC2). Paradoxically, MNC1 exhibit superior capacity to harbor viable Mtb. This paradox is partly explained by Mtb's ESX-1, which actively recruits lysosome-impaired MNC1 to lung tissue, creating protective niches for bacterial persistence. Targeting this host vulnerability, c-Abl inhibitors (e.g., nilotinib) restore lysosomal function via TFEB activation, proposing a novel host-directed therapy (HDT) to eliminate Mtb reservoirs (Zheng et al., 2024). Moreover, the Mtb Type VII secretion system effector Rv2347c employs a dual mechanism to subvert host defenses: it employs a dual mechanism to subvert host defenses, and it not only suppresses phagosome maturation by downregulating early markers (RAB5/EEA1), but also compromises lysosomal membrane integrity, ultimately facilitating bacterial escape from the degradative compartment (Jiang et al., 2024). MptpB, encoded by Rv0153c, as an effector molecule of the type VII secretion system of Mtb, is a key TB virulence factor with phosphoinositide phosphatase activity (Singh et al., 2005; Beresford et al., 2007). By dephosphorylating PI3P, it impedes phagosome maturation and lysosome–phagosome fusion, protecting Mtb from destruction (Beresford et al., 2007). On the basis of this, the MptpB inhibitor C13 enhances mycobacterial clearance through dual mechanisms: restructuring PI3P–phagosome interactions to promote phagolysosomal fusion, evidenced by increased LAMP-1 colocalization, and exhibiting synergistic bactericidal activity with frontline antibiotics (rifampin, bedaquiline, and pretomanid) through accelerated lysosomal trafficking and intracellular burden reduction (Rodríguez-Fernández et al., 2024). Similarly, AcpM, encoded by Rv2244, plays a crucial role in the biosynthetic pathway of the cell wall and closely related to the pathogenicity and drug resistance of Mtb (Miotto et al., 2022; Ling et al., 2024). It orchestrates immune evasion through dual posttranscriptional sabotage: miR-155-5p-mediated Akt-mTOR activation suppresses TFEB-driven lysosomal biogenesis, while coordinated repression of TFEB-regulated vesicular trafficking (e.g., LAMP1/RAB7) blocks phagolysosomal maturation, creating protected niches for Mtb persistence (Paik et al., 2022). Instead, the sulfolipid SL-1 of Mtb is encoded by Rv3821 and Rv3822 (Seeliger et al., 2012). It suppresses mTORC1 activity to promote TFEB nuclear translocation, thereby activating lysosomal biogenesis and potentiating lysosomal function. Intriguingly, SL-1 demonstrates complementary phagosomal acidification capacity, whereas SL-1-deficient mutants show impaired lysosomal trafficking concomitant with elevated intracellular bacterial survival rates (Sachdeva et al., 2020).

Apart from these, research has identified other influencers. For example, 1-TbAd, an abundant lipid in Mtb that is biosynthesized involving Rv3377c and Rv3378c, has been proven to be a naturally evolved phagolysosome disruptor (Mayfield et al., 2024) (Buter et al., 2019). It penetrates lysosomes, protonates, and concentrates within the acidic lysosomal environment, causing both lysosomal swelling and pH elevation. This cascade inactivates hydrolytic enzymes while hindering autophagosome maturation, thereby facilitating Mtb

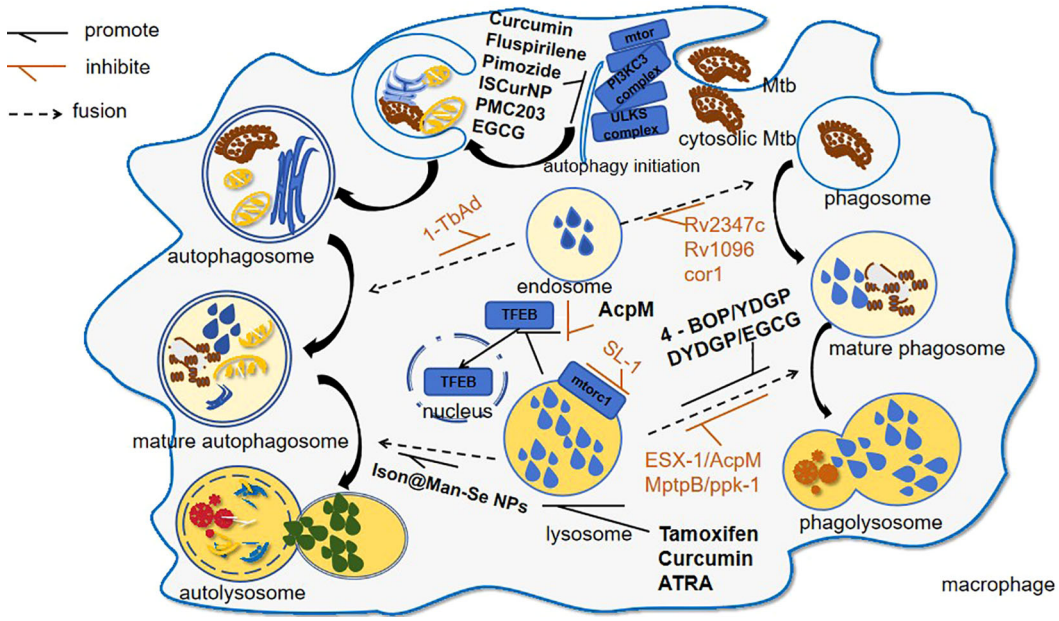

FIGURE 1
Mtb-induced lysosomal modulation and drug interventions following host invasion. This schematic delineates the autophagic and phagocytic pathways activated during Mtb infection: 1. Pathogen-Driven immune evasion: Mtb virulence factors, such as 1-TbAb, inhibit autophagosome maturation; 2. Therapeutic interventions: ① lysosomal potentiators like curcumin through upregulating lysosomal biogenesis; ② autophagy enhancers like Ison@Man-Se NPs through enhancing autophagosome–lysosome fusion.

infection (Bedard et al., 2023). Beyond that, Rv1096 can inhibit the maturation of phagosomes, allowing Mtb to escape into the host cell cytoplasm (Deng et al., 2020). Additionally, PPK, which stands for "Polyphosphate kinase," primarily includes ppk-1 (encoded by Rv2984) and ppk-2 (encoded by Rv3232c) (Singh et al., 2016). They critically regulate Mtb stress adaptation, enhancing resistance to thermal, acidic, oxidative, and hypoxic challenges while potentiating intramacrophage replication through polyP-mediated homeostasis (Cole et al., 1998; Sureka et al., 2007, Sureka et al., 2009; Singh et al., 2013). Chugh et al. (2024 PNAS) revealed polyphosphate kinase-1 (PPK-1) as a central metabolic regulator in Mtb pathogenesis through two complementary mechanisms: PPK-1 deficiency disrupts phthiocerol dimycocerosate (PDIM) biosynthesis to enhance phagolysosomal fusion-mediated bacterial clearance, while pharmacological inhibition of PPK-1 with raloxifene synergizes with frontline anti-TB drugs (isoniazid/bedaquiline) by subverting bacterial metabolic networks, collectively demonstrating the potential to shorten chemotherapy duration and combat MDR-TB through this dual host–pathogen targeting strategy (Chugh et al., 2024).

In addition to the factors aforementioned in TB, it is noteworthy that Coronin 1 (Cor1), a 57-kDa trimeric actin-binding protein essential for leukocyte cytoskeletal dynamics, emerges as a critical mediator of macrophage–Mtb interactions (Stocker et al., 2018). Its structural capacity to orchestrate actin remodeling becomes indispensable for pathogen containment during Mtb phagocytosis (Jayachandran et al., 2007; Bravo-Cordero et al., 2013). Mtb strategically hijacks Cor1 to orchestrate phagosomal arrest through a cAMP–cofilin1 signaling axis. Upon macrophage infection, Cor1 recruitment to phagosomal membranes coincides with cAMP elevation, which activates Slingshot phosphatase to dephosphorylate cofilin1. This cascade induces F-actin depolymerization, disrupting actin remodeling essential for phagosomal trafficking. Crucially, Cor1-mediated dual blockade of both actin cytoskeletal dynamics and vesicular fusion machinery creates protected compartments that evade lysosomal destruction (Saha et al., 2021). Mtb PknG is encoded by Rv0410c (Wang et al., 2021). It subverts host autophagy–lysosome fusion, impairs lysosomal acidification via V-ATPase inhibition, and destabilizes lysosomal membrane integrity, thereby hijacking autophagic flux to establish intracellular survival niches while evading lysosomal degradation, which underscores the therapeutic promise of dual-targeting PknG kinase activity and lysosomal functional restoration in TB treatment (Ge et al., 2022). The molecular mechanisms through which Mtb subverts host lysosomal function via key virulence determinants, along with corresponding therapeutic interventions, are systematically shown in (Table 1).

3 The defense mechanisms of lysosomes against Mtb

3.1 Regulating the homeostasis of lysosomes

Lysosomal damage is a feature in many diseases and hinders cellular health. Inner membrane damage causes organelle instability. How cells stabilize the damaged inner membrane for repair is unclear. Current research shows that under various stresses, cells form stress granules. Stress granules modulate

TABLE 1 The impact of Mtb pathogenic factors on lysosomes.

Virulence Factor	Encoding Genes	Mechanism of Action	Potential Therapeutic Targets
ESX-1 Secretion System	RD1 (Behr et al., 1999)	Secretes ESAT-6/CFP-10 to disrupt host membrane integrity (Simeone et al., 2009); damaging phagosome membranes, preventing the fusion of autophagosomes with lysosomes and so on (Simeone et al., 2012) (Lienard et al., 2023); ESX-1 recruits lysosome-impaired MNC1 to form protective niches; TFEB suppression reduces lysosomal biogenesis (Zheng et al., 2024).	Inhibitors of ESX-1 secretion; c-Abl inhibitors (e.g., nilotinib); lysosome-targeted nanoparticles.
Rv2347c (T7SS effector)	Rv2347c	Downregulates RAB5/EEA1 to block phagosome maturation; disrupts lysosomal membrane integrity (Jiang et al., 2024).	Small-molecule inhibitors of Rv2347c.
MptpB	Rv0153c (Singh et al., 2005)	Dephosphorylates PI3P to impair phagosome–lysosome fusion (Beresford et al., 2007).	MptpB inhibitor (e.g., C13) (Rodríguez-Fernández et al., 2024).
AcpM	Rv2244	Suppresses TFEB-mediated lysosomal biogenesis; blocks RAB7/LAMP1-dependent phagolysosomal fusion (Paik et al., 2022).	miR-155-5p antagonists; Akt-mTOR inhibitors.
SL-1 (Sulfolipid)	Rv3821 and Rv3822 (Seeliger et al., 2012)	Inhibits mTORC1 to activate TFEB, enhancing lysosomal function; promotes phagosomal acidification (Sachdeva et al., 2020).	SL-1 biosynthesis enzyme inhibitors
1-TbAd	Rv3377c and Rv3378c (Mayfield et al., 2024)	Elevates lysosomal pH to inactivate hydrolases; blocks autophagosome maturation (Bedard et al., 2023).	1-TbAd synthase inhibitors.
Rv1096	Rv1096	Inhibits phagosomal maturation (Deng et al., 2020).	Targeted degradation of Rv1096.
PPK-1	Rv2984 and Rv293232c (Singh et al., 2016)	Disrupts PDIM biosynthesis to enhance phagolysosomal fusion; synergizes with isoniazid/bedaquiline (Chugh et al., 2024).	PPK-1 inhibitors [e.g., raloxifene (Chugh et al., 2024)].
Coronin 1	None (it is a protein in macrophage)	Activates cAMP–cofilin1 axis to block phagosomal trafficking; inhibits lysosomal fusion (Saha et al., 2021).	Coronin 1-cAMP interaction inhibitors.
PknG	Rv0410c (Wang et al., 2021)	Inhibits V-ATPase to impair lysosomal acidification; destabilizes lysosomal membranes (Ge et al., 2022).	PknG kinase inhibitors; lysosomal acidification enhancers.

mRNA stability and translation to help cells cope with adverse environments (Protter and Parker, 2016). When host cells are infected with Mtb, lysosomal inner membrane is damaged. Stress granules form at the damage site, prevent further membrane rupture, and assist lysosome repair. They can inhibit Mtb proliferation and spread (Bussi et al., 2023). Simultaneously, Galectin-3 (Gal3), which is involved in processes such as cell adhesion, apoptosis, immune response, and autophagy, recognizes the glycans exposed after lysosomal inner membrane damage and recruits ESCRT components (e.g., ALIX and CHMP4) to promote the repair process (Jia et al., 2020b). The dual repair mechanisms of Mtb-induced lysosomal membrane damage—stress granule stabilization and Galectin-3/ESCRT-mediated remodeling and their role in suppressing bacterial proliferation are shown in (Figure 2a). Therefore, modulating stress granule formation or associated pathways can develop treatment strategies, targeting pathogen and host cell mechanisms to enhance treatment effectiveness and address drug resistance.

Except for lysosomal damage, lysosomes have abnormal functions related to various diseases like Gaucher disease (GD), which is an autosomal recessive genetic disorder classified under lysosomal storage diseases, and is caused by mutations in the GBA1 gene, disrupting glucocerebrosidase in lysosomes, leading to accumulation and dysfunctions (Andrzejczak and Karabon, 2024). However, it is surprising to see that zebrafish with GBA1 deletion showed resistance to infections by Mtb. GBA1 mutations confer resistance to mycobacterial infections in zebrafish by enhancing lysosomal bactericidal activity through glucosylsphingosine accumulation in macrophage lysosomes (as shown in Figure 2b). This lysosomal metabolite exerts bactericidal effects either by modifying membrane properties or by activating enzymatic pathways that potentiate macrophage microbicidal capacity (Fan et al., 2023).

3.2 Affect autophagy

Autophagy is an evolutionarily conserved process where cells employ lysosomes to selectively degrade damaged, senescent, or superfluous biomacromolecules and organelles, with the breakdown products recycled to fuel metabolism and facilitate organelle renewal. This lysosome-mediated degradation pathway serves as a fundamental cellular quality control system (Mizushima and Komatsu, 2011). The autophagic cascade consists of crucial steps: initiation, isolation membrane formation, autophagosome generation, and its fusion with lysosomes, ending in degradation and recycling (Mariño et al., 2014). The regulation of autophagy can be achieved through the following key factors: (1) mTOR (mechanistic target of rapamycin): functions as a central nutrient sensor and master autophagy regulator. In nutrient-abundant conditions, it phosphorylates proteins such as the ULK1 complex, inhibiting the initiation of autophagy. However, in situations of starvation, hypoxia, stress, or under the influence of drugs, the activity of mTOR decreases, triggering autophagy (Kim et al., 2011). (2) The AMPK

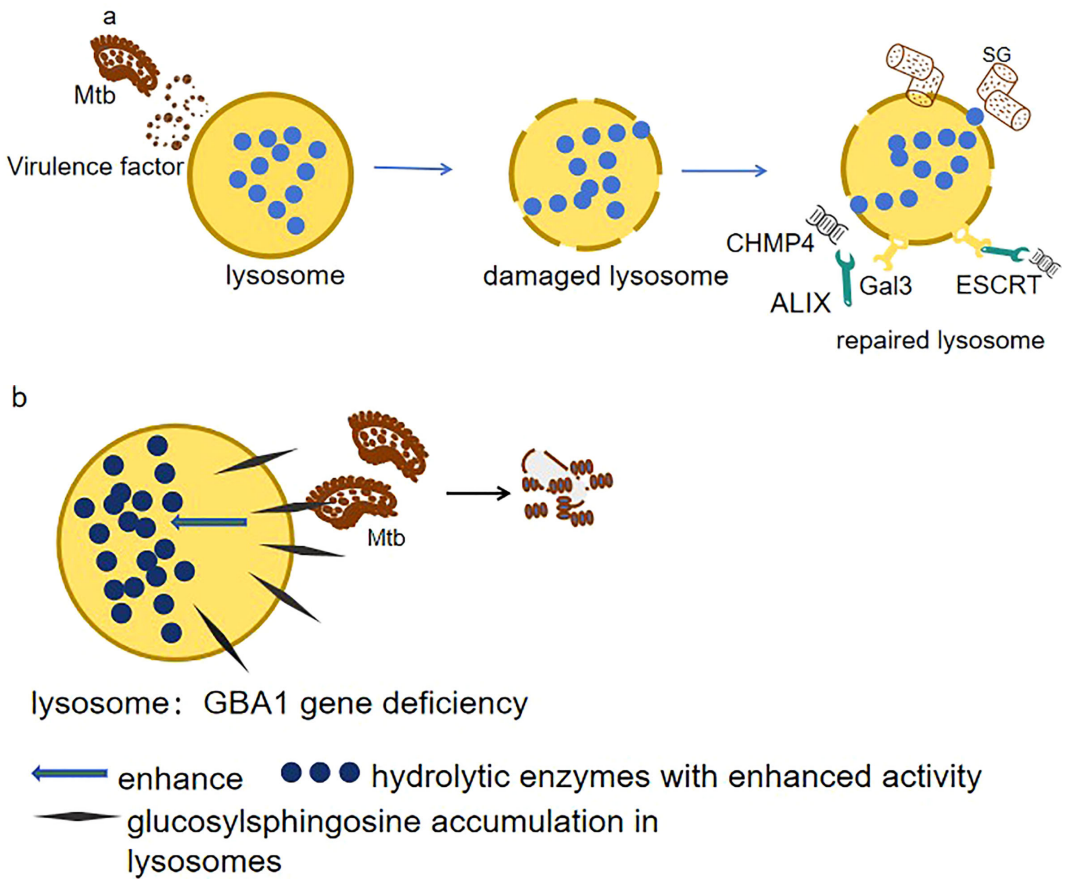

FIGURE 2
(a) Membrane damage resolution. Mtb disrupts lysosomal integrity via ESX-1 secretion system. Host cells counteract this by mobilizing two repair pathways: 1. ESCRT machinery (ALIX/CHMP4): Mediates membrane scission and vesicle shedding to restore lysosomal continuity. 2. Galectin-3 (Gal3)–ubiquitin axis: Recognizes exposed glycans on damaged membranes, recruiting TRIM16 ubiquitin ligase to tag compromised lysosomes for selective autophagy (lysophagy). These coordinated responses inhibit Mtb proliferation by maintaining lysosomal bactericidal capacity. **(b)** Metabolic reprogramming in GBA1 deficiency. Loss of GBA1 elevates glucosylsphingosine (GlcSph) levels in lysosomes, which paradoxically 1. Enhances hydrolase activity: GlcSph stabilizes lysosomal enzymes (e.g., cathepsins), boosting proteolytic degradation of Mtb. 2. Disrupts lipid hijacking: Counters Mtb's strategy to exploit MMGT1-GPR156 lipid droplet axis for survival.

(AMP-activated protein kinase) signaling pathway dominates cellular energy homeostasis. Sensing ATP/AMP ratio, it kicks in when energy wanes (Hardie et al., 2012). Once activated, it curbs mTOR and jump-starts autophagy via the ULK1 (Unc-51 like autophagy activating kinase 1) complex and downstream effectors (Kim et al., 2011). (3) Beclin-1 and the PI3K (phosphatidylinositol 3-kinase) complex: Beclin-1 and the PI3K complex are pivotal in autophagy onset. Their interaction yields PI3P, vital for isolation membrane formation (Tran et al., 2021). (4) TFEB (transcription factor EB): a transcriptional maestro for autophagy and lysosomal biogenesis that relocates to the nucleus during nutrient scarcity or stress to activate both, augmenting intracellular autophagic clearance (Settembre et al., 2011). (5) Oxidative stress: Oxidative stress tweaks autophagy as ROS levels vary. Mild ROS prompts autophagy, and excessive amounts impede and harm cells. Cells deploy antioxidants, e.g., Nrf2, to balance stress and modulate autophagy, safeguarding cell viability in complex settings (Finkel, 2011).

TB infection commonly induces lysosomal dysfunction (Berg et al., 2016; Rombouts and Neyrolles, 2023). Autophagy-related genes (ATGs), in conjunction with their associated proteins and regulatory elements, play pivotal roles in orchestrating cellular responses to lysosomal damage (Cross et al., 2023). Notably, during TB-induced lysosomal damage, membrane Atg8ylation emerges as a central coordinator of stress adaptation. This ubiquitin-like modification directly recruits stress granule (SG) proteins NUFIP2 and G3BP1 to damaged lysosomal membranes, bypassing SG condensate formation. Crucially, NUFIP2 engages the Ragulator-RagA/B complex to suppress mTOR activity, thereby activating autophagy and lysosomal repair programs. These Atg8ylation-driven responses enable cells to survive Mtb infection by restoring lysosomal homeostasis (Jia et al., 2022). When lysosomal membrane repair fails, Gal3 recruits ubiquitin ligases (e.g., TRIM16) to tag damaged lysosomes with ubiquitin signals, initiating lysophagy for their selective autophagic clearance. Concurrently, TFEB activation drives lysosomal biogenesis, ensuring replenishment of functional lysosomes (Jia et al., 2020b). Furthermore, during lysosomal damage, Galectin-9 (Gal9) coordinates AMPK activation by stabilizing ubiquitin signals

through enhanced lysosomal glycoprotein binding and dissociation from the deubiquitinase USP9X, thereby driving metabolic and autophagic adaptation (Jia et al., 2020a). This process directly induces autophagy, leading to autophagy-mediated clearance of the membrane-damaged Mtb.

During TB infection, the host cell initiates a series of defense mechanisms to combat the invading pathogen. For example, during Mtb infection, NCoR1 (nuclear receptor co-repressor 1) acts as a metabolic-immune checkpoint in myeloid cells, dynamically balancing antibacterial responses through AMPK–mTOR–TFEB axis regulation. Early infection upregulates NCoR1 to activate AMPK, which inhibits mTOR and releases TFEB, driving lysosomal autophagy to restrict bacterial growth. NCoR1 depletion disrupts this pathway, accelerating Mtb proliferation, while AMPK agonists (e.g., AICAR) or mTOR inhibitors (e.g., rapamycin) restore lysosomal function and bacterial clearance (Biswas et al., 2023). In another experiment, an interesting phenomenon has been observed: Mesenchymal stem cells (MSCs) expel anti-TB drugs via host ABC transporters, reducing drug efficacy and promoting Mtb survival. In contrast, Mtb's own ABC systems primarily import nutrients (Soni et al., 2020). Targeting both host drug-efflux pumps and pathogen nutrient-import pathways may overcome this dual resistance mechanism. However, recent studies by Aqdas et al. have shed light on a potential countermeasure. They discovered that co-stimulating NOD-2/TLR-4 (N2.T4) in mesenchymal stem cells eliminates intracellular Mtb by enhancing lysosomal degradation (3.8-fold Mtb-lysosome fusion↑) and amplifying autophagy through NF-κB/p38 MAPK signaling, achieving 89% bacterial clearance ($p < 0.001$) and highlighting therapeutic potential (Aqdas et al., 2021). This finding strongly suggests that N2.T4 co-stimulation holds great promise as a potential strategy for eradicating Mtb harbored within MSCs, opening up new avenues for TB treatment research. (Figure 3) shows the integrated autophagy-lysosomal repair network during Mtb infection, including Atg8ylation-driven stress adaptation, Galectin-mediated lysophagy, and NOD-2/TLR-4 co-stimulation as a therapeutic strategy to enhance bacterial clearance.

3.3 Affect phagosomes, lysosomes, and their fusion

Lysosomes are often dubbed the "scavengers" in the body. In the process of lysosomes eliminating foreign substances, the fusion of phagosomes and lysosomes plays a crucial step (Huynh et al., 2007). During phagosome–lysosome fusion, the phagosome's internal pH is gradually lowered to 4.5 by proton pumps, creating an optimal environment for enzyme-mediated degradation upon fusion with lysosomes, which is regulated by GTPase Rab7 and SNARE proteins such as VAMP8 (Hyttinen et al., 2013). Aylan et al. identified ATG7 and ATG14 as essential regulators of Mtb clearance in human macrophages through compartment-specific autophagy mechanisms. ATG14 drives phagosome–lysosome fusion, limiting phagosomal Mtb survival, while ATG7 enables autophagosome formation to restrict cytosolic replication (Aylan et al., 2023). Mtb subverts macrophage defenses by hijacking the p38 MAPK-CREB signaling axis. Upon infection, Mtb activates transcription factor CREB via the p38 MAPK pathway. This CREB-mediated response suppresses phosphorylation of the necroptotic effectors RIPK3 (receptor-interacting serine) and MLKL (mixed lineage kinase domain-like protein), thereby dampening necroptotic signaling. Consequently, the inhibition of necroptosis disrupts phagolysosome fusion, creating a permissive niche for Mtb to evade lysosomal degradation and sustain intracellular proliferation (Leopold Wager et al., 2023). Considering this, targeting the CREB-mediated pathway with small-molecule inhibitors or modulators could avert the drug resistance risk of direct antibacterial therapies. Additionally, uncovering the specific early genes upregulated by M.tb-induced CREB activation and their functions may reveal novel therapeutic targets. Moreover, SLAMF1 (signaling lymphocytic activation molecule family member 1) serves as a critical regulator of Mtb containment in macrophages. Mtb infection upregulates SLAMF1 expression, which directly enhances bacterial uptake through receptor-mediated phagocytosis. Strikingly, stimulation of SLAMF1 with agonistic antibodies further amplifies this phagocytic capacity. Mechanistically, SLAMF1 colocalizes with Mtb-containing phagosomes and dynamically associates with both early (Rab5) and late (Rab7/LAMP1) endolysosomal markers, driving phagosome maturation toward bactericidal lysosomal compartments. This SLAMF1-dependent endolysosomal reprogramming potently restricts intracellular Mtb survival (Barbero et al., 2021). Similarly, BTLA, an immunoregulatory receptor highly expressed on lymphocytes and macrophages, modulates immune responses through interaction with its ligand HVEM. This BTLA-HVEM signaling axis critically balances immune activation and tolerance to maintain homeostasis (Andrzejczak and Karabon, 2024). Subsequent experiments have indicated that BTLA orchestrates autophagic clearance of Mtb through AKT/mTOR signaling in macrophages. Mtb infection upregulates BTLA expression, which suppresses AKT/mTOR pathway activity to activate autophagic flux. This is evidenced by increased LC3-II conversion and enhanced autophagosome–lysosome fusion, culminating in lysosomal degradation of intracellular bacteria (Liu et al., 2021).

Recent studies reveal that Mtb differentially manipulates lysosomal pathways across host cells to determine infection outcomes. In endothelial cells, Mtb is targeted to acidified phagolysosomes for degradation through itgb3-mediated activation of Rab GTPases, which drive endosomal maturation and autophagic flux (Bussi and Gutierrez, 2019). Conversely, in macrophages and epithelial cells, Mtb suppresses lysosomal acidification by disrupting V-ATPase assembly via virulence factors like LpqH, while coopting the MMGT1-GPR156 lipid droplet axis to sequester antimicrobial lipids and stabilize non-acidified niches (Kalam et al., 2023). These dual strategies—exploiting host ITGB3 (Integrin Subunit Beta 3) for lysosomal clearance in endothelia versus hijacking MMGT1-GPR156

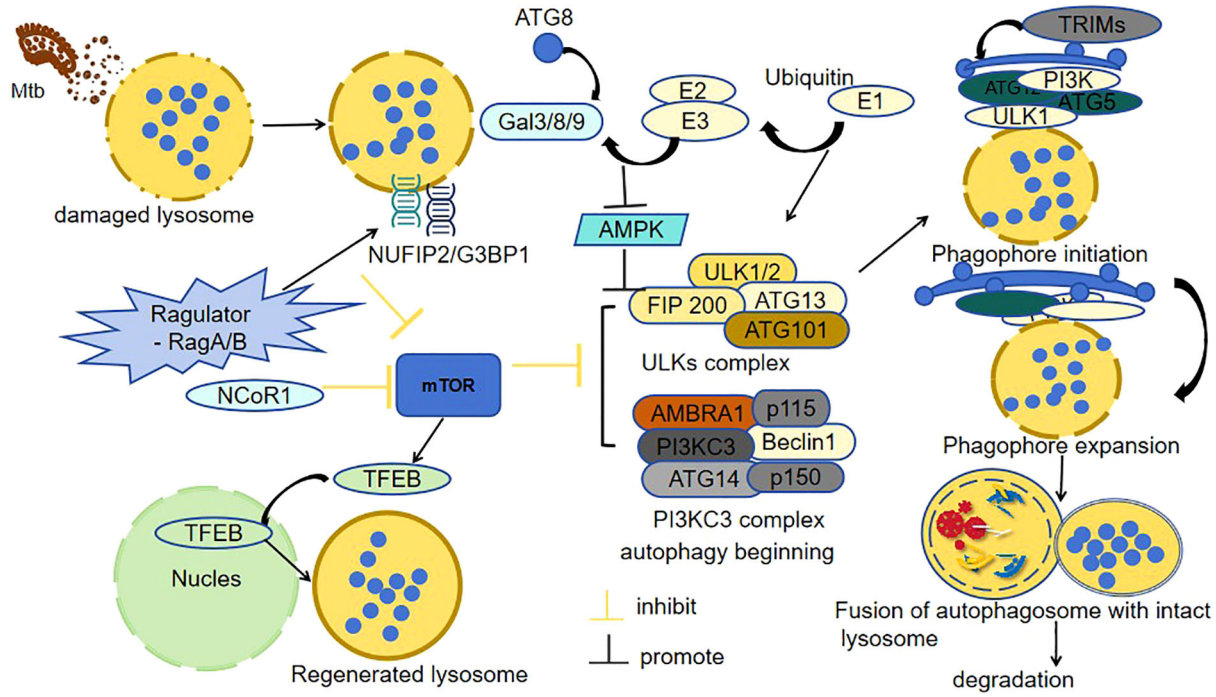

FIGURE 3
Mtb-induced lysosomal damage and autophagic defense. (Mtb) disrupts lysosomal integrity to evade immune clearance. In response, host cells deploy a coordinated defense: 1. Damage sensing: Galectins (Gal3/8/9) detect lysosomal membrane damage and initiate repair. 2. Autophagy activation: The NUFIP2/G3BP1-Ragulator-RagA/B complex suppresses mTOR, enabling ULK1-mediated autophagosome formation, while AMPK amplifies this signal via energy stress sensing. 3. Lysosomal regeneration: Nuclear translocation of TFEB drives lysosomal biogenesis to replenish functional lysosomes. 4. Quality control: Irreparable lysosomes undergo TRIM-mediated ubiquitination for selective lysophagic degradation. 5. Pathogen clearance: Autophagosomes fuse with intact lysosomes, enabling enzymatic degradation of intracellular Mtb. This integrated response highlights the synergy between lysosomal repair and autophagy in combating TB infection.

for lipid-dependent persistence in phagocytes—highlight cell type-specific vulnerabilities that could be therapeutically targeted to restore lysosomal bactericidal functions.

While cellular-level research has its own charm, the clinical realm has unveiled a treasure trove of fascinating phenomena that captivate our attention. Deng et al. found that miRNA-215-5p expression was upregulated in patients with TB compared to healthy controls. Upregulation of miRNA-215-5p inhibited autophagy maturation by preventing autophagosome–lysosome fusion (Deng et al., 2023). Thus, regulating miRNA-215-5p may offer a new anti-TB treatment strategy. Further research on its specific regulation of the autophagy pathway may elucidate its role in TB immunopathology. Another study showed that phospholipids and ceramides in the plasma of patients with active TB exhibited significant abnormalities. Notably, lipid metabolic reprogramming emerges as a promising theranostic target in TB. Elevated lysophosphatidic acid species [LPA(16:0/18:0)] in active TB patients' plasma show perfect diagnostic accuracy (AUC = 1.0), while ceramides enhance antibacterial immunity through autophagy–lysosome coordination, proposing a novel "diagnosis-to-therapy" biomarker strategy (Chen et al., 2021). Thus, targeting lipid metabolism emerges as a novel TB treatment strategy, while lipid biomarkers like LPA serve as dual-purpose biomarkers for diagnosis and treatment monitoring. Furthermore, Mtb accumulates more extracellular polyphosphate than non-pathogenic bacteria, hindering phagocyte killing by inhibiting phagosome acidification and lysosomal activity (Rijal et al., 2020). Genetic deletion of BCG_2432c in the BCG vaccine strain augments autophagy-mediated antimycobacterial immunity through enhanced autophagosome–lysosome fusion and lysosomal proteolytic activity, providing superior protection against Mtb infection compared to parental BCG in preclinical models (Wu et al., 2022).

3.4 The communication between lysosomes and other organelles

Lysosomes are crucial intracellular digestive and defensive organelles, and their normal functions are vital for resisting Mtb infection. Lysosomes directly degrade invading pathogens via their hydrolases for preliminary defense and interact with other organelles to combat pathogen invasion and replication (Repnik et al., 2013). For instance, lysosomes and mitochondria maintain cellular homeostasis through reciprocal metabolic exchange: lysosomal metabolites fuel oxidative phosphorylation, while mitochondrial ATP powers lysosomal acidification and function (Deus et al., 2020). Research by Bussi et al. shows that under

physiological conditions, lysosomes degrade Mtb through enzymatic activity while exporting metabolites to sustain mitochondrial oxidative phosphorylation; reciprocally, mitochondria generate ATP to power lysosomal acidification and proteolytic functions. However, Mtb disrupts this partnership by compromising lysosomal integrity, triggering cathepsin-mediated degradation of mitochondrial electron transport chain components. The resultant energy crisis forces metabolic reprogramming toward glycolysis, paradoxically enhancing Mtb survival through nutrient enrichment. Therapeutic intervention with α-ketoglutarate restores lysosomal–mitochondrial crosstalk, simultaneously rescuing mitochondrial metabolism and lysosomal bactericidal capacity—demonstrating how leveraging this organelle partnership can overcome pathogen-evolved immunosuppression strategies (Bussi et al., 2022). Moreover, lysosomes and the endoplasmic reticulum (ER) coordinate a multilayered defense against Mtb through dynamic membrane interactions. When Mtb damages lysosomal membranes via its ESX-1, ER-resident oxysterol-binding protein 8 (OSBP8) is recruited to membrane contact sites, where it mediates PI4P-cholesterol exchange to restore lysosomal integrity. This lipid transfer mechanism accomplishes dual protective roles: clearing pathogenic PI4P microdomains to reactivate V-ATPase-driven acidification (pH ≤4.5), and providing cholesterol to stabilize lysosomal membranes against bacterial phospholipase assaults. Concurrently, ER-derived calcium signaling enhances lysosomal protease activation, enabling efficient bacterial degradation. Disruption of this partnership (e.g., OSBP8 deficiency) triggers PI4P overload (>3-fold increase), elevates lysosomal pH (≥6.2), and reduces bacterial killing efficacy by 4.7-fold (Anand et al., 2023). Therapeutic strategies targeting this collaborative axis—such as small molecules enhancing ER-lysosome lipid flux—could counteract Mtb's membrane sabotage tactics, positioning organelle cooperation as a frontier in host-directed TB therapies.

4 Drug research on tuberculosis

4.1 Drug repurposing

Although drugs like bedaquiline and delamanid are clinically used for DR-TB, no lysosome-targeted anti-TB drugs have been developed or widely applied thus far. Notably, tamoxifen, widely recognized as a breast cancer drug, has recently been reported to exhibit a direct antibacterial effect on Mtb and to synergize with first-line TB antibiotics (Chen et al., 2014; Jang et al., 2015). In Boland et al.'s study of the zebrafish *Mycobacterium marinum* infection model, tamoxifen's anti-mycobacterial activity was shown to be independent of its established estrogen receptor pathway function. Instead, it appears to enhance lysosomal function, facilitating the transport of mycobacteria to lysosomes for degradation, thereby suggesting a host-directed mechanism centered on lysosomal modulation (Boland et al., 2023). However, whether tamoxifen directly targets TFEB or LC3 to enhance lysosomal function and promote mycobacterial trafficking to lysosomes for degradation requires further investigation into the molecular mechanisms. These findings especially support the repurposing of tamoxifen for HDT in the treatment of drug-resistant infections, but studies have shown that long-term tamoxifen use significantly increases risks of endometrial cancer, venous thromboembolism (VTE), and non-alcoholic fatty liver disease (NAFLD) (Davies et al., 2013). Moreover, ibrutinib was proved to increase the colocalization of the autophagy marker LC3b with Mtb, promotes the fusion of autophagy–lysosomes, and significantly inhibits the intracellular growth of Mtb. It revealed that ibrutinib increases autophagy in Mtb-infected macrophages by inhibiting the BTK/Akt/mTOR pathway (Hu et al., 2020). However, ibrutinib use may cause cardiotoxicity (e.g., atrial fibrillation) and increase the risk of bleeding and opportunistic infections (Byrd et al., 2013; Yin et al., 2017; Buck et al., 2023). Singh et al. also found that all-trans retinoic acid (ATRA) can enhance the acidification and increase the number of lysosomes by activating the MEK/ERK and p38 MAPK signaling pathways and upregulating the expressions of lysosome-related genes (such as TFEB) (Singh et al., 2024). These changes effectively promote the phagocytosis and elimination of Mtb by cells. Adding ATRA to the standard TB treatment may help clear bacteria more quickly. Therefore, it is necessary to conduct further research on its potential for human use. Additionally, the hepatotoxicity, cutaneous-mucosal toxicity, and increased intracranial pressure associated with ATRA administration must be considered (Tallman et al., 2002). Heemskerk and others found that two antipsychotic drugs, fluspirilene and pimozide, can inhibit the growth of Mtb. On the one hand, these two drugs mainly enhance autophagy by inhibiting calmodulin activity and blocking the Dopamine D2 Receptor (D2R), which promotes more bacteria to be localized in autophagolysosomes. On the other hand, they both can increase the presence of TFEB in the nucleus, thereby enhancing the lysosomal response. In addition, pimozide can also reduce the degradation of lysosomal V-ATPase mediated by cytokine-inducible SH2-containing protein (CISH) induced by Mtb, thus enhancing the acidification of lysosomes and ultimately effectively inhibiting the growth of Mtb (Heemskerk et al., 2021). These two approved antipsychotic drugs are promising candidates for HDT against drug-resistant Mtb infections (Zumla et al., 2016). While specific clinical data are currently lacking, neurotoxicity and cardiotoxicity should be monitored during use (Frangos et al., 1978; Shi et al., 2015). 4-BOP (4-(benzyloxy)phenol) can be found in cosmetics or food packaging materials and acts as an antioxidant to prevent product deterioration due to oxidation. It can activate p53 expression by inhibiting its interaction with KDM1A, resulting in the generation of reactive oxygen species (ROS) and an increase in intracellular calcium levels. These changes trigger phagosome–lysosome fusion and enhance the killing effect on intracellular mycobacteria (Naik et al., 2024). However, 4-(benzyloxy)phenol may have potential carcinogenicity and cytotoxicity at high concentrations.

4.2 Phytochemicals

Clinical chemical drugs occupy a pivotal position in contemporary medicine; however, recent research has progressively concentrated on plant-derived compounds, termed phytochemicals, owing to their potential therapeutic advantages, such as epigallocatechin gallate, abbreviated as EGCG, which is a polyphenolic compound that widely exists in nature and has important biological activities. It is especially abundant in green tea. However, clinical studies have shown that daily intake exceeding 600 mg may increase the risk of liver damage, and after oral administration, it is easily and rapidly biotransformed and degraded in the gastrointestinal tract and liver, resulting in low bioavailability and ultimately limiting its clinical application effectiveness (Dekant et al., 2017; Peng et al., 2024). It can downregulate TACO gene transcription, weakening TACO's inhibition of phagosome–lysosome fusion. The activation of AMPK inhibits mTORC1 activity, thereby relieving its suppression on ULK1 and initiating the formation of autophagosome precursors. Moreover, it promotes TFEB nuclear translocation and induces mitochondrial ROS generation and activates the MAPK/ERK pathway to upregulate the expression of V-ATPase subunits and enhance the acidic environment within lysosomes. Moreover, compared with oral administration, pulmonary delivery of EGCG could enhance drug concentration in the lungs, avoid metabolism, and reduce systemic side effects (Sharma et al., 2020). Another is curcumin, a natural polyphenolic compound extracted from the rhizomes of *Curcuma longa* of the Zingiberaceae family, which has remarkable anti-inflammatory, antioxidant, anti-tumor, antibacterial, and antiviral effects (Chen et al., 2018; Eke-Okoro et al., 2018). Owing to its diverse biological activities, curcumin has garnered extensive attention in the fields of medicine and healthcare. Similarly, curcumin enhances autophagy through the AMPK/mTOR/ULK1 pathway, downregulates TACO expression, activates Rab7, and upregulates LAMP1 to promote phagosome–lysosome fusion, while further promoting TFEB (transcription factor EB) nuclear translocation and upregulating V-ATPase subunit expression driving lysosomal acidification and thereby clearing intracellular Mtb (Gupta et al., 2023). As a natural compound, curcumin has relatively low toxicity and may offer good safety in clinical applications. In the context of the growing problem of DR-TB, it presents a new option for treatment.

4.3 Nanomedicines

Nanomaterials, as an emerging class of materials, are being actively explored for their unique properties and promising applications across various fields, including medicine, where they hold potential for novel therapeutic and diagnostic approaches. Gupta et al. demonstrated that ISCurNP significantly reduced the CFU count in Mtb-infected RAW cells, and the synergistic combination of ISCurNP with isoniazid markedly enhanced Mtb killing (Gupta et al., 2023). ISCurNP not only targets macrophages and boosts curcumin's bioavailability but also chelates free iron within lysosomes to block the iron uptake pathway of Mtb, thereby inhibiting its growth. This dual mechanism effectively combats Mtb, offering new therapeutic possibilities for TB, particularly in drug-resistant cases. Similarly, Se NPs and Ison@Man-Se NPs preferentially accumulate in macrophages where they activate AMPK, inhibit mTORC1 to initiate autophagosome formation, and upregulate LAMP1 to promote phagosome–lysosome fusion, thereby enhancing the clearance of intracellular Mtb (Pi et al., 2020).

Regarding other aspects, YDGP is a porous microparticle derived from the yeast cell wall. It serves as a targeted drug delivery system to macrophages by binding to surface receptors Dectin-1. This binding initiates NADPH oxidase-dependent ROS production and regulates the LC3-associated autophagy pathway, which jointly facilitate phagosomal maturation. Through these synergistic mechanisms, YDGP not only improves the anti-TB effect by clearing intracellular pathogens but also offers a strategic framework for developing immunotherapeutic agents targeting macrophage-mediated immunity (Fatima et al., 2021). Similarly, Ahmad et al. demonstrated that rifabutin-loaded β-glucan microparticles (DYDGP) targeted macrophage Dectin-1 receptors to activate NOX2-dependent ROS burst and LC3-II-mediated macroautophagy. This dual mechanism enhanced phagolysosomal fusion (a 2.7-fold increase in LAMP-1 expression) and autophagosome maturation (an 83% enhancement in AVO formation), achieving a 3.1-log reduction in CFU counts of multidrug-resistant MDR-M.tb strains (Ahmad et al., 2024). Although YDGP exhibits excellent biocompatibility as a natural polysaccharide, prolonged administration at high doses may lead to excessive immune activation, oxidative tissue damage, and cellular toxicity. Consequently, meticulous dose optimization and functional modifications such as ligand conjugation are essential to ensure optimal therapeutic safety and efficacy.

4.4 Probiotic preparations

Alongside the emerging field of nanomaterials, microorganisms are indispensable to life, with their diverse functions ranging from nutrient cycling to disease pathogenesis, making them a central focus of scientific inquiry and biotechnological innovation. Rahim et al. demonstrated that PMC203 (*Lactobacillus rhamnosus*) significantly induces autophagy and lysosomal biosynthesis, thereby reducing Mtb load in macrophages (Rahim et al., 2024). Although the exact mechanisms remain to be elucidated, it may involve gene expression regulation or other pathways. These findings underscore the potential of probiotic-mediated autophagy as a novel therapeutic approach for TB. Although *in vitro* studies have demonstrated its favorable safety profile, further *in vivo* animal studies remain needed to confirm its efficacy and safety (Rahim et al., 2024). These findings are summarized in (Table 2), which highlights candidate therapeutics – including repurposed drugs, phytochemicals, nanomedicines, and probiotics – that target lysosomal-autophagy pathways to eliminate Mtb, along with their mechanistic insights and clinical translational challenges.

TABLE 2 Potential drugs for treating Mtb.

Mechanism	Drugs	Potential Targets	Mode of Action
Lysosomal Function Enhancement			
TFEB-mediated biogenesis	Tamoxifen	TFEB, LC3	Promotes lysosomal trafficking and bacterial degradation via ER-independent pathways (Boland et al., 2023).
Lysosomal acidification	4-BOP	p53-KDM1A, V-ATPase	Induces ROS/calcium signaling to activate lysosomal acidification (Naik et al., 2024).
Phagosome–Lysosome Fusion			
TACO suppression	EGCG	TACO, AMPK/mTOR/ULK1	Downregulates TACO; activates AMPK/mTOR/ULK1-TFEB axis (Sharma et al., 2020).
Rab7/LAMP1 activation	Curcumin	Rab7, LAMP1, V-ATPase	Enhances vesicular trafficking and acidification via TFEB-driven V-ATPase upregulation (Gupta et al., 2023).
Calmodulin/D2R blockade	Fluspirilene/Pimozide	Calmodulin, D2R, CISH	Stabilizes V-ATPase by inhibiting CISH-mediated degradation (Heemskerk et al., 2021).
Autophagy Regulation			
mTOR pathway inhibition	Ibrutinib	BTK/Akt/mTOR, LC3	Enhances LC3-II-dependent autophagosome–lysosome fusion (Hu et al., 2020).
Iron chelation	ISCurNP	Lysosomal iron transport	Depletes iron availability while boosting autophagy flux (Pi et al., 2020).
Dectin-1/LC3 activation	YDGP/DYDGP	Dectin-1, NOX2, LC3	Triggers NADPH oxidase-dependent ROS and LC3-II-mediated phagosomal maturation (Fatima et al., 2021).
Probiotic-Induced Autophagy			
TFEB pathway activation	PMC203	TFEB	Induces lysosomal biogenesis through undefined autophagy initiation mechanisms (Rahim et al., 2024).

5 Conclusions and prospects

Researching on the interaction mechanism between TB and lysosomes, significant progress has been achieved. Numerous mycobacterial factors affecting lysosomal impact have been identified. These findings provide crucial insights into TB pathogenesis. However, current research faces limitations; some results remain inconsistent or contradictory. Future studies require more precise and comprehensive methods, such as advanced imaging and molecular biology techniques, to better monitor the dynamic interaction between lysosomes and Mtb for obtaining more reliable data.

The defense mechanisms of lysosomes against Mtb exhibit multifaceted characteristics. Studies on lysosome–mitochondria communication have uncovered novel pathways for intracellular material transport and metabolic regulation, informing new treatment strategies based on organelle interactions. Future research should explore both the synergistic effects among these mechanisms and their variations during different infection stages and cell types.

In the realm of TB drug research, while certain drugs have demonstrated some anti-TB potential, they still encounter numerous formidable challenges in widespread clinical applications. However, the efficacy, safety, and long-term stability of these drugs and formulations require rigorous validation through large-scale, multi-center clinical trials. Therefore, future drug development efforts should focus on optimizing drug structures and formulations, significantly improving drug targeting and bioavailability, and actively exploring rational and effective combination therapies to effectively address TB drug resistance and enhance treatment efficacy.

The strategy of targeting lysosomes for TB treatment holds great application prospects and is anticipated to overcome many limitations of traditional TB treatment modalities. By implementing a series of effective measures, such as enhancing lysosomal function and adopting advanced lysosome-targeted drug delivery systems, the treatment outcomes of Mtb and drug-resistant Mtb can be significantly improved. Nevertheless, this strategy still faces multiple challenges in clinical application, including the optimization of drug design, in-depth exploration of the mechanism of action, the formulation of personalized treatment regimens, and clinical translation.

With the continuous advancement of science and technology and deeper interdisciplinary collaboration, it is expected that in the foreseeable future, the strategy of targeting lysosomes for TB treatment will achieve significant breakthroughs, bringing new hope for improving the treatment outcomes and quality of life of patients with TB.

Author contributions

GF: Conceptualization, Funding acquisition, Supervision, Validation, Writing – review & editing. CB: Writing – original draft, Data curation, Formal analysis, Investigation, Methodology, Validation, Visualization. YZ: Data curation, Investigation, Resources, Supervision, Writing – review & editing. JF: Data curation, Investigation, Supervision, Writing – review & editing. XH: Supervision, Validation, Writing – review & editing. NG: Supervision, Validation, Writing – review & editing.

Conflict of interest

The authors declare that the research was conducted in the absence of any commercial or financial relationships that could be construed as a potential conflict of interest.

Generative AI statement

The author(s) declare that no Generative AI was used in the creation of this manuscript.

Publisher's note

All claims expressed in this article are solely those of the authors and do not necessarily represent those of their affiliated organizations, or those of the publisher, the editors and the reviewers. Any product that may be evaluated in this article, or claim that may be made by its manufacturer, is not guaranteed or endorsed by the publisher.

Funding

The author(s) declare that financial support was received for the research and/or publication of this article. This research was funded by the National Natural Science Foundation of China (grant number 82070017).

References

Ahmad, F., Fatima, N., Ahmad, S., Upadhyay, T. K., Jain, P., Saeed, M., et al. (2024). Treatment of Mycobacterium tuberculosis infected macrophages with rifabutin loaded β-glucan microparticles induces macroautophagy mediated bacillary killing. *Int. J. Biol. Macromol* 283, 137256. doi: 10.1016/j.ijbiomac.2024.137256

Anand, A., Mazur, A. C., Rosell-Arevalo, P., Franzkoch, R., Breitsprecher, L., Listian, S. A., et al. (2023). ER-dependent membrane repair of mycobacteria-induced vacuole damage. *mBio* 14, e0094323. doi: 10.1128/mbio.00943-23

Andrzejczak, A., and Karabon, L. (2024). BTLA biology in cancer: from bench discoveries to clinical potentials. *Biomark Res.* 12, 8. doi: 10.1186/s40364-024-00556-2

Appelqvist, H., Wäster, P., Kågedal, K., and Öllinger, K. (2013). The lysosome: from waste bag to potential therapeutic target. *J. Mol. Cell Biol.* 5, 214–226. doi: 10.1093/jmcb/mjt022

Aqdas, M., Singh, S., Amir, M., Maurya, S. K., Pahari, S., and Agrewala, J. N. (2021). Cumulative signaling through NOD-2 and TLR-4 eliminates the mycobacterium tuberculosis concealed inside the mesenchymal stem cells. *Front. Cell Infect. Microbiol* 11. doi: 10.3389/fcimb.2021.669168

Armstrong, J. A., and Hart, P. D. (1971). Response of cultured macrophages to Mycobacterium tuberculosis, with observations on fusion of lysosomes with phagosomes. *J. Exp. Med.* 134, 713–740. doi: 10.1084/jem.134.3.713

Aylan, B., Bernard, E. M., Pellegrino, E., Botella, L., Fearns, A., Athanasiadi, N., et al. (2023). ATG7 and ATG14 restrict cytosolic and phagosomal Mycobacterium tuberculosis replication in human macrophages. *Nat. Microbiol* 8, 803–818. doi: 10.1038/s41564-023-01335-9

Barbero, A. M., Trotta, A., Genoula, M., Pino, R., Estermann, M. A., Celano, J., et al. (2021). SLAMF1 signaling induces Mycobacterium tuberculosis uptake leading to endolysosomal maturation in human macrophages. *J. Leukoc Biol.* 109, 257–273. doi: 10.1002/jlb.4ma0820-655rr

Bedard, M., van der Niet, S., Bernard, E. M., Babunovic, G., Cheng, T. Y., Aylan, B., et al. (2023). A terpene nucleoside from M. tuberculosis induces lysosomal lipid storage in foamy macrophages. *J. Clin. Invest.* 133 (6). doi: 10.1172/jci161944

Behr, M. A., Wilson, M. A., Gill, W. P., Salamon, H., Schoolnik, G. K., Rane, S., et al. (1999). Comparative genomics of BCG vaccines by whole-genome DNA microarray. *Science* 284, 1520–1523. doi: 10.1126/science.284.5419.1520

Beresford, N., Patel, S., Armstrong, J., Szöor, B., Fordham-Skelton, A. P., and Tabernero, L. (2007). MptpB, a virulence factor from Mycobacterium tuberculosis, exhibits triple-specificity phosphatase activity. *Biochem. J.* 406, 13–18. doi: 10.1042/bj20070670

Berg, R. D., Levitte, S., O'Sullivan, M. P., O'Leary, S. M., Cambier, C. J., Cameron, J., et al. (2016). Lysosomal disorders drive susceptibility to tuberculosis by compromising macrophage migration. *Cell* 165, 139–152. doi: 10.1016/j.cell.2016.02.034

Biswas, V. K., Sen, K., Ahad, A., Ghosh, A., Verma, S., Pati, R., et al. (2023). NCoR1 controls Mycobacterium tuberculosis growth in myeloid cells by regulating the AMPK-mTOR-TFEB axis. *PLoS Biol.* 21, e3002231. doi: 10.1371/journal.pbio.3002231

Boland, R., Heemskerk, M. T., Forn-Cuní, G., Korbee, C. J., Walburg, K. V., Esselink, J. J., et al. (2023). Repurposing tamoxifen as potential host-directed therapeutic for tuberculosis. *mBio* 14, e0302422. doi: 10.1128/mbio.03024-22

Bravo-Cordero, J. J., Magalhaes, M. A., Eddy, R. J., Hodgson, L., and Condeelis, J. (2013). Functions of cofilin in cell locomotion and invasion. *Nat. Rev. Mol. Cell Biol.* 14, 405–415. doi: 10.1038/nrm3609

Buck, B., Chum, A. P., Patel, M., Carter, R., Nawaz, H., Yildiz, V., et al. (2023). Cardiovascular magnetic resonance imaging in patients with ibrutinib-associated cardiotoxicity. *JAMA Oncol.* 9, 552–555. doi: 10.1001/jamaoncol.2022.6869

Bussi, C., and Gutierrez, M. G. (2019). Mycobacterium tuberculosis infection of host cells in space and time. *FEMS Microbiol Rev.* 43, 341–361. doi: 10.1093/femsre/fuz006

Bussi, C., Heunis, T., Pellegrino, E., Bernard, E. M., Bah, N., Dos Santos, M. S., et al. (2022). Lysosomal damage drives mitochondrial proteome remodelling and reprograms macrophage immunometabolism. *Nat. Commun.* 13, 7338. doi: 10.1038/s41467-022-34632-8

Bussi, C., Mangiarotti, A., Vanhille-Campos, C., Aylan, B., Pellegrino, E., Athanasiadi, N., et al. (2023). Stress granules plug and stabilize damaged endolysosomal membranes. *Nature* 623, 1062–1069. doi: 10.1038/s41586-023-06726-w

Buter, J., Cheng, T. Y., Ghanem, M., Grootemaat, A. E., Raman, S., Feng, X., et al. (2019). Mycobacterium tuberculosis releases an antacid that remodels phagosomes. *Nat. Chem. Biol.* 15, 889–899. doi: 10.1038/s41589-019-0336-0

Byrd, J. C., Furman, R. R., Coutre, S. E., Flinn, I. W., Burger, J. A., Blum, K. A., et al. (2013). Targeting BTK with ibrutinib in relapsed chronic lymphocytic leukemia. *N Engl. J. Med.* 369, 32–42. doi: 10.1056/NEJMoa1215637

Chai, Q., Zhang, Y., and Liu, C. H. (2018). Mycobacterium tuberculosis: an adaptable pathogen associated with multiple human diseases. *Front. Cell Infect. Microbiol* 8. doi: 10.3389/fcimb.2018.00158

Chen, J. X., Han, Y. S., Zhang, S. Q., Li, Z. B., Chen, J., Yi, W. J., et al. (2021). Novel therapeutic evaluation biomarkers of lipid metabolism targets in uncomplicated pulmonary tuberculosis patients. *Signal Transduct Target Ther.* 6, 22. doi: 10.1038/s41392-020-00427-w

Chen, C. Y., Kao, C. L., and Liu, C. M. (2018). The cancer prevention, anti-inflammatory and anti-oxidation of bioactive phytochemicals targeting the TLR4 signaling pathway. *Int. J. Mol. Sci.* 19 (9). doi: 10.3390/ijms19092729

Chen, F. C., Liao, Y. C., Huang, J. M., Lin, C. H., Chen, Y. Y., Dou, H. Y., et al. (2014). Pros and cons of the tuberculosis drugome approach–an empirical analysis. *PLoS One* 9, e100829. doi: 10.1371/journal.pone.0100829

Chugh, S., Tiwari, P., Suri, C., Gupta, S. K., Singh, P., Bouzeyen, R., et al. (2024). Polyphosphate kinase-1 regulates bacterial and host metabolic pathways involved in pathogenesis of Mycobacterium tuberculosis. *Proc. Natl. Acad. Sci. U S A* 121, e2309664121. doi: 10.1073/pnas.2309664121

Cole, S. T., Brosch, R., Parkhill, J., Garnier, T., Churcher, C., Harris, D., et al. (1998). Deciphering the biology of Mycobacterium tuberculosis from the complete genome sequence. *Nature* 393, 537–544. doi: 10.1038/31159

Cross, J., Durgan, J., McEwan, D. G., Tayler, M., Ryan, K. M., and Florey, O. (2023). Lysosome damage triggers direct ATG8 conjugation and ATG2 engagement via non-canonical autophagy. *J. Cell Biol.* 222 (12). doi: 10.1083/jcb.202303078

Davies, C., Pan, H., Godwin, J., Gray, R., Arriagada, R., Raina, V., et al. (2013). Long-term effects of continuing adjuvant tamoxifen to 10 years versus stopping at 5 years after diagnosis of oestrogen receptor-positive breast cancer: ATLAS, a randomised trial. *Lancet* 381, 805–816. doi: 10.1016/s0140-6736(12)61963-1

de Duve, C. (2005). The lysosome turns fifty. *Nat. Cell Biol.* 7, 847–849. doi: 10.1038/ncb0905-847

Dekant, W., Fujii, K., Shibata, E., Morita, O., and Shimotoyodome, A. (2017). Safety assessment of green tea based beverages and dried green tea extracts as nutritional supplements. *Toxicol. Lett.* 277, 104–108. doi: 10.1016/j.toxlet.2017.06.008

Deng, G., Ji, N., Shi, X., Zhang, W., Qin, Y., Sha, S., et al. (2020). Effects of Mycobacterium tuberculosis Rv1096 on mycobacterial cell division and modulation on macrophages. *Microb Pathog* 141, 103991. doi: 10.1016/j.micpath.2020.103991

Deng, F., Xu, P., Miao, J., Jin, C., Tu, H., and Zhang, J. (2023). Pulmonary tuberculosis biomarker miR-215-5p inhibits autophagosome-lysosome fusion in macrophages. *Tuberculosis (Edinb)* 143, 102422. doi: 10.1016/j.tube.2023.102422

Deus, C. M., Yambire, K. F., Oliveira, P. J., and Raimundo, N. (2020). Mitochondria-lysosome crosstalk: from physiology to neurodegeneration. *Trends Mol. Med.* 26, 71–88. doi: 10.1016/j.molmed.2019.10.009

Eke-Okoro, U. J., Raffa, R. B., Pergolizzi, J. V. Jr., Breve, F., and Taylor, R. Jr. (2018). Curcumin in turmeric: Basic and clinical evidence for a potential role in analgesia. *J. Clin. Pharm. Ther.* 43, 460–466. doi: 10.1111/jcpt.12703

Fan, J., Hale, V. L., Lelieveld, L. T., Whitworth, L. J., Busch-Nentwich, E. M., Troll, M., et al. (2023). Gaucher disease protects against tuberculosis. *Proc. Natl. Acad. Sci. U S A* 120, e2217673120. doi: 10.1073/pnas.2217673120

Fatima, N., Upadhyay, T., Ahmad, F., Arshad, M., Kamal, M. A., Sharma, D., et al. (2021). Particulate β-glucan activates early and delayed phagosomal maturation and autophagy within macrophage in a NOX-2 dependent manner. *Life Sci.* 266, 118851. doi: 10.1016/j.lfs.2020.118851

Finkel, T. (2011). Signal transduction by reactive oxygen species. *J. Cell Biol.* 194, 7–15. doi: 10.1083/jcb.201102095

Frangos, H., Zissis, N. P., Leontopoulos, I., Diamantas, N., Tsitouridis, S., Gavriil, I., et al. (1978). Double-blind therapeutic evaluation of fluspirilene compared with fluphenazine decanoate in chronic schizophrenics. *Acta Psychiatr. Scand.* 57, 436–446. doi: 10.1111/j.1600-0447.1978.tb06912.x

Ge, P., Lei, Z., Yu, Y., Lu, Z., Qiang, L., Chai, Q., et al. (2022). M. tuberculosis PknG manipulates host autophagy flux to promote pathogen intracellular survival. *Autophagy* 18, 576–594. doi: 10.1080/15548627.2021.1938912

Gupta, P. K., Jahagirdar, P., Tripathi, D., Devarajan, P. V., and Kulkarni, S. (2023). Macrophage targeted polymeric curcumin nanoparticles limit intracellular survival of Mycobacterium tuberculosis through induction of autophagy and augment anti-TB activity of isoniazid in RAW 264.7 macrophages. *Front. Immunol.* 14. doi: 10.3389/fimmu.2023.1233630

Hardie, D. G., Ross, F. A., and Hawley, S. A. (2012). AMPK: a nutrient and energy sensor that maintains energy homeostasis. *Nat. Rev. Mol. Cell Biol.* 13, 251–262. doi: 10.1038/nrm3311

Heemskerk, M. T., Korbee, C. J., Esselink, J. J., Dos Santos, C. C., van Veen, S., Gordijn, I. F., et al. (2021). Repurposing diphenylbutylpiperidine-class antipsychotic drugs for host-directed therapy of Mycobacterium tuberculosis and Salmonella enterica infections. *Sci. Rep.* 11, 19634. doi: 10.1038/s41598-021-98980-z

Hu, Y., Wen, Z., Liu, S., Cai, Y., Guo, J., Xu, Y., et al. (2020). Ibrutinib suppresses intracellular mycobacterium tuberculosis growth by inducing macrophage autophagy. *J. Infect.* 80, e19–e26. doi: 10.1016/j.jinf.2020.03.003

Huynh, K. K., Eskelinen, E. L., Scott, C. C., Malevanets, A., Saftig, P., and Grinstein, S. (2007). LAMP proteins are required for fusion of lysosomes with phagosomes. *EMBO J.* 26, 313–324. doi: 10.1038/sj.emboj.7601511

Hyttinen, J. M., Niittykoski, M., Salminen, A., and Kaarniranta, K. (2013). Maturation of autophagosomes and endosomes: a key role for Rab7. *Biochim. Biophys. Acta* 1833, 503–510. doi: 10.1016/j.bbamcr.2012.11.018

Jang, W. S., Kim, S., Podder, B., Jyoti, M. A., Nam, K. W., Lee, B. E., et al. (2015). Anti-mycobacterial activity of tamoxifen against drug-resistant and intra-macrophage mycobacterium tuberculosis. *J. Microbiol Biotechnol.* 25, 946–950. doi: 10.4014/jmb.1412.12023

Jayachandran, R., Sundaramurthy, V., Combaluzier, B., Mueller, P., Korf, H., Huygen, K., et al. (2007). Survival of mycobacteria in macrophages is mediated by coronin 1-dependent activation of calcineurin. *Cell* 130, 37–50. doi: 10.1016/j.cell.2007.04.043

Jia, J., Bissa, B., Brecht, L., Allers, L., Choi, S. W., Gu, Y., et al. (2020a). AMPK, a regulator of metabolism and autophagy, is activated by lysosomal damage via a novel galectin-directed ubiquitin signal transduction system. *Mol. Cell* 77, 951–969.e959. doi: 10.1016/j.molcel.2019.12.028

Jia, J., Claude-Taupin, A., Gu, Y., Choi, S. W., Peters, R., Bissa, B., et al. (2020b). Galectin-3 coordinates a cellular system for lysosomal repair and removal. *Dev. Cell* 52, 69–87.e68. doi: 10.1016/j.devcel.2019.10.025

Jia, J., Wang, F., Bhujabal, Z., Peters, R., Mudd, M., Duque, T., et al. (2022). Stress granules and mTOR are regulated by membrane atg8ylation during lysosomal damage. *J. Cell Biol.* 221 (11). doi: 10.1083/jcb.202207091

Jiang, Z., Zhen, J., Abulikena, Y., Gao, C., Huang, L., Huang, T., et al. (2024). Mycobacterium tuberculosis VII secretion system effector molecule Rv2347c blocks the maturation of phagosomes and activates the STING/TBK1 signaling pathway to inhibit cell autophagy. *Microbiol Spectr.* 12, e0118824. doi: 10.1128/spectrum.01188-24

Kalam, H., Chou, C. H., Kadoki, M., Graham, D. B., Deguine, J., Hung, D. T., et al. (2023). Identification of host regulators of Mycobacterium tuberculosis phenotypes uncovers a role for the MMGT1-GPR156 lipid droplet axis in persistence. *Cell Host Microbe* 31, 978–992.e975. doi: 10.1016/j.chom.2023.05.009

Kim, J., Kundu, M., Viollet, B., and Guan, K. L. (2011). AMPK and mTOR regulate autophagy through direct phosphorylation of Ulk1. *Nat. Cell Biol.* 13, 132–141. doi: 10.1038/ncb2152

Leopold Wager, C. M., Bonifacio, J. R., Simper, J., Naoun, A. A., Arnett, E., and Schlesinger, L. S. (2023). Activation of transcription factor CREB in human macrophages by Mycobacterium tuberculosis promotes bacterial survival, reduces NF-kB nuclear transit and limits phagolysosome fusion by reduced necroptotic signaling. *PLoS Pathog* 19, e1011297. doi: 10.1371/journal.ppat.1011297

Levine, B., and Kroemer, G. (2008). Autophagy in the pathogenesis of disease. *Cell* 132, 27–42. doi: 10.1016/j.cell.2007.12.018

Lienard, J., Munke, K., Wulff, L., Da Silva, C., Vandamme, J., Laschanzky, K., et al. (2023). Intragranuloma accumulation and inflammatory differentiation of neutrophils underlie mycobacterial ESX-1-dependent immunopathology. *mBio* 14, e0276422. doi: 10.1128/mbio.02764-22

Ling, X., Liu, X., Wang, K., Guo, M., Ou, Y., Li, D., et al. (2024). Lsr2 acts as a cyclic di-GMP receptor that promotes keto-mycolic acid synthesis and biofilm formation in mycobacteria. *Nat. Commun.* 15, 695. doi: 10.1038/s41467-024-44774-6

Liu, J., Ming, S., Song, W., Meng, X., Xiao, Q., Wu, M., et al. (2021). B and T lymphocyte attenuator regulates autophagy in mycobacterial infection via the AKT/mTOR signal pathway. *Int. Immunopharmacol* 91, 107215. doi: 10.1016/j.intimp.2020.107215

Luies, L., and du Preez, I. (2020). The echo of pulmonary tuberculosis: mechanisms of clinical symptoms and other disease-induced systemic complications. *Clin. Microbiol Rev.* 33 (4). doi: 10.1128/cmr.00036-20

Luzio, J. P., Pryor, P. R., and Bright, N. A. (2007). Lysosomes: fusion and function. *Nat. Rev. Mol. Cell Biol.* 8, 622–632. doi: 10.1038/nrm2217

Mariño, G., Niso-Santano, M., Baehrecke, E. H., and Kroemer, G. (2014). Self-consumption: the interplay of autophagy and apoptosis. *Nat. Rev. Mol. Cell Biol.* 15, 81–94. doi: 10.1038/nrm3735

Mayfield, J. A., Raman, S., Ramnarine, A. K., Mishra, V. K., Huang, A. D., Dudoit, S., et al. (2024). Mycobacteria that cause tuberculosis have retained ancestrally acquired genes for the biosynthesis of chemically diverse terpene nucleosides. *PLoS Biol.* 22, e3002813. doi: 10.1371/journal.pbio.3002813

Miotto, P., Sorrentino, R., De Giorgi, S., Provvedi, R., Cirillo, D. M., and Manganelli, R. (2022). Transcriptional regulation and drug resistance in Mycobacterium tuberculosis. *Front. Cell Infect. Microbiol* 12. doi: 10.3389/fcimb.2022.990312

Mizushima, N., and Komatsu, M. (2011). Autophagy: renovation of cells and tissues. *Cell* 147, 728–741. doi: 10.1016/j.cell.2011.10.026

Naik, L., Patel, S., Kumar, A., Ghosh, A., Mishra, A., Das, M., et al. (2024). 4-(Benzyloxy)phenol-induced p53 exhibits antimycobacterial response triggering phagosome-lysosome fusion through ROS-dependent intracellular Ca(2+) pathway in THP-1 cells. *Microbiol Res.* 282, 127664. doi: 10.1016/j.micres.2024.127664

Organization, W. H. (2024). *Global tuberculosis report 2024*. (Geneva: World Health Organization).

Paik, S., Kim, K. T., Kim, I. S., Kim, Y. J., Kim, H. J., Choi, S., et al. (2022). Mycobacterial acyl carrier protein suppresses TFEB activation and upregulates miR-155 to inhibit host defense. *Front. Immunol.* 13. doi: 10.3389/fimmu.2022.946929

Peng, X., McClements, D. J., Liu, X., and Liu, F. (2024). EGCG-based nanoparticles: synthesis, properties, and applications. *Crit. Rev. Food Sci. Nutr.* 65 (12), 2177–2198. doi: 10.1080/10408398.2024.2328184

Pi, J., Shen, L., Yang, E., Shen, H., Huang, D., Wang, R., et al. (2020). Macrophage-targeted isoniazid-selenium nanoparticles promote antimicrobial immunity and synergize bactericidal destruction of tuberculosis bacilli. *Angew Chem. Int. Ed Engl.* 59, 3226–3234. doi: 10.1002/anie.201912122

Protter, D. S. W., and Parker, R. (2016). Principles and properties of stress granules. *Trends Cell Biol.* 26, 668–679. doi: 10.1016/j.tcb.2016.05.004

Rahim, M. A., Seo, H., Kim, S., Barman, I., Ghorbanian, F., Hossain, M. S., et al. (2024). Exploring the potential of Lactocaseibacillus rhamnosus PMC203 in inducing autophagy to reduce the burden of Mycobacterium tuberculosis. *Med. Microbiol Immunol.* 213, 14. doi: 10.1007/s00430-024-00794-z

Repnik, U., Česen, M. H., and Turk, B. (2013). The endolysosomal system in cell death and survival. *Cold Spring Harb Perspect. Biol.* 5, a008755. doi: 10.1101/cshperspect.a008755

Rijal, R., Cadena, L. A., Smith, M. R., Carr, J. F., and Gomer, R. H. (2020). Polyphosphate is an extracellular signal that can facilitate bacterial survival in eukaryotic cells. *Proc. Natl. Acad. Sci. U S A* 117, 31923–31934. doi: 10.1073/pnas.2012009117

Rodríguez-Fernández, P., Botella, L., Cavet, J. S., Domínguez, J., Gutierrez, M. G., Suckling, C. J., et al. (2024). MptpB Inhibitor Improves the Action of Antibiotics against Mycobacterium tuberculosis and Nontuberculous Mycobacterium avium Infections. *ACS Infect. Dis.* 10, 170–183. doi: 10.1021/acsinfecdis.3c00446

Rombouts, Y., and Neyrolles, O. (2023). The fat is in the lysosome: how Mycobacterium tuberculosis tricks macrophages into storing lipids. *J. Clin. Invest.* 133 (6). doi: 10.1172/jci168366

Russell, D. G. (2011). Mycobacterium tuberculosis and the intimate discourse of a chronic infection. *Immunol. Rev.* 240, 252–268. doi: 10.1111/j.1600-065X.2010.00984.x

Sachdeva, K., Goel, M., Sudhakar, M., Mehta, M., Raju, R., Raman, K., et al. (2020). Mycobacterium tuberculosis (Mtb) lipid mediated lysosomal rewiring in infected macrophages modulates intracellular Mtb trafficking and survival. *J. Biol. Chem.* 295, 9192–9210. doi: 10.1074/jbc.RA120.012809

Saftig, P., and Klumperman, J. (2009). Lysosome biogenesis and lysosomal membrane proteins: trafficking meets function. *Nat. Rev. Mol. Cell Biol.* 10, 623–635. doi: 10.1038/nrm2745

Saha, S., Hazra, A., Ghatak, D., Singh, A. V., Roy, S., and BoseDasgupta, S. (2021). A bumpy ride of mycobacterial phagosome maturation: roleplay of coronin1 through cofilin1 and cAMP. *Front. Immunol.* 12. doi: 10.3389/fimmu.2021.687044

Seeliger, J. C., Holsclaw, C. M., Schelle, M. W., Botyanszki, Z., Gilmore, S. A., Tully, S. E., et al. (2012). Elucidation and chemical modulation of sulfolipid-1 biosynthesis in Mycobacterium tuberculosis. *J. Biol. Chem.* 287, 7990–8000. doi: 10.1074/jbc.M111.315473

Settembre, C., Di Malta, C., Polito, V. A., Garcia Arencibia, M., Vetrini, F., Erdin, S., et al. (2011). TFEB links autophagy to lysosomal biogenesis. *Science* 332, 1429–1433. doi: 10.1126/science.1204592

Sharma, A., Vaghasiya, K., Ray, E., Gupta, P., Gupta, U. D., Singh, A. K., et al. (2020). Targeted pulmonary delivery of the green tea polyphenol epigallocatechin gallate controls the growth of mycobacterium tuberculosis by enhancing the autophagy and suppressing bacterial burden. *ACS Biomater Sci. Eng* 6, 4126–4140. doi: 10.1021/acsbiomaterials.0c00823

Shi, X. N., Li, H., Yao, H., Liu, X., Li, L., Leung, K. S., et al. (2015). In silico identification and *in vitro* and *in vivo* validation of anti-psychotic drug fluspirilene as a potential CDK2 inhibitor and a candidate anti-cancer drug. *PLoS One* 10, e0132072. doi: 10.1371/journal.pone.0132072

Simeone, R., Bobard, A., Lippmann, J., Bitter, W., Majlessi, L., Brosch, R., et al. (2012). Phagosomal rupture by Mycobacterium tuberculosis results in toxicity and host cell death. *PLoS Pathog* 8, e1002507. doi: 10.1371/journal.ppat.1002507

Simeone, R., Bottai, D., and Brosch, R. (2009). ESX/type VII secretion systems and their role in host-pathogen interaction. *Curr. Opin. Microbiol* 12, 4–10. doi: 10.1016/j.mib.2008.11.003

Singh, B., Pahuja, I., Yadav, P., Shaji, A., Chaturvedi, S., Ranganathan, A., et al. (2024). Adjunct therapy with all-trans-retinoic acid improves therapeutic efficacy through immunomodulation while treating tuberculosis with antibiotics in mice. *J. Infect. Dis.* 229, 1509–1518. doi: 10.1093/infdis/jiad460

Singh, R., Singh, M., Arora, G., Kumar, S., Tiwari, P., and Kidwai, S. (2013). Polyphosphate deficiency in Mycobacterium tuberculosis is associated with enhanced drug susceptibility and impaired growth in Guinea pigs. *J. Bacteriol* 195, 2839–2851. doi: 10.1128/jb.00038-13

Singh, R., Singh, A., and Tyagi, A. K. (2005). Deciphering the genes involved in pathogenesis of Mycobacterium tuberculosis. *Tuberculosis (Edinb)* 85, 325–335. doi: 10.1016/j.tube.2005.08.015

Singh, M., Tiwari, P., Arora, G., Agarwal, S., Kidwai, S., and Singh, R. (2016). Establishing Virulence Associated Polyphosphate Kinase 2 as a drug target for Mycobacterium tuberculosis. *Sci. Rep.* 6, 26900. doi: 10.1038/srep26900

Soni, D. K., Dubey, S. K., and Bhatnagar, R. (2020). ATP-binding cassette (ABC) import systems of Mycobacterium tuberculosis: target for drug and vaccine development. *Emerg Microbes Infect.* 9, 207–220. doi: 10.1080/22221751.2020.1714488

Stocker, T. J., Pircher, J., Skenderi, A., Ehrlich, A., Eberle, C., Megens, R. T. A., et al. (2018). The actin regulator coronin-1A modulates platelet shape change and consolidates arterial thrombosis. *Thromb. Haemost.* 118, 2098–2111. doi: 10.1055/s-0038-1675604

Sureka, K., Dey, S., Datta, P., Singh, A. K., Dasgupta, A., Rodrigue, S., et al. (2007). Polyphosphate kinase is involved in stress-induced mprAB-sigE-rel signalling in mycobacteria. *Mol. Microbiol* 65, 261–276. doi: 10.1111/j.1365-2958.2007.05814.x

Sureka, K., Sanyal, S., Basu, J., and Kundu, M. (2009). Polyphosphate kinase 2: a modulator of nucleoside diphosphate kinase activity in mycobacteria. *Mol. Microbiol* 74, 1187–1197. doi: 10.1111/j.1365-2958.2009.06925.x

Tallman, M. S., Andersen, J. W., Schiffer, C. A., Appelbaum, F. R., Feusner, J. H., Woods, W. G., et al. (2002). All-trans retinoic acid in acute promyelocytic leukemia: long-term outcome and prognostic factor analysis from the North American Intergroup protocol. *Blood* 100, 4298–4302. doi: 10.1182/blood-2002-02-0632

Tran, S., Fairlie, W. D., and Lee, E. F. (2021). BECLIN1: protein structure, function and regulation. *Cells* 10 (6). doi: 10.3390/cells10061522

Wang, J., Ge, P., Lei, Z., Lu, Z., Qiang, L., Chai, Q., et al. (2021). Mycobacterium tuberculosis protein kinase G acts as an unusual ubiquitinating enzyme to impair host immunity. *EMBO Rep.* 22, e52175. doi: 10.15252/embr.202052175

Wu, Y., Tian, M., Zhang, Y., Peng, H., Lei, Q., Yuan, X., et al. (2022). Deletion of BCG_2432c from the Bacillus Calmette-Guérin vaccine enhances autophagy-mediated immunity against tuberculosis. *Allergy* 77, 619–632. doi: 10.1111/all.15158

Yin, Q., Sivina, M., Robins, H., Yusko, E., Vignali, M., O'Brien, S., et al. (2017). Ibrutinib therapy increases T cell repertoire diversity in patients with chronic lymphocytic leukemia. *J. Immunol.* 198, 1740–1747. doi: 10.4049/jimmunol.1601190

Zheng, W., Chang, I. C., Limberis, J., Budzik, J. M., Zha, B. S., Howard, Z., et al. (2024). Mycobacterium tuberculosis resides in lysosome-poor monocyte-derived lung cells during chronic infection. *PLoS Pathog* 20, e1012205. doi: 10.1371/journal.ppat.1012205

Zumla, A., Nahid, P., and Cole, S. T. (2013). Advances in the development of new tuberculosis drugs and treatment regimens. *Nat. Rev. Drug Discov.* 12, 388–404. doi: 10.1038/nrd4001

Zumla, A., Rao, M., Wallis, R. S., Kaufmann, S. H., Rustomjee, R., Mwaba, P., et al. (2016). Host-directed therapies for infectious diseases: current status, recent progress, and future prospects. *Lancet Infect. Dis.* 16, e47–e63. doi: 10.1016/s1473-3099(16)00078-5

frontiers | Frontiers in Cellular and Infection Microbiology

TYPE Original Research
PUBLISHED 06 June 2025
DOI 10.3389/fcimb.2025.1607127

OPEN ACCESS

EDITED BY
Valerio Baldelli,
University of Milan, Italy

REVIEWED BY
Andrew Fenton,
The University of Sheffield, United Kingdom
Matteo Boattini,
Azienda Ospedaliera Citta' Della Salute E Della Scienza Di Torino, Italy

*CORRESPONDENCE
Aili He
heaili@xjtu.edu.cn

RECEIVED 07 April 2025
ACCEPTED 19 May 2025
PUBLISHED 06 June 2025

CITATION
Liu Z, Lei J, Zhang X, Yin J, Zhang Y, Lei K, Geng Y, Huang L, Han Q and He A (2025) Evolution of ceftazidime-avibactam resistance driven by variation in *bla*$_{KPC-2}$ to *bla*$_{KPC-190}$ during treatment of ST11-K64 hypervirulent *Klebsiella pneumoniae*. *Front. Cell. Infect. Microbiol.* 15:1607127. doi: 10.3389/fcimb.2025.1607127

Evolution of ceftazidime-avibactam resistance driven by variation in *bla*$_{KPC-2}$ to *bla*$_{KPC-190}$ during treatment of ST11-K64 hypervirulent *Klebsiella pneumoniae*

Zeshi Liu[1], Jing Lei[1], Xue Zhang[1], Jian Yin[1], Yanping Zhang[1], Ke Lei[1], Yan Geng[1], Lingjuan Huang[2], Qiang Han[3] and Aili He[4,5,6]*

[1]Department of Clinical Laboratory, The Second Affiliated Hospital of Xi'an Jiaotong University, Xi'an, China, [2]Geriatrics Department, The First Affiliated Hospital of Xi'an Medical College, Xi'an, China, [3]Department of Gynaecology and Obstetrics, The Second Affiliated Hospital of Xi'an Jiaotong University, Xi'an, China, [4]Department of Hematology, The Second Affiliated Hospital of Xi'an Jiaotong University, Xi'an, China, [5]National-Local Joint Engineering Research Center of Biodiagnostics and Biotherapy, The Second Affiliated Hospital of Xi'an Jiaotong University, Xi'an, China, [6]Xi'an Key Laboratory of Hematological Diseases, The Second Affiliated Hospital of Xi'an Jiaotong University, Xi'an, China

Introduction: The emergence of *Klebsiella* pneumoniae carbapenemase (KPC) variants has significantly compromised the efficacy of ceftazidime-avibactam (CZA), a critical antibiotic for treating carbapenem-resistant *K. pneumoniae* (CRKP) infections. This study investigates the novel KPC-190 variant, identified in a hypervirulent ST11-K64 *K. pneumoniae* strain during CZA therapy, which confers resistance to CZA while partially restoring carbapenem susceptibility.

Methods: The *K. pneumoniae* clinical isolate LX02 harboring *bla*$_{KPC-190}$ was characterized using antimicrobial susceptibility testing, whole-genome sequencing (Illumina and Nanopore), and plasmid analysis. Functional studies included plasmid transformation, cloning assays, and enzyme kinetics (spectrophotometric analysis of purified KPC-190 protein). Genetic context was mapped using bioinformatics tools (RAST, ResFinder, Proksee), and virulence determinants were identified.

Results: KPC-190 exhibited a unique resistance profile: high-level CZA resistance (MIC >64 μg/mL) with reduced carbapenem MICs (imipenem MIC = 2 μg/mL). Enzyme kinetics revealed decreased *K*cat/Km for carbapenems and ceftazidime, alongside a 9-fold higher IC50 for avibactam (0.13 μM vs. KPC-2's 0.014 μM). Genomic analysis identified *bla*$_{KPC-190}$ within an IS26 flanked mobile element (IS26-ISKpn8-*bla*$_{KPC}$-ΔISKpn6-ΔtnpR-IS26) on an IncFII plasmid. The strain also carried hypervirulence markers (*rmpA2*, *iucABCD-iutA*, and type 1/3 fimbriae).

Discussion: The KPC-190 variant underscores the adaptive evolution of *bla*$_{KPC}$ under antibiotic pressure, combining CZA resistance via enhanced ceftazidime

affinity and avibactam evasion with retained carbapenem hydrolysis. Its association with hypervirulence plasmids and IS26-mediated mobility poses a dual threat for dissemination. These findings highlight the urgent need for genomic surveillance and alternative therapies (e.g., meropenem-vaborbactam) to address KPC-190-mediated resistance.

KEYWORDS

KPC-190, *Klebsiella pneumoniae*, ceftazidime-avibactam, blaKPC variants, antibiotic resistance

Introduction

Carbapenem-resistant *Klebsiella pneumoniae* (CRKP) poses a severe threat to global healthcare systems due to its ability to evade the effects of multiple antibiotics (Gonçalves Barbosa et al., 2022; Chou et al., 2024). A major driver of carbapenem resistance in CRKP is the production of *Klebsiella pneumoniae* carbapenemases (KPCs), encoded by the bla_{KPC} gene. Ceftazidime-avibactam (CZA), a combination of a third-generation cephalosporin and an innovative β-lactamase inhibitor, was designed to effectively target carbapenemase-producing pathogens, including strains that produce Ambler class A, class C and some class D β-lactamases (Sharma et al., 2016; van Duin and Bonomo, 2016). Studies have shown the superiority of ceftazidime-avibactam over colistin in the initial treatment of the infections caused by CRE (carbapenem-resistant Enterobacterales), and the use of ceftazidime-avibactam can reduce hospital mortality from all causes and improve risk-benefit outcomes (Karaiskos et al., 2021; Castón et al., 2022). However, since its introduction in China in 2019, ceftazidime-avibactam has exerted selective pressure on KPC-producing K. pneumoniae populations, particularly in nosocomial settings (Boattini et al., 2024). While metallo-β-lactamase-producing strains exhibit intrinsic resistance, recent studies demonstrate the emergence of ceftazidime-avibactam-resistant variants specifically among KPC-producers through acquired mutations (Oliva et al., 2024).

The resistance mechanisms of ceftazidime-avibactam predominantly involve the alterations of the major porins that allow the diffusion of CZA across the outer membrane (*OmpK35* and *OmpK36* porins), the increased gene expression and/or copy number of bla_{KPC}, and alterations in cell permeability or efflux pump activity, with amino acid substitutions in the KPC enzyme constituting a primary mechanism (Wang et al., 2020). Since its discovery, more than 200 bla_{KPC} variants have been reported globally, with variations in bla_{KPC-2} being the primary mechanism for the evolution of these variants. Amino acid variations in the bla_{KPC} gene are primarily located in the loop region near the active site (Hobson et al., 2020). These variations often result in resistance to advanced β-lactam/β-lactamase inhibitor combinations, such as ceftazidime-avibactam. Notably, these resistant isolates may demonstrate cross-resistance to FDC (cefiderocol), which has been attributed to multiple mechanisms including structural similarities between FDC and ceftazidime, porin modifications, and enhanced efflux pump activity (Findlay et al., 2025). The mechanism underlying the resistance to FDC is a combination of different mechanisms including the co-expression of different β-lactamases (NDM (New Delhi metallo-β-lactamase) and KPC variants), variations affecting siderophore–drug receptor expression/function (*cir*A and *fiu* of *Escherichia coli*), overexpression of efflux pumps (*OmpK35* and *OmpK36*), and target modification (penicillin-binding protein 3, PBP-3 coded by the *fts*I gene) (Karakonstantis et al., 2022; Lan et al., 2022).

This study describes the first identification of KPC-190 in a clinical setting, isolated from a patient undergoing prolonged ceftazidime-avibactam therapy. Through whole-genome sequencing and enzymatic characterization, we explored the genetic and functional features of KPC-190, shedding light on its resistance profile and implications for therapy. The findings emphasize the need for vigilant monitoring and innovative treatment strategies for combating KPC-190-mediated resistance.

Methods

Strain identification and antimicrobial susceptibility testing

Strain identification was performed using MALDI-TOF MS (bioMérieux, France). Minimal inhibitory concentrations (MICs) were determined by broth microdilution following Clinical and Laboratory Standards Institute (CLSI) guidelines, with *Escherichia coli* ATCC 25922 as the quality control strain. MIC interpretation adhered to CLSI breakpoints, except for tigecycline (S ≤ 0.5 mg/L; R > 0.5 mg/L) and eravacycline (S ≤ 0.5 mg/L), which followed EUCAST and FDA breakpoints, respectively. Rapid carbapenemase detection utilized a colloidal gold immunoassay (CGI) kit (Gold Mountain River Tech Development Co., Beijing, China) and the carbapenemase inhibitor enhancement test.

Molecular characterization of carbapenemase genes

Whole-genome DNA from the isolates carrying bla_{KPC-2}, and $bla_{KPC-190}$ was extracted using the QIAamp DNA minikit (Qiagen, France). PCR amplification of bla_{KPC} variants employed primers Kpc-rbs (5'-CTCCACCTTCAAACAAGGAAT-3') and Kpc-rev (5'-ATCTGCAGAATTCGCCCTTCGCCATCGTCAGTGCTC TAC-3'), and the resulting products were cloned into plasmid pHSG398 downstream of the *pLac* promoter for phenotypic studies. Recombinant plasmids were electroporated into *E. coli* DH5α and *K. pneumonia* 13882, and constructs were sequenced using T7 promoter/terminator primers. Gene sequences were analyzed via NCBI tools.

Whole-genome sequencing and bioinformatics analysis

Genomic DNA was sequenced on the Illumina MiSeq platform (paired-end, 2×300 bp) and supplemented with Oxford Nanopore long-read sequencing. Hybrid *de novo* assembly was conducted using Unicycler v0.4.8. Resistance genes, plasmid replicons, and sequence types were annotated using RAST v2.0, MLST, PlasmidFinder, and ResFinder. Single nucleotide polymorphism (SNP) analysis was performed with Snippy v4.4.3 using *K. pneumoniae* 5055 as a reference. The genetic environment of bla_{KPC} was examined with VRprofile, and plasmid drafts were generated via Proksee.

Plasmid transformation and conjugation experiments

To evaluate the transferability of ceftazidime-avibactam resistance, a conjugation experiment was performed using *Klebsiella pneumoniae* LX02 as the donor strain and *Escherichia coli* J53 and EC600 as the recipient. Transconjugants were selected on Luria–Bertani (LB) agar plates containing ceftazidime-avibactam (1 μg/mL) and sodium azide or Rifampin (150 μg/mL). In addition, a transformation experiment was carried out by extracting plasmid DNA from *K. pneumoniae* LX02 using the phenol–chloroform method, followed by electroporation into *E. coli* DH5α as the recipient strain. Transformants were grown on LB agar plates supplemented with ampicillin (50 μg/mL), screened for the presence of the bla_{KPC} gene via PCR, and further analyzed through sequencing and comparison using the BLAST program (http://blast.ncbi.nlm.nih.gov/Blast.cgi) (Poirel et al., 2011).

Protein purification and enzyme kinetics

The bla_{KPC} coding region (amino acids 25-293) was inserted into the pET-28a expression plasmid to generate an N-terminally His-tagged recombinant protein. Following transformation into *E. coli* BL21(DE3) cells, the expressed protein was isolated using immobilized metal affinity chromatography followed by size-exclusion purification (Pemberton et al., 2017). Protein quantification was achieved through UV absorbance at 280 nm, applying a molar extinction coefficient of 39,545 $M^{-1}cm^{-1}$, with final concentrations adjusted to 10-20 mg/mL.

Enzyme activity measurements were conducted spectrophotometrically under ambient conditions using purified protein preparations. Reactions were carried out in phosphate-buffered saline (pH7.4), with kinetic constants derived by nonlinear regression analysis of the Michaelis-Menten model (Winkler et al., 2015). Nitrocefin hydrolysis was assessed by tracking absorbance changes at 482 nm across a concentration gradient. Ceftazidime turnover rates were quantified by monitoring absorbance at 257 nm, while meropenem and imipenem degradation were both followed at 299 nm, both using identical experimental setups with appropriate substrate concentration ranges.

Inhibitor potency (IC_{50}) against KPC-2 and KPC-190 variants was evaluated using nitrocefin hydrolysis as reporter activity. Protein samples were pre-incubated with serial dilutions (0-30 μM) of avibactam for 10 minutes prior to substrate addition (100 μM final nitrocefin concentration). After 30 minutes incubation, 482 nm absorbance measurements were collected and dose-response curves generated using Prism analysis software.

Results

Overview of the *K. pneumoniae* clinical isolate

K. pneumoniae LX01 and LX02 were sequentially isolated from a 65-year-old male patient hospitalized at the Second Affiliated Hospital of Xi'an Jiaotong University for hospital-acquired pneumonia (HAP) complicating acute liver failure. The patient had significant comorbidities including hypertension, and type 2 diabetes.

On admission, he was empirically treated with meropenem (1 g q8h for 5 d) for suspected Gram-negative infection. Despite therapy, persistent fever (38.5-39.2°C), leukocytosis (WBC 15.3×10^9/L), and elevated procalcitonin (2.8 ng/mL) were observed, with *K. pneumoniae* LX01 (carbapenem-resistant) isolated from sputum cultures (≥10^5 CFU/mL). Treatment was escalated to ceftazidime-avibactam (2.5 g q8h).

After 10 days, while fever subsided, inflammatory markers remained elevated (CRP 48 mg/L, PCT 1.2 ng/mL), and *K. pneumoniae* LX02 (ceftazidime-avibactam-resistant) was isolated. Rectal screening confirmed did not carry KPC-producing *K. pneumoniae* in the intestine before treatment. Final clearance was achieved with tigecycline (100 mg q12h for 4 d), with normalization of clinical (afebrile) and laboratory (WBC 8.7×10^9/L, CRP <10 mg/L) parameters before discharge. A comprehensive timeline of the patient's medication history is shown in Figure 1.

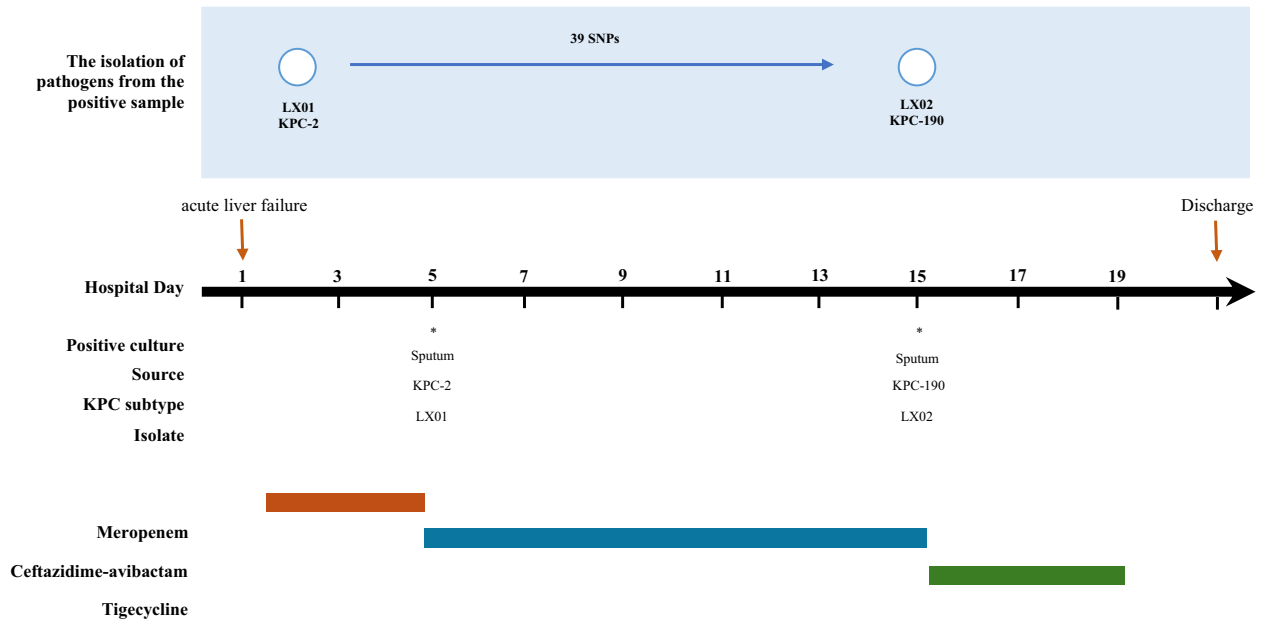

FIGURE 1
Timeline clinical history of the case patient. * indicates the isolation of KPC-positive Klebsiella pneumoniae.

Antimicrobial susceptibility testing and *bla*$_{KPC}$ gene expression

Antimicrobial susceptibility testing revealed distinct resistance profiles for the *K. pneumoniae* clinical isolates carrying KPC-2 and its variants (Table 1). The initial strain, LX01 (KPC-2), displayed high resistance to carbapenems (imipenem MIC = 32 μg/mL, meropenem MIC = 16 μg/mL). After 10 days of ceftazidime-avibactam therapy, the second isolate, LX02 (KPC-190), exhibited resistance to ceftazidime-avibactam (MIC > 64 μg/mL) and carbapenems (imipenem MIC = 2 μg/mL, meropenem MIC = 4 μg/mL). These findings suggest that the evolution from KPC-2 to KPC-190 resulted in partial restoration of carbapenem susceptibility, while maintaining high level resistance to ceftazidime-avibactam. The two isolates were resistant to all the β-lactams tested, quinolones, and aminoglycosides but they were susceptible to colistin and tigecycline. Concerning the BLICs, the isolate was resistant to CZA and susceptible to meropenem-vaborbactam, imipenem-relebactam and aztreonam-avibactam. Resistance to FDC (MIC = 8 mg/L) was also detected. In addition, there was a significant upward trend in the *bla*$_{KPC}$ gene expression during treatment in *K. pneumoniae* LX02. This strain showed a 4-fold increase in gene expression when compared to the initially isolated *K. pneumoniae* LX01.

WGS analysis of the *bla*$_{KPC}$-carrying plasmid

Comparative analysis revealed that the two isolates differed by 39 SNPs, which showed a high degree of homology (Figure 1). Whole-genome sequencing analysis confirmed that the two strains belonged to clone ST11-KL64 with the *iucABCD-iutA* virulence cluster and *rmpA/rmpA2* genes, which could be identified as hypervirulent *K. pneumoniae* (Li et al., 2018) in association with the patient's poor prognosis. In addition, several resistance genes were found, including the β-lactamase genes *bla*$_{CTX-M-65}$, *bla*$_{SHV-12}$, and *bla*$_{TEM-1B}$, the aminoglycoside resistance genes *rmtB* and *aadA2*, the fluoroquinolone resistance gene *qnrS1*, the fosfomycin resistance gene *fosA3*, the trimethoprim-sulfamethoxazole resistance genes *dfrA14* and *sul2*. The *bla*$_{KPC-2}$ gene was detected in *K. pneumoniae* LX01. Notably, whole-genome comparative analysis also revealed one novel *bla*$_{KPC-2}$ variants in *K. pneumoniae* LX02, designated *bla*$_{KPC-190}$. Nucleotide alignment of *bla*$_{KPC}$ variants revealed variations in both the Ω-loop and the 237-243 loop (D179Y and A243V) (Figure 2).

The complete sequence was also obtained for plasmid characterization. *bla*$_{KPC-2}$-positive *K. pneumoniae* LX01 was used as a representative strain. This strain had five plasmids pVir-LX01, pKPC-LX01, p3-LX01, p4-LX01, and p5-LX01 with sizes of approximately 193, 136, 87, 12, 0.5kb. Virulence factors including iroN, rmpA, iucA, iucB, iucC, iucD, iutA, rmpA2 were identified on the virulence plasmid pVir-LX01. The *bla*$_{KPC}$ was located on the IncFII-type plasmid, pKPC-LX01, which was reported to be one of the key vectors mediating transmission of *bla*$_{KPC}$ (Yang et al., 2021). The multi-replicon enhanced the ability to replicate in a wider range of hosts (Li et al., 2019). *bla*$_{CTX-M-65}$, *bla*$_{TEM-1B}$, *rmtB* were also identified in this plasmid. In addition, several resistance genes including qnrS1, dfrA14 were carried by the plasmid p3-LX01. BLAST analysis revealed that the plasmid pKPC-LX01 had high coverage with the plasmid pNC75-5 in the NCBI database, which carries *bla*$_{KPC-2}$ isolated from clinical *K. pneumoniae* (Figure 3).

TABLE 1 Antimicrobial susceptibility profiles of clinical strains of *K. pneumoniae* (LX01 and LX02), bla_{KPC}-positive conjugants and transformants, recipient strain.

Antimicrobials	MIC							
	LX01 (KPC-2)	LX02 (KPC-190)	pHSG398-*E. coli* DH5a	KPC-2-*E. coli* DH5a	KPC-190-*E. coli* DH5a D179Y and A243V	*K. pneumoniae* 13882-pHSG398	*K. pneumoniae* 13882-KPC-2	*K. pneumoniae* 13882-KPC-190
Imipenem	32	2	0.125	16	0.5	0.125	16	0.5
Meropenem	16	4	≤0.06	4	0.25	≤0.06	16	0.25
Meropenem-vaborbactam	2	2	≤0.06	≤0.06	≤0.06	≤0.06	≤0.06	≤0.06
Ceftazidime	>32	>32	0.5	16	128	0.5	8	128
Ceftazidime-avibactam	8	>64	0.125	0.125	32	0.125	0.5	128
Imipenem-relebactam	0.5	0.5	0.125	0.125	0.125	0.125	0.125	0.125
Amikacin	>128	>128	1	0.5	1	1	1	1
Aztreonam	>128	>128	0.125	128	1	0.125	64	32
Aztreonam-avibactam	1	2	0.125	0.125	0.125	0.125	0.125	0.125
Cefiderocol	8	8	0.06	0.06	0.06	0.06	0.06	0.06
Ciprofloxacin	>8	>8	≤0.06	≤.06	≤.06	≤0.06	≤0.06	≤0.06
Polymyxin B	0.25	0.25	0.5	0.5	0.5	0.5	0.5	0.5
Tigecycline	0.5	0.25	0.25	0.25	0.25	0.25	0.25	0.25

Grey shading indicates resistance to antimicrobials.

Plasmid transformation assay

Plasmid transformation assays yielded significant results (Table 1). Transformants KPC-190-*E. coli* DH5a increased the MICs of ceftazidime-avibactam and ceftazidime by at least 256- and 256-fold, respectively compared with the recipient *E. coli* DH5α. KPC-190 mediated a 4-fold increase in MICs for imipenem, for meropenem, KPC-190 mediated an at least 4-fold

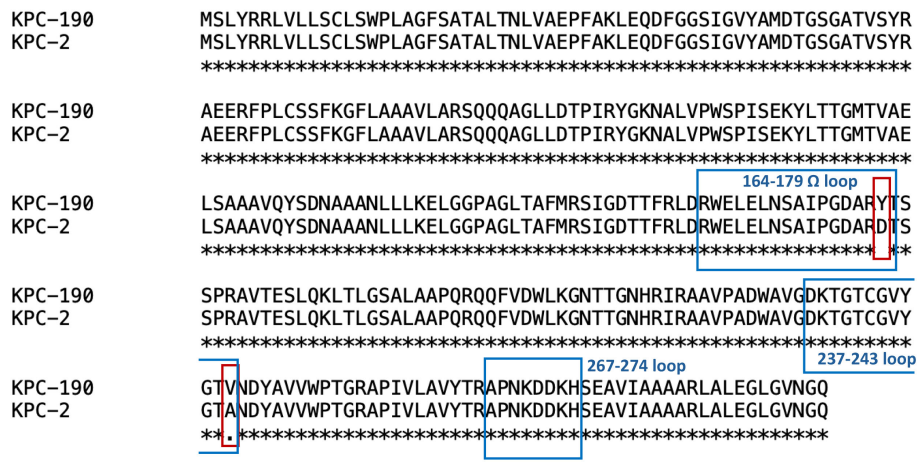

FIGURE 2
Amino acid sequence alignment of KPC-2 and KPC-190. Amino acids that don't match the reference are marked with red frame.

10.3389/fcimb.2025.1607127

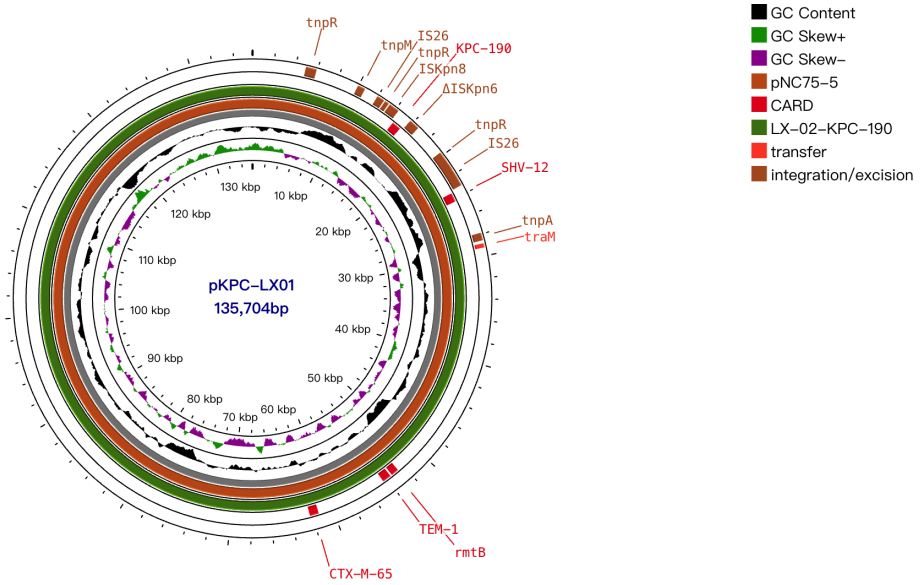

FIGURE 3
Alignments of plasmids. Comparison of the plasmids pKPC-LX01 with plasmid pNC75-5 (134,876 bp, GenBank accession no. CP163294.1). Pivotal genes related to replication, transfer, transposition, and resistance are labeled.

increase in the MIC of imipenem. Notably, no bla_{KPC}-containing conjugants were detectable when either *E. coli* EC600 or J53 were used as recipients. The bla_{KPC}-containing plasmids in this study do not appear to be self-conjugative, potentially due to the absence of relaxase and T4CP.

Functional characterization of KPC variants

The recombinant plasmids carrying bla_{KPC} were successfully introduced into the recipient strain *K. pneumoniae* ATCC 13882. bla_{KPC-2} conferred resistance to most β-lactams including ceftazidime, cefepime, imipenem, and meropenem, but retained susceptibility to ceftazidime-avibactam (Table 1). In contrast to the bla_{KPC-2}-positive clonal strains, the MICs of the $bla_{KPC-190}$ strains decreased at least 32-fold towards carbapenems and increased at least 64-fold to ceftazidime-avibactam. In general, the bla_{KPC-2} variants conferred resistance to ceftazidime-avibactam and susceptibility to carbapenems compared to bla_{KPC-2}. Importantly, the bla_{KPC-2} variants appeared to confer a higher ceftazidime-avibactam MIC in *K. pneumoniae* than in *E. coli*. This suggests that variations in strain backgrounds may influence the expression of bla_{KPC} variants. In addition, emerging carbapenemase inhibitor combinations, namely imipenem-relebactam, aztreonam-avibactam, and meropenem-vaborbactam, showed superior inhibitory performance against both bla_{KPC-2} and variants.

Enzyme kinetic data

The enzyme kinetics and IC_{50} values of KPC-2 and KPC variants were determined. Enzymatic assays demonstrated that the hydrolytic activity (*Kcat/Km*) of KPC-190 against carbapenems was reduced compared to KPC-2. Hydrolytic activity against ceftazidime was significantly decreased for KPC-190 compared to KPC-2, indicating that the KPC-190 enzymes exhibited reduced hydrolysis and higher affinity for ceftazidime compared with wild-type KPC-2 (Table 2). Notably, the KPC variants had almost no detectable hydrolysis activity

TABLE 2 Kinetic parameters and IC_{50} of the β-lactamases KPC-2 and KPC-190.

Antimicrobials	bla_{KPC} variants	K_m(μM)	K_{cat}(s^{-1})	K_{cat}/K_m ($\mu M^{-1}s^{-1}$)	IC_{50}(μM)
Imipenem	bla_{KPC-2}	450.3	74	0.16	/
	$bla_{KPC-190}$	522.13	62.15	0.12	/
Meropenem	bla_{KPC-2}	96.35	89.21	0.93	/
	$bla_{KPC-190}$	241.61	62.31	0.26	/
Ceftazidime	bla_{KPC-2}	78.32	2.5	0.032	/
	$bla_{KPC-190}$	87.86	0.87	0.001	/
Avibactam	bla_{KPC-2}	/	/	/	0.014
	$bla_{KPC-190}$	/	/	/	0.13

of carbapenems (ertapenem, imipenem, and meropenem), indicating reduced activity to carbapenems. To evaluate the inhibitory activity of the inhibitor against the KPC-2 and KPC-190 enzymes, the 50% inhibitory concentration (IC_{50}) values for avibactam were also measured. The IC_{50} values for avibactam were markedly higher for KPC-190 (0.13 μM) compared to KPC-2 (0.014 μM), indicating a significant reduction in avibactam binding affinity. This low affinity for avibactam, coupled with the retained hydrolytic activity against carbapenems, accounts for the resistance phenotype of KPC-190.

Genetic context of *bla*$_{KPC-190}$ and virulence factors of *K. pneumoniae* LX01

Whole-genome sequencing revealed that *bla*$_{KPC-190}$ is located on an IncFII plasmid within the translocatable unit: IS*26*-IS*Kpn8*-*bla*$_{KPC}$-ΔIS*Kpn6*-ΔtnpR-IS*26*, which contrasts with previous studies where three different variants of Tn*1721* harbouring *bla*$_{KPC-2}$ (referred to as A1-, A2-, and B-type) predominated in China (Figure 4). Here, IS*26* replaced Tn*1721* to form a transposable structure with double IS*26* flanking the IS*Kpn6*-*bla*$_{KPC}$-IS*Kpn27* core structure, a configuration rarely observed in *bla*$_{KPC}$ variants.

The ST11-K64 *Klebsiella pneumoniae* LX02 strain harbored a variety of virulence factors (Table 3). Notably, it contained a large virulence plasmid approximately 200 kb in size, which carried genes conferring resistance to heavy metals such as copper and silver, alongside virulence-related genes responsible for capsular polysaccharide synthesis regulation (*rmpA*/*rmpA2*) and iron acquisition systems (*iucABCD*-*iutA*). This plasmid shared significant similarity with the widely disseminated pLVPK-like plasmids (reference sequence GenBank accession number CP094941) but lacked a ~25-kb pathogenicity island that includes *rmpA*, *fecAIR*, and *iroBCDN*.

In addition to the plasmid, the bacterial chromosome encoded multiple virulence-associated gene clusters. These included the *fim* and *mrk* clusters, which are responsible for the production of type 1 and type 3 fimbriae, respectively. These fimbriae, in combination with capsule production, represented the primary virulence mechanisms of *K. pneumoniae* LX02. Interestingly, copy number variations (CNVs) were observed in some chromosomal genes, with a slight reduction in *mrkA* and an increase in *pgaA*.

Discussion

The *bla*$_{KPC-2}$-positive ST11 type CRKP strains have emerged as a formidable clonal lineage in China, posing a threat in clinical settings (Shi et al., 2020; Huang et al., 2023). Ceftazidime-avibactam, an effective antibiotic, has been clinically approved in China since 2019, with a predicted increase in resistance following extensive use (Dietl et al., 2020). Resistance to ceftazidime-avibactam in CRKP strains has typically been correlated with various variations in the *bla*$_{KPC-2}$ gene (Wang et al., 2020). More than 60% of novel KPC gene subtypes have emerged since 2019, with variations primarily occurring in four loops surrounding the active site core: the 105-loop (Leu102 to Ser106), Ω-loop (Arg164 to Asp179), 240-loop (Cys238 to Thr243) and 270-loop (Ala267 to Ser275) (Hobson et al., 2020). Amino acid substitutions in the Ω-loop of the KPC-2, particularly at position 179, are the major contributors to resistance against ceftazidime-avibactam (Li et al., 2021). In this study, *bla*$_{KPC-190}$ was identified as a novel variant arising during ceftazidime-avibactam therapy in a patient with CRKP infection. This variant exhibited resistance to both ceftazidime-avibactam and carbapenems. The reduced hydrolytic activity of KPC-190 towards ceftazidime, coupled with its decreased affinity for avibactam, highlights the complex interplay of structural variations that contribute to its resistance phenotype. This structural characteristic likely makes ceftazidime more susceptible to "capture" by KPC-190 variants compared to the KPC-2 enzyme (Barnes et al., 2017; Alsenani et al., 2022). Ceftazidime contains

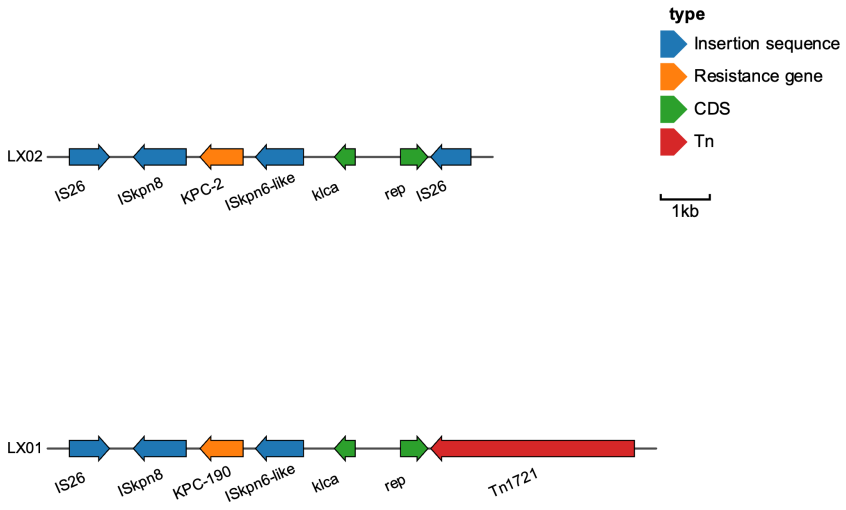

FIGURE 4
Genetic environment of blaKPC-2 and blaKPC-190 and comparative analysis.

TABLE 3 Genetic characterization of strains *K. pneumoniae* LX01 and *K. pneumoniae* LX02.

Strain	contig	Size (bp)	Resistance and virulence genes	Inc type
LX01	chromosome	5435629	*aadA2b*, $bla_{SHV-182}$, fosA6, sul1, *yagV/ecpE, yagW/ecpD, yagX/ecpC, yagY/ecpB, yagZ/ecpA, ykgK/ecpR, galF, cpsACP, wzi, wza, wcaJ, gnd, manC, manB, wbtL, ugd, wzm, wzt, wbbM, glf, wbbN, wbbO, rcsA*	–
	pVir-LX01	192901	*iroN, rmpA, iucA, iucB, iucC, iucD, iutA, rmpA2*	IncHI1B, repB
	pKPC-LX01	135704	bla_{SHV-12}, $bla_{CTX-M-65}$, bla_{TEM-1B}, *rmtB*, bla_{KPC-2}	IncFII
	p3-LX01	87095	*qnrS1*, bla_{LAP-2}, *tet(A), sul2, dfrA14*, catA2	–
	p4-LX01	11970	-	ColRNAI
	p5-LX01	5596		–
LX02	chromosome	5435629	*aadA2b*, $bla_{SHV-182}$, fosA6, sul1, *yagV/ecpE, yagW/ecpD, yagX/ecpC, yagY/ecpB, yagZ/ecpA, ykgK/ecpR, galF, cpsACP, wzi, wza, wcaJ, gnd, manC, manB, wbtL, ugd, wzm, wzt, wbbM, glf, wbbN, wbbO, rcsA*	–
	pVir-LX01	192957	*iroN, rmpA, iucA, iucB, iucC, iucD, iutA, rmpA2*	IncHI1B, repB
	pKPC-LX01	135704	bla_{SHV-12}, $bla_{CTX-M-65}$, bla_{TEM-1B}, *rmtB*, $bla_{KPC-190}$	IncFII
	p3-LX01	87095	*qnrS1*, bla_{LAP-2}, *tet(A), sul2, dfrA14*, catA2	–
	p4-LX01	11970	-	ColRNAI
	p5-LX01	5596		–

10.3389/fcimb.2025.1607127

bulky R1 substituents and small pyridine R2 substituents, which enhance its intrinsic rigidity. This structural feature may influence the two-component regulatory system, thereby contributing to bacterial resistance mechanisms (Alsenani et al., 2022).

The detection rate of KPC variants has risen sharply in recent years, with the number of newly identified bla_{KPC} subtypes in the past two years surpassing the total discovered over the previous two decades. These KPC variations are strongly linked to ceftazidime-avibactam treatment (especially in sporadic cases). A recent study reported that up to 48.4% (15/31) of *K. pneumoniae* isolates carrying KPC variants were identified following ceftazidime-avibactam therapy. In our study, the KPC variant developed as a result of prolonged exposure to ceftazidime-avibactam. As the existing studies have shown (Zhang et al., 2023), with the widespread use of ceftazidime-avibactam, the bla_{KPC} copy number increases under ceftazidime-avibactam pressure, accompanied by further variations in single bla_{KPC}.

Unlike the Tn*4401* transposon, the most prevalent bla_{KPC}-containing mobile element, genomic analysis revealed that $bla_{KPC-190}$ is located on an IncFII plasmid within the conserved genetic context IS26-ISKpn8-blaKPC-ΔISKpn6-ΔtnpR- IS26. The presence of two IS26 components is noteworthy, previous studies have shown that many deletions and insertions were accompanied by one or two tandem copies of IS26 (Varani et al., 2021; Shi et al., 2024). This suggests the possibility of IS26-mediated transposition, which may contribute to the diversity of resistance mechanisms and facilitate transmission (Varani et al., 2021).

The evolution of blaKPC-190 presents significant clinical and diagnostic challenges. Conventional detection methods may fail to identify this variant due to enzyme conformational changes, potentially yielding false-negative results. The strain's atypical susceptibility profile - resistant to ceftazidime-avibactam but variably susceptible to carbapenems - complicates routine antimicrobial susceptibility testing. Chromogenic media (e.g., chromID® CARBA SMART) could support diagnostic surveillance by improving detection of such KPC variants (Bianco et al., 2022). Furthermore, the risk of misidentification as ESBL-producing strains remains a concern, particularly given the current lack of standardized protocols for KPC-variant detection.

Therapeutically, the emergence of KPC-190 highlights the limitations of current treatment regimens for CRKP infections. Although alternative β-lactam/β-lactamase inhibitor combinations, such as meropenem-vaborbactam, show promise, their availability remains limited in many regions. The use of combination therapies, as seen in this case, may delay the onset of resistance but does not prevent the evolution of bla_{KPC} variants. Adjusting dosage regimens and incorporating therapeutic drug monitoring (TDM) for ceftazidime-avibactam may mitigate the risk of resistance variations. Additionally, novel diagnostic tools capable of rapidly identifying bla_{KPC} variants are essential for guiding treatment decisions.

In conclusion, KPC-190 exemplifies the dynamic evolution of bla_{KPC} genes under antibiotic pressure and highlights the urgent need for enhanced global surveillance systems to monitor the emergence of novel KPC variants. Addressing the diagnostic and therapeutic challenges posed by KPC-190 will require a multifaceted approach, including the development of robust diagnostic assays, the optimization of treatment strategies, and the establishment of comprehensive surveillance networks to track the spread of resistant strains. These efforts are critical for mitigating the impact of KPC-190 and preserving the efficacy of current therapeutic options.

Data availability statement

The datasets presented in this study can be found in online repositories. The names of the repository/repositories and accession number(s) can be found in the article/supplementary material.

Author contributions

ZL: Conceptualization, Data curation, Formal analysis, Methodology, Writing – original draft, Writing – review & editing. JL: Data curation, Investigation, Project administration, Resources, Writing – original draft. XZ: Investigation, Project administration, Writing – review & editing. JY: Formal analysis, Investigation, Methodology, Writing – review & editing. YZ: Formal analysis, Methodology, Writing – review & editing. KL: Conceptualization, Formal analysis, Visualization, Writing – review & editing. YG: Conceptualization, Project administration, Software, Validation, Writing – review & editing. LH: Conceptualization, Supervision, Writing – review & editing. QH: Formal analysis, Resources, Writing – review & editing. AH: Conceptualization, Funding acquisition, Investigation, Methodology, Project administration, Writing – original draft, Writing – review & editing.

Funding

The author(s) declare that financial support was received for the research and/or publication of this article. This work was supported by the Key Research and Development Plan of Shaanxi Province (2024SF-YBXM-160), the Key Research and Development Plan of Shaanxi Province (2020SF-173), Innovation Capability Support Program-Medical Research Projects of Xi'an Science and Technology Bureau (23YXYJ0123) and the project of the First Affiliated Hospital of Xi'an Medical University (XYYFY-2023-08).

Conflict of interest

The authors declare that the research was conducted in the absence of any commercial or financial relationships that could be construed as a potential conflict of interest.

Generative AI statement

The author(s) declare that no Generative AI was used in the creation of this manuscript.

Publisher's note

References

Alsenani, T. A., Viviani, S. L., Kumar, V., Taracila, M. A., Bethel, C. R., Barnes, M. D., et al. (2022). Structural characterization of the D179N and D179Y variants of KPC-2 β-lactamase: Ω-loop destabilization as a mechanism of resistance to ceftazidime-avibactam. *Antimicrob Agents Chemother.* 66, e0241421. doi: 10.1128/aac.02414-21

Barnes, M. D., Winkler, M. L., Taracila, M. A., Page, M. G., Desarbre, E., Kreiswirth, B. N., et al. (2017). Klebsiella pneumoniae Carbapenemase-2 (KPC-2), Substitutions at Ambler Position Asp179, and Resistance to Ceftazidime-Avibactam: Unique Antibiotic-Resistant Phenotypes Emerge from β-Lactamase Protein Engineering. *mBio* 8 (5), e00528-17. doi: 10.1128/mBio.00528-17

Bianco, G., Boattini, M., Comini, S., Leone, A., Bondi, A., Zaccaria, T., et al. (2022). Implementation of Chromatic Super CAZ/AVI(®) medium for active surveillance of ceftazidime-avibactam resistance: preventing the loop from becoming a spiral. *Eur. J. Clin. Microbiol Infect. Dis.* 41, 1165–1171. doi: 10.1007/s10096-022-04480-x

Boattini, M., Bianco, G., Bastos, P., Comini, S., Corcione, S., Almeida, A., et al. (2024). Prevalence and mortality of ceftazidime/avibactam-resistant KPC-producing Klebsiella pneumoniae bloodstream infections (2018-2022). *Eur. J. Clin. Microbiol Infect. Dis.* 43, 155–166. doi: 10.1007/s10096-023-04712-8

Castón, J. J., Cano, A., Pérez-Camacho, I., Aguado, J. M., Carratalá, J., Ramasco, F., et al. (2022). Impact of ceftazidime/avibactam versus best available therapy on mortality from infections caused by carbapenemase-producing Enterobacterales (CAVICOR study). *J. Antimicrob Chemother.* 77, 1452–1460. doi: 10.1093/jac/dkac049

Chou, S. H., Chuang, C., Juan, C. H., Ho, Y. C., Liu, S. Y., Chen, L., et al. (2024). Mechanisms and fitness of ceftazidime/avibactam-resistant Klebsiella pneumoniae clinical strains in Taiwan. *Int. J. Antimicrob Agents* 64, 107244. doi: 10.1016/j.ijantimicag.2024.107244

Dietl, B., Martínez, L. M., Calbo, E., and Garau, J. (2020). Update on the role of ceftazidime-avibactam in the management of carbapenemase-producing Enterobacterales. *Future Microbiol* 15, 473–484. doi: 10.2217/fmb-2020-0012

Findlay, J., Bianco, G., Boattini, M., and Nordmann, P. (2025). High-level cefiderocol and ceftazidime/avibactam resistance in KPC-producing Klebsiella pneumoniae associated with mutations in KPC and the sensor histidine kinase EnvZ. *J. Antimicrob Chemother.* 80, 1155–1157. doi: 10.1093/jac/dkaf048

Gonçalves Barbosa, L. C., Silva, E. S. J. A., Bordoni, G. P., Barbosa, G. O., and Carneiro, L. C. (2022). Elevated mortality risk from CRKp associated with comorbidities: systematic review and meta-analysis. *Antibiotics (Basel)* 11 (7), 874. doi: 10.3390/antibiotics11070874

Hobson, C. A., Bonacorsi, S., Jacquier, H., Choudhury, A., Magnan, M., Cointe, A., et al. (2020). KPC beta-lactamases are permissive to insertions and deletions conferring substrate spectrum modifications and resistance to ceftazidime-avibactam. *Antimicrob Agents Chemother.* 64 (12), e01175-20. doi: 10.1128/AAC.01175-20

Huang, X., Shen, S., Chang, F., Liu, X., Yue, J., Xie, N., et al. (2023). Emergence of KPC-134, a KPC-2 variant associated with ceftazidime-avibactam resistance in a ST11 Klebsiella pneumoniae clinical strain. *Microbiol Spectr.* 11, e0072523. doi: 10.1128/spectrum.00725-23

Karaiskos, I., Daikos, G. L., Gkoufa, A., Adamis, G., Stefos, A., Symbardi, S., et al. (2021). Ceftazidime/avibactam in the era of carbapenemase-producing Klebsiella pneumoniae: experience from a national registry study. *J. Antimicrob Chemother.* 76, 775–783. doi: 10.1093/jac/dkaa503

Karakonstantis, S., Rousaki, M., and Kritsotakis, E. I. (2022). Cefiderocol: systematic review of mechanisms of resistance, heteroresistance and *in vivo* emergence of resistance. *Antibiotics (Basel)* 11 (6), 723. doi: 10.3390/antibiotics11060723

Lan, P., Lu, Y., Jiang, Y., Wu, X., Yu, Y., and Zhou, J. (2022). Catecholate siderophore receptor CirA impacts cefiderocol susceptibility in Klebsiella pneumoniae. *Int. J. Antimicrob Agents* 60, 106646. doi: 10.1016/j.ijantimicag.2022.106646

Li, D., Li, K., Dong, H., Ren, D., Gong, D., Jiang, F., et al. (2021). Ceftazidime-Avibactam Resistance in Klebsiella pneumoniae Sequence Type 11 Due to a Mutation in Plasmid-Borne bla (kpc-2) to bla (kpc-33), in Henan, China. *Infect. Drug Resist.* 14, 1725–1731. doi: 10.2147/IDR.S306095

Li, J., Ren, J., Wang, W., Wang, G., Gu, G., Wu, X., et al. (2018). Risk factors and clinical outcomes of hypervirulent Klebsiella pneumoniae induced bloodstream infections. *Eur. J. Clin. Microbiol Infect. Dis.* 37, 679–689. doi: 10.1007/s10096-017-3160-z

Li, Y., Shen, H., Zhu, C., and Yu, Y. (2019). Carbapenem-Resistant Klebsiella pneumoniae Infections among ICU Admission Patients in Central China: Prevalence and Prediction Model. *BioMed. Res. Int.* 2019, 9767313. doi: 10.1155/2019/9767313

Oliva, A., Volpicelli, L., Gigante, A., Di Nillo, M., Trapani, S., Viscido, A., et al. (2024). Impact of renal-adjusted ceftazidime/avibactam in patients with KPC-producing Klebsiella pneumoniae bloodstream infection: a retrospective cohort study. *JAC Antimicrob Resist.* 6, dlae201. doi: 10.1093/jacamr/dlae201

Pemberton, O. A., Zhang, X., and Chen, Y. (2017). Molecular basis of substrate recognition and product release by the klebsiella pneumoniae carbapenemase (KPC-2). *J. Med. Chem.* 60, 3525–3530. doi: 10.1021/acs.jmedchem.7b00158

Poirel, L., Walsh, T. R., Cuvillier, V., and Nordmann, P. (2011). Multiplex PCR for detection of acquired carbapenemase genes. *Diagn. Microbiol Infect. Dis.* 70, 119–123. doi: 10.1016/j.diagmicrobio.2010.12.002

Sharma, R., Park, T. E., and Moy, S. (2016). Ceftazidime-avibactam: A novel cephalosporin/β-lactamase inhibitor combination for the treatment of resistant gram-negative organisms. *Clin. Ther.* 38, 431–444. doi: 10.1016/j.clinthera.2016.01.018

Shi, Q., Shen, S., Tang, C., Ding, L., Guo, Y., Yang, Y., et al. (2024). Molecular mechanisms responsible KPC-135-mediated resistance to ceftazidime-avibactam in ST11-K47 hypervirulent Klebsiella pneumoniae. *Emerg Microbes Infect.* 13, 2361007. doi: 10.1080/22221751.2024.2361007

Shi, Q., Yin, D., Han, R., Guo, Y., Zheng, Y., Wu, S., et al. (2020). Emergence and Recovery of Ceftazidime-avibactam Resistance in blaKPC-33-Harboring Klebsiella pneumoniae Sequence Type 11 Isolates in China. *Clin. Infect. Dis.* 71, S436–s439. doi: 10.1093/cid/ciaa1521

van Duin, D., and Bonomo, R. A. (2016). Ceftazidime/avibactam and ceftolozane/tazobactam: second-generation β-lactam/β-lactamase inhibitor combinations. *Clin. Infect. Dis.* 63, 234–241. doi: 10.1093/cid/ciw243

Varani, A., He, S., Siguier, P., Ross, K., and Chandler, M. (2021). The IS6 family, a clinically important group of insertion sequences including IS26. *Mob DNA* 12, 11. doi: 10.1186/s13100-021-00239-x

Wang, Y., Wang, J., Wang, R., and Cai, Y. (2020). Resistance to ceftazidime-avibactam and underlying mechanisms. *J. Glob Antimicrob Resist.* 22, 18–27. doi: 10.1016/j.jgar.2019.12.009

Winkler, M. L., Papp-Wallace, K. M., and Bonomo, R. A. (2015). Activity of ceftazidime/avibactam against isogenic strains of Escherichia coli containing KPC and SHV β-lactamases with single amino acid substitutions in the Ω-loop. *J. Antimicrob Chemother.* 70, 2279–2286. doi: 10.1093/jac/dkv094

Yang, X., Dong, N., Chan, E. W., Zhang, R., and Chen, S. (2021). Carbapenem resistance-encoding and virulence-encoding conjugative plasmids in klebsiella pneumoniae. *Trends Microbiol* 29, 65–83. doi: 10.1016/j.tim.2020.04.012

Zhang, P., Hu, H., Shi, Q., Sun, L., Wu, X., Hua, X., et al. (2023). The effect of β-lactam antibiotics on the evolution of ceftazidime/avibactam and cefiderocol resistance in KPC-producing klebsiella pneumoniae. *Antimicrob Agents Chemother.* 67, e0127922. doi: 10.1128/aac.01279-22

frontiers | Frontiers in Cellular and Infection Microbiology

TYPE Original Research
PUBLISHED 30 June 2025
DOI 10.3389/fcimb.2025.1583926

OPEN ACCESS

EDITED BY
Daniela Visaggio,
Roma Tre University, Italy

REVIEWED BY
Yahan Wei,
The University of Texas Rio Grande Valley, United States
Karl Pedersen,
Aarhus University, Denmark

*CORRESPONDENCE
Marte Glambek
marte.glambek@uib.no

RECEIVED 26 February 2025
ACCEPTED 11 June 2025
PUBLISHED 30 June 2025

CITATION
Glambek M, Kjos M, Mårli MT, Salehian Z, Skrede S, Sivertsen A, Kittang BR and Oppegaard O (2025) *TrexAB*, a novel tetracycline resistance determinant in *Streptococcus dysgalactiae*. *Front. Cell. Infect. Microbiol.* 15:1583926. doi: 10.3389/fcimb.2025.1583926

TrexAB, a novel tetracycline resistance determinant in *Streptococcus dysgalactiae*

Marte Glambek[1,2]*, Morten Kjos[3], Marita T. Mårli[3], Zhian Salehian[3], Steinar Skrede[1,2], Audun Sivertsen[4], Bård R. Kittang[2,5] and Oddvar Oppegaard[1,2]

[1]Department of Medicine, Haukeland University Hospital, Bergen, Norway, [2]Department of Clinical Science, Faculty of Medicine, University of Bergen, Bergen, Norway, [3]Faculty of Chemistry, Biotechnology and Food Science, Norwegian University of Life Sciences, Ås, Norway, [4]Department of Microbiology, Haukeland University Hospital, Bergen, Norway, [5]Department of Internal Medicine, Haraldsplass Deaconess Hospital, Bergen, Norway

Background: *Streptococcus dysgalactiae* (SD) is a potent pathogen associated with infections in a broad range of host species. Notably, a substantial proportion of SD isolates exhibit reduced susceptibility to tetracycline but lack identifiable resistance determinants. In the present study, we wanted to explore the genetic basis for this low-grade resistance to tetracycline.

Methods: Genome-wide association studies were performed on a collection of 407 SD genomes to identify potential novel resistance determinants. Two strains of SD, belonging to each of the subspecies *dysgalactiae* and *equisimilis* were used for mutagenesis. Natural transformation was exploited to knock out resistance gene candidates, and the resultant mutants were compared with their respective wildtypes regarding susceptibility to tetracycline, doxycycline, minocycline, tigecycline, erythromycin, gentamicin, clindamycin and ciprofloxacin.

Results: We identified a two gene operon, herein designated *trexAB*, significantly associated with reduced susceptibility to tetracycline. The proteins encoded by the operon were predicted *in silico* to constitute a heterodimeric efflux transporter. The knockout of *trexAB* led to a 16- to 32-fold reduction in minimum inhibitory concentration (MIC) for tetracycline and a 4-fold reduction in MIC for tigecycline in the investigated strains. No differences between mutants and wildtypes were observed for other antibiotics included in the test panel. Whole genome alignment of mutants and their respective wildtypes revealed no differences other than the expected differences caused by the knockout.

Conclusion: We have characterized a novel operon causing low-grade resistance to tetracycline in SD. The MIC distribution of *trexAB*-positive isolates is intersected by the current EUCAST susceptibility breakpoint, and our findings are relevant for future revisions and determinations of adequate breakpoints for tetracycline in *S. dysgalactiae*.

KEYWORDS

antibiotic resistance, tetracycline, *Streptococcus dysgalactiae*, natural transformation, ABC transporter

Introduction

Tetracyclines were among the first broad-spectrum antibiotics discovered. The limited number of side-effects together with the availability of oral formulations, made tetracyclines attractive choices in both clinical and agricultural settings. The tetracyclines are divided into three different generations, where the first generation comprises tetracycline, oxytetracycline and chlortetracycline, the second generation includes minocycline and doxycycline, and the glycylcycline tigecycline constitutes the third generation (Thaker et al., 2010).

The tetracyclines inhibit bacterial protein synthesis by binding to the bacterial ribosome, disturbing the bacteria's ability to synthesize proteins. Bacterial resistance against tetracycline occurs by different mechanisms, which mainly fit into the categories of efflux systems, ribosomal protection and drug destruction (Thaker et al., 2010). The more than 60 unique tetracycline resistance determinants characterized to date, indicate that drug efflux is the main resistance strategy in gram-negative bacteria, whereas ribosomal protection is the most common mechanism in gram-positive bacteria (Roberts, 2024). To be defined as a unique resistance gene in this setting, the sequence homology to genes of known function must be lower than 79% at the amino acid level (Levy et al., 1999).

We recently characterized antimicrobial susceptibility patterns of *Streptococcus dysgalactiae* (SD), a gram-positive pathogen known to infect a broad range of host species (Glambek et al., 2024). We explored resistance in a One Health perspective, including both *S. dysgalactiae* subspecies *dysgalactiae* (SDSD) associated with bovine and ovine infections, and *S. dysgalactiae* subspecies *equisimilis* (SDSE) predominantly targeting other animals and humans. Surprisingly, we observed a trimodal distribution of minimum inhibitory concentrations (MIC) values to tetracycline, and a relative high proportion of low-grade tetracycline resistant isolates without an identifiable genetic resistance determinant.

The central cluster of SD isolates had MIC values ranging between 0.5 and 4 µg/ml (herein referred to as the transition zone), and thus encircled the EUCAST breakpoint between sensitive and resistant, suggestive of low-grade phenotypic resistance. Canonical *tet*-genes were identified in nearly all isolates with MIC values above the transition zone, whereas isolates in the central cluster generally did not encode identifiable resistance genes.

In the present study, we explore the underlying mechanism for this low-grade resistance using genome-wide association studies and mutant construction. We report the identification of a novel two-gene operon associated with the low-grade resistance phenotype, likely encoding proteins that together function as an ABC efflux transporter.

Materials and methods

Bacterial isolates

A collection of 407 SD strains procured from human and animal associated infections in Norway during 2018–2019 was investigated in this study. The isolates have previously been whole genome sequenced, examined for antibiotic resistance genes and susceptibility tested for tetracycline (Glambek et al., 2024).

In accordance with the phenotypic definition proposed by Vieira et al (Vieira et al., 1998), we defined SDSD *in silico* as genomes harboring the Lancefield group C-antigen operon, lacking the streptolysin S operon (corresponding to an α- or nonhemolytic reaction on blood agar), and lacking the streptokinase gene (inferring that streptokinase activity on human plasminogen does not occur). All other genomes were classified as SDSE (Glambek et al., 2024).

In silico analysis

DBGWAS was used to search for genetic variants associated with low-grade tetracycline resistance (Jaillard et al., 2018). Strains harboring known tetracycline resistance genes were excluded from the analyses, and minimum inhibitory concentration (MIC) level was used as phenotype-indicator, with a MIC phenoThreshold of 0.5 µg/ml. Genetic variants identified by DBGWAS were mapped to genomic location and inspected using the Geneous Prime v 2024.0 software. The predicted function of annotated genes at matching loci was evaluated by screening for conserved functional domains using CD search (Wang et al., 2022) and InterProScan 102.0 (Blum et al., 2024), with default settings. Searches for homologue genes and proteins to our candidate tetracycline resistance genes were done using megaBLASTn and BLASTp, respectively.

A core genome single-nucleotide polymorphism phylogeny was generated by CSI Phylogeny at the Center for Genomic Epidemiology (Kaas et al., 2014) using default settings and the SDSE type strain NCTC13762 as a reference. The resulting maximum likelihood phylogenetic tree was visualized and annotated using the Interactive Tree of Life platform, iTol v6 (Letunic and Bork, 2021).

Screening of global collection of SD genomes

For comparative analysis, we downloaded a global collection of SD genomes from published epidemiological studies available from GenBank and PubMLST. These included human associated isolates collected in Australia (Xie et al., 2024), Canada (Lother et al., 2017) and Japan (Shinohara et al., 2023), bovine isolates from Canada (Vélez et al., 2017), as well as swine and horse isolates from Italy, US and Portugal (Pinho et al., 2016; Cinthi et al., 2023). The genomes were *de novo* assembled using SPAdes v 5.14 (Bankevich et al., 2012), annotated using RAST v 1.073 (Aziz et al., 2008), and screened for the presence of candidate genes using the Geneious Prime v 2024.0 software.

Growth conditions and susceptibility testing

In the knockout experiments, bacteria were grown in airtight tubes in C-medium (Lacks and Hotchkiss, 1960) or on brain heart

infusion (BHI) agar plates at 37 °C in 10% CO_2. For selection of knock out mutants, kanamycin was added to the BHI agar to a final concentration of 400 µg/ml.

Knockout mutants and their respective wild types were examined for susceptibility to tetracycline, doxycycline, minocycline, tigecycline, erythromycin, gentamicin, clindamycin and ciprofloxacin according to the NORM protocol (NORM, 2019). Briefly, isolates were plated on Mueller-Hinton agar supplemented with defibrinated horse blood and β-NAD. MIC-levels were determined using MIC-gradient strips.

Synthetic peptides

Synthetic nature quorum sensing peptide pheromones, XIP1 (aa: EFDWWNLG) and XIP2 (aa: QVDWWRL) were purchased from Thermo Scientific.

Construction of deletion fragment and deletion of *trexAB* by natural transformation

A linear DNA fragment for homologous recombination to delete *trexAB* was assembled using overlap extension PCR (Higuchi et al., 1988). Amplicons of approximately 2 kb length of flanking sequences to the *trexAB*-operon in addition to a core sequence consisting of the so-called Janus cassette (Sung et al., 2001), encoding a kanamycin resistance cassette and a *rpsL*-allele, were made by PCR and extracted from agarose gel. The *trexAB* upstream and downstream fragments were merged to the 5' end and 3' end of the Janus cassette, respectively, making a DNA construct to create genetic knockouts (Higuchi et al., 1988). Primers used are listed in Table 1.

Two SD isolates were selected for functional studies of the *trexAB* operon, the human associated isolate iSDSE_NORM6 of subspecies *equisimilis*, and the bovine associated isolate SDSD24 of subspecies *dysgalactiae*. These strains contained an intact *trexAB* operon and displayed low grade resistance to tetracycline, without possessing any validated tetracycline resistance genes. These strains also possessed a complete and intact apparatus for competence and natural transformation (Mårli et al., 2024).

The natural transformation procedure was adapted from the protocol described by Mårli and co-workers (Mårli et al., 2024). Briefly, overnight cultures of isolates to be transformed were diluted in C-medium to an initial OD_{600} of 0.05 for further incubation until reaching OD_{600} 0.2. The cultures were again diluted to OD_{600} 0.03 and finally grown to OD_{600} 0.05 before approximately 400 ng of DNA-construct and 250 ng of XIP1 (iSDSE_NORM6) or XIP2 (SDSD24) was added to 1 ml culture. Cultures were further incubated at 37°C for 3–4 hours and then plated on BHI agar containing 400 µg/ml kanamycin and grown overnight for selection of kanamycin resistant mutants. Cultures without the added DNA-construct, were used as negative controls.

Whole genome sequencing

Genomic DNA was purified using MagNA Pure extraction kit (Roche Life Science). Whole genome sequencing of knockout mutant strains was performed at Haukeland University Hospital on an Illumina 4,000 HiSeq system to produce 150 bp paired end reads, as previously described (Oppegaard et al., 2017). The genomes of mutant and wildtype strains were aligned with Mauve, and manually compared for insertion, deletion, and mutation events.

Results

Identification of tetracycline resistance determinants

Genome-wide associating studies with DBGWAS identified fifteen genetic regions with at least one polymorphism significantly associated with variations in MIC-level. Only two regions were associated with an increased MIC-level. One of these was a single C/G synonymous mutation in the YidA sugar phosphatase gene, which was deemed unlikely to confer tetracycline resistance. The other was 149 overlapping significant hits constituting a two-gene operon of unknown function. This

TABLE 1 Primers.

Purpose	Primer sequence 5'-3'	Reference
Amplifying upstream fragment	**GAAGACTGAGAAGCCATCAC**	This study
Amplifying upstream fragment	CACATTATCCATTAAAAATCAAAC**GTTATCCTCCTTCTTCTTTTCAG**	This study
Amplifying downstream fragment	GTCCAAAAGCATAAGGAAAG**AATCGTGGCAAGCGTCGTC**	This study
Amplifying downstream fragment	**GCATCTGGTAAGTCCTTTGTC**	This study
Sequence confirmation *trexAB*	**CCCATTAGCATCATGATGGTC**	This study
Sequence confirmation *trexAB*	**TCTGCGACAACAGATTGTCG**	This study
Sequence confirmation *kan* gene	**GTTTGATTTTTAATGGATAATGTG**	Johnsborg et al, 2008
Sequence confirmation *kan* gene	**CTTTCCTTATGCTTTTGGAC**	Johnsborg et al, 2008

Sequence tails not matching target for PCR are marked in grey.

operon was observed in 167 of the 172 strains with MIC values in the transition zone, but only in 13 of the 184 strains with lower MIC values (Figure 1), among which 5 strains contained an intact operon, and the remaining 8 strains had one or both genes truncated (Supplementary Table).

We compared the products of the two novel genes to previously characterized tetracycline resistance determinants using BLASTp. A low-level homology to TetA(46) and TetB(46) was detected (55% and 59% pairwise amino acid sequence identity, respectively), a tetracycline efflux pump encoded by a two gene operon in *Streptococcus australis* (Warburton et al., 2013). We thus decided to further explore the potential role in tetracycline resistance of our newly discovered operon, herein designated *trexAB* (Tetracycline Resistance EffluX, gene A and gene B).

Genetic characterization of the *trexAB* operon

The operon comprised the *trexA* gene (1722 base pairs) and *trexB* gene (1743 base pairs). Both genes showed high interstrain homology within our collection of SD, with nucleotide sequence similarity ranging from 98 to 100%.

Screening the predicted proteins for conserved domains revealed that both TrexA and TrexB harbored MdlB superfamily domains (COG1132), which represent a group of well-characterized ABC-type multidrug transport systems. Typically, these systems are composed of two proteins constituting a dimer spanning the cell membrane, actively exporting toxic substances out of the cell, fueled by the energy generated from hydrolyzing ATP to ADP. In line with this, InterProScan detected the presence of several transmembrane regions gathered in a transmembrane domain (TMD) and an ABC transporter domain constituting the P-loop nucleoside triphosphate hydrolase domain in both TrexA and TrexB (Figure 2).

Genomic context of *trexAB*

The *trexAB* operon had a conserved genomic location between an operon containing four genes of the mevalonate pathway and the *s5nA*-nucleotidase gene. In strains lacking *trexAB*, the same genomic location was found to be occupied by a three-gene operon of unknown function (Figure 3). The predicted proteins of these three genes all appear to be involved in signal transduction mechanisms, harboring the domains belonging to YjbM superfamily (COG2357), OmpR superfamily (COG0745) and BaeS superfamily (COG0642), respectively. All isolates harbored one of the two operons, and they were mutually exclusive. The genetic region was highly conserved, and we did not find any association between *trexAB* or the alternative operon and known conjugative mobile genetic elements. Differently, IS-elements were found immediately upstream or downstream of *trexAB* in 55 of the isolates.

Distribution of *trexAB*

The *trexAB* operon was distributed among SD collected from all ecovars. Notably, all strains (83 SDSD and 2 SDSE) originating from cattle and sheep possessed this operon, as did all isolates (SDSE) from pigs and horses, while only 69 out of 274 isolates (SDSE) associated with humans harbored *trexAB*. The operon was limited to specific phylogenetic clades of human associated SD, predominantly belonging to multilocus sequence type 29 clonal complex. Among the SD isolates (SDSE) procured from dogs, four of 20 isolates were lacking *trexAB*. However, phylogenetically these four isolates clustered with human-associated SD isolates also lacking *trexAB* (Figure 4).

Further examination of collections of SD genomes available online revealed results in accordance with the findings regarding our strain collection. We found *trexAB* to be present in 22% (n = 294) isolates

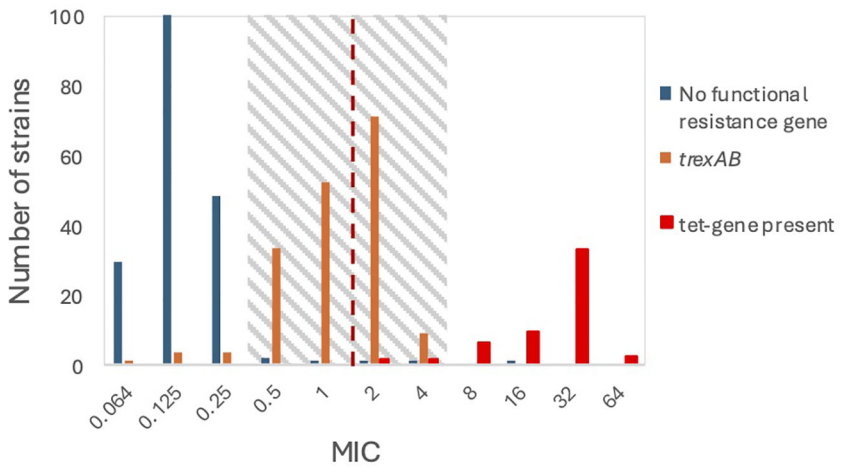

FIGURE 1
Susceptibility in relation to genes known or presumed to be associated with resistance to tetracycline. The dotted line represents the EUCAST breakpoint between susceptibility and resistance. The MIC transition zone is highlighted with grey shading.

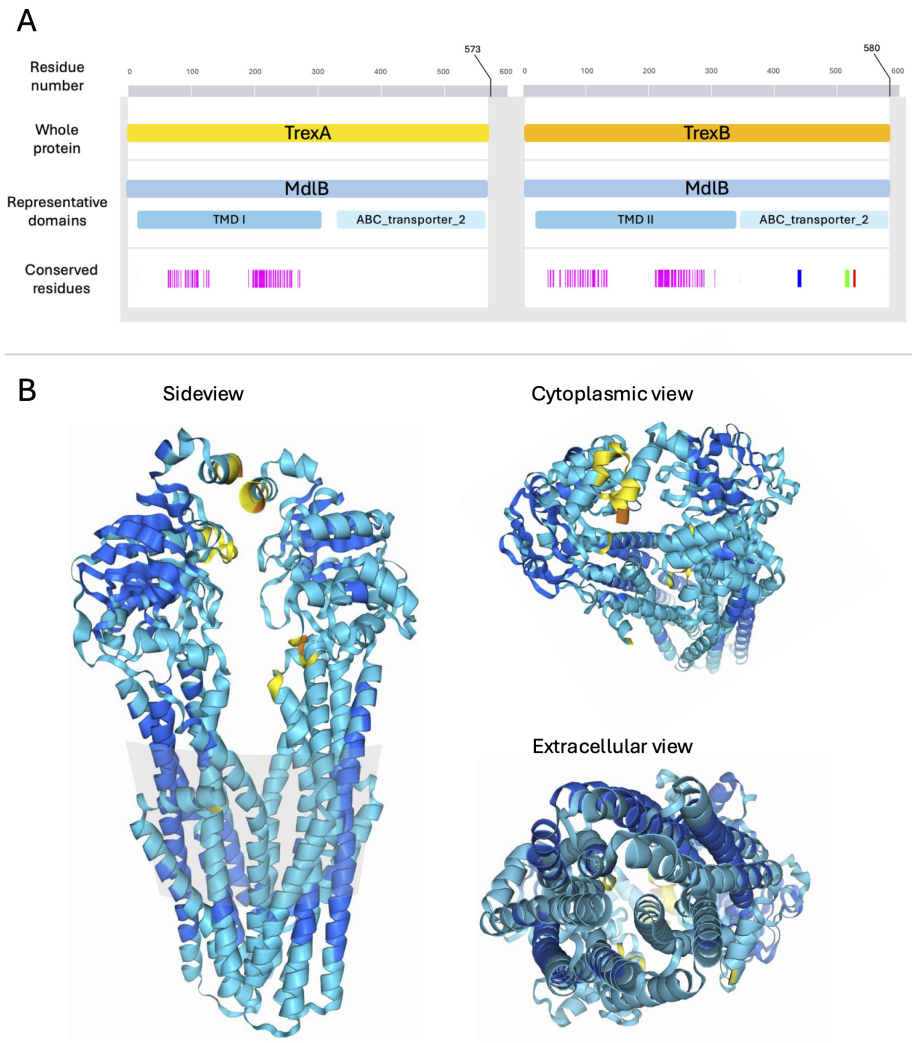

FIGURE 2
Domains and predicted structure of TrexAB. **(A)** The amino acid sequence of TrexA and TrexB where the numbering of amino acids in the primary sequence is marked in grey scale. Representative domains are highlighted in light blue shades. Conserved residues in TrexA and TrexB determined by InterPro-search representing the heterodimeric interface, the Walker A/P-loop motif, the ABC transporter signature motif, and the Walker B motif are highlighted in pink, blue, green and red, respectively. **(B)** Structures of the heterodimeric TrexAB predicted using Alpha Fold 3. The colors in this model represent per-atom prediction confidence where dark blue, light blue, yellow and orange represent very high, confident, low and very low accuracy, respectively.

originating from Australia, 23% (n = 137) isolates from Japan and 7% (n = 122) isolates from Canada, all isolates associated with human infection or carriage. The *trexAB* carriage of SD isolates from livestock was higher and found in 100% of SD isolates in three different collections of isolates from cattle (n = 86), swine (n = 97) and horses (n = 14), respectively. These animal associated SD were isolated from widespread geographical areas, including locations in China, North America and Europe, confirming a global distribution of *trexAB*.

In BLASTp searches for TrexA and TrexB homologs in other bacterial species, the closest match was found in *Streptococcus canis*, with 100% query coverage and sequence identity of 88% and 89% on the aa level regarding TrexA and TrexB, respectively. Homologs with limited sequence identity (60 – 75%) were also detected in other animal associated streptococcal species, such as *Streptococcus suis*, *Streptococcus phocae* and *Streptococcus iniae*. No homologs were detected among typical human pathogenic species. Interestingly, the only significant homology found to the gene products of the alternative operon was in *Streptococcus pyogenes*, with both query coverage and sequence identity approximating 100% both on the aa and on the nucleotide level (Figure 3).

Knockout of *trexAB*

Successful construct of SDSD24Δ*trexAB* and iSDSE_NORM6Δ*trexAB* knockout mutants was confirmed by whole genome sequencing, and the difference between wild type and mutant was limited to the expected exchange of *trexAB* with the kanamycin cassette. In susceptibility testing for tetracycline, minocycline, tigecycline, doxycycline, erythromycin, gentamicin,

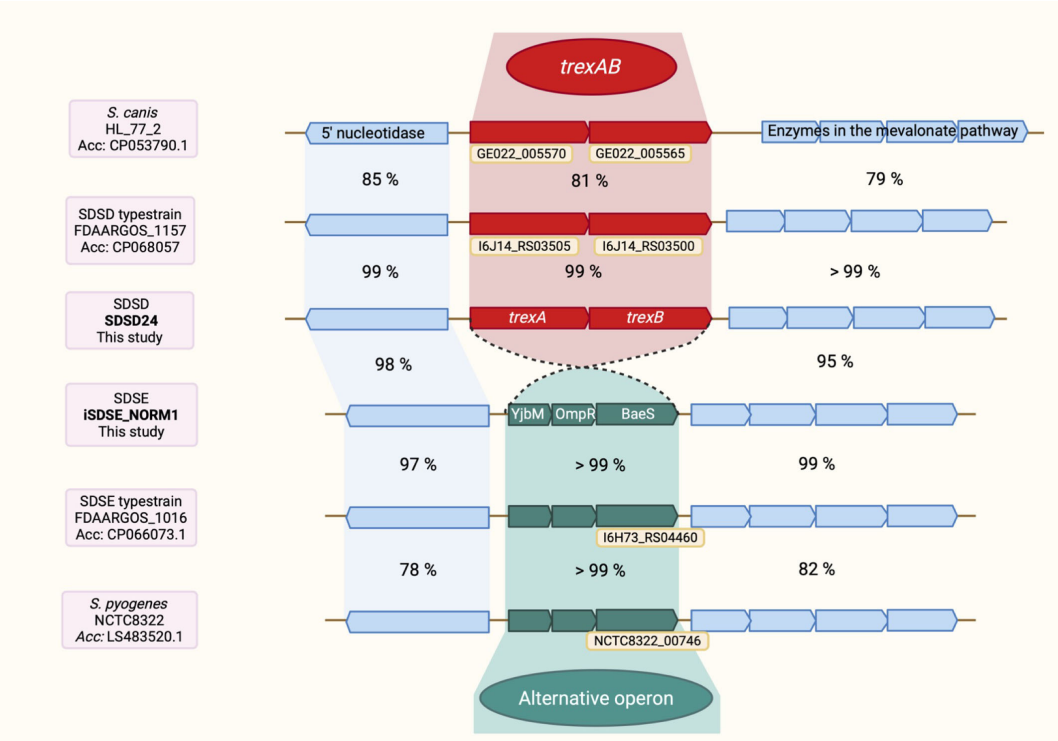

FIGURE 3
The chromosomal location of *trexAB*. *trexAB* has the closest homolog in *S. canis*, with a sequence identity of 81% at the nucleotide level. The alternative operon is found in *S. pyogenes* in addition to *S. dysgalactiae*. The sequence identity of the alternative operon between *S. pyogenes* and *S. dysgalactiae* is significantly higher than the sequence identity of *trexAB* and its closest homolog in *S. canis*. The close resemblance of the alternative operon in *S. pyogenes* and *S. dysgalactiae* is also in contrast with the flanking regions, which has a much lower sequence identity between the two species. Corresponding ProteinID (to locus tags): "TrexA": QKG75729.1 (GE022_005570), QQT04366.1 (I6J14_03505); "TrexB": QKG75728.1 (GE022_005565), QQT04365.1 (I6J14_03500); Alt. operon, 3. gene: QQC56251.1 (I6H73_04460), SRX87322.1 (NCTC8322_00746). Created with Biorender.com, https://app.biorender.com/illustrations/6836d76968fa6ae428cd3cb3.

clindamycin and ciprofloxacin, both transformant strains showed an increased susceptibility for tetracycline and tigecycline compared to their respective wild types, with a 16- to 32-fold reduction in MIC for tetracycline and a 4-fold reduction in MIC for tigecycline (Table 2). For iSDSE_NORM6Δ*trexAB*, a small difference was noted also regarding susceptibility to minocycline, with MIC of 0.032 µg/ml compared to 0.064 µg/ml for the wild type. For all other antibiotics tested, no difference in susceptibility between mutant and wild type was observed.

Discussion

In the present study, we demonstrate that a two-gene operon designated *trexAB* is associated with reduced susceptibility to tetracycline in SD, and that a targeted knockout of the operon lead to a 16- to 32-fold decrease in tetracycline MIC-values compared to the wildtype strains. The operon has a widespread dissemination and conserved chromosomal location without indications of being located on a mobile genetic element.

Notably, the *trexAB*-operon appears to have a skewed phylogenetic ecological distribution. Whereas only 25% of the human associated isolates in our collection contained the operon, almost all animal-associated isolates were found to carry *trexAB*. A similar distribution is evident in epidemiological collections of SD genomes available in GenBank and PubMLST.

Interestingly, the skewed distribution of *trexAB* between human- and animal-associated isolates is in line with the detection of the closest homolog to *trexAB* in a dog-associated species, *S. canis*, while the alternative operons dissemination is limited to the strictly human pathogen *S. pyogenes*. Combined with the mutual exclusivity of these two operons, this could point to interspecies horizontal genetic exchange and SD evolution occurring within their respective ecological niches. A similar evolutionary phenomenon has also been inferred in several previous genomic studies (Bessen et al., 2005; Ward et al., 2009; Porcellato et al., 2021). Moreover, extensive exchange of genetic material between SD and *S. pyogenes* has previously been documented *in silico* (Xie et al., 2024), as have adaptations of SD to host species through presumed tailored genetic content specific to SD of each host species (Porcellato et al., 2021). Nevertheless, further studies are needed to elucidate the potential origin of these operons.

In silico predictions of the domain architecture of the two amino acid sequences encoded in *trexAB*, revealed typical features of a heterodimeric multidrug resistance transporter (MDR) transporter (Lubelski et al., 2004; Matsuo et al., 2007; Torres et al., 2009; Reilman et al., 2014; Hürlimann et al., 2016). These transporters are

10.3389/fcimb.2025.1583926

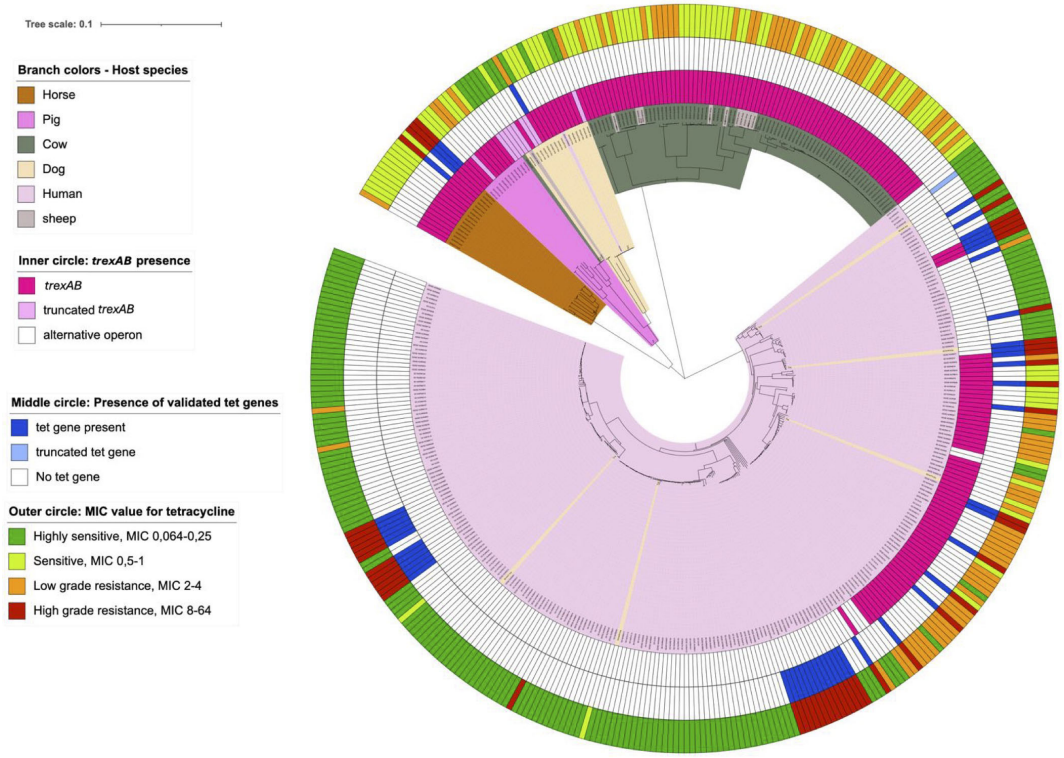

FIGURE 4
The relationship between genotypic and phenotypic tetracycline resistance and their linkage to phylogenetic distribution. Scale indicates substitutions per site. The phylogenetic tree is constructed based on a core genome single nucleotide polymorphism alignment on maximum likelihood method.

typically shown capable of exporting a selection of substances across the cell membrane. Susceptibility testing for several antibiotics demonstrated an effect by *trexAB* only for tetracycline and to a lesser extent tigecycline, which provides a tenuous foundation for interpreting *trexAB* as a multidrug transporter. However, we only evaluated *trexAB* in relation to antibiotics, whereas tests of other MDR transporters have included a wider range of noxious substances like ethidium bromide, safranin, doxorubicin, pyrroles and acriflavine (Orelle et al., 2019). Thus, a broader selection of substrates for efflux by *trexAB* than demonstrated here is possible.

The level of resistance to tetracycline caused by *trexAB* seems to be modest, and the impact on susceptibility to tigecycline even more so. As such, the clinical significance of harboring this operon on treatment efficacy is uncertain. Notwithstanding, future vigilance towards potential treatment failures is warranted. Regardless of clinical impact, interpretation of tetracycline resistance in *trexAB*-positive isolates undoubtably represent a challenge, as the MIC distribution of this population is intersected by the current EUCAST breakpoint. Due to inherent technical and analytical variability in susceptibility testing, such isolates will thus be

TABLE 2 MIC values for wildtype and knockout strains.

	MIC for strain iSDSE_NORM6 (*)	MIC for strain iSDSE_NORM6 Δ*trexAB* (*)	MIC for strain SDSD24 (*)	MIC for strain SDSD24Δ*trexAB* (*)
Tetracycline	2 (2)	0.125 (0.125)	4 (4-8)	0.125 (0.125)
Doxycycline	0.125 (0.125-0.25)	0.125 (0,125)	0.25 (0.125-0.25)	0.125 (0.125)
Minocycline	0.064 (0.064)	0.032 (0.032)	0.064 (0.064)	0.064 (0.064)
Tigecycline	0.125 (0.125)	0.032 (0.032)	0.125 (0.125)	0.032 (0.032)
Erythromycin	0.25 (0.25)	0.25 (0.25)	0.25 (0.25)	0.25 (0.25)
Gentamicin	16 (8-16)	8 (8-16)	8 (8)	8 (8)
Clindamycin	0.25 (0.25)	0.25 (0.25)	0.25 (0.25)	0.25 (0.25)
Ciprofloxacin	0.5 (0.5)	0.5 (0.5)	1 (1)	0.5 (0.5-1)

*Range of values for 3 biological replicates.

interchangeably classified as resistant or susceptible to tetracycline. Notably, in 2023 EUCAST removed the category "Susceptible, increased exposure" for tetracycline in beta-hemolytic streptococcal species, including SD. They argued that a pharmacodynamic and pharmacokinetic rationale for an intermediate category was not evident, and lowered the breakpoint for resistance from "above 2 µg/ml" to "above 1 µg/ml". Considering the widespread distribution of low-grade resistant *trexAB*-positive SD isolates, the implications for dosage and clinical efficacy need to be carefully evaluated before further revising the EUCAST breakpoints.

A limitation of the knockout experiments in this study is the fact that both resistance genes were removed in one maneuver, making it difficult to decipher the individual contribution of TrexA and TrexB. However, several others have documented the need for the contribution from both half transporters for the function of a heterodimeric efflux pump (Matsuo et al., 2007; Garvey et al., 2010; Warburton et al., 2013). In addition, our collection contained isolates where *trexA* alone was truncated, which in each case was associated with full susceptibility to tetracycline.

Another potential limitation is the use of MIC-strips for susceptibility testing, as broth microdilution or disc diffusion are the reference methods proposed by EUCAST (EUCAST, 2025). Nevertheless, a distribution of tetracycline susceptibility encircling the current breakpoint is evident also in studies of SD using broth microdilution methodology (McDougall et al., 2014; Jensen et al., 2024). Moreover, we have disc diffusion data for one third of the isolates in the present study, and the susceptibility distribution is congruent with the MIC-strip results (data not shown).

In conclusion, we have investigated the cause for low grade tetracycline resistance in *S. dysgalactiae* and found the underlying genetic factor to be the two gene operon *trexAB* encoding a hitherto uncharacterized ABC transporter. The tetracycline MIC distribution of the *trexAB*-positive isolates is intersected by the current EUCAST breakpoint, and the clinical implications of this should be subject to scrutiny.

Data availability statement

The datasets presented in this study can be found in online repositories. The names of the repository/repositories and accession number(s) can be found in the article/Supplementary Material.

Author contributions

MG: Conceptualization, Data curation, Formal analysis, Writing – original draft, Writing – review & editing. MK: Conceptualization, Project administration, Supervision, Writing – review & editing. MM: Methodology, Supervision, Writing – review & editing. ZS: Methodology, Supervision, Writing – review & editing. SS: Funding acquisition, Supervision, Writing – review & editing. AS: Writing – review & editing. BK: Writing – review & editing. OO: Conceptualization, Data curation, Formal analysis, Funding acquisition, Methodology, Project administration, Supervision, Writing – review & editing.

Funding

The author(s) declare that financial support was received for the research and/or publication of this article. This work was supported by grants from the Norwegian surveillance program for antimicrobial resistance (NORM) (Grant number: 19/08, to OO). The genomic Core Facility (GCF) at the University of Bergen, which is part of the NorSeq consortium, provided services on the whole genome sequencing in this study; GCF is supported by major grants from the Research Council of Norway (grant no. 245979/F50) and Trond Mohn Foundation (grant no. BFS2017TMT04/BFS2017TMT08). This study was received also financial contributions from the Western Norway Regional Health Authority (grant no. 912231). SS received grants from the Norwegian Research Council under the frames of NordForsk (Project: 90456, PerAID) and ERA PerMed (Project: 2018-151, PerMIT).

Acknowledgments

We thank the staff at Microbiological Department at Haukeland University Hospital for excellent technical assistance and for providing access to their laboratory facilities.

Conflict of interest

The authors declare that the research was conducted in the absence of any commercial or financial relationships that could be construed as a potential conflict of interest.

Generative AI statement

The author(s) declare that Generative AI was used in the creation of this manuscript. As a dictionary for word expressions. Not for generating text or images.

Publisher's note

Supplementary material

The Supplementary Material for this article can be found online at: https://www.frontiersin.org/articles/10.3389/fcimb.2025.1583926/full#supplementary-material

References

Aziz, R. K., Bartels, D., Best, A. A., DeJongh, M., Disz, T., Edwards, R. A., et al. (2008). The RAST server: rapid annotations using subsystems technology. *BMC Genom.* 9, 75. doi: 10.1186/1471-2164-9-75

Bankevich, A., Nurk, S., Antipov, D., Gurevich, A. A., Dvorkin, M., Kulikov, A. S., et al. (2012). SPAdes: A new genome assembly algorithm and its applications to single-cell sequencing. *J. Comput. Biol.* 19, 455–477. doi: 10.1089/cmb.2012.0021

Bessen, D. E., Manoharan, A., Luo, F., Wertz, J. E., and Robinson, D. A. (2005). Evolution of transcription regulatory genes is linked to niche specialization in the bacterial pathogen *Streptococcus pyogenes*. *J. Bacteriol.* 187, 4163–4172. doi: 10.1128/jb.187.12.4163-4172.2005

Blum, M., Andreeva, A., Florentino, L. C., Chuguransky, S. R., Grego, T., Hobbs, E., et al. (2024). InterPro: the protein sequence classification resource in 2025. *Nucleic Acids Res.* 53, D444–D456. doi: 10.1093/nar/gkae1082

Cinthi, M., Massacci, F. R., Coccitto, S. N., Albini, E., Cucco, L., Orsini, M., et al. (2023). Characterization of a prophage and a defective integrative conjugative element carrying the optrA gene in linezolid-resistant *Streptococcus dysgalactiae* subsp. *equisimilis* isolates from pigs, Italy. *J. Antimicrob. Chemother.* 78, 1740–1747. doi: 10.1093/jac/dkad164

EUCAST (2025).European Committee on Antimicrobial Susceptibility Testing. Breakpoint tables for interpretation of MICs and zone diameters version 15.0, 2025. Available online at: https://www.eucast.org/clinical_breakpoints (Accessed February 24, 2025).

Garvey, M. I., Baylay, A. J., Wong, R. L., and Piddock, L. J. V. (2010). Overexpression of patA and patB, Which Encode ABC Transporters, Is Associated with Fluoroquinolone Resistance in Clinical Isolates of *Streptococcus pneumoniae*. *Antimicrob. Agents Chemother.* 55, 190–196. doi: 10.1128/aac.00672-10

Glambek, M., Skrede, S., Sivertsen, A., Kittang, B. R., Kaci, A., Jonassen, C. M., et al. (2024). Antimicrobial resistance patterns in *Streptococcus dysgalactiae* in a One Health perspective. *Front. Microbiol.* 15. doi: 10.3389/fmicb.2024.1423762

Higuchi, R., Krummel, B., and Saiki, R. (1988). A general method of *in vitro* preparation and specific mutagenesis of DNA fragments: study of protein and DNA interactions. *Nucleic Acids Res.* 16, 7351–7367. doi: 10.1093/nar/16.15.7351

Hürlimann, L. M., Corradi, V., Hohl, M., Bloemberg, G. V., Tieleman, D. P., and Seeger, M. A. (2016). The heterodimeric ABC transporter efrCD mediates multidrug efflux in enterococcus faecalis. *Antimicrob. Agents Chemother.* 60, 5400–5411. doi: 10.1128/aac.00661-16

Jaillard, M., Lima, L., Tournoud, M., Mahé, P., Belkum, A., Lacroix, V., et al. (2018). A fast and agnostic method for bacterial genome-wide association studies: Bridging the gap between k-mers and genetic events. *PLoS Genet.* 14, e1007758. doi: 10.1371/journal.pgen.1007758

Jensen, V. F., Damborg, P., Norström, M., Nonnemann, B., Slettemeås, J. S., Smistad, M., et al. (2024). Estimation of epidemiological cut-off values for eight antibiotics used for treatment of bovine mastitis caused by *Streptococcus uberis* and *Streptococcus dysgalactiae* subsp. *dysgalactiae*. *Vet. Microbiol.* 290, 109994. doi: 10.1016/j.vetmic.2024.109994

Johnsborg, O., Eldholm, V., Bjørnstad, M. L., and Håvarstein, L. S. (2008). A predatory mechanism dramatically increases the efficiency of lateral gene transfer in Streptococcus pneumoniae and related commensal species. *Mol. Microbiol.* 69, 245–253. doi: 10.1111/j.1365-2958.2008.06288.x

Kaas, R. S., Leekitcharoenphon, P., Aarestrup, F. M., and Lund, O. (2014). Solving the problem of comparing whole bacterial genomes across different sequencing platforms. *PLoS One* 9, e104984. doi: 10.1371/journal.pone.0104984

Lacks, S., and Hotchkiss, R. D. (1960). A study of the genetic material determining an enzyme activity in *Pneumococcus*. *Biochim. Biophys. Acta* 39, 508–518. doi: 10.1016/0006-3002(60)90205-5

Letunic, I., and Bork, P. (2021). Interactive Tree Of Life (iTOL) v5: an online tool for phylogenetic tree display and annotation. *Nucleic Acids Res.* 49, gkab301–. doi: 10.1093/nar/gkab301

Levy, S. B., McMurry, L. M., Barbosa, T. M., Burdett, V., Courvalin, P., Hillen, W., et al. (1999). Nomenclature for new tetracycline resistance determinants. *Antimicrob. Agents Chemother.* 43, 1523–1524. doi: 10.1128/aac.43.6.1523

Lother, S. A., Demczuk, W., Martin, I., Mulvey, M. R., Dufault, B., Lagacé-Wiens, P., et al. (2017). Clonal clusters and virulence factors of group C and G streptococcus causing severe infections, manitoba, Canada 2012–2014 - volume 23, number 7—July 2017 - emerging infectious diseases journal - CDC. *Emerg. Infect. Dis.* 23, 1079–1088. doi: 10.3201/eid2307.161259

Lubelski, J., Mazurkiewicz, P., Merkerk, R., Konings, W. N., and Driessen, A. J. M. (2004). ydaG and ydbA of *Lactococcus lactis* Encode a Heterodimeric ATP-binding Cassette-type Multidrug Transporter*. *J. Biol. Chem.* 279, 34449–34455. doi: 10.1074/jbc.m404072200

Mårli, M. T., Oppegaard, O., Porcellato, D., Straume, D., and Kjos, M. (2024). Genetic modification of *Streptococcus dysgalactiae* by natural transformation. *mSphere* 9, e0021424. doi: 10.1128/msphere.00214-24

Matsuo, T., Chen, J., Minato, Y., Ogawa, W., Mizushima, T., Kuroda, T., et al. (2007). SmdAB, a heterodimeric ABC-type multidrug efflux pump, in *Serratia marcescens*. *J. Bacteriol.* 190, 648–654. doi: 10.1128/jb.01513-07

McDougall, S., Hussein, H., and Petrovski, K. (2014). Antimicrobial resistance in *Staphylococcus aureus*, *Streptococcus uberis* and *Streptococcus dysgalactiae* from dairy cows with mastitis. *N. Z. Vet. J.* 62, 68–76. doi: 10.1080/00480169.2013.843135

NORM (2019).NORM/NORM-VET 2018. Usage of antimicrobial agents and occurrence of antimicrobial resistance in Norway. Tromsø/Oslo 2019. Available online at: https://www.unn.no/4a79d7/siteassets/documents/kompetansetjenester–sentre-og-fagrad/norm—norsk-overvakingssystem-for-antibiotikaresistens-hos-mikrober/rapporter/norm-norm-vet-2018.pdf (Accessed 2019).

Oppegaard, O., Mylvaganam, H., Skrede, S., Lindemann, P. C., and Kittang, B. R. (2017). Emergence of a *Streptococcus dysgalactiae* subspecies *equisimilis* stG62647-lineage associated with severe clinical manifestations. *Sci. Rep.* 7, 7589. doi: 10.1038/s41598-017-08162-z

Orelle, C., Mathieu, K., and Jault, J.-M. (2019). Multidrug ABC transporters in bacteria. *Res. Microbiol.* 170, 381–391. doi: 10.1016/j.resmic.2019.06.001

Pinho, M. D., Erol, E., Ribeiro-Gonçalves, B., Mendes, C. I., Carriço, J. A., Matos, S. C., et al. (2016). Beta-hemolytic *Streptococcus dysgalactiae* strains isolated from horses are a genetically distinct population within the *Streptococcus dysgalactiae* taxon. *Sci. Rep.* 6, 31736. doi: 10.1038/srep31736

Porcellato, D., Smistad, M., Skeie, S. B., Jørgensen, H. J., Austbø, L., and Oppegaard, O. (2021). Whole genome sequencing reveals possible host species adaptation of *Streptococcus dysgalactiae*. *Sci. Rep.* 11, 17350. doi: 10.1038/s41598-021-96710-z

Reilman, E., Mars, R. A. T., van Dijl, J. M., and Denham, E. L. (2014). The multidrug ABC transporter BmrC/BmrD of Bacillus subtilis is regulated via a ribosome-mediated transcriptional attenuation mechanism. *Nucleic Acids Res.* 42, 11393–11407. doi: 10.1093/nar/gku832

Roberts, M. (2024).Tetracycline genes Modified 1. Available online at: https://faculty.washington.edu/marilynr/tetweb4.pdf (Accessed February 10, 2025).

Shinohara, K., Murase, K., Tsuchido, Y., Noguchi, T., Yukawa, S., Yamamoto, M., et al. (2023). Clonal Expansion of Multidrug-Resistant *Streptococcus dysgalactiae* Subspecies *equisimilis* Causing Bacteremia, Japan 2005–2021 - Volume 29, Number 3—March 2023 - Emerging Infectious Diseases journal - CDC. *Emerg. Infect. Dis.* 29, 528–539. doi: 10.3201/eid2903.221060

Sung, C. K., Li, H., Claverys, J. P., and Morrison, D. A. (2001). An rpsL Cassette, Janus, for Gene Replacement through Negative Selection in *Streptococcus pneumoniae*. *Appl. Environ. Microbiol.* 67, 5190–5196. doi: 10.1128/aem.67.11.5190-5196.2001

Thaker, M., Spanogiannopoulos, P., and Wright, G. D. (2010). The tetracycline resistome. *Cell. Mol. Life Sci.* 67, 419–431. doi: 10.1007/s00018-009-0172-6

Torres, C., Galián, C., Freiberg, C., Fantino, J.-R., and Jault, J.-M. (2009). The YheI/YheH heterodimer from *Bacillus subtilis* is a multidrug ABC transporter. *Biochim. Biophys. Acta (BBA) - Biomembr.* 1788, 615–622. doi: 10.1016/j.bbamem.2008.12.012

Vélez, J. R., Cameron, M., Rodríguez-Lecompte, J. C., Xia, F., Heider, L. C., Saab, M., et al. (2017). Whole-Genome Sequence Analysis of Antimicrobial Resistance Genes in *Streptococcus uberis* and *Streptococcus dysgalactiae* Isolates from Canadian Dairy Herds. *Front. Vet. Sci.* 4. doi: 10.3389/fvets.2017.00063

Vieira, V. V., Teixeira, L. M., Zahner, V., Momen, H., Facklam, R. R., Steigerwalt, A. G., et al. (1998). Genetic relationships among the different phenotypes of *Streptococcus dysgalactiae* strains. *Int. J. Syst. Evol. Micr* 48, 1231–1243. doi: 10.1099/00207713-48-4-1231

Wang, J., Chitsaz, F., Derbyshire, M. K., Gonzales, N. R., Gwadz, M., Lu, S., et al. (2022). The conserved domain database in 2023. *Nucleic Acids Res.* 51, D384–D388. doi: 10.1093/nar/gkac1096

Warburton, P. J., Ciric, L., Lerner, A., Seville, L. A., Roberts, A. P., Mullany, P., et al. (2013). TetAB(46), a predicted heterodimeric ABC transporter conferring tetracycline resistance in *Streptococcus australis* isolated from the oral cavity. *J. Antimicrob. Chemother.* 68, 17–22. doi: 10.1093/jac/dks351

Ward, P. N., Holden, M. T., Leigh, J. A., Lennard, N., Bignell, A., Barron, A., et al. (2009). Evidence for niche adaptation in the genome of the bovine pathogen *Streptococcus uberis*. *BMC Genom.* 10, 54. doi: 10.1186/1471-2164-10-54

Xie, O., Zachreson, C., Tonkin-Hill, G., Price, D. J., Lacey, J. A., Morris, J. M., et al. (2024). Overlapping *Streptococcus pyogenes* and *Streptococcus dysgalactiae* subspecies *equisimilis* household transmission and mobile genetic element exchange. *Nat. Commun.* 15, 3477. doi: 10.1038/s41467-024-47816-1

frontiers | Frontiers in Cellular and Infection Microbiology

TYPE Original Research
PUBLISHED 27 August 2025
DOI 10.3389/fcimb.2025.1617614

OPEN ACCESS

EDITED BY
Valerio Baldelli,
University of Milan, Italy

REVIEWED BY
Dao-Feng Zhang,
Hohai University, China
Rhishita Chourashi,
University of Maryland, United States
Shijun Sun,
First Affiliated Hospital of Zhengzhou University, China

*CORRESPONDENCE
Lin Zheng
zl050514@163.com
Lingwei Zhu
lingweiz@126.com
Xuejun Guo
xuejung2021@163.com

†These authors have contributed equally to this work

RECEIVED 24 April 2025
ACCEPTED 14 July 2025
PUBLISHED 27 August 2025

CITATION
Zheng L, Wang Z, Zhang X, Lu G, Jing J, Sun S, Sun Y, Ji X, Jiang B, Zhu L and Guo X (2025) Genomic features and fitness cost of co-existence of *bla*$_{KPC-2}$ and *bla*$_{VIM-2}$ plasmids in ICU-derived pan-drug resistant *Pseudomonas aeruginosa*. *Front. Cell. Infect. Microbiol.* 15:1617614. doi: 10.3389/fcimb.2025.1617614

Genomic features and fitness cost of co-existence of *bla*$_{KPC-2}$ and *bla*$_{VIM-2}$ plasmids in ICU-derived pan-drug resistant *Pseudomonas aeruginosa*

Lin Zheng[1*†], Zixian Wang[1†], Xin Zhang[2], Gejin Lu[1], Jie Jing[1], Shiwen Sun[1], Yang Sun[1], Xue Ji[1], Bowen Jiang[1], Lingwei Zhu[1*] and Xuejun Guo[1*]

[1]Key Laboratory of Jilin Province for Zoonosis Prevention and Control, Changchun Veterinary Research Institute, Chinese Academy of Agriculture Sciences, Changchun, Jilin, China, [2]China-Japan Union Hospital, Jilin University, Changchun, Jilin, China

Background: The emergence of carbapenem-resistant *Pseudomonas aeruginosa* (CRPA) co-producing KPC-2 and VIM-2 has increased the healthcare threats.

Results: In this study, a CRPA strain 18102011, was isolated from the bile of a burn patient in ICU of China. Its whole genome was sequenced via the PacBio platform. The molecular characteristics of the genome were analyzed to assess the genetic environment of the carbapenemase genes *bla*$_{KPC-2}$ and *bla*$_{VIM-2}$. Antimicrobial susceptibility, plasmid stability, bacterial growth curves, and plasmid conjugation were measured. Strain 18102011 exhibited a resistant pattern to all 23 antibiotics tested, which could be defined as a pan-drug resistant *P. aeruginosa* strain. Two plasmids were identified in this strain: the Inc$_{pRBL16}$ mega-plasmid pP2011–1 carrying *bla*$_{VIM-2}$ and the IncP6 plasmid pP2011–2 carrying *bla*$_{KPC-2}$. *bla*$_{VIM-2}$ was located in the region of In2057 (a novel class 1 integron) that was inserted into pP2011-1, and the expression of the *bla*$_{VIM-2}$ gene was increased by the PcW$_{TGN-10}$ promoter located at the 5'-CS. For the *bla*$_{KPC-2}$ gene, the core module Tn*3*-IS*Kpn27*-*bla*$_{KPC}$-ΔIS*Kpn6* served as the *bla*$_{KPC-2}$ platform in pP2011-2, and the expression of the *bla*$_{KPC-2}$ gene was achieved via the P1 promoter located downstream of IS*Kpn27*. This expression pattern resulted in MICs of 4,096 μg/mL of imipenem for both strain 18102011 and its transconjugant D2011. Both plasmids were stable in strain 18102011 and could be co-transferred to other strains.

Conclusion: This study raised concerns regarding the high stability and non-inferior fitness of *bla*$_{KPC-2}$-*bla*$_{VIM-2}$-CRPA, shed light on its genomic characteristics, and underscored the importance of continued surveillance of CRPA.

KEYWORDS

carbapenem-resistant *Pseudomonas aeruginosa*, blaKPC-2, blaVIM-2, plasmid, fitness cost

Introduction

Pseudomonas aeruginosa accounts for 10-15% of nosocomial infections worldwide (Blanc et al., 1998). It can attach to the surfaces of medical instruments through biofilm formation, facilitating its spread within hospitals, particularly in the ICU (Cornaglia et al., 2000; Li et al., 2022). Most ICU patients use broad-spectrum antimicrobials to treat bacterial infections, and the prolonged use of antibiotics to eradicate bacterial infections is commonly practiced (Pang et al., 2019). However, the acquisition of antibiotic resistance genes by mobile genetic elements (e.g., plasmids, transposons, integrative elements, and conjugative elements), combined with their transfer among bacterial strains, leads to the development of multidrug-resistant *P. aeruginosa* strains in patients (De Vos et al., 1997; Partridge et al., 2018; Botelho et al., 2019; Allameh et al., 2020; Mohammadnejad et al., 2023). Such infections are associated with high mortality rates, ranging from 18 to 61% (Kang et al., 2003). Although carbapenems are the most important antibiotics for treating their *P. aeruginosa* infections, the bacteria can be resistant to them due in part to the acquisition of carbapenemase genes, complicating treatment (Partridge et al., 2018; Botelho et al., 2019). Some strains even exhibit pan-drug resistance, rendering subsequent treatments with drugs such as colistin and amikacin ineffective, which creates a therapeutic dilemma. Consequently, antimicrobial resistance has become a global health challenge that threatens many medical achievements of the last century and causing serious harm to health system outcomes.

In this study, *P. aeruginosa* strain 18102011 was isolated from the bile of a burn patient in a hospital ICU in 2018 (Changchun, China). The strain was genetically investigated to evaluate the genetic mechanism of its drug resistance. The whole-genome sequence of the strain was generated, and its molecular characteristics were subsequently investigated. The strain belonged to multi-locus sequence typing (ST2374) and serotype O4. Furthermore, the strain co-harbored the bla_{KPC-2} and bla_{VIM-2} genes, enabling it to resist carbapenems. The MICs of imipenem and meropenem (carbapenem) were both >256 μg/mL. Additionally, it was a pan-drug resistant *P. aeruginosa* that was resistant to 23 antibiotics, including amikacin, colistin, and fosfomycin. Further genetic analyses were applied to the plasmids pP2011–1 carrying bla_{VIM-2}, and pP2011–2 carrying bla_{KPC-2} to characterize their genetic environments. The transcriptional expression of resistance genes bla_{KPC-2} and bla_{VIM-2} changed after imipenem exposure. Moreover, the fitness cost, loss of resistance genes under serially passage, and horizontal transmission ability of the bla_{KPC-2} and bla_{VIM-2} genes in bacteria were analyzed. These results provide a deeper understanding of the acquisition of drug resistance genes in *P. aeruginosa*.

Materials and methods

Identification of bla_{KPC-2}-bla_{VIM-2}-CRPA

A CRPA obtained from bile collected from a patient in the intensive care unit (ICU) of a public Chinese hospital in 2018, exhibited resistance to both imipenem and meropenem. This isolate was forwarded to our laboratory for species identification and antimicrobial susceptibility testing via the BD Phoenix-100 system, using *Escherichia coli* ATCC25922 as the quality control for susceptibility testing (The antibiotics tested were shown in Supplementary Table S1). Additionally, the isolate was stored at -80°C for potential future use. The experimental protocols were approved by the Ethics Committee of the Jilin University (JDKQ202316EC).

To ensure the accuracy of our findings, the MICs of imipenem and meropenem were determined by E-test. Furthermore, the MICs for other antibiotics that have not been tested in the BD Phoenix-100 system, such as colistin, ceftazidime-avibactam, and fosfomycin, which were commonly used to treat carbapenem-resistant bacteria, were also ascertained using E-test (The antibiotics tested were shown in Supplementary Table S2). And the quality control strain was *E. coli* ATCC25922. Drug-resistance levels, including resistance, intermediary, and sensitivity thresholds, were assessed by the guidelines established by the Clinical and Laboratory Standards Institute.

It was subject to polymerase chain reaction (PCR) and Sanger sequencing and targets the *oprL* gene (which was specific to *P. aeruginosa*), which encoded a peptidoglycan-associated lipoprotein (De Vos et al., 1997). Additionally, PCR assays were performed to detect the presence of carbapenemase genes, including bla_{IMP}, bla_{SPM}, bla_{AIM}, bla_{VIM}, bla_{GIM}, bla_{BIC}, bla_{SIM}, bla_{NDM}, bla_{DIM}, bla_{KPC} and bla_{OXA-48} (Poirel et al., 2011) (The primer sequences and PCR conditions were listed in Supplementary Table S3).

Sequencing and genome sequence assembly

Bacterial genomic DNA was isolated using the UltraClean microbial DNA extraction kit (Qiagen, Germany) and sequenced via a PacBio RS II sequencer (Pacific Biosciences, USA). The sequence reads were *de novo* assembled using the SMARTdenovo assembler (http://github.com/ruanjue/smartdenovo). The assembly results were corrected based on sequencing data through three rounds of error correction by using the Racon software (version 1.4.13). Subsequently, three rounds of error correction were performed using the Pilon software (version 1.22) with second-generation reads, yielding the final assembly results.

Genome annotation and comparison

Precise bacterial species identification was evaluated using pair-wise ANI (http://www.ezbiocloud.net/tools/ani) analysis between the genomes generated in this study and the *P. aeruginosa* reference genome sequence PAO1 (GenBank ID: NC_002516.2). A ≥95% ANI cut-off was used to define bacterial species (Yoon et al., 2017). The PAst (https://cge.food.dtu.dk/services/PAst/) server was used to perform O-antigen classification. In addition, *RAST 2.0* (Brettin et al., 2015) and *BLASTP*/*BLASTN* (Boratyn et al., 2013) searches were used to predict open reading frames (ORFs), whereas comparisons with the ResFinder 4.0 (Bortolaia et al., 2020) (https://cge.cbs.dtu.dk/services/ResFinder/), CARD (https://

card.mcmaster.ca) (Alcock et al., 2023) and VFDB (Liu et al., 2022) (http://www.mgc.ac.cn/VFs/) databases were used to identify acquired resistance genes and virulence genes. In addition, the ISfinder (Varani et al., 2011) (https://www-is.biotoul.fr/; Lastest Database Update 2021-9-21), TnCentral (https://tncentral.ncc.unesp.br), INTEGRAL (Moura et al., 2009) (http://integrall.bio.ua.pt/), and ICEberg 2.0 (Liu et al., 2019) (http://db-mml.sjtu.edu.cn/ICEberg/) platforms were used to identify mobile elements. The online database BPROM (Cassiano and Silva-Rocha, 2020) was used for promoter prediction. Pairwise sequence comparisons were conducted using *BLASTN* searches. Functional analysis of proteins in families and domain prediction was conducted using the InterPro (https://www.ebi.ac.uk/interpro) database. Gene organization diagrams were drawn in Inkscape 1.0 (http://inkscape.org/en/).

Multilocus sequence typing (ST) was conducted by evaluating gene sequence data (including seven conserved housekeeping genes: *acsA*, *aroE*, *gtaA*, *mutL*, *nuoD*, *ppsA*, and *trpE*) with the pubMLST platform (https://pubmlst.org/).

Conjugation experiments

Plasmid transferability was tested using *E. coli* EC600 (rifampicin resistant) and strain 18102011 as the recipient strain and donor strain, respectively. Both the donor and recipient strains were cultured separately overnight at 37°C. Adjust the bacterial concentrations of both recipient strain EC600 and the donor strain 18102011 to 10^9 CFU/mL. The donor and recipient strains were then subsequently mixed at a 1:1 ratio. The mixture was then spotted onto a $1cm^2$ hydrophilic nylon membrane filter (Millipore; 0.45 μm pore size), which was placed on an LB agar plate and incubated at 37°C for 6 h to initiate mating. After incubation, cells were recovered from the filter and serially diluted from 10^{-1} to 10^{-9}, with three parallel replicates per dilution. The dilution was spotted onto LB agar (containing 80 μg/mL rifampicin and 4 μg/mL imipenem) and LB agar (containing 80 μg/mL rifampicin) to select the carbapenem-resistant *E. coli* transconjugants and recipient strain *E. coli* EC600, respectively. The entire experimental procedure was repeated three times. The conjugation transfer efficiency between strain 18102011 and EC600 was calculated using the Equation (1.1). Antimicrobial susceptibility of transconjugants was determined using the BD Phoenix-100 system, while the MIC of imipenem for both strain 18102011 and its transconjugant D2011 was determined by the broth dilution method.

$$\textbf{Conjugation transfer efficiency} = \frac{\textbf{Number of exconjugants (CFU/mL)}}{\textbf{Number of recipient bacteria (CFU/mL)}} \quad (1.1)$$

Bacterial growth curve assay

In studies assessing plasmid fitness burden, it's standard and scientifically appropriate to compare an isogenic pair. To specifically determine the fitness cost associated with the presence of plasmids harboring bla_{KPC-2} and bla_{VIM-2} genes in strain 18102011, bacterial growth curves were constructed for both transconjugant D2011 (carrying bla_{KPC-2} and bla_{VIM-2}) of strain 18102011 and recipient strain *E. coli* EC600. The overnight culture of strain D2011 and EC600 were diluted to 0.5 McFarland standard and subsequently diluted 1:100 in antibiotic-free LB broth. Over the next 12 hours, the optical density (OD_{600}) of each culture was monitored at 2-hour intervals via a NanoPhotometer N60 (Implen, Germany). The data represent the mean ± SEM of two independent experiments. Statistical differences were determined by two-tailed *t*-test (*$p< 0.05$).

Plasmid stability testing

Strain 18102011 was grown at 37°C in a shaking incubator set to 200 rpm and serially passaged for 10 days, with each passage diluted 1:500 in antibiotic-free LB broth. After 5 and 10 days, the cultures were serially diluted and plated on antibiotic-free LB agar. Fifty single colonies were randomly selected for detection of the bla_{KPC-2} and bla_{VIM-2} genes by PCR on the 5^{th} and 10^{th} day, respectively, and were used as markers to reflect the loss of their plasmid. The data represent the mean ± SEM of two independent experiments. Statistical differences were determined by two-tailed *t*-test (*$p< 0.05$).

RNA preparation and transcriptome sequencing

Bacterial genomic RNA (before and after the addition of imipenem) was isolated using the RNAprep Pure Cell/Bacteria Kit RNAprep Pure (TianGen, China). Starting with total RNA, the mRNA was purified by rRNA depletion. And cDNA libraries were constructed using mRNA. Transcriptome sequencing was performed on triplicate samples, which was carried out by Illumina NovaSeq. Using HTSeq v0.6.1, the number of reads mapped to each gene was counted. FPKM values for each gene were then calculated based on gene length and the corresponding read counts. FPKM, which stands for Fragments Per Kilobase of transcript sequence per Million base pairs sequenced, accounts for both sequencing depth and gene length, making it a widely used method for estimating gene expression levels. The DESeq R package (1.18.0) was employed to determine differential expression of strain 18102011 carrying plasmids before and after the addition of imipenem, using a model based on the negative binomial distribution. Using the Equstion (1.2), we calculate the fold change in expression levels of the resistance genes (bla_{KPC-2} and bla_{VIM-2}), conjugative transfer genes, and replicon genes, before and after antibiotic treatment. The resulting *p*-values were adjusted using the Benjamini-Hochberg method to control the false discovery rate. Genes with an adjusted *p*-value<0.05, identified by DESeq, were classified as differentially expressed.

$$\mathbf{log2FoldChange} = \mathbf{log2}\frac{\mathbf{antibiotic\ \ treated\ \ group}}{\mathbf{antibiotic-free\ \ group}} \quad (1.2)$$

Quantitative real-time polymerase chain reaction

All primers and probes for bla_{KPC-2} gene, bla_{VIM-2} gene, and *repA* genes (Inc_{pRBL16} and IncP6) were designed using Primer 5.0 software, based on the sequences from strain 18102011 carrying plasmid 1 (CP116229) and plasmid 2 (CP116230) (The primer sequences are listed in Supplementary Table S4). DNA contamination was removed from RNA samples using the 4x gDNA wiper rMix (reaction conditions: 42°C for 2 min). cDNA was then synthesized using the used 5x HiScripII qRT SuperMIx II. The reverse transcription program included incubation at 50 °C for 15 min, followed by incubation at 85 °C for 5 s. Quantitative real-time polymerase (qPCR) analysis specifically targeted four key genetic elements. These included the bla_{KPC-2} gene and bla_{VIM-2} gene responsible for encoding KPC-2 and VIM-2 carbapenemases respectively. The analysis also targeted the Inc_{pRBL16} *repA* and IncP6 *repA* genes, which encode essential replication initiation proteins for plasmid 1 and plasmid 2 (The qPCR conditions were listed in Supplementary Table S5). The experiment was conducted with three technical replicates using three-fold serial dilutions of cDNA. The entire experimental procedure was repeated three times.

Nucleotide sequence accession numbers

The complete sequences of strain 18102011, plasmid pP2011-1, and plasmid pP2011–2 have been submitted to GenBank under the accession numbers CP116228, CP116229, and CP116230, respectively. The transcriptome data of strain 18102011 and its plasmids before and after the addition of imipenem have been uploaded to the China National Center for Bioinformatics (CNCB) (http://ngdc.cncb.ac.cn/gsub/) under accession number CRA023298.

Results and discussion

Identification and antimicrobial resistance profile of strain 18102011

After strain 18102011 was cultured overnight at 37°C on Brain Heart Infusion (BHI) agar containing an imipenem concentration of 4 μg/mL, distinct colonies with smooth and regular edges, measuring approximately 0.5 mm in diameter, were observed. These colonies exhibited non-fusion growth, and pyocyanin production, and were devoid of metallic sheens. Subsequently, strain 18102011 was identified as *P. aeruginosa* using the BD Phoenix-100 automated identification system and sequencing of the *oprL* gene, a marker specific to this species. Following this identification, a comprehensive analysis of its drug resistance spectrum was conducted, revealing resistance to all evaluated antibiotics (Supplementary Tables S1, S2).

Genomic characterization of the *P. aeruginosa* strain 18102011

To characterize the genome of the bacterium thoroughly, we employed Single Molecule Real-Time (SMRT) sequencing. The genome sequencing data revealed a 6.6 Mb chromosome in strain 18102011 (GenBank ID: CP116228), exhibiting a GC content of 66.2%. Additionally, the presence of two plasmids was detected in this bacterium. This strain's genome revealed an ANI value of ≥95% with the reference strain *P. aeruginosa* PAO1 (GenBank ID: NC_002516.2), verifying the species information for this bacterium again.

The molecular genetic characteristics of the bacterium were analyzed to determine whether it was a member of a potential epidemic clone group. The isolate belonged to the multi-locus sequence type ST2374 and serotype O4 based on MLST and PAst identification, respectively. As of March 2024, the pbMLST database contained two total strains of ST2374 *P. aeruginosa*, including strain SX69 from a sputum origin in China and strain 127Gr isolated from soft tissue in Belarus in 2016. More than twenty serotypes of *P. aeruginosa* were known, of which serotype O4 was not known as a multidrug-resistant serotype (Nasrin et al., 2022). However, serotype switching from O4 to the multidrug-resistant serotype O12 had been observed under specific conditions (Thrane et al., 2015).

Three virulence genes were detected on the chromosome of strain 18102011: the phospholipase C (PLC) gene (*plcH*) and exotoxin genes (*exoS* and *exoT*). PLC was a thermolabile hemolysin that degrades phospholipid surfactants and reduces surface tension, thus preventing alveoli from collapsing completely when air leaves them during breathing (Khan et al., 2021; Wang et al., 2021). The ExoS and ExoT proteins could be secreted via the type III secretion system (T3SS) and could disrupt the cytoskeleton, induce host cell rounding, disrupt intercellular tight junctions, prevent wound healing, and inhibit bacterial internalization into epithelial cells and macrophages (Rao et al., 2021; Jouault et al., 2022). Consistent with previous reports, the isolate harboring *exoS*-like sequences did not contain *exoU*-like sequences (Feltman et al., 2001). In this study, in addition to the *exoU* gene encoding ExoU (a T3SS effector), the *exoA* gene encoding Exotoxin A (ExoA), which was also a strong pathogenic virulence factor such as ExoU, was not identified (Jørgensen et al., 2005; Foulkes et al., 2019; Morgan et al., 2021). Additionally, the *exoY* gene encoding ExoY (another T3SS effector) was also not detected in this study. It might exhibit greater cytotoxicity to epithelial cells than strains secreting active ExoY, as ExoY had been found to possibly play a protective role at certain stages of bacterial infection, either to facilitate host colonization or to establish and/or maintain chronic infection in the host (Silistre et al., 2021). Thus, this strain might cause cellular damage in immunocompromised patients, but it didn't cause acute toxicity.

According to the Resfinder database, CARD database, and PCR results, the bacteria carried the acquired genes bla_{VIM-2} and bla_{KPC-2} simultaneously. Furthermore, through the Resfinder platform, other acquired resistance genes were identified in strain 18102011, including aminoglycoside resistance genes (*aph(3')-IIb*, *aac(6')-Ib-cr*, *ant(2")-Ia*), β-lactam resistance genes ($bla_{OXA-396}$, bla_{PAO}, bla_{PER-1}), a sulfonamide resistance gene (*sul1*), a chloramphenicol resistance gene (*catB7*), a quinolone resistance gene (*qnrVC6*), and a fosfomycin resistance gene (*fosA*). These resistance genes were inserted into chromosomes and plasmids by mobile elements. Plasmid-mediated drug resistance genes could lead to their rapid spread among bacteria. Pan-resistance *P. aeruginosa* co-carrying bla_{VIM-2} and bla_{KPC-2} genes was first reported in Colombia and had subsequently spread in this country, harboring many resistance genes (Correa et al., 2015; Rada et al., 2021), which was not common in China.

Overview of plasmid pP2011–1 carrying bla_{VIM-2}

The bacteria carried two plasmids, which were named pP2011–1 and pP2011-2, in this study. The mega-plasmid pP2011-1 (GenBank ID: CP116229) carrying bla_{VIM-2} was 474 kb and exhibited a GC content of 56.9%. The plasmid harbored a *repA* (replication initiation) gene sharing ≥96% nucleotide identity to $repA_{IncpRBL16}$. The Inc_{pRBL16} plasmid was first reported in the mega-plasmid p12969-DIM (GenBank ID: KU130294) of strain *P. aeruginosa* 12969 (Sun et al., 2016). As of March 2024, there were many genomes containing $repA_{IncpRBL16\text{-}like}$ sequences in the GenBank database, all of which belonged to *Pseudomonas* spp. However, the pP2011–1 plasmid had a low genetic identified with the previously reported Inc_{pRBL16} family plasmid (Jiang et al., 2020; Dong et al., 2022), and there were large structural variations. The Inc_{pRBL16} family plasmids carried by bacteria may have co-evolved with their chromosomes to maintain their presence in the host bacteria.

As shown in Figure 1, the backbone of plasmid pP2011–1 contained genes for partitioning (*parB2-parAB*), conjugal transfer (*cpl* and *tivF*), chemotaxis (*che*), pilus assembly (*pil*), and tellurium resistance (*ter*), in addition to $repA_{IncpRBL16}$ (Figure 1). The plasmid also contained 3 novel recombination sites in addition to the common recombination site 2 for Inc_{pRBL16} family plasmids (Jiang et al., 2020). IS*Pa75* (IS*66* family) and *fosA* formed the accessory module 1 region that was inserted between two hypothetical proteins of the tellurium resistance region. In addition, *dnaK* and *yaeT*, along with several phage integrase genes and stress protein genes, form the accessory module 2 region that was inserted into the region of the catalytic subunit of Pol V (UmuC), which was a major recombination site of Inc_{pRBL16} family plasmids. During conjugation, plasmids were transferred as single-stranded DNA, which in turn activates the bacterial SOS stress response. The SOS response coordinated the expression of dozens of bacterial genes involved in DNA repair and cell cycle control, and it was known to fuel bacterial evolvability through an increase in recombination and mutagenesis (Rodríguez-Beltrán et al., 2021). The accessory module 3 region comprised heavy-metal efflux protein genes (*merE*, *merD*, *merA*, *merP*, *merT*, and *merR*), Tn*6001* (Tn*3* family), two copies of IS*CR1* (IS*91* family), bla_{PER-1}, and *qnrVC6*, and a novel class 1 integron In2057 carrying *ant(2")-IIa*, bla_{VIM-2} and *aac(6')-Ib-cr*, which was inserted between the hypothetical protein genes that were 708 bp and 1,257 bp in length. Finally, the accessory module 4 region included IS*Pa141* (IS*30* family), IS*Pa61* (IS*L3* family), IS*Pst3* (IS*21* family), IS*Pa60* (IS*As1* family), Tn*4662a* (Tn*3* family), and Tn*5046.1* (Tn*3* family), which were inserted between the hypothetical protein and phage protein genes.

Overview of plasmid pP2011–2 carrying bla_{KPC-2}

As shown in Figure 2, the pP2011–2 plasmid (GenBank ID: CP116230) carrying bla_{KPC-2} was 40 kb in length and exhibited a GC content of 58.1%. The plasmid harbored a *repA* gene sharing ≥96% nucleotide identity to $repA_{Incp6}$. The IncP6 plasmid was first identified in pRms149 (GenBank ID: GCA_019400855.1) of the *P. aeruginosa* JX05 strain in 2005 (Haines et al., 2005). According to the GenBank database, this replicon sequence could be found in Enterobacteriaceae, *P. aeruginosa*, and *Aeromonas* strains. The backbone of the $repA_{Incp6}$ family plasmid included $repA_{Incp6}$, genes for partitioning (*parABC*), and a mobilization region (*mobABCDE*), in addition to two accessory modules in this study. The accessory module 1 region comprised Tn*5563a* (Tn*3* family) and IS*Pa19*, whereas accessory module 2 includes IS*Ec33*-Tn*3*-IS*Apu2*-IS*Apu2-orf7*-IS*Kpn27*-bla_{KPC-2}-ΔIS*Kpn6-korC-orf6-klcA*-Δ*repB*. Typical transposons Tn*4401* and Tn*1722*, both members of Tn*3* family, have been demonstrated to mobilize the bla_{KPC-2} at high transposition frequencies (Song et al., 2024). KPC-1/KPC-2 was first identified in *Klebsiella pneumoniae* in 2001 (Yigit et al., 2001). While KPC carried by Enterobacteriaceae, it has also been detected in non-Enterobacteriaceae due to horizontal gene transfer, such as *P. aeruginosa*. Tn*4401* is a removable element that commonly carries the bla_{KPC-2} gene in Europe, Brazil, and the United States. In Asia, bla_{KPC-2} is mainly located on different variants of Tn*1722*-like transposons (Song et al., 2024). Zhang DF et al. found that there were three divergent forms of bla_{KPC-2} transposon unit in *K. pneumoniae*, including Tn*1721*-bla_{KPC-2} transposon, IS*26*-Tn*1721*-bla_{KPC-2} transposon and IS*26*-bla_{KPC-2} transposon (Zhang et al., 2022). The IncP6 plasmid (p10265-KPC) was first characterized in 2016, different from the Tn*1722*/Tn*1721*-like unit transposons (pKP048 from *K. pneumoniae*), the IS*Apu1-orf7*-IS*Apu2* structure truncates the Tn*3* transposase and inserts a truncated bla_{TEM-1} gene downstream of IS*Kpn27* (Dai et al., 2016). In this study, the distinction lines in the fact that p10265-KPC has a truncated bla_{TEM-1} gene inserted between IS*Kpn27* and the bla_{KPC-2} gene (Dai et al., 2016).

10.3389/fcimb.2025.1617614

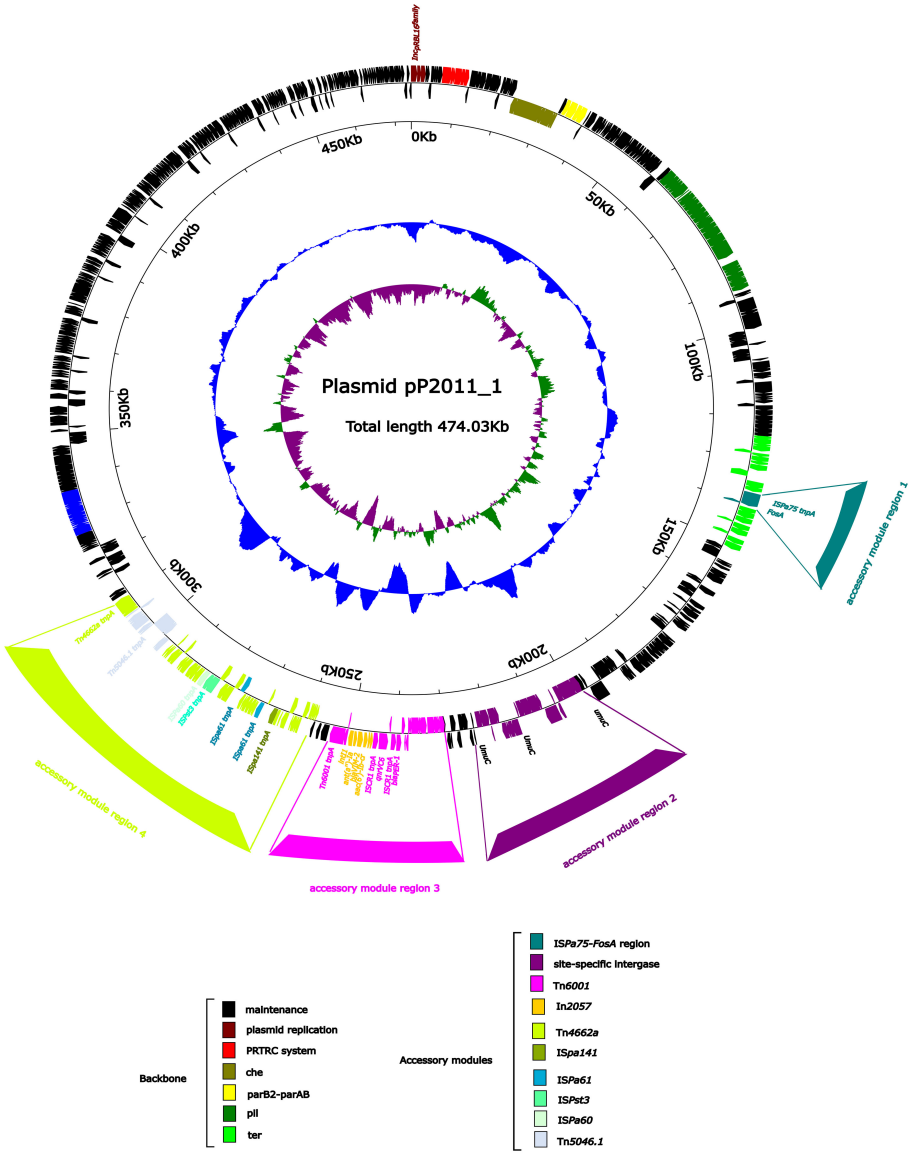

FIGURE 1
Annotation of the plasmid pP2011-1. The circles represented (from outside to inside) the following: (1) Genome functional annotation. The backbone region was black, the plasmid replicon was brown, the PRTRC system was red, the *che* region was dark green, the parB2-parAB region was yellow, the *pil* region was lighter green, and the *ter* region was bright green. The IS*Pa75* and *fosA* genes form the accessory module 1 region (dark cyan), whereas the *dnaK* and *yaeT* genes, along with several phage integrase genes and stress protein genes, form the accessory module 2 region (purple), which was inserted into the UmuC region (purple). The accessory module 3 region (pink) comprises Tn*6011* (pink) and In2057 (orange). The accessory module 4 region (green-yellow) comprises IS*pa141* (olive), IS*pa61* (dark blue), IS*pst3* (turquoise), IS*Pa60* (honeydew), Tn*4662a* (green-yellow) and Tn*5046.1* (alice blue); (2) GC skew calculated as [(G-C)/(G+C)]; and (3) GC content.

Conjugative transfer and resistance phenotype dissemination of bla_{VIM-2} and bla_{KPC-2}-encoding plasmids

To evaluate the transferability of plasmids harboring bla_{KPC-2} and bla_{VIM-2}, conjugation assays were performed by co-culturing the strain 18102011 with *E. coli* EC600. Conjugants grown on dilution gradients of 10^{-1}, 10^{-2}, and 10^{-3}. And recipient bacteria can grow on all dilution gradients from 10–^{1} to 10–^{9} on a medium containing only rifampicin. The conjugation transfer efficiency was calculated to be 10–^{6} using the Equation (1.1). Because the IncP6 plasmid lacked a conjugation-transfer region and only had a mobile region, the plasmid could only carry out horizontal transfer under the synergistic action of the conjugation plasmid Inc_{pRBL16} (Coluzzi et al., 2022). In this study, all suspected transconjugants were picked from the culture medium at 10^{3} dilution gradients, with number of 19, 15, and 21 respectively (corresponding to three parallel replicates). A single carbapenem-resistant gene, namely bla_{KPC-2} or bla_{VIM-2}, was not found by conjugation assays. Although the MICs of transconjugant D2011 for many antibiotics tested

FIGURE 2
Annotation of plasmid pP2011-2. The circles represented (from outside to inside) the following: (1) Genome functional annotation. The backbone region was black, in which the plasmid replicon was green. Tn*5563a* (pink) and IS*Pa19* (sea-green) comprise the accessory module 1 region (pink), whereas the module 2 region (orange) comprises IS*Kpn6* (red), bla_{KPC-2} (magenta), IS*Kpn27* (yellow), Tn*3* (orange), IS*Apu2* (blue), and IS*Ec33* (purple); (2) the GC skew was calculated as [(G-C)/(G+C)]; and (3) the GC content.

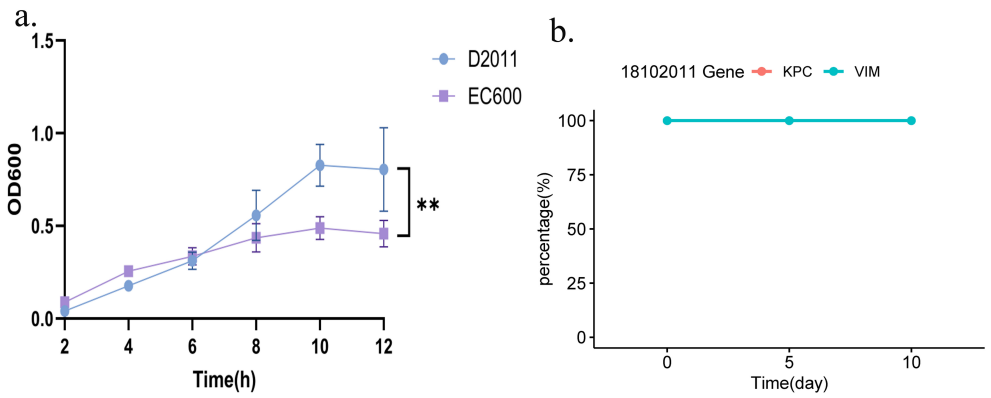

FIGURE 3
Growth curves of strain D2011 and stability of the bla_{KPC-2} or bla_{VIM-2} gene. **(a)** Growth curve of strain D2011 carrying the bla_{KPC-2} and bla_{VIM-2} genes and *E. coli* EC600. **(b)** Stability of the bla_{KPC-2} and bla_{VIM-2} genes during the 10-day serial passage. $p< 0.05$ *(significant), $p< 0.01$ ** (highly significant).

decreased significantly, indicating susceptibility, it was still resistant to imipenem and meropenem (Supplementary Tables S1, S2). The MICs of strain 18102011 and its transconjugant D2011 against imipenem were determined by broth method, both of which were 4,096 μg/mL. Therefore, the main resistance mechanism of strain 18102011 to carbapenem antibiotics was plasmid-mediated bla_{VIM-2} and bla_{KPC-2} genes, resulting in a stable carbapenem-resistant transmission phenotype.

Plasmid stability and fitness cost analysis of bla_{KPC-2} and bla_{VIM-2}-co-harboring strain 18102022

The impact of the acquisition of both plasmids carrying bla_{KPC-2} and bla_{VIM-2} on the biological fitness cost was evaluated. Notably, the OD_{600} of recipient strain *E. coli* EC600 was significantly lower than that of the transconjugant D2011 (carrying bla_{KPC-2} and

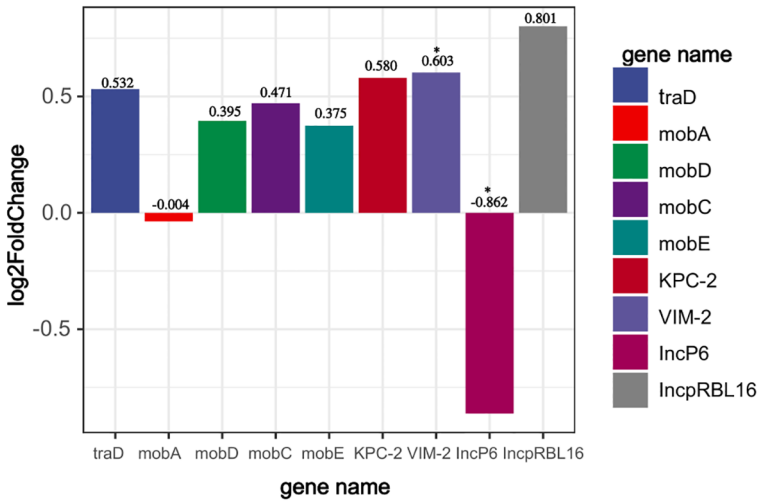

FIGURE 4
Read counts of the Inc_{pRBL16} (*repA*), IncP6 (*repA*), bla_{VIM-2}, bla_{KPC-2}, conjugative transfer genes (*tra*), and mobile genetic genes (*mob*) in strain 18102011. The horizontal axis represents gene name, whereas the vertical axis represents change in read counts (FPKM) of genes after imipenem addition (expressed as log_2FoldChange). $p<0.05$ *(significant), $p<0.01$ **(highly significant).

bla_{VIM-2}) in 12h. Taken together, these microbiological characteristics indicated that strain 18102011 could carry both the bla_{KPC-2} and bla_{VIM-2} genes without compromising their fitness and maintaining them stably over time (Figure 3a). Furthermore, during serial passage in the laboratory for 10 days to evaluate the stability of plasmids carrying bla_{KPC-2} and bla_{VIM-2} from strain 1810211. Interestingly, both the bla_{KPC-2} and bla_{VIM-2} plasmids were present in 50 colonies (100%, 50/50) on the 5^{th} and 10^{th} day, respectively, indicating high stability (Figure 3b, PCR identification of bla_{KPC-2} and bla_{VIM-2} genes of the strain D2011 on 5^{th} and 10^{th} day were shown in Supplementary Figure S1). This increased our concern about bla_{KPC-2}-bla_{VIM-2}-CRPA, as it posed not only significant challenges in treatment but also a remarkable ability to stably maintain these plasmids without apparent fitness costs, making it difficult to retrogress.

Transcriptional regulation of bla_{VIM-2} and bla_{KPC-2} under carbapenem pressure

The integron In2057-bla_{VIM-2} sequence was uploaded into the BPROM database, revealing only one promoter with the -10/-35

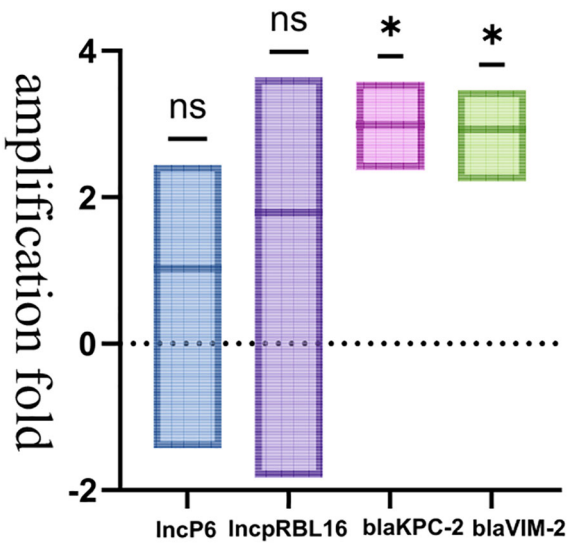

FIGURE 5
Results of qPCR identification of the Inc_{pRBL16} (*repA*), IncP6 (*repA*), bla_{VIM-2}, and bla_{KPC-2} in strain 18102011. The horizontal axis represents group classifications (IncP6; Inc_{pRBL16}; bla_{KPC-2}; bla_{VIM-2}), whereas the vertical axis represents amplification fold. $p<0.05$ *(significant), $p<0.01$ **(highly significant), $p>0.05$ ns (not significant).

region (AGCTTACCA/TGTCCA) located within In2057's integrase. This promoter sequence matched the PcW_{TGN-10} promoter sequence identified in the research by Nesvera J et al., driving the expression of the downstream gene cassette (Nesvera et al., 1998). It had been reported that the TGN-10 motif increased the PcW promoter strength efficiency 15-fold (Jové et al., 2010). Therefore, this promoter might have increased the expression of a series of downstream gene cassettes in this study, including bla_{VIM-2}. This might be one of the reasons for the high resistance of bacteria to carbapenem.

The IS*Kpn27*-bla_{KPC-2} sequence was uploaded into the BPROM database. Only one promoter with the -10/-35 region (ATGTAA/GGATTA) was identified between the IS*Kpn27* and bla_{KPC-2} genes. This promoter sequence was consistent with the P1 promoter sequence commonly found in IS*Kpn7*-bla_{KPC-2}, which drove the expression of the downstream bla_{KPC-2} gene (Huang et al., 2019; Huang et al., 2020).

Through transcriptome analysis of the expression of the bla_{VIM-2} gene carried by plasmid pP2011–1 and the bla_{KPC-2} gene carried by plasmid pP2011-2, it was found that both genes were up-regulated when imipenem was added to the culture medium (Figure 4, the data for Figure 4 can be found in Supplementary Table S6). However, after the addition of imipenem, the expression level of bla_{VIM-2} significantly increased, which might be related to the regulatory effect of its upstream strong promoter (Figures 4, 5, the data for Figure 4 can be found in Supplementary Table S7). Additionally, under the influence of imipenem, the expression levels of some other genes on the plasmid also changed. For example, the expression levels of plasmid conjugative transfer gene (*tra*), the mobilization genes (*mob*, excluding *mobA*), and the *repA* gene on the IncpRBL16 plasmid all showed increase, although this increase was not significant (Figures 4, 5). The low levels of read counts (FPKM) for the replicon genes *repA* (located on the Inc_{pRBL16} plasmids) and the conjugative transfer gene (*traD*) indicated their low expression levels (Supplementary Table S6). Since the *repA* gene is a key factor for initiating plasmid replication, its low expression leads to a reduction in plasmid copy number. This could be a strategy employed by the Inc_{pRBL16} plasmid to decrease its fitness cost to the host bacterium by maintaining a lower copy number (Figure 4).

Conclusion

Currently, there were relatively few reports on pan-resistant *P. aeruginosa* co-carrying bla_{VIM-2} and bla_{KPC-2} genes in China, which were mostly concentrated in Columbia. The limited existing reports also lacked an analysis of the fitness costs associated with the plasmids carried by these bacteria. In this study, the presence of bla_{KPC-2} and bla_{VIM-2} plasmids didn't cause fitness costs to the growth of the host bacteria. Since the IncP6 plasmid lacked a conjugation transfer region, its horizontal transfer required the assistance of Inc_{pRBL16} conjugation plasmids for co-transfer into *E. coli* EC600. Through horizontal plasmid transfer, high-level resistance to imipenem was stably maintained within the bacterial population. However, there were differences in the composition of the cell membranes between *P. aeruginosa* and *E. coli*, causing the pan-drug resistant phenotype to not be shared between the donor and recipient bacteria through plasmid conjugation transfer. As the treatment of pan-drug resistant bacteria was extremely challenging, their epidemiological and molecular genetics across the world should be closely monitored.

Data availability statement

Publicly available datasets were analyzed in this study. This data can be found here: The complete sequences of strain 18102011, plasmid pP2011-1, and plasmid pP2011-2 have been submitted to GenBank under the accession numbers CP116228, CP116229, and CP116230, respectively. The transcriptome data of strain 18102011 and its plasmids before and after the addition of imipenem have been uploaded to the China National Center for Bioinformatics (CNCB) (http://ngdc.cncb.ac.cn/gsub/) under accession number CRA023298.

Author contributions

LZ: Conceptualization, Investigation, Writing – original draft, Writing – review & editing, Data curation, Validation, Visualization, Methodology. ZW: Writing – original draft. GL: Writing – original draft, Supervision. XZ: Supervision, Validation, Writing – original draft. JJ: Writing – original draft, Supervision, Validation. SS: Project administration, Writing – original draft. YS: Writing – original draft, Resources, Project administration, Funding acquisition. XJ: Writing – original draft, Project administration. BJ: Project administration, Writing – original draft. LWZ: Conceptualization, Resources, Funding acquisition, Methodology, Supervision, Writing – review & editing. XG: Methodology, Investigation, Data curation, Funding acquisition, Resources, Project administration, Conceptualization, Writing – review & editing.

Funding

The author(s) declare financial support was received for the research and/or publication of this article. Funding for the study design, data collection, data generation, and publication costs was provided by Jilin Provincial Department of Finance (jcsz2023481-1) and the National Science and Natural Science Foundation of China (Grant agreement 31872486).

Acknowledgments

We are grateful to the members of the China-Japan Union Hospital, Jilin University.

Conflict of interest

The authors declare that the research was conducted in the absence of any commercial or financial relationships that could be construed as potential conflicts of interest.

Generative AI statement

The author(s) declare that no Generative AI was used in the creation of this manuscript.

Publisher's note

All claims expressed in this article are solely those of the authors and do not necessarily represent those of their affiliated organizations, or those of the publisher, the editors and the reviewers. Any product that may be evaluated in this article, or claim that may be made by its manufacturer, is not guaranteed or endorsed by the publisher.

Supplementary material

The Supplementary Material for this article can be found online at: https://www.frontiersin.org/articles/10.3389/fcimb.2025.1617614/full#supplementary-material

SUPPLEMENTARY FIGURE 1
PCR identification of *bla*$_{KPC-2}$ and *bla*$_{VIM-2}$ genes of strain 18102011 on the 5th and 10th day. (a) PCR identification of *bla*$_{KPC-2}$ and *bla*$_{VIM-2}$ genes of strain 18102011 on the 5th day; (b) PCR identification of *bla*$_{KPC-2}$ and *bla*$_{VIM-2}$ genes of strain 18102011 on the 10th day; (c) PCR identification of *bla*$_{KPC-2}$ and *bla*$_{VIM-2}$ genes of strain 18102011 on the 5th day (repeat); (d) PCR identification of *bla*$_{KPC-2}$ and *bla*$_{VIM-2}$ genes of strain 18102011 on the 10th day (repeat).

References

Alcock, B. P., Huynh, W., Chalil, R., Smith, K. W., Raphenya, A. R., Wlodarski, M. A., et al. (2023). CARD 2023: expanded curation, support for machine learning, and resistome prediction at the Comprehensive Antibiotic Resistance Database. *Nucleic Acids Res.* 51, D690–d699. doi: 10.1093/nar/gkac920

Allameh, S. F., Nemati, S., Ghalehtaki, R., Mohammadnejad, E., Aghili, S. M., Khajavirad, N., et al. (2020). Clinical characteristics and outcomes of 905 COVID-19 patients admitted to imam khomeini hospital complex in the capital city of tehran, Iran. *Arch. Iran Med.* 23, 766–775. doi: 10.34172/aim.2020.102

Blanc, D. S., Petignat, C., Janin, B., Bille, J., and Francioli, P. (1998). Frequency and molecular diversity of *Pseudomonas aeruginosa* upon admission and during hospitalization: a prospective epidemiologic study. *Clin. Microbiol. Infect.* 4, 242–247. doi: 10.1111/j.1469-0691.1998.tb00051.x

Boratyn, G. M., Camacho, C., Cooper, P. S., Coulouris, G., Fong, A., Ma, N., et al. (2013). BLAST: a more efficient report with usability improvements. *Nucleic Acids Res.* 41, W29–W33. doi: 10.1093/nar/gkt282

Bortolaia, V., Kaas, R. S., Ruppe, E., Roberts, M. C., Schwarz, S., Cattoir, V., et al. (2020). ResFinder 4.0 for predictions of phenotypes from genotypes. *J. Antimicrob. Chemother.* 75, 3491–3500. doi: 10.1093/jac/dkaa345

Botelho, J., Grosso, F., and Peixe, L. (2019). Antibiotic resistance in *Pseudomonas aeruginosa* - Mechanisms, epidemiology and evolution. *Drug Resist. Updat* 44, 100640. doi: 10.1016/j.drup.2019.07.002

Brettin, T., Davis, J. J., Disz, T., Edwards, R. A., Gerdes, S., Olsen, G. J., et al. (2015). RASTtk: a modular and extensible implementation of the RAST algorithm for building custom annotation pipelines and annotating batches of genomes. *Sci. Rep.* 5, 8365. doi: 10.1038/srep08365

Cassiano, M. H. A., and Silva-Rocha, R. (2020). Benchmarking bacterial promoter prediction tools: potentialities and limitations. *mSystems* 5. doi: 10.1128/mSystems.00439-20

Coluzzi, C., Garcillán-Barcia, M. P., de la Cruz, F., and Rocha, E. P. C. (2022). Evolution of plasmid mobility: origin and fate of conjugative and nonconjugative plasmids. *Mol. Biol. Evol.* 39. doi: 10.1093/molbev/msac115

Cornaglia, G., Mazzariol, A., Lauretti, L., Rossolini, G. M., and Fontana, R. (2000). Hospital outbreak of carbapenem-resistant *Pseudomonas aeruginosa* producing VIM-1, a novel transferable metallo-beta-lactamase. *Clin. Infect. Dis.* 31, 1119–1125. doi: 10.1086/317448

Correa, A., Del Campo, R., Perenguez, M., Blanco, V. M., Rodríguez-Baños, M., Perez, F., et al. (2015). Dissemination of high-risk clones of extensively drug-resistant *Pseudomonas aeruginosa* in Colombia. *Antimicrob. Agents Chemother.* 59, 2421–2425. doi: 10.1128/AAC.03926-14

Dai, X., Zhou, D., Xiong, W., Feng, J., Luo, W., Luo, G., et al. (2016). The IncP-6 Plasmid p10265-KPC from Pseudomonas aeruginosa Carries a Novel ΔIS*Ec33*-Associated *bla* $_{KPC-2}$ Gene Cluster. *Front. Microbiol.* 7, 310. doi: 10.3389/fmicb.2016.00310

De Vos, D., Lim, A. Jr., Pirnay, J. P., Struelens, M., Vandenvelde, C., Duinslaeger, L., et al. (1997). Direct detection and identification of *Pseudomonas aeruginosa* in clinical samples such as skin biopsy specimens and expectorations by multiplex PCR based on two outer membrane lipoprotein genes, oprI and oprL. *J. Clin. Microbiol.* 35, 1295–1299. doi: 10.1128/jcm.35.6.1295-1299.1997

Dong, N., Liu, C., Hu, Y., Lu, J., Zeng, Y., Chen, G., et al. (2022). Emergence of an Extensive Drug Resistant *Pseudomonas aeruginosa* Strain of Chicken Origin Carrying bla(IMP-45), tet(X6), and tmexCD3-toprJ3 on an Inc(pRBL16) Plasmid. *Microbiol. Spectr* 10, e0228322. doi: 10.1128/spectrum.02283-22

Feltman, H., Schulert, G., Khan, S., Jain, M., Peterson, L., and Hauser, A. R. (2001). Prevalence of type III secretion genes in clinical and environmental isolates of Pseudomonas aeruginosa. *Microbiol. (Reading)* 147, 2659–2669. doi: 10.1099/00221287-147-10-2659

Foulkes, D. M., McLean, K., Haneef, A. S., Fernig, D. G., Winstanley, C., Berry, N., et al. (2019). *Pseudomonas aeruginosa* toxin exoU as a therapeutic target in the treatment of bacterial infections. *Microorganisms* 7. doi: 10.3390/microorganisms7120707

Haines, A. S., Jones, K., Cheung, M., and Thomas, C. M. (2005). The IncP-6 plasmid Rms149 consists of a small mobilizable backbone with multiple large insertions. *J. Bacteriol.* 187, 4728–4738. doi: 10.1128/JB.187.14.4728-4738.2005

Huang, J., Hu, X., Zhao, Y., Shi, Y., Ding, H., Wu, R., et al. (2019). Comparative analysis of bla(KPC) expression in tn*4401* transposons and the tn*3*-tn*4401* chimera. *Antimicrob. Agents Chemother.* 63:e02434-18. doi: 10.1128/AAC.02434-18

Huang, J., Hu, X., Zhao, Y., Shi, Y., Ding, H., Xv, J., et al. (2020). Genetic factors associated with enhanced bla(KPC) expression in tn*3*/tn*4401* chimeras. *Antimicrob. Agents Chemother.* 64. :e01836-19. doi: 10.1128/AAC.01836-19

Jiang, X., Yin, Z., Yuan, M., Cheng, Q., Hu, L., Xu, Y., et al. (2020). Plasmids of novel incompatibility group IncpRBL16 from *Pseudomonas* species. *J. Antimicrob. Chemother.* 75, 2093–2100. doi: 10.1093/jac/dkaa143

Jørgensen, R., Merrill, A. R., Yates, S. P., Marquez, V. E., Schwan, A. L., Boesen, T., et al. (2005). Exotoxin A-eEF2 complex structure indicates ADP ribosylation by ribosome mimicry. *Nature* 436, 979–984. doi: 10.1038/nature03871

Jouault, A., Saliba, A. M., and Touqui, L. (2022). Modulation of the immune response by the *Pseudomonas aeruginosa* type-III secretion system. *Front. Cell Infect. Microbiol.* 12, 1064010. doi: 10.3389/fcimb.2022.1064010

Jové, T., Da Re, S., Denis, F., Mazel, D., and Ploy, M. C. (2010). Inverse correlation between promoter strength and excision activity in class 1 integrons. *PloS Genet.* 6, e1000793. doi: 10.1371/journal.pgen.1000793

Kang, C. I., Kim, S. H., Kim, H. B., Park, S. W., Choe, Y. J., Oh, M. D., et al. (2003). Pseudomonas aeruginosa bacteremia: risk factors for mortality and influence of delayed receipt of effective antimicrobial therapy on clinical outcome. *Clin. Infect. Dis.* 37, 745–751. doi: 10.1086/377200

Khan, M., Willcox, M. D. P., Rice, S. A., Sharma, S., and Stapleton, F. (2021). Development of antibiotic resistance in the ocular *Pseudomonas aeruginosa* clone ST308 over twenty years. *Exp. Eye Res.* 205, 108504. doi: 10.1016/j.exer.2021.108504

Li, X., Gu, N., Huang, T. Y., Zhong, F., and Peng, G. (2022). *Pseudomonas aeruginosa*: A typical biofilm forming pathogen and an emerging but underestimated pathogen in food processing. *Front. Microbiol.* 13, 1114199. doi: 10.3389/fmicb.2022.1114199

Liu, M., Li, X., Xie, Y., Bi, D., Sun, J., Li, J., et al. (2019). ICEberg 2.0: an updated database of bacterial integrative and conjugative elements. *Nucleic Acids Res.* 47, D660–d665. doi: 10.1093/nar/gky1123

Liu, B., Zheng, D., Zhou, S., Chen, L., and Yang, J. (2022). VFDB 2022: a general classification scheme for bacterial virulence factors. *Nucleic Acids Res.* 50, D912–d917. doi: 10.1093/nar/gkab1107

Mohammadnejad, E., Seifi, A., Ghanei Gheshlagh, R., Aliramezani, A., Fattah Ghazi, S., Salehi, M., et al. (2023). Determine phenotypical patterns of resistance to antibiotics in COVID-19 patients with associated bacterial infection: largest medical center in Iran. *Iran J. Microbiol.* 15, 336–342. doi: 10.18502/ijm.v15i3.12893

Morgan, R. N., Saleh, S. E., Aboshanab, K. M., and Farrag, H. A. (2021). ADP-ribosyl transferase activity and gamma radiation cytotoxicity of *Pseudomonas aeruginosa* exotoxin A. *AMB Express* 11, 173. doi: 10.1186/s13568-021-01332-3

Moura, A., Soares, M., Pereira, C., Leitão, N., Henriques, I., and Correia, A. (2009). INTEGRALL: a database and search engine for integrons, integrases and gene cassettes. *Bioinformatics* 25, 1096–1098. doi: 10.1093/bioinformatics/btp105

Nasrin, S., Hegerle, N., Sen, S., Nkeze, J., Sen, S., Permala-Booth, J., et al. (2022). Distribution of serotypes and antibiotic resistance of invasive *Pseudomonas aeruginosa* in a multi-country collection. *BMC Microbiol.* 22, 13. doi: 10.1186/s12866-021-02427-4

Nesvera, J., Hochmannová, J., and Pátek, M. (1998). An integron of class 1 is present on the plasmid pCG4 from gram-positive bacterium Corynebacterium glutamicum. *FEMS Microbiol. Lett.* 169, 391–395. doi: 10.1111/j.1574-6968.1998.tb13345.x

Pang, Z., Raudonis, R., Glick, B. R., Lin, T. J., and Cheng, Z. (2019). Antibiotic resistance in *Pseudomonas aeruginosa*: mechanisms and alternative therapeutic strategies. *Biotechnol. Adv.* 37, 177–192. doi: 10.1016/j.biotechadv.2018.11.013

Partridge, S. R., Kwong, S. M., Firth, N., and Jensen, S. O. (2018). Mobile genetic elements associated with antimicrobial resistance. *Clin. Microbiol. Rev.* 31. doi: 10.1128/CMR.00088-17

Poirel, L., Walsh, T. R., Cuvillier, V., and Nordmann, P. (2011). Multiplex PCR for detection of acquired carbapenemase genes. *Diagn. Microbiol. Infect. Dis.* 70, 119–123. doi: 10.1016/j.diagmicrobio.2010.12.002

Rada, A. M., de la Cadena, E., Agudelo, C. A., Pallares, C., Restrepo, E., Correa, A., et al. (2021). Genetic Diversity of Multidrug-Resistant *Pseudomonas aeruginosa* Isolates Carrying bla (VIM-2) and bla (KPC-2) Genes That Spread on Different Genetic Environment in Colombia. *Front. Microbiol.* 12, 663020. doi: 10.3389/fmicb.2021.663020

Rao, L., de la Rosa, I., Xu, Y., Sha, Y., Bhattacharya, A., Holtzman, M. J., et al. (2021). Pseudomonas aeruginosa survives in epithelia by ExoS-mediated inhibition of autophagy and mTOR. *EMBO Rep.* 22, e50613. doi: 10.15252/embr.202050613

Rodríguez-Beltrán, J., DelaFuente, J., León-Sampedro, R., MacLean, R. C., and San Millán, Á. (2021). Beyond horizontal gene transfer: the role of plasmids in bacterial evolution. *Nat. Rev. Microbiol.* 19, 347–359. doi: 10.1038/s41579-020-00497-1

Silistre, H., Raoux-Barbot, D., Mancinelli, F., Sangouard, F., Dupin, A., Belyy, A., et al. (2021). Prevalence of exoY activity in *pseudomonas aeruginosa* reference panel strains and impact on cytotoxicity in epithelial cells. *Front. Microbiol.* 12, 666097. doi: 10.3389/fmicb.2021.666097

Song, J. M., Long, H. B., Ye, M., Yang, B. R., Wu, G. J., He, H. C., et al. (2024). Genomic characterization of a bla (KPC-2)-producing IncM2 plasmid harboring transposon ΔTn*6296* in Klebsiella michiganensis. *Front. Cell Infect. Microbiol.* 14, 1492700. doi: 10.3389/fcimb.2024.1492700

Sun, F., Zhou, D., Wang, Q., Feng, J., Feng, W., Luo, W., et al. (2016). Genetic characterization of a novel $bla_{\mathrm{DIM\text{-}2}}$-carrying megaplasmid p12969-DIM from clinical Pseudomonas putida. *J. Antimicrob. Chemother.* 71, 909–912. doi: 10.1093/jac/dkv426

Thrane, S. W., Taylor, V. L., Freschi, L., Kukavica-Ibrulj, I., Boyle, B., Laroche, J., et al. (2015). The Widespread Multidrug-Resistant Serotype O12 *Pseudomonas aeruginosa* Clone Emerged through Concomitant Horizontal Transfer of Serotype Antigen and Antibiotic Resistance Gene Clusters. *mBio* 6, e01396–e01315. doi: 10.1128/mBio.01396-15

Varani, A. M., Siguier, P., Gourbeyre, E., Charneau, V., and Chandler, M. (2011). ISsaga is an ensemble of web-based methods for high throughput identification and semi-automatic annotation of insertion sequences in prokaryotic genomes. *Genome Biol.* 12, R30. doi: 10.1186/gb-2011-12-3-r30

Wang, J., Chen, Y. L., Li, Y. K., Chen, D. K., He, J. F., and Yao, N. (2021). Functions of sphingolipids in pathogenesis during host-pathogen interactions. *Front. Microbiol.* 12, 701041. doi: 10.3389/fmicb.2021.701041

Yigit, H., Queenan, A. M., Anderson, G. J., Domenech-Sanchez, A., Biddle, J. W., Steward, C. D., et al. (2001). Novel carbapenem-hydrolyzing beta-lactamase, KPC-1, from a carbapenem-resistant strain of Klebsiella pneumoniae. *Antimicrob. Agents Chemother.* 45, 1151–1161. doi: 10.1128/AAC.45.4.1151-1161.2001

Yoon, S. H., Ha, S. M., Lim, J., Kwon, S., and Chun, J. (2017). A large-scale evaluation of algorithms to calculate average nucleotide identity. *Antonie Van Leeuwenhoek* 110, 1281–1286. doi: 10.1007/s10482-017-0844-4

Zhang, D. F., Zhang, Z. F., Li, P. D., and Qu, P. H. (2022). Characterization of carbapenem-resistant Acinetobacter baumannii ST540 and *Klebsiella pneumoniae* ST2237 isolates in a pneumonia case from China. *J. Appl. Microbiol.* 133, 1434–1445. doi: 10.1111/jam.15648

frontiers | Frontiers in Cellular and Infection Microbiology

TYPE Original Research
PUBLISHED 08 September 2025
DOI 10.3389/fcimb.2025.1618815

OPEN ACCESS

EDITED BY
Massimiliano Lucidi,
Roma Tre University, Italy

REVIEWED BY
Yongqin Wu,
Anhui Provincial Hospital, China
Ifeanyi Elibe Mba,
University of Ibadan, Nigeria
Aswathy Narayanan,
Jawaharlal Nehru Centre for Advanced Scientific Research, India

*CORRESPONDENCE
Liangsheng Guo
gls2135@sina.com

†These authors have contributed equally to this work

RECEIVED 27 April 2025
ACCEPTED 25 August 2025
PUBLISHED 08 September 2025

CITATION
Wei Y, Wang J, Tang N, Lin Z, Li W, Xu Y and Guo L (2025) Caspofungin paradoxical growth in *Candida albicans* requires stress pathway activation and promotes unstable echinocandin resistance mediated by aneuploidy.
Front. Cell. Infect. Microbiol. 15:1618815.
doi: 10.3389/fcimb.2025.1618815

Caspofungin paradoxical growth in *Candida albicans* requires stress pathway activation and promotes unstable echinocandin resistance mediated by aneuploidy

Ying Wei[1†], Jing Wang[2†], Nan Tang[3], Ziwei Lin[1], Wenhui Li[1], Yi Xu[4] and Liangsheng Guo[1*]

[1]Department of Obstetrics and Gynecology, The Second Affiliated Hospital of Soochow University, Suzhou, China, [2]Department of Pharmacy, Zibo Zhoucun People's Hospital, Zibo, China, [3]Department of Public Health, Zibo Zhoucun People's Hospital, Zibo, China, [4]Department of Pharmacy, The 960th Hospital of PLA, Jinan, China

Paradoxical growth (PG) is a counterintuitive phenomenon in which otherwise susceptible fungal cells resume proliferation at supra-MIC concentrations of echinocandins, thereby undermining the efficacy of these frontline antifungals. Despite its clinical significance, the genetic basis of PG remains poorly understood. Here, we systematically dissect the roles of key stress response pathways—Hsp90, PKC, calcineurin, and TOR—in mediating caspofungin (CSP)-induced PG in *Candida albicans* and uncover a novel genetic mechanism involving segmental aneuploidy. Disruption of these pathways via pharmacological inhibition or targeted gene deletion abolished PG, confirming their essential roles in mediating adaptive stress responses. Whole-genome sequencing of CSP-tolerant isolates revealed a recurrent segmental monosomy on the right arm of Chromosome R (SegChrRx1). Phenotypic reversion analyses demonstrated that CSP resistance is reversible and directly linked to the presence of this aneuploidy. Transcriptomic profiling of SegChrRx1 strains showed broad transcriptional remodeling, including upregulation of *GSC1* (encoding β-1,3-glucan synthase), *CHS3* and *CHS4* (chitin synthases), and key regulators of the PKC and calcineurin pathways, alongside downregulation of dosage-sensitive genes whose deletion enhances CSP resistance. Collectively, our findings reveal a dual mechanism of PG: activation of stress response pathways confers initial survival, while segmental aneuploidy enables reversible transcriptional reprogramming that promotes drug resistance. This study establishes segmental aneuploidy as a dynamic and previously underappreciated mechanism of echinocandin adaptation in *C. albicans*, with important implications for antifungal therapy.

KEYWORDS

***Candida albicans*, paradoxical growth, stress pathway, aneuploidy, transient resistance**

Introduction

Invasive fungal infections caused by *Candida albicans* remain a major source of morbidity and mortality, particularly in immunocompromised individuals (Pfaller and Diekema, 2007). Echinocandins—such as caspofungin (CSP), micafungin (MCF), and anidulafungin (ANF)—have emerged as first-line antifungal agents due to their fungicidal activity and selective inhibition of β-1,3-glucan synthase, a critical enzyme in fungal cell wall biosynthesis (Pappas et al., 2016). However, the clinical efficacy of echinocandins is increasingly compromised by the emergence of resistance mechanisms (Kanafani and Perfect, 2008). While paradoxical growth (PG) has been well-documented *in vitro*, its clinical relevance remains to be fully elucidated [reviewed in (Wagener and Loiko, 2017)].

PG refers to regrowth of *Candida* spp. at higher but not lower supra-MIC concentrations of echinocandins (Valero et al., 2020). This phenomenon has been consistently observed in *C. albicans* and other fungal species (Toth et al., 2020). PG has been linked to cell wall remodeling, particularly increased chitin deposition (Walker et al., 2013), and activation of conserved stress response pathways, including the PKC, calcineurin, and TOR signaling cascades. Heat shock protein 90 (Hsp90) plays a central role in stabilizing these pathways and has been shown to be essential for PG in both *C. albicans* and *Aspergillus fumigatus* (Reinoso-Martin et al., 2003; Lesage et al., 2004; Fortwendel et al., 2009; Singh et al., 2009; Lamoth et al., 2014; Caplan et al., 2018; Rivera and Heitman, 2023; Lefranc et al., 2024).

Beyond transcriptional responses, *C. albicans* exhibits remarkable genomic plasticity, often employing chromosomal aneuploidy to rapidly adapt to antifungal stress (Selmecki et al., 2006; Yang et al., 2013, Yang et al., 2017, Yang et al., 2019; Li et al., 2022; Sun et al., 2023; Yang et al., 2023; Zheng et al., 2023; Guo et al., 2024; Zheng et al., 2024). Whole-chromosome aneuploidies have been implicated in resistance to azoles and other stressors, yet the role of segmental chromosomal changes in mediating resistance remains largely unexplored. Segmental aneuploidy offers a mechanism for fine-tuned adaptation with potentially lower fitness costs compared to whole-chromosome alterations. The transient and reversible nature of PG suggests the involvement of epigenetic or unstable genetic mechanisms. Given that aneuploidy can reversibly alter gene dosage and broadly rewire cellular pathways, we hypothesized that segmental aneuploidy may contribute to PG in *C. albicans*.

In this study, we combined genetic perturbation, pharmacological inhibition, whole-genome sequencing, and transcriptomic profiling to dissect the molecular basis of CSP-induced PG. We demonstrate that PG arises from a dual mechanism: (1) activation of conserved stress response pathways that mediate immediate resistance, and (2) acquisition of a recurrent segmental aneuploidy on Chromosome R that promotes genome-wide transcriptional remodeling. These findings uncover a novel paradigm for antifungal resistance and underscore the therapeutic potential of targeting aneuploidy-stabilizing mechanisms or stress pathway hubs.

Materials and methods

Strains and growth conditions

The *C. albicans* reference strain SC5314 was used as the progenitor for this study. Gene knock strains are listed in Supplementary Table S1. Stock cultures were preserved in 25% glycerol and stored at -80°C. Cells were routinely cultured in Yeast Extract-Peptone-Dextrose (YPD) medium, which contains 1% (w/v) yeast extract, 2% (w/v) peptone, and 2% (w/v) D-glucose, at 37°C using a shaking incubator set to 150–200 rpm. Caspofungin (HY-17006), anidulafungin (HY-13553), micafungin (HY-16321), rapamycin (HY-10219), and NVP-HSP990 (HY-15190) were purchased from MedChemExpress (MCE). Drug solutions were prepared in dimethyl sulfoxide (DMSO) and stored at -20°C.

Broth microdilution assay

Broth microdilution assay was performed according to the CLSI guidelines (CLSI, 2017) with minor modifications. Briefly, fungal cells were suspended in YPD broth and adjusted to a density of 2.5×10^3 cells/mL. A serial dilution of echinocandins was tested across a concentration range of 0.0125–12.8 μg/mL. The inoculated 96-well plates were incubated at 37°C for 48 hours. Paradoxical growth was assessed by measuring optical density at 600 nm (OD_{600}) using a NanoPhotometer (Implen, California, USA). PG was defined as fungal growth in consecutive wells at supra-MIC concentrations after the incubation period (Chamilos et al., 2007).

Spot assay

Cells were suspended in distilled water and adjusted to a concentration of 1×10^7 cells/mL. 3 μL of 10-fold serial dilutions were spotted on YPD plates containing the indicated drug concentrations, with specific compounds and doses shown in Figures 1–3 top and bottom panels, and Figure 4 top right panel. The plates were incubated at 37°C and photographed after 48 hours.

Obtaining PG adaptor strains

SC5314 cells were suspended in distilled water, and cell density was determined using a hemocytometer. Approximately 50 cells were plated on YPD agar supplemented with CSP (0.05 to 12.8 μg/mL). The plates were incubated at 37°C for 5 days. All colonies that grew on the drug-containing plates were collected for further analysis.

Colony instability assay

One SegChrRx1 adaptor (selected at 1.6 μg/mL CSP) was chosen as the representative strain for subsequent experiments

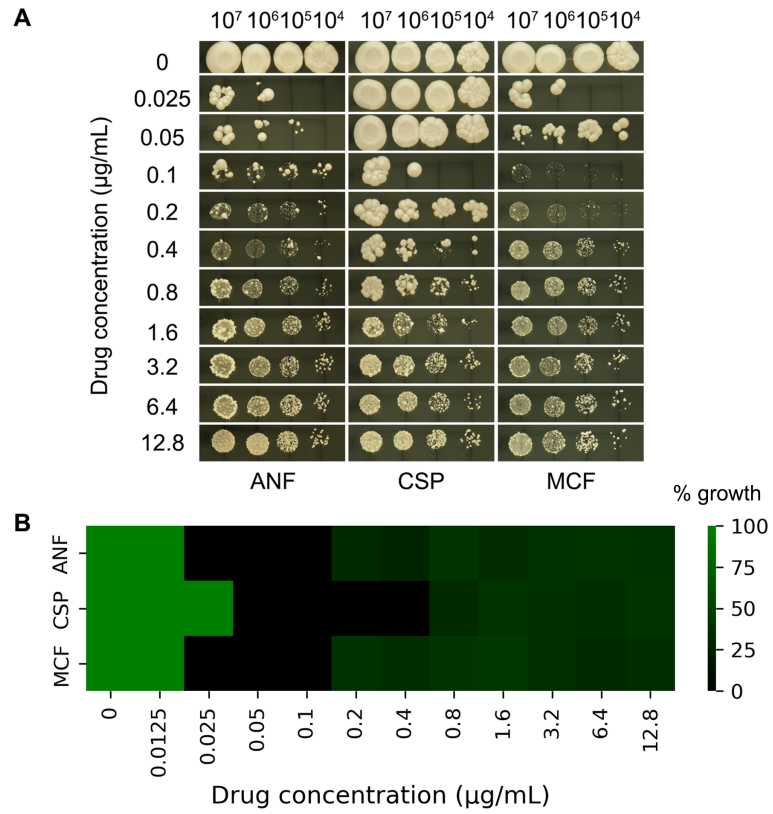

FIGURE 1
Paradoxical growth of **(C)** *albicans* in response to echinocandins. **(A)** Spot assay: Serial 10-fold dilutions (3 µL) of cultures were spotted onto YPD agar plates containing anidulafungin (ANF), caspofungin (CSP), or micafungin (MCF) at concentrations ranging from 0.025 to 12.8 µg/mL. Plates were incubated at 37°C for 48 hours. **(B)** Broth microdilution assay: Cells were grown in YPD broth in 96-well plates containing ANF, CSP, or MCF at concentrations ranging from 0.0125 to 12.8 µg/mL. Plates were incubated at 37°C for 48 hours, and growth was quantified by measuring OD_{600}. Values were normalized against the drug-free control well.

due to its prevalence among adapted clones. The adaptor strain was streaked from a –80°C glycerol stock onto a YPD agar plate and incubated at 37°C for 36 hours. A single colony was randomly selected, resuspended in distilled water, and serially diluted. Approximately 200 cells were plated onto a fresh YPD agar plate and incubated again at 37°C for 36 hours. After incubation, one small colony and five large colonies were randomly picked for further analysis.

Whole genome sequencing

DNA extraction, library construction and sequencing were performed as described previously (Guo et al., 2024). Briefly, cells were cultured on YPD plates at 30°C (~300 colonies/plate), with only small colonies selected. Colonies were resuspended in 1 mL distilled water, pelleted by centrifugation (1 min, microcentrifuge), and processed for genomic DNA extraction using phenol-chloroform. DNA libraries were prepared by BGI (Wuhan, China) as follows: 1 µg genomic DNA was sheared (Covaris LE220), followed by size selection (300–400 bp), end repair, and adapter ligation using Agencourt AMPure XP-Medium kits. After PCR amplification and purification, single-strand circular DNA libraries were prepared and quality-controlled. Sequencing was performed on the BGISEQ-500 platform using DNA nanoball technology, with 100 bp paired-end reads generated through combinatorial Probe-Anchor Synthesis (cPAS).

Data was visualized using Y_{MAP} (Abbey et al., 2014). Raw fastq files were uploaded to Y_{MAP} (version 1.0) (http://lovelace.cs.umn.edu/Ymap/). Read depth (normalized to that of the diploid parent) is shown on the y-axis on a log2 scale converted to absolute copy numbers (1-4). Copy number is indicated on the vertical axis such that trisomy is reflected in black bars above the lengthwise 2N midpoint of each chromosome. Homologs A and B for each chromosome based on the reference genotype are indicated by cyan and magenta, respectively. Heterozygous positions are marked in grey. Allelic ratios (A:B) are color-coded: grey, 1:1 (A/B); cyan, 1:0 (A or A/A); magenta, 0:1 (B or B/B); purple, 1:2 (A/B/B); blue, 2:1 (A/A/B); light blue, 3:1 (A/A/A/B)). Read depth was plotted as a function of chromosome position using the Assembly 22 version of the SC5314 reference genome (http://www.candidagenome.org/download/sequence/*C_albicans*_SC5314/Assembly22/current/*C_albicans*_SC5314_A22_current_chromosomes.fasta.gz).

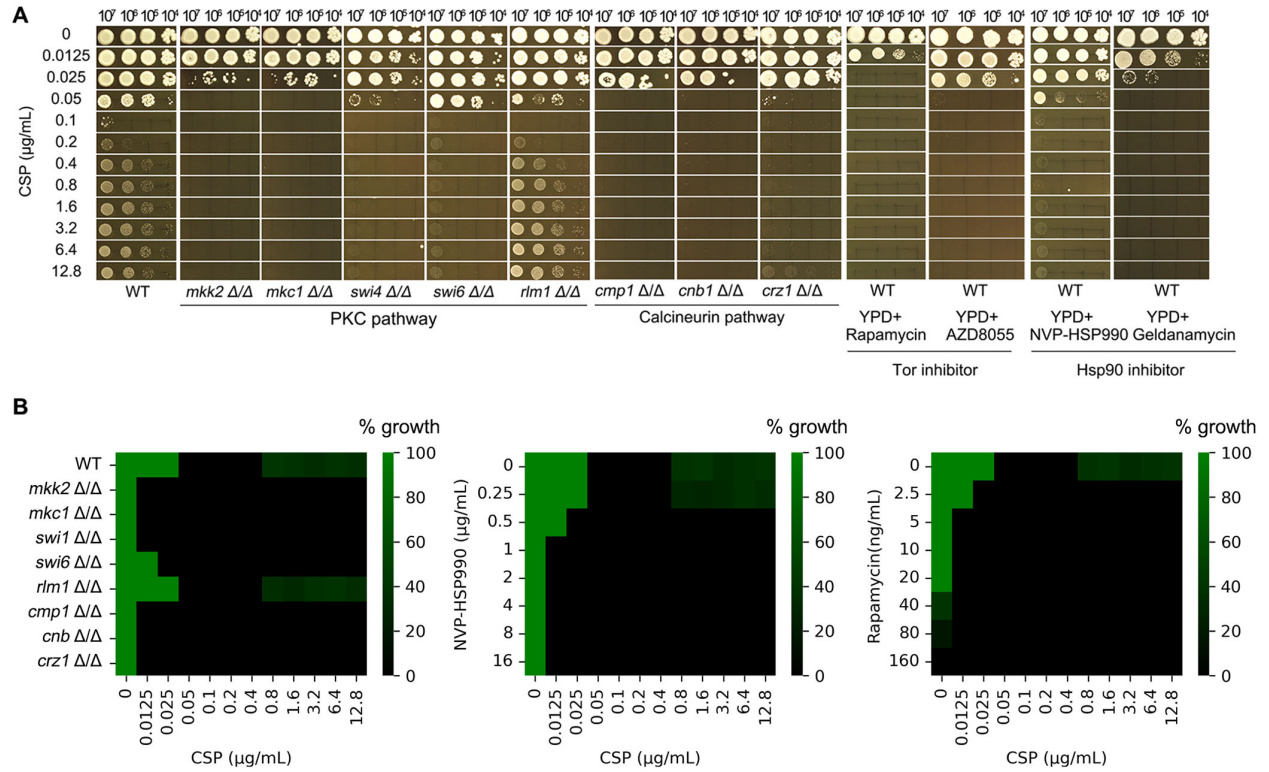

FIGURE 2
Genetic and pharmacological requirements for caspofungin paradoxical growth in (*C*) *albicans*. **(A)** The wild-type (WT) strain SC5314 was tested on YPD plates containing caspofungin (CSP; 0.0125-12.8 μg/mL) with or without inhibitors of key signaling pathways: TOR inhibitors rapamycin (10 ng/mL) and AZD8055 (4 μg/mL) or Hsp90 inhibitor NVP-HSP990 (1 μg/mL) and geldanamycin (0.5 μg/mL). Additionally, deletion strains of the PKC and calcineurin pathways were examined under the same conditions. All plates were incubated at 37°C for 48 hours before imaging. **(B)** Requirement of stress pathways for maintenance of PG evaluated with liquid assay. (Left) Broth microdilution assay of PKC pathway mutants (*mkk2Δ/Δ, mkc1Δ/Δ, swi4Δ/Δ, swi6Δ/Δ, rlm1Δ/Δ*), and alcineurin pathway mutants (*cmp1Δ/Δ, cnb1Δ/Δ, crz1Δ/Δ* CSP (0.0125-12.8 μg/mL). (Middle) WT (SC5314) exposed to CSP (0.0125-12.8 μg/mL) with HSP90 inhibitor NVP-HSP990 at concentrations indicated. (Right) WT (SC5314) exposed to CSP (0.0125-12.8 μg/mL) with Tor inhibitor rapamycin at concentrations indicated. Growth after 48 h at 37°C was quantified by OD_{600} and normalized to drug-free controls.

RNA-seq

Strains were streaked onto YPD plates from the -80˚C freezer. After 36h incubation at 37°C, several colonies of similar sizes were chosen. Colonies were suspended in distilled water and adjusted to $1x10^4$ cells/mL. 100 μL of cell suspension were spread on YPD plates. The plates were incubated at 37°C for 36 hours. Cells were collected by centrifugation, washed and flash frozen in liquid nitrogen. Total RNA extraction and purification, library construction, and sequencing were performed as described in (Yang et al., 2013). Briefly, total RNA was extracted and purified using the RNeasy Mini Kit (Qiagen, Hilden, Germany). RNA concentration was quantified using a Qubit 4.0 fluorometer (Thermo Fisher Scientific, Waltham, USA), and integrity was assessed with the Agilent 4200 system (Agilent Technologies, Waldbronn, Germany). Libraries were prepared using the ALFA-SEQ RNA Library Prep Kit (Findrop Biosafety Technology, Guangzhou, China), and sequencing was performed on an Illumina MiSeq i100 platform (Illumina,San Diego, USA).

Raw sequence files (.fastq files) underwent quality control analysis using the FastQC tool (http://www.bioinformatics.babraham.ac.uk/projects/fastqc). Reads were mapped to the *C. albicans* SC5314 reference genome (http://www.candidagenome.org/download/sequence/*C_albicans*_SC5314/Assembly22/current/). Differential gene expression profiling was carried out using DESeq2 (Love et al., 2014) with standard parameters. Genes with relative fold changes >1.5 and false discovery rate (FDR)-adjusted P-values <0.05 were considered differentially expressed.

Data availability

The sequencing data have been deposited in the ArrayExpress database at EMBL-EBI (www.ebi.ac.uk/arrayexpress) under accession number E-MTAB-12336 (DNA-Seq) and E-MTAB-12323 (RNA-Seq).

Results

Paradoxical growth of *C. albicans* in the presence of echinocandins

To assess PG in *C. albicans*, we performed serial dilution spot assays of reference strain SC5314 on YPD agar plates containing graded concentrations of three echinocandins: CSP, ANF, and

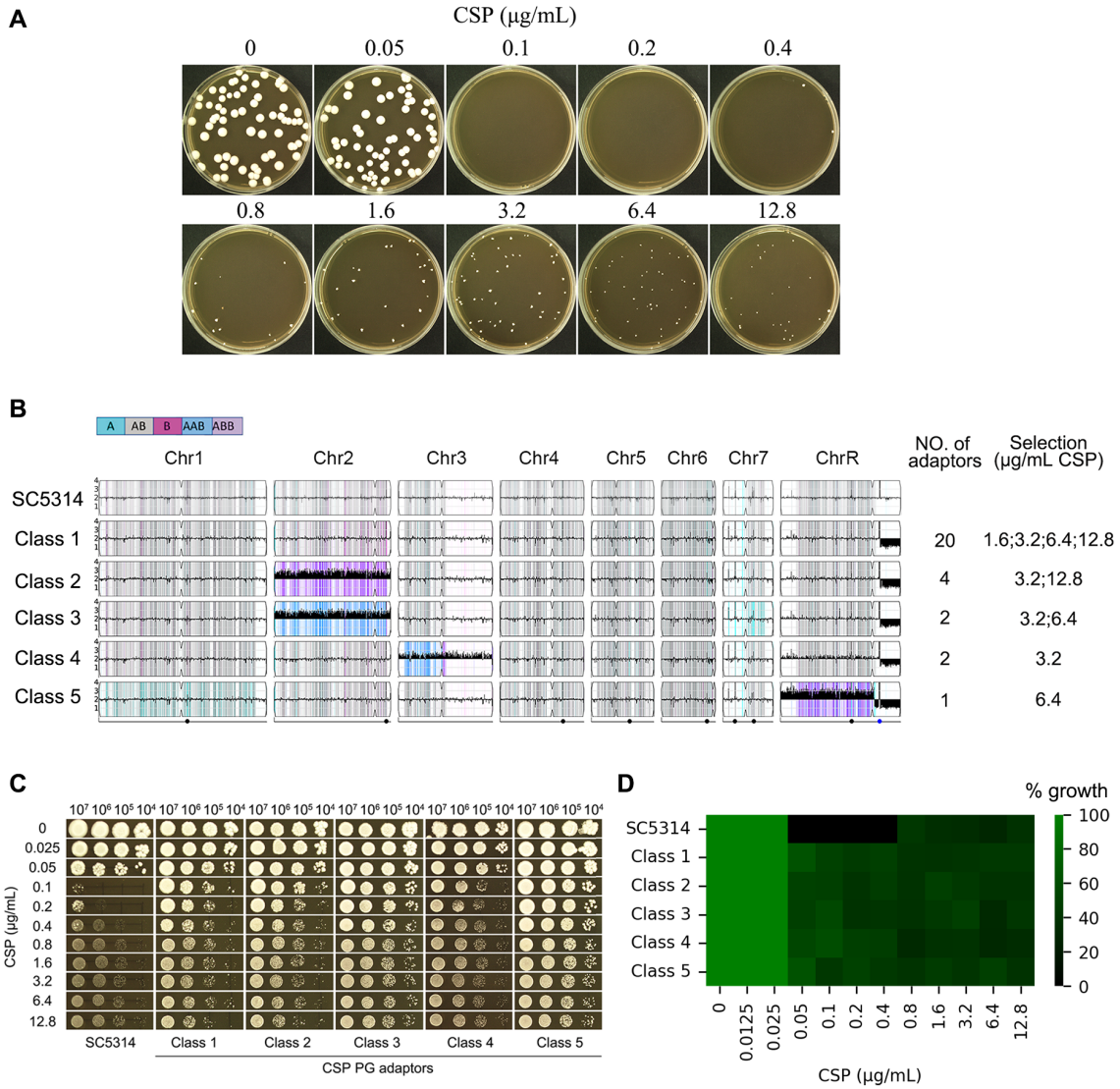

FIGURE 3
Paradoxical growth promotes caspofungin resistance through aneuploidy formation. **(A)** Isolation of adaptor strains: Approximately 50 SC5314 cells were plated on YPD agar containing caspofungin (CSP; 0.05-12.8 μg/mL) and incubated at 37°C for 5 days. All resulting colonies were collected for analysis. **(B)** Genomic characterization: 29 CSP-tolerant adaptor strains were sequenced. Karyotype analysis revealed these adaptor strains clustered into 5 distinct classes. The figure displays the distribution of adaptors across classes and their selection conditions. **(C, D)** Phenotypic validation: Representative adaptor strains from each class were assessed for CSP resistance using spot assays **(C)** and broth microdilution assay **(D)**.

MCF. Following 48-hour incubation at 37°C, SC5314 consistently exhibited PG with all three compounds. Complete growth inhibition occurred at 0.1-0.2 μg/mL CSP and 0.025-0.05 μg/mL ANF/MCF, while growth restoration was observed at 0.4-12.8 μg/mL CSP, 0.1 and 12.8 μg/mL ANF and MCF, respectively. Notably, a subset of colonies developed papillary morphologies (Figure 1A), suggesting potential selection of resistant subpopulations through mutational adaptation.

The broth microdilution assay revealed MIC values of 0.025 μg/mL for ANF, 0.05 μg/mL for CSP, and 0.025 μg/mL for MCF. No fungal growth was observed at 0.025–0.1 μg/mL (ANF), 0.05–0.4 μg/mL (CSP), or 0.025–0.1 μg/mL (MCF). However, PG occurred at higher concentrations, specifically within 0.2–12.8 μg/mL (ANF), 0.8–12.8 μg/mL (CSP), and 0.2–12.8 μg/mL (MCF) (Figure 1B).

Roles of PKC, calcineurin, TOR, and Hsp90 in CSP-induced paradoxical growth in *C. albicans*

We investigated the roles of the PKC, calcineurin, and TOR pathways, as well as Hsp90, in PG. The canonical PKC cell wall integrity pathway in yeast consists of a phosphorylation cascade involving *PKC1* (upstream kinase), *BCK1* (MAPKKK), *MKK2* (MAPKK), and *MKC1* (terminal MAPK), which activates transcription factors *RLM1* and the *SWI4*/*SWI6* (SBF) complex to regulate stress response genes, cell wall biosynthesis, and cell cycle progression (LaFayette et al., 2010). The calcineurin signaling pathway comprises the heterodimeric calcineurin phosphatase (encoded by *CMP1*/catalytic subunit and *CNB1*/regulatory

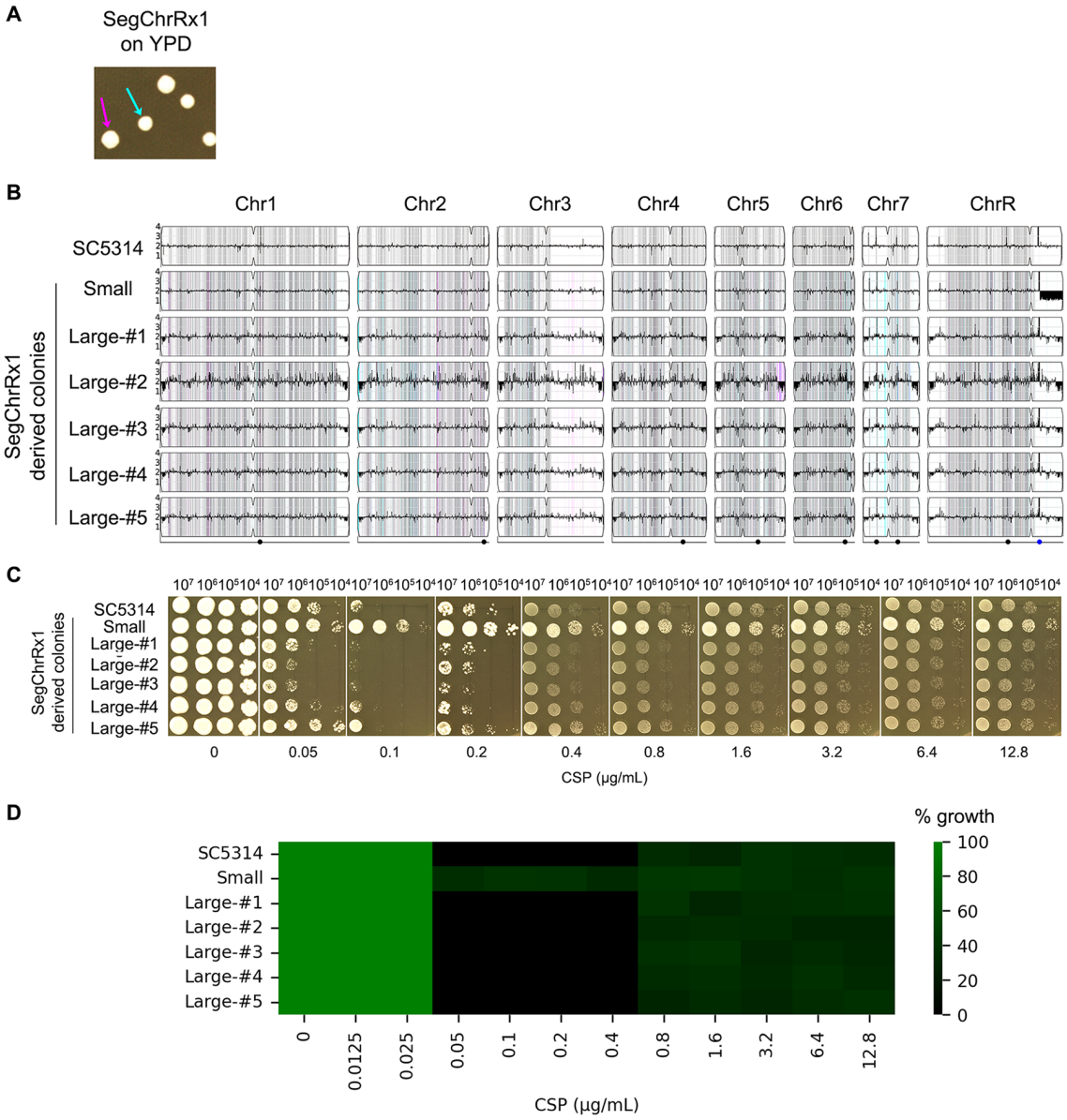

FIGURE 4
Phenotypic and genomic instability of aneuploid strains. **(A)** Colony morphology variation. A SegChrRx1 adaptor strain grown on YPD agar for 36 hours exhibited colony size polymorphism, with distinct small (cyan arrow) and large (magenta arrow) colonies. **(B)** Karyotype analysis. Whole-genome sequencing revealed that the progenitor SC5314 and all large colonies maintained euploid diploid genomes, while the small colony retained the SegChrRx1 aneuploidy. **(C, D)** Drug sensitivity profiling. Spot assays on YPD containing 0.05-12.8 μg/mL caspofungin **(C)** and broth microdilution assay using 0.0125-12.8 μg/mL CSP **(D)** showed complete inhibition of SC5314 and large colonies at lower supra-MIC CSP concentrations but PG at higher supra-MIC concentrations, while the small SegChrRx1 colony displayed ability to grow at both lower and higher supra-MIC CSP concentrations.

subunit) and its downstream transcription factor *CRZ1* (Park et al., 2019). The Hsp90 and TOR pathways can be selectively inhibited using well-characterized pharmacological agents: NVP-HSP990 and geldanamycin (Hsp90 inhibitors), and rapamycin and AZD8055 (TOR pathway inhibitors) (Raught et al., 2001; Menezes et al., 2012).

Here we found, supplementation with the Hsp90 inhibitors NVP-HSP990 (1 μg/mL) and geldanamycin (0.5 μg/mL), or the TOR inhibitor rapamycin (10 ng/mL) and AZD8055 (4 μg/mL), increased *C. albicans* SC5314 susceptibility to CSP (growth inhibition at 0.025 and 0.5 μg/mL CSP, respectively) and abolished PG (Figure 2A). Control experiments confirmed that the inhibitor concentrations used (1 μg/mL NVP-HSP990, 0.5 μg/mL geldanamycin,10 ng/mL rapamycin, 4 μg/mL AZD8055) did not affect growth when administered alone, with no inhibition observed even at 10× higher concentrations (data not shown). Similarly, deletions of PKC pathway genes (*MKK2*, *MKC1*, *SWI4*) increased CSP susceptibility and abolished PG, whereas *SWI6* deletion abolished PG without altering susceptibility. In contrast, *RLM1* deletion neither altered CSP susceptibility nor abolished PG.

Deletion of calcineurin components *CMP1* or *CNB1* completely abolished PG and increased susceptibility (growth inhibition at 0.05 μg/mL CSP). While *CRZ1* deletion similarly increased susceptibility, it only attenuated - rather than eliminated - PG, with residual growth observed at the highest CSP concentration (12.8 μg/mL). This suggests calcineurin regulates PG primarily through *CRZ1* but retains some *CRZ1*-independent capacity to mediate the response (Figure 2A).

In broth microdilution assay, the wild type strain SC5314 exhibited PG in the presence of CSP, while strains with deletions of PKC pathway genes (*MKK2*, *MKC1*, *SWI4*, *SWI6*) and calcineurin pathway genes (*CMP1*, *CNB1*, *CRZ1*) did not exhibit PG. But *rlm1 Δ/Δ* strain still had PG (Figure 2B left panel).

In checkerboard assay, SC5314 was grown in YPD broth supplemented with or without NVP-HSP990 (Hsp90 inhibitor) and rapamycin (Tor pathway inhibitor). NVP-HSP990 alone did not exhibit inhibitory effect against SC5314 at the concentrations of 0.25-16 μg/mL. Addition of 0.5-16 μg/mLNVP-HSP990 abolished PG, but addition of 0.25 μg/mL failed to abolish PG (Figure 2B middle panel). Rapamycin alone at 40–160 ng/mL had inhibitory effect against SC5314. Addition of subinhibitory concentrations of rapamycin (2.5–20 ng/mL) abolished PG (Figure 2B right panel).

Collectively, our findings demonstrate that Hsp90, TOR, PKC, and calcineurin are all essential for maintaining PG in *C. albicans*.

The discontinuous growth patterns in *MKK2* and *MKC1* deletion strains reflect stochastic emergence of drug-tolerant variants. While the papillary colony morphology strongly suggests mutational resistance, comprehensive genomic analysis would be required to definitively exclude other adaptation mechanisms.

Paradoxical growth is linked to aneuploidy formation

PG in *C. albicans* may result from stress response mechanisms, including compensatory increases in cell wall chitin content (Walker et al., 2013) and the formation of aneuploid subpopulations (Li et al., 2022). To investigate whether exposure to CSP induces genetic adaptations that contribute to PG, we plated approximately 50 cells of the reference strain SC5314 on YPD agar containing CSP concentrations ranging from 0.05 to 12.8 μg/mL (Figure 3A). No colonies appeared on plates containing 0.1–0.2 μg/mL CSP, which we define as "lower supra-MIC concentrations". A few colonies were observed on plates containing 0.4–12.8 μg/mL CSP, which we refer to as "higher supra-MIC concentrations". From these plates, we isolated all 163 colonies that emerged at CSP concentrations between 0.4-12.8 μg/mL. Subsequent spot assays using 0.1 μg/mL CSP identified 29 colonies (termed "adaptors") that demonstrated enhanced growth compared to the parental SC5314 strain (data not shown). Whole-genome sequencing analysis of these adaptors revealed they could be categorized into five distinct classes based on their karyotypic alterations. The majority of adaptors (Class 1, n=20) exhibited segmental monosomy of Chromosome R (SegChrRx1), with the deleted region spanning from the ribosomal DNA (rDNA) repeats on the right arm to the right telomere. These Class 1 adaptors were recovered across a broad range of CSP concentrations (1.6, 3.2, 6.4 and 12.8 μg/mL). Class 2 adaptors (n=4) displayed the same SegChrRx1 alteration plus trisomy of Chromosome 2 resulting from amplification of the B homolog (Chr2x3, ABB) and were isolated at 3.2 and 12.8 μg/mL CSP. Class 3 adaptors (n=2) showed SegChrRx1 with an alternative Chr2 trisomy pattern (AAB) and were selected at 3.2 and 6.4 μg/mL CSP. Class 4 adaptors (n=2) had SegChrRx1 combined with trisomy of Chromosome 3 (Chr3x3, AAB) and were recovered at 3.2 μg/mL CSP. The single Class 5 adaptor contained SegChrRx1 along with trisomy of the remaining portion of Chromosome R (SegChrRx3) and was isolated at 6.4 μg/mL CSP. Collectively, all adaptor strains shared SegChrRx1, either as a sole genomic alteration or in combination with additional aneuploidies involving trisomy of Chr2, Chr3, or the remaining segment of ChrR. (Figure 3B). Representative spot assays from each adaptor class demonstrated their ability to grow across the full range of CSP concentrations tested (0.1-12.8 μg/mL), in contrast to the parental SC5314 strain which exhibited characteristic PG - showing growth inhibition at 0.1 and 0.2 μg/mL CSP but resumed growth at higher concentrations (0.4-12.8 μg/mL) (Figure 3C). Broth microdilution assays showed that the parental strain SC5314 had clear wells at 0.1–0.4 μg/mL CSP, indicating an MIC of 0.1 μg/mL. In contrast, all five adaptor classes exhibited turbid growth across the entire range tested (0.1–12.8 μg/mL CSP), suggesting an MIC of ≥12.8 μg/mL (Figure 3D). These results demonstrate that the adaptors are resistant to caspofungin.

Clinical resistance to caspofungin in *C. albicans* is primarily mediated by point mutations in the conserved hotspot regions of *FKS* genes (Perlin, 2015). To determine whether similar mutations arose in our adaptor strains, we examined all three *FKS* genes (*GSC1*, *GSL1*, and *GSL2*) using the Integrative Genomics Viewer (IGV). After visually inspecting the sequencing reads across all 29 adaptor strains, we found no evidence of mutations in any of the FKS genes.

Unstable resistance to CSP is due to reversible copy number variation

Aneuploidy represents an unstable genetic state that often reverts spontaneously to euploidy in the absence of selective pressure (Yang et al., 2023). To evaluate this genomic instability, we analyzed a SegChrRx1 adaptor strain that exhibited bimodal colony morphology on YPD plates, with distinct small (1.99 ± 0.14 mm diameter) and large (2.59 ± 0.27 mm diameter) colony populations (Figure 4A). This size variation likely reflects differential adaptation states, where smaller colonies may maintain the aneuploid genotype while larger colonies represent potential revertants. Whole-genome sequencing of randomly selected colonies (one small and five large) revealed that the small colony maintained SegChrRx1 and retained the ability to grow at lower supra-MIC concentrations of CSP (0.1 and 0.2 μg/Ml), while all five large colonies had reverted to euploidy and lost the ability of growth in the presence of lower

supra-MIC CSP concentrations. Both small and large colonies could grow at higher supra-MIC CSP concentrations (Figures 4B–D). These findings demonstrate that CSP resistance is mediated by reversible copy number variation of the monosomic region on Chromosome R.

SegChrRx1 regulates multiple genes associated with CSP resistance

As described above, the parental strain SC5314 exhibits classic PG, showing inhibition at intermediate CSP concentrations (0.1-0.2 μg/ml) but resuming growth at higher concentrations. In contrast, the aneuploid adaptor strains grow across all tested CSP concentrations (Figure 3), including the 0.1-0.2 μg/mL range that inhibits the parent. Importantly, when these adaptors revert to euploidy, they regain the parental PG phenotype (Figure 4), demonstrating that their extended growth range is directly linked to their aneuploid state. To identify the molecular basis for this phenotypic difference, we performed comparative transcriptomic analysis between a representative SegChrRx1 adaptor strain and the parental SC5314. This approach allowed us to distinguish gene expression changes associated with the aneuploidy-mediated growth capacity from those involved in the parent strain's paradoxical growth response.

Our analysis revealed that SegChrRx1 mediates complex transcriptional reprogramming involving multiple CSP response pathways (Table 1). Notably, we observed upregulation of *GSC1* (encoding the CSP target protein β-1,3-glucan synthase) and chitin synthase genes (*CHS3*, *CHS4*), consistent with established cell wall remodeling responses to echinocandin exposure. Conversely, the chitinase gene *CHT3* was downregulated, suggesting a coordinated modulation of cell wall homeostasis. Key stress response pathways were also affected, with upregulation of calcineurin components (*CNB1*, *CRZ1*) and PKC signaling elements (*MKC1*, *SWI4*). Within the monosomic ChrR region, we identified five dosage-sensitive genes (*ALO1*, *MAL2*, *AHA1*, *SPT3*, *PRE8*) that were downregulated and, according to the Candida Genome Database (Lew-Smith et al., 2025), are associated with CSP resistance when deleted. This observation suggests that reduced gene dosage in this region may contribute to the adapted phenotype through haploinsufficiency effects.

Divergent mutation frequencies at supra-MIC versus paradoxical growth concentrations of caspofungin in *C. albicans*

As previously described, when fewer than one hundred cells of the SC5314 were spread on CSP plates, colonies formed exclusively on plates containing 0.4-12.8 μg/mL CSP, with no colonies observed at 0.1 or 0.2 μg/mL CSP. Among the 163 colonies that emerged across these plates, only 29 colonies (17.8%) selected by

TABLE 1 Differentially expressed genes in SegChrRx1 as compared to parent.

Systematic name	Gene	Chromosome	Ratio (allele A; allele B)
			SegChrRx1/ Parent
β-1,3-glucan synthase genes			
C1_02420C	*GSC1*	Chr1	**3.55; 3.54***
C1_05600W	*GSL1*	Chr1	1.03; 0.96
CR_00850C	*GSL2*	ChrR	0.83; 0.83
Chitin synthase genes			
C7_02770W	*CHS1*	Chr7	0.92; 0.82
CR_09020C	*CHS2*	ChrR	1.39; 1.39
C1_13110C	*CHS3*	Chr1	**2.00; 2.16***
C3_05700W	*CHS4*	Chr3	**1.27;1.25***
C2_04140W	*CHS5*	Chr2	0.96; 0.91
C7_03060C	*CHS6*	Chr7	1.02; 1.28
C1_06010W	*CHS7*	Chr1	1.32; 1.24
C3_00710W	*CHS8*	Chr3	1.20; 0.97
Chitinase genes			
CR_00180C	*CHT1*	ChrR	1.04; 1.04
C5_04130C	*CHT2*	Chr5	0.93; 0.86
CR_10110W	*CHT3*	ChrR	**0.58; 0.58***
C2_02010C	*CHT4*	Chr2	0.81; 1.36
Calcineurin genes			
C1_00730C	*CMP1*	Chr1	1.19; 1.52
C5_05160C	*CNB1*	Chr5	1.49*; 1.19
C3_05780C	*CRZ1*	Chr3	**1.33; 1.33***
PKC genes			
C3_04470W	*PKC1*	Chr3	1.09; 1.09
C7_02990W	*BCK1*	Chr7	1.19; 1.31
C2_05780C	*MKK2*	Chr2	1.18; 1.11
CR_00120C	*MKC1*	ChrR	**1.36; 1.36***
C1_01790W	*SWI4*	Chr1	**1.45; 1.50***
C1_08670W	*SWI6*	Chr1	0.97; 1.20
C4_01260W	*RLM1*	Chr4	1.39; 1.09
ChrR genes in the segmental monosomy region			
CR_09790W	*ALO1*	ChrR	**0.56; 0.56***
CR_10790W	*MAL2*	ChrR	**0.19; 0.19***
CR_10270C	*AHA1*	ChrR	**0.21; 0.21***

(Continued)

TABLE 1 Continued

Systematic name	Gene	Chromosome	Ratio (allele A; allele B)
			SegChrRx1/ Parent
ChrR genes in the segmental monosomy region			
CR_10450C	*SPT3*	ChrR	**0.42; 0.42***
CR_09380W	*PRE8*	ChrR	**0.53; 0.53***

*q<0.05. Bold values are siginificantly differential genes.

1.6-12.8 µg/mL CSP exhibited CSP resistance. In contrast, when one million SC5314 cells were plated, the 0.1 and 0.2 µg/mL CSP plates each produced several hundred colonies, while plates containing 0.4-12.8 µg/mL CSP showed lawn growth (Figure 5A). From the colonies appearing on 0.1 and 0.2 µg/mL CSP plates, we randomly selected and tested 16 colonies (8 from each concentration). We found that 6 out of 8 colonies (75%) from the 0.1 µg/mL plates and 7 out of 8 colonies (87.5%) from the 0.2 µg/mL plates demonstrated CSP resistance, confirmed by their ability to grow in the presence of 0.1 and 0.2 µg/mL CSP respectively. Importantly, all 16 tested colonies maintained PG phenotypes (Figure 5B). These results demonstrate that the frequency of induced CSP-tolerant mutations is substantially higher at 0.1-0.2 µg/mL compared to concentrations of 0.4 µg/mL and above.

PG-deficient isolate adapts only to lower supra-MIC concentrations of CSP

A PG-deficient clinical isolate, G309, was tested for adaptation to CSP using two approaches.

In Approach #1, fewer than one hundred G309 cells were spread on CSP plates (0.05–12.8 µg/mL). Colonies appeared only on the control (no drug) and 0.05 µg/mL CSP plates (Figure 6A, top panel). Eight randomly selected colonies from the drug plates were tested using a spot assay, but none exhibited growth on 0.05–12.8 µg/mL CSP plates (Figure 6A, bottom panel).

In Approach #2, one million G309 cells were spread on CSP plates. Lawn growth occurred on both the control and 0.5 µg/mL CSP plates. A few colonies appeared on the 0.1 µg/mL CSP plate, but no colonies appeared on the 0.2–12.8 µg/mL CSP plates (Figure 6B, top panel). Eight randomly selected colonies from the 0.1 µg/mL CSP plate were tested with a spot assay. All colonies grew

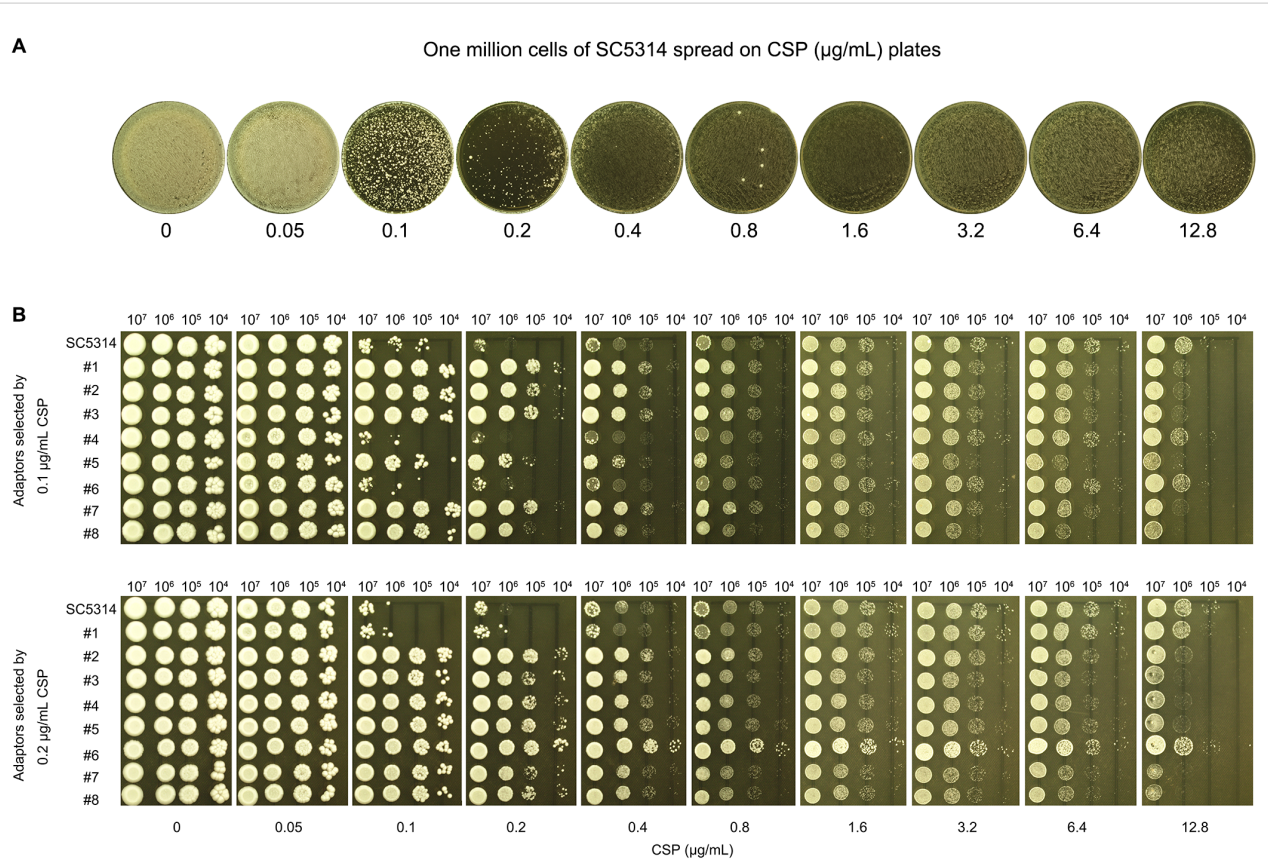

FIGURE 5
High-frequency selection of CSP-tolerant mutants at supra-MIC concentrations **(A)** Colony formation assay: One million cells of strain SC5314 spread on YPD agar plates containing CSP concentrations (0.05-12.8 µg/mL). The plates were incubated at 37°C for 72h. **(B)** Spot assays: Eight colonies each from 0.1 µg/mL and 0.2 µg/mL CSP plates **(A)** were spotted in serial dilution onto YPD agar with CSP (0.05-12.8 µg/mL). The plates were incubated at 37°C for 72h.

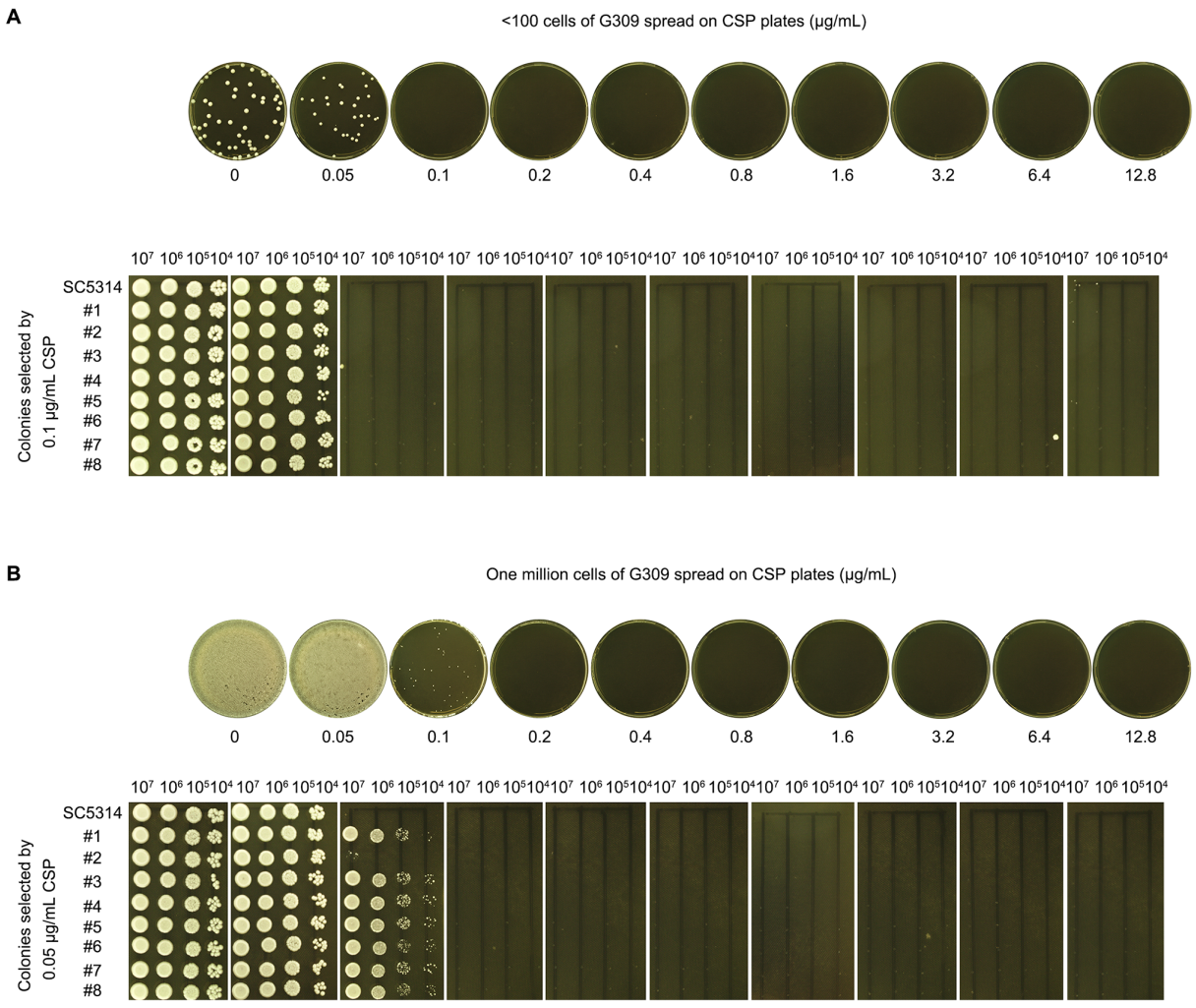

FIGURE 6
Adaptation of PG-deficient isolate to CSP **(A)** Low-density plating: <100 G309 cells spread on YPD agar plates containing CSP (concentrations are shown in the figure). Colonies from 0.05 μg/mL plate isolated for spot assay. **(B)** High-density plating: 10^6 G309 cells spread on CSP plates. Colonies from 0.1 μg/mL plate isolated for spot assay. For both panels, all plates incubated at 37°C for 72 h before imaging.

on the 0.1 μg/mL CSP plate but failed to grow on 0.2–12.8 μg/mL CSP plates (Figure 6B, bottom panel).

Discussion

Our study demonstrates that CSP paradoxical growth in *C. albicans* depends on stress pathway activation and facilitates transient echinocandin resistance through adaptive aneuploidy. While PG has long been recognized as a stress-responsive phenomenon, our work provides the first direct evidence that segmental aneuploidy—specifically, SegChrRx1—plays a pivotal role in mediating reversible resistance to CSP. This finding represents a significant advance in understanding the genetic and cellular processes that underpin fungal drug resistance.

Our findings demonstrate that Hsp90, TOR, PKC, and calcineurin pathways all play essential but mechanistically distinct roles in CSP PG in *C. albicans*. Pharmacological inhibition of Hsp90 (NVP-HSP990) or TOR (rapamycin) abolished PG while increasing basal CSP susceptibility, suggesting these chaperone and nutrient-sensing pathways maintain both general stress resistance and PG-specific responses. Genetic dissection revealed hierarchical organization within the PKC pathway, where upstream MAPK components (*MKK2*/MKC1) and *SWI4* governed both susceptibility and PG, while *SWI6* deletion only affected PG - indicating functional divergence within the SBF transcription complex. In contrast, calcineurin pathway deletions showed identical phenotypes with complete PG loss and intermediate susceptibility shifts, suggesting this calcium-dependent pathway operates as a unified module. These differential genetic requirements highlight how PG integrates inputs from multiple stress-responsive systems: Hsp90 likely stabilizes key signaling components, TOR modulates adaptive responses, PKC coordinates cell wall remodeling through both MAPK and SBF-

dependent outputs, while calcineurin provides a central regulatory hub, together enabling *C. albicans* to overcome CSP stress at supra-inhibitory concentrations.

Strikingly, our genomic analyses reveal that segmental aneuploidy, particularly SegChrRx1, is a recurrent and dominant feature among CSP-resistant isolates. This structural alteration confers broad-spectrum growth across inhibitory CSP concentrations and defines a previously unrecognized route to PG. The identification of five distinct karyotypic classes, all sharing SegChrRx1, suggests that this chromosomal change serves as a core adaptive strategy that may facilitate subsequent acquisition of additional aneuploidies to enhance fitness. Notably, SegChrRx1 is not a fixed genetic trait but a reversible, dynamic adaptation—supporting the concept of aneuploidy as a transient survival mechanism under antifungal pressure (Yang et al., 2023).

Transcriptomic profiling revealed extensive transcriptional rewiring in SegChrRx1-bearing strains, encompassing both direct and indirect effects. On one hand, increased expression of drug target genes (e.g., *GSC1*), chitin biosynthesis enzymes, and components of the calcineurin and PKC pathways collectively support enhanced stress resistance. On the other hand, downregulation of five dosage-sensitive genes within the deleted ChrR region—*ALO1*, *MAL2*, *AHA1*, *SPT3*, and *PRE8*—likely contributes to resistance through haploinsufficiency. These genes are annotated as CSP resistance modulators in *C. albicans* (Lew-Smith et al., 2025), and their decreased dosage appears to recapitulate drug-adapted phenotypes. These findings underscore the nuanced regulatory potential of segmental aneuploidy, which enables coordinated tuning of stress networks and core cellular processes.

The reversibility of CSP resistance following the loss of SegChrRx1 further implicates aneuploidy as a key driver of non-heritable, yet stable, drug adaptation. This phenomenon blurs the line between resistance and tolerance, emphasizing the need to consider chromosomal instability in antifungal susceptibility testing and resistance monitoring. While resistance mutations in *FKS* genes are well-established (Perlin, 2015), our results highlight an alternative and potentially more plastic mechanism of survival—one that evades current diagnostic paradigms focused solely on point mutations.

Clinically, the implications are significant. Aneuploidy-mediated PG may underlie persistent or relapsing infections despite echinocandin therapy, particularly in immune-compromised hosts where fungal stress responses are hyper-activated. Targeting the stress response hubs (e.g., Hsp90 or calcineurin) or pathways that stabilize aneuploidy may represent novel therapeutic strategies. Importantly, combination regimens involving echinocandins and Hsp90 or TOR inhibitors may suppress PG and improve treatment outcomes, as suggested by our inhibitor assays and recent synergistic drug studies (Cowen et al., 2009; Lefranc et al., 2024).

Conclusions

In conclusion, our work establishes that caspofungin paradoxical growth in *C. albicans* hinges on stress pathway activation for immediate survival, while transient segmental aneuploidy—particularly ChrR monosomy—mediates unstable echinocandin resistance. These findings redefine paradoxical growth as a gateway to adaptive, yet reversible, resistance mechanisms. Future studies should investigate the clinical prevalence of stress-induced aneuploidy and its role in echinocandin treatment failure, offering insights for antifungal strategies targeting genomic instability or stress response pathways.

Data availability statement

The datasets presented in this study can be found in online repositories. The names of the repository/repositories and accession number(s) can be found in the article/Supplementary Material.

Author contributions

YW: Writing – review & editing, Formal Analysis, Investigation, Validation, Methodology. JW: Validation, Methodology, Writing – review & editing, Investigation. NT: Formal Analysis, Visualization, Writing – review & editing. ZL: Formal Analysis, Writing – review & editing, Visualization. WL: Writing – review & editing, Visualization, Data curation. YX: Writing – review & editing, Funding acquisition, Formal Analysis, Visualization. LG: Supervision, Conceptualization, Project administration, Writing – review & editing, Funding acquisition, Writing – original draft, Visualization, Resources.

Funding

The author(s) declare financial support was received for the research and/or publication of this article. The authors declare financial support was received for the research, authorship, and/or publication of this article. This study was supported by the Suzhou City Applied Basic Research Science and Technology Innovation Project (SYWD2024002), Scientific Research Pre-research Fund Project of the Second Affiliated Hospital of Soochow University (SDFEYBS2424), Science and Technology Development Plan of Suzhou (SLJ2022018), and Scientific Research Project of Suzhou Commission of Health (GSWS2020028) to LG, the National Natural Science Foundation of China (81402978), Natural Science Foundation of Shandong Province (ZR2023MH227), Medical and Health Science and Technology Project of Shandong Province (202402041035) to YX.

Acknowledgments

We sincerely thank Dr. Feng Yang for generously providing the deletion strains and for his valuable assistance in analyzing the NGS data using Y_{MAP}.

Conflict of interest

The authors declare that the research was conducted in the absence of any commercial or financial relationships that could be construed as a potential conflict of interest.

Generative AI statement

The author(s) declare that no Generative AI was used in the creation of this manuscript.

Any alternative text (alt text) provided alongside figures in this article has been generated by Frontiers with the support of artificial intelligence and reasonable efforts have been made to ensure accuracy, including review by the authors wherever possible. If you identify any issues, please contact us.

Publisher's note

Supplementary material

The Supplementary Material for this article can be found online at: https://www.frontiersin.org/articles/10.3389/fcimb.2025.1618815/full#supplementary-material

References

Abbey, D. A., Funt, J., Lurie-Weinberger, M. N., Thompson, D. A., Regev, A., Myers, C. L., et al. (2014). YMAP: a pipeline for visualization of copy number variation and loss of heterozygosity in eukaryotic pathogens. *Genome Med.* 6, 100. doi: 10.1186/s13073-014-0100-8

Caplan, T., Polvi, E. J., Xie, J. L., Buckhalter, S., Leach, M. D., Robbins, N., et al. (2018). Functional genomic screening reveals core modulators of echinocandin stress responses in candida albicans. *Cell Rep.* 23, 2292–2298. doi: 10.1016/j.celrep.2018.04.084

Chamilos, G., Lewis, R. E., Albert, N., and Kontoyiannis, D. P. (2007). Paradoxical effect of Echinocandins across Candida species *in vitro*: evidence for echinocandin-specific and candida species-related differences. *Antimicrob. Agents Chemother.* 51, 2257–2259. doi: 10.1128/AAC.00095-07

CLSI (2017). "Reference method for broth dilution antifungal susceptibility testing of yeasts," in *CLSI standard M27, 4th ed* (Clinical and Laboratory Standards Institute, Wayne, PA).

Cowen, L. E., Singh, S. D., Kohler, J. R., Collins, C., Zaas, A. K., Schell, W. A., et al. (2009). Harnessing Hsp90 function as a powerful, broadly effective therapeutic strategy for fungal infectious disease. *Proc. Natl. Acad. Sci. U.S.A.* 106, 2818–2823. doi: 10.1073/pnas.0813394106

Fortwendel, J. R., Juvvadi, P. R., Pinchai, N., Perfect, B. Z., Alspaugh, J. A., Perfect, J. R., et al. (2009). Differential effects of inhibiting chitin and 1,3-beta-D-glucan synthesis in ras and calcineurin mutants of Aspergillus fumigatus. *Antimicrob. Agents Chemother.* 53, 476–482. doi: 10.1128/AAC.01154-08

Guo, L., Zheng, L., Dong, Y., Wang, C., Deng, H., Wang, Z., et al. (2024). Miconazole induces aneuploidy-mediated tolerance in Candida albicans that is dependent on Hsp90 and calcineurin. *Front. Cell. Infection Microbiol.* 14. doi: 10.3389/fcimb.2024.1392564

Kanafani, Z. A., and Perfect, J. R. (2008). Antimicrobial resistance: resistance to antifungal agents: mechanisms and clinical impact. *Clin. Infect. Dis.* 46, 120–128. doi: 10.1086/524071

LaFayette, S. L., Collins, C., Zaas, A. K., Schell, W. A., Betancourt-Quiroz, M., Gunatilaka, A. A., et al. (2010). PKC signaling regulates drug resistance of the fungal pathogen Candida albicans via circuitry comprised of Mkc1, calcineurin, and Hsp90. *PloS Pathog.* 6, e1001069. doi: 10.1371/journal.ppat.1001069

Lamoth, F., Juvvadi, P. R., Gehrke, C., Asfaw, Y. G., and Steinbach, W. J. (2014). Transcriptional activation of heat shock protein 90 mediated via a proximal promoter region as trigger of caspofungin resistance in Aspergillus fumigatus. *J. Infect. Dis.* 209, 473–481. doi: 10.1093/infdis/jit530

Lefranc, M., Accoceberry, I., Fitton-Ouhabi, V., Biteau, N., and Noel, T. (2024). Rapamycin and caspofungin show synergistic antifungal effects in caspofungin-susceptible and caspofungin-resistant Candida strains in *vitro*. *J. Antimicrob. Chemother.* 79, 151–156. doi: 10.1093/jac/dkad359

Lesage, G., Sdicu, A. M., Menard, P., Shapiro, J., Hussein, S., and Bussey, H. (2004). Analysis of beta-1,3-glucan assembly in Saccharomyces cerevisiae using a synthetic interaction network and altered sensitivity to caspofungin. *Genetics* 167, 35–49. doi: 10.1534/genetics.167.1.35

Lew-Smith, J., Binkley, J., and Sherlock, G. (2025). The Candida Genome Database: annotation and visualization updates. *Genetics* 229. doi: 10.1093/genetics/iyaf001

Li, H., Cao, Y. B., Yan, T. H., Jiang, Y. Y., and Yang, F. (2022). Aneuploidy underlies paradoxical growth of rezafungin and enables cross-tolerance to echinocandins in Candida albicans. *J. Infect.* 85, 702–769. doi: 10.1016/j.jinf.2022.09.028

Love, M. I., Huber, W., and Anders, S. (2014). Moderated estimation of fold change and dispersion for RNA-seq data with DESeq2. *Genome Biol.* 15, 550. doi: 10.1186/s13059-014-0550-8

Menezes, D. L., Taverna, P., Jensen, M. R., Abrams, T., Stuart, D., Yu, G. K., et al. (2012). The novel oral Hsp90 inhibitor NVP-HSP990 exhibits potent and broad-spectrum antitumor activities *in vitro* and in *vivo*. *Mol. Cancer Ther.* 11, 730–739. doi: 10.1158/1535-7163.MCT-11-0667

Pappas, P. G., Kauffman, C. A., Andes, D. R., Clancy, C. J., Marr, K. A., Ostrosky-Zeichner, L., et al. (2016). Clinical practice guideline for the management of candidiasis: 2016 update by the infectious diseases society of america. *Clin. Infect. Dis.* 62, e1–50. doi: 10.1093/cid/civ933

Park, H. S., Lee, S. C., Cardenas, M. E., and Heitman, J. (2019). Calcium-calmodulin-calcineurin signaling: A globally conserved virulence cascade in eukaryotic microbial pathogens. *Cell Host Microbe* 26, 453–462. doi: 10.1016/j.chom.2019.08.004

Perlin, D. S. (2015). Echinocandin resistance in candida. *Clin. Infect. Dis.* 61 Suppl 6, S612–S617. doi: 10.1093/cid/civ791

Pfaller, M. A., and Diekema, D. J. (2007). Epidemiology of invasive candidiasis: a persistent public health problem. *Clin. Microbiol. Rev.* 20, 133–163. doi: 10.1128/CMR.00029-06

Raught, B., Gingras, A. C., and Sonenberg, N. (2001). The target of rapamycin (TOR) proteins. *Proc. Natl. Acad. Sci. U.S.A.* 98, 7037–7044. doi: 10.1073/pnas.121145898

Reinoso-Martin, C., Schuller, C., Schuetzer-Muehlbauer, M., and Kuchler, K. (2003). The yeast protein kinase C cell integrity pathway mediates tolerance to the antifungal drug caspofungin through activation of Slt2p mitogen-activated protein kinase signaling. *Eukaryot Cell* 2, 1200–1210. doi: 10.1128/EC.2.6.1200-1210.2003

Rivera, A., and Heitman, J. (2023). Natural product ligands of FKBP12: Immunosuppressive antifungal agents FK506, rapamycin, and beyond. *PloS Pathog.* 19, e1011056. doi: 10.1371/journal.ppat.1011056

Selmecki, A., Forche, A., and Berman, J. (2006). Aneuploidy and isochromosome formation in drug-resistant Candida albicans. *Science* 313, 367–370. doi: 10.1126/science.1128242

Singh, S. D., Robbins, N., Zaas, A. K., Schell, W. A., Perfect, J. R., and Cowen, L. E. (2009). Hsp90 governs echinocandin resistance in the pathogenic yeast Candida albicans via calcineurin. *PloS Pathog.* 5, e1000532. doi: 10.1371/journal.ppat.1000532

Sun, L. L., Li, H., Yan, T. H., Fang, T., Wu, H., Cao, Y. B., et al. (2023). Aneuploidy mediates rapid adaptation to a subinhibitory amount of fluconazole in candida albicans. *Microbiol. Spectr.*, e0301622. doi: 10.1128/spectrum.03016-22

Toth, Z., Forgacs, L., Kardos, T., Kovacs, R., Locke, J. B., Kardos, G., et al. (2020). Relative frequency of paradoxical growth and trailing effect with caspofungin, micafungin, anidulafungin, and the novel echinocandin rezafungin against candida species. *J. Fungi (Basel)* 6. doi: 10.3390/jof6030136

Valero, C., Colabardini, A. C., Chiaratto, J., Pardeshi, L., de Castro, P. A., Ferreira Filho, J. A., et al. (2020). Aspergillus fumigatus transcription factors involved in the caspofungin paradoxical effect. *mBio* 11. doi: 10.1128/mBio.00816-20

Wagener, J., and Loiko, V. (2017). Recent insights into the paradoxical effect of echinocandins. *J. Fungi (Basel)* 4. doi: 10.3390/jof4010005

Walker, L. A., Gow, N. A., and Munro, C. A. (2013). Elevated chitin content reduces the susceptibility of Candida species to caspofungin. *Antimicrob. Agents Chemother.* 57, 146–154. doi: 10.1128/AAC.01486-12

Yang, F., Kravets, A., Bethlendy, G., Welle, S., and Rustchenko, E. (2013). Chromosome 5 monosomy of Candida albicans controls susceptibility to various toxic agents, including major antifungals. *Antimicrob. Agents Chemother.* 57, 5026–5036. doi: 10.1128/AAC.00516-13

Yang, F., Scopel, E. F. C., Li, H., Sun, L. L., Kawar, N., Cao, Y. B., et al. (2023). Antifungal Tolerance and Resistance Emerge at Distinct Drug Concentrations and Rely upon Different Aneuploid Chromosomes. *mBio*, e0022723. doi: 10.1128/mbio.00227-23

Yang, F., Teoh, F., Tan, A. S. M., Cao, Y., Pavelka, N., and Berman, J. (2019). Aneuploidy enables cross-adaptation to unrelated drugs. *Mol. Biol. Evol.* 36, 1768–1782. doi: 10.1093/molbev/msz104

Yang, F., Zhang, L., Wakabayashi, H., Myers, J., Jiang, Y., Cao, Y., et al. (2017). Tolerance to Caspofungin in Candida albicans Is Associated with at Least Three Distinctive Mechanisms That Govern Expression of FKS Genes and Cell Wall Remodeling. *Antimicrob. Agents Chemother.* 61. doi: 10.1128/AAC.00071-17

Zheng, L., Xu, Y., Dong, Y., Ma, X., Wang, C., Yang, F., et al. (2023). Chromosome 1 trisomy confers resistance to aureobasidin A in Candida albicans. *Front. Microbiol.* 14. doi: 10.3389/fmicb.2023.1128160

Zheng, L., Xu, Y., Wang, C., and Guo, L. (2024). Ketoconazole induces reversible antifungal drug tolerance mediated by trisomy of chromosome R in Candida albicans. *Front. Microbiol.* 15. doi: 10.3389/fmicb.2024.1450557

frontiers | Frontiers in Cellular and Infection Microbiology

TYPE Original Research
PUBLISHED 03 October 2025
DOI 10.3389/fcimb.2025.1628036

OPEN ACCESS

EDITED BY
Daniela Visaggio,
Roma Tre University, Italy

REVIEWED BY
Marta Laranjo,
University of Evora, Portugal
Valentine Usongo,
Health Canada, Canada

*CORRESPONDENCE
Ihab Habib
i.habib@uaeu.ac.ae
Mushtaq Khan
mushtaq.khan@uaeu.ac.ae
Abiola Senok
Abiola.senok@dubaihealth.ae

RECEIVED 16 May 2025
ACCEPTED 22 September 2025
PUBLISHED 03 October 2025

CITATION
Habib I, Mohamed M-YI, Lakshmi GB, Anes F, Goering R, Khan M and Senok A (2025) Prevalence, antimicrobial resistance, and distribution of toxin genes in methicillin-resistant *Staphylococcus aureus* from retail meat and fruit and vegetable cuts in the United Arab Emirates. *Front. Cell. Infect. Microbiol.* 15:1628036. doi: 10.3389/fcimb.2025.1628036

Prevalence, antimicrobial resistance, and distribution of toxin genes in methicillin-resistant *Staphylococcus aureus* from retail meat and fruit and vegetable cuts in the United Arab Emirates

Ihab Habib[1,2], Mohamed-Yousif Ibrahim Mohamed[1,2], Glindya Bhagya Lakshmi[1,2], Febin Anes[3], Richard Goering[4], Mushtaq Khan[3,5]* and Abiola Senok[6,7]*

[1]Department of Veterinary Medicine, College of Agriculture and Veterinary Medicine, United Arab Emirates University, Al Ain, United Arab Emirates, [2]ASPIRE Research Institute for Food Security in the Drylands (ARIFSID), United Arab Emirates University, Al Ain, United Arab Emirates, [3]Department of Medical Microbiology and Immunology, College of Medicine and Health Sciences, United Arab Emirates University, Al Ain, United Arab Emirates, [4]Department of Medical Microbiology and Immunology, Creighton University School of Medicine, Omaha, Nebraska, NE, United States, [5]Zayed Centre for Health Sciences, United Arab of Emirates University, Al Ain, United Arab Emirates, [6]College of Medicine, Mohammed Bin Rashid University of Medicine and Health Sciences, Dubai, United Arab Emirates, [7]School of Dentistry, Cardiff University, Cardiff, United Kingdom

Introduction: Methicillin-resistant *Staphylococcus aureus* (MRSA) is an emerging foodborne hazard with significant public health implications under the One Health framework. Data on MRSA in retail foods from the United Arab Emirates (UAE) remain scarce, despite the country's heavy reliance on diverse food supply chains. This study aimed to investigate the prevalence, antimicrobial resistance (AMR) profiles, and toxin gene distribution of MRSA in retail foods of animal and plant origin in Dubai, UAE.

Methods: A total of 260 food samples—including beef, sheep, camel, and chicken meat, as well as ready-to-eat fruit and vegetable cuts—were collected from major supermarkets. MRSA screening was performed using enrichment culture, followed by dual confirmation with MALDI-TOF MS for species identification and triplex PCR targeting the mecA gene. Antimicrobial susceptibility was assessed in 87 confirmed isolates against multiple antibiotic classes. Logistic regression analysis was applied to assess associations between product forms and MRSA contamination. Detection of enterotoxin and exfoliative toxin genes was performed using PCR assays.

Results: MRSA was detected in 47.7% of samples, with the highest prevalence in chicken meat (75%), followed by camel (55%) and beef (45.7%). Contamination was lower in fruit (16.7%) and vegetable cuts (30%). Minced beef exhibited significantly higher contamination (78.5%) compared to other beef forms. All 87 isolates were resistant to β-lactam antibiotics. Resistance varied across food

groups for gentamicin, ciprofloxacin, erythromycin, and tetracycline. Multidrug resistance (≥3 classes) was found in 79.3% of isolates, with extensive resistance (≥4 classes) more frequent in camel (75%) and beef (65.4%) isolates. Enterotoxin genes were identified in 42.5% of isolates, predominantly sea (29.1%). Exfoliative toxin gene type A was detected most often in vegetable cuts. Dual toxin gene carriage was rare (4.6%).

Discussion/Conclusion: Retail foods in the UAE, particularly chicken and camel meat, represent an important reservoir of multidrug-resistant and toxigenic MRSA. The findings highlight the One Health risks of MRSA in the food chain and underscore the need for coordinated surveillance and intervention strategies across human, animal, and environmental health sectors to mitigate transmission risks and safeguard public health.

KEYWORDS

methicillin-resistant *staphylococcus aureus*, retail food, antimicrobial resistance, OneHealth, United Arab Emirates

1 Introduction

Staphylococcus aureus, a Gram-positive microorganism, naturally colonizes the skin and mucosal surfaces of approximately one-third of the healthy human population and is similarly found in various domestic and wild animals, including birds (Kadariya et al., 2014). Beyond its commensal existence, *S. aureus* is a known contaminant of various food items and is capable of causing staphylococcal food poisoning (SFP) through consuming food containing pre-synthesized enterotoxins (Léguillier et al., 2024). Staphylococcal enterotoxins (SEs) are typically grouped into two major categories: classical SEs and more recently identified non-classical forms (Shalaby et al., 2024). Among these, *sea* to *see*—classified as classical SEs—are the most commonly reported. Strains of *S. aureus* harboring genes that encode these enterotoxins and can express them under conducive conditions in food are thus considered potential foodborne pathogens (Léguillier et al., 2024; Shalaby et al., 2024).

Methicillin-resistant *S. aureus* first emerged in the 1960s and has since spread to be of global concern (Kadariya et al., 2014). Historically, MRSA was associated with nosocomial infections (HA-MRSA) in patients with co-morbidities. In the 1990s, community-associated MRSA (CA-MRSA) emerged and were associated with community acquired infections in previously healthy individuals (Enright et al., 2002; Roy et al., 2024). These CA-MRSA lineages have now evolved to be the main drivers of nosocomial infections in many regions globally. In the United Arab Emirates (UAE), national antimicrobial resistance surveillance data spanning over a decade reveals an alarming upward trend of MRSA infections from 21.9% in 2010 to 33.5% in 2021 (Thomsen et al., 2023). Notably, CA-MRSA lineages dominate clinical settings across the UAE, and their considerable genetic diversity suggests a dynamic epidemiological landscape likely driven by the country's status as a global hub with a highly diverse population (Moradigaravand et al., 2023).

The emergence of MRSA in the food chain has garnered global attention, particularly its detection in raw and processed meat products (González-Machado et al., 2024; Khalifa et al., 2025). A systematic review revealed that MRSA was detected in 84.3% of the studies (n= 165) conducted on retail foods, even though the actual sample-level prevalence often remained below 20% (González-Machado et al., 2024). Beyond meat, fresh produce—including leafy greens, fruits, and vegetables—may also become contaminated with *Staphylococcus* spp. at various points in the food supply chain (Khalifa et al., 2025). Recently, our group reported the first isolation in the UAE of a *mecA*-positive MRSA strain belonging to sequence type ST-672 and spa type t384 from imported fresh dill (Habib et al., 2024). The principal public health concerns surrounding MRSA in food include its potential for community transmission and the risk of staphylococcal foodborne illness. In extreme cases, the ingestion of MRSA-contaminated food by a colonized or susceptible individual undergoing antibiotic treatment could allow for enterotoxin production in the gut, leading to disease (Sergelidis and Angelidis, 2017).

Despite the growing relevance of MRSA in food safety (Sergelidis and Angelidis, 2017), there remains a significant data gap in the UAE concerning its prevalence and antimicrobial resistance in meat products. This study addressed that gap by assessing MRSA prevalence in raw meats (beef, sheep meat, camel meat, and chicken) and fresh produce (ready-to-eat fruit and vegetable cuts) available in UAE retail outlets. Specifically, this work investigates the carriage of classical enterotoxin genes, evaluates antibiotic resistance patterns, and identifies the extent of multidrug resistance among MRSA isolates. This study represents the first comprehensive examination of MRSA prevalence, resistance profiles, and enterotoxin gene occurrence in retail foods of animal origin in the UAE. The findings from this study

TABLE 1 Distribution of methicillin-resistant *Staphylococcus aureus*-positive samples across different food types (n = 260) collected from retail outlets in Dubai, United Arab Emirates.

Food type	No. of samples	No. of positive samples (%)	95% Confidence interval
Beef	70	32 (45.7)	33.7; 58.1
Sheep meat	50	22 (44.0)	30.0; 58.7
Camel meat	20	11 (55.0)	31.5; 76.9
Chicken meat	60	45 (75.0)	62.1; 85.3
Fruit cuts	30	5 (16.6)	5.6; 34.7
Vegetables cuts	30	9 (30.0)	14.7; 49.4
Total	260	124 (47.7)	41.5; 54.0

contribute valuable data to the global understanding of foodborne MRSA transmission risks, particularly from underreported regions.

2 Materials and methods

2.1 Study design and sampling

This cross-sectional study was carried out in Dubai, one of the UAE's largest and most diverse retail markets. The sample size was calculated using an expected MRSA prevalence of 20% (González-Machado et al., 2024), with a 95% confidence level and a 5% margin of error, yielding a minimum required sample size of 246. To ensure comprehensive coverage and account for diversity in sample sources, 260 food samples were collected over six months (between September 2024 to February 2025). The sampling strategy included various food types to reflect dietary diversity and possible exposure routes. These included raw meat samples from beef (n = 70), sheep (n = 50), camel (n = 20), and chicken (n = 60), as well as ready-to-eat fresh produce items (n = 60), including fruit (n = 30) and vegetable cuts (n = 30). Red meat samples were in the form of boneless cuts, pieces with bones, and mince. Chicken meat was either whole carcasses or parts (breast, thigh, and wings) (Table 1). Samples were randomly collected from major supermarket outlets (n = 15) distributed across different districts in Dubai. All samples were aseptically collected in sterile containers, kept in insulated coolers with ice packs at a temperature lower than 4°C, and transported to the laboratory within 3 hours of collection to maintain microbial integrity. Upon arrival, samples were processed for microbiological analysis following standard protocols.

2.2 Isolation and identification of MRSA

A 25-gram portion from each food sample was aseptically transferred into 225 mL of Mueller–Hinton broth supplemented with 6.5% sodium chloride (HiMedia, India) to enhance selective enrichment (González-Machado et al., 2024). The inoculated broths were incubated at 37°C for 18 to 24 hours. Following incubation, a 10 µL loopful of the enriched culture was streaked onto CHROMagar MRSA (Paris, France), a chromogenic medium selective for MRSA, and incubated at 37°C for 18 to 24 hours (Diederen et al., 2005). Colonies exhibiting rose to mauve pigmentation—indicative of presumptive MRSA—were further subcultured onto nutrient agar plates to obtain pure isolates. Up to five suspect colonies per plate were selected for further identification. Species confirmation as *S. aureus* was achieved using matrix-assisted laser desorption ionization-time of flight mass spectrometry (MALDI-TOF MS), utilizing the Autobio ms1000 platform (Autobio Diagnostics, China). For DNA isolation, a commercial kit (Wizard® Genomic DNA Purification Kit ((Promega, United States)) was used according to the supplier's instructions. A multiplex polymerase chain reaction (PCR) assay targeting the *16S rRNA*, *mecA*, and *nuc* genes was performed to validate the MRSA status of the isolates, following the protocol of Maes et al. (2002) (Maes et al., 2002). Confirmed MRSA strains were then preserved in cryogenic storage at −80°C for downstream analyses.

2.3 Antibiotic susceptibility testing

Antimicrobial susceptibility testing of MRSA isolates was enabled using the VITEK-2 automated system (bioMérieux, France), utilizing the AST-P592 card designed specifically for *Staphylococcus*/*Enterococcus* species. A total of 15 clinically relevant antibiotics were included in the testing panel. These comprised β-lactams such as benzylpenicillin and oxacillin, with cefoxitin employed as a qualitative screen for methicillin resistance (reported as positive or negative). The panel also evaluated aminoglycoside susceptibility using gentamicin, and fluoroquinolone resistance was tested through both ciprofloxacin and moxifloxacin. Macrolide-lincosamide-streptogramin B (MLSB) resistance was assessed by including tests for erythromycin and clindamycin minimum inhibitory concentrations (MICs) alongside a qualitative screen for inducible clindamycin resistance. Glycopeptides such as teicoplanin, vancomycin, and linezolid (an oxazolidinone) were also included. Additional antimicrobials tested were tigecycline, tetracycline, rifampicin, and a combination of trimethoprim/sulfamethoxazole. Automated interpretation of MIC results was achieved using the bioMérieux VITEK-2 Advanced Expert System (AES) (bioMérieux, France). Isolates were considered multidrug-resistant (MDR) when they exhibited resistance to at least three distinct antimicrobial categories in the test panel (Magiorakos et al., 2012).

2.4 PCR testing for toxins encoding genes

All MRSA isolates tested for antimicrobial susceptibility testing were examined for seven toxin-encoding genes. This included

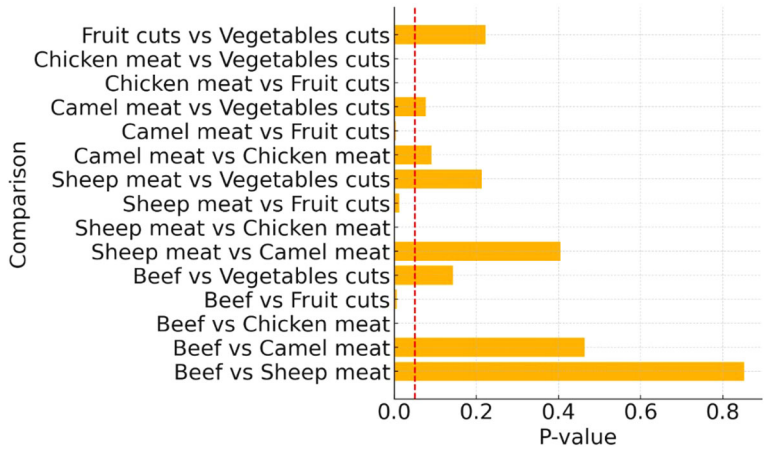

FIGURE 1
Pairwise comparison of methicillin-resistant *Staphylococcus aureus* detection in different food types. Red dashed line indicates the significance threshold at *p*-value = 0.05.

screening for the five classical staphylococcal enterotoxin genes (*sea*, *seb*, *sec*, *sed*, and *see*), as well as two exfoliative toxin genes (*eta* and *etb*), using gene-specific primers (Leke et al., 2017). PCR amplification was performed on a QIAamplifier 96 thermocycler (Qiagen, Germany). The cycling protocol began with an initial denaturation at 94°C for 5 minutes, followed by 35 amplification cycles consisting of denaturation at 94°C for 2 minutes, primer annealing at 57°C for 2 minutes, and extension at 72°C for 1 minute. A final extension step was conducted at 72°C for 7 minutes to complete the reaction. The resulting PCR products were separated by electrophoresis using a 1.5% agarose gel run at 110V for 45 minutes (Leke et al., 2017). DNA bands were then visualized and documented using the GelDoc-Go imaging system (Bio-Rad, USA).

2.5 Statistical analysis

All statistical analyses were performed using STATA version 16.1 (StataCorp; Texas, USA). Descriptive statistics were applied to summarize the prevalence of MRSA across different food categories. Frequencies and proportions were reported and compared across MRSA-positive samples, with exact binomial 95% confidence intervals (CI) calculated to assess the precision of prevalence estimates. To investigate potential predictors of MRSA occurrence, pairwise comparisons using two-sample z-tests for proportions and logistic regression models were used. The primary outcome variable was the presence or absence of MRSA in a given food sample. Explanatory variables included food type (categorical: beef, sheep meat, camel meat, chicken meat, fruits and vegetables), and product form—stratified by commodity group. For red meat samples (beef, sheep, camel), product form was categorized as minced, bone-in cuts, and boneless cuts. The form was grouped into whole birds versus parts (e.g., wings, legs, breasts) for chicken samples. Logistic regression analyses were conducted, and odds ratios (OR) with corresponding 95% CIs were reported, and model fit was assessed using likelihood-ratio tests. A two-sided *p*-value of <0.05 was considered statistically significant for all inferential tests.

3 Results

3.1 MRSA across different food types

A total of 260 food samples were tested, of which 124 (47.7%; 95% confidence interval 41.5%; 54.0%) were positive for MRSA (Table 1). The highest proportion of MRSA-positive samples was observed in chicken meat (75.0%), followed by camel meat (55.0%) and beef (45.7%). Lower prevalence rates were recorded in vegetables (30.0%) and fruit cuts (16.7%) (Table 1).

A chi-square test for independence indicated a statistically significant difference in MRSA prevalence across the different food categories ($\chi^2 = 35.46$, $p < 0.001$). Pairwise comparisons using two-sample z-tests for proportions revealed that several food type comparisons had statistically significant differences in MRSA contamination levels (Figure 1). Chicken meat had significantly higher contamination rates than fruit cuts, vegetables, and sheep meat ($p < 0.05$ in each comparison). The differences between beef, sheep, and camel meats were less pronounced, with some comparisons approaching but not reaching statistical significance (Figure 1).

3.2 Product forms and variation in MRSA contamination

Logistic regression analysis was conducted to evaluate the association between product form and MRSA contamination across various food types (Table 2). Within beef products, both "pieces with bones" and "boneless cuts" were significantly less likely to be MRSA-positive compared to minced beef, which served as the reference category. Specifically, "pieces with bones" had an odds

TABLE 2 Association between product form and methicillin-resistant *Staphylococcus aureus* contamination across different meat types based on logistic regression analysis.

Food type	Product form	Number of samples	Number of positive samples (%)	Odds ratio	*P*-value	95% Confidence interval
Beef	Mince	28	22 (78.5)	Reference category		
	Pieces with bones	14	2 (14.2)	0.04	0.001	0.007-0.261
	Boneless cuts	28	8 (28.5)	0.10	<0.001	0.032-0.369
Sheep meat	Pieces with bones	41	17 (41.4)	Reference category		
	Boneless cuts	7	2 (42.8)	1.05	0.945	0.209-5.354
Camel meat	Pieces with bones	11	8 (72.7)	Reference category		
	Boneless cuts	9	3 (33.3)	0.18	0.087	0.027-1.277
Chicken meat	Parts (breast, legs, wings)	31	23 (74.2)	Reference category		
	Whole carcass	29	22 (75.8)	1.09	0.881	0.339-3.524

ratio (OR) of 0.04 ($p = 0.001$), and "boneless cuts" had an OR of 0.10 ($p < 0.001$), indicating a strong negative association (Table 2).

In sheep meat, the odds of MRSA contamination were nearly identical between "pieces with bones" and "boneless cuts" (OR = 1.05, $p = 0.945$), suggesting no significant association between product form and contamination (Table 2). For camel meat, "boneless cuts" showed lower odds of MRSA contamination compared to "pieces with bones" (OR = 0.18), though this association did not reach statistical significance ($p = 0.087$) (Table 2). Among chicken meat samples, no significant difference in MRSA contamination was found between "parts" (breasts, legs, wings) and whole carcasses (OR = 1.09, $p = 0.881$), indicating that product form was not a predictor of MRSA presence in poultry (Table 2).

3.3 Antibiotic Susceptibility of MRSA isolates

From the 124 food samples confirmed positive for MRSA, a subset of 87 non-duplicate isolates (one isolate per positive food sample) was selected for further antimicrobial susceptibility testing and toxin gene screening. The 87 isolates were selected to be proportionally representative of MRSA isolates across different foods, distinct sampling locations, and sampling events/months.

All MRSA isolates (n = 87) from the six food categories were confirmed positive by the cefoxitin screen test (100%). High levels of resistance were also observed to benzylpenicillin and oxacillin, with near-universal resistance in the characterized isolates; only one camel meat isolate (12.5%) showed oxacillin susceptibility and a single chicken isolate (5%) was susceptible to benzylpenicillin (Table 3). None of the isolates exhibited non-susceptibility to linezolid, vancomycin, and teicoplanin. Only one sheep isolate (5.9%) showed resistance to rifampicin, and resistance to moxifloxacin was detected only in a single chicken isolate (5%) (Table 3).

Resistance to gentamicin, ciprofloxacin, and erythromycin varied across the confirmed MRSA isolates from different foods. Notably, camel meat isolates exhibited the highest gentamicin resistance (50%) and ciprofloxacin resistance (87.5%), whereas sheep meat isolates showed the lowest resistance to gentamicin (11.8%) ($p = 0.042$, Fisher's exact test). Similarly, ciprofloxacin resistance was significantly more prevalent in beef (78.6%) and camel (87.5%) compared to chicken meat (40%) and vegetable cuts (33.3%) ($p < 0.05$, chi-square test).

Inducible clindamycin resistance (ICR) was detected in 53.6% of beef isolates and 41.2% of sheep isolates but was absent in all fruit and vegetable isolates. The absence of ICR in fruit/vegetable isolates was noticeable, although not statistically significant ($p = 0.07$), compared to livestock-associated strains. Erythromycin resistance was widespread in meat isolates, particularly in chicken (85%), while fruit and vegetable isolates showed universal susceptibility (100%). Clindamycin resistance followed a similar pattern, with the highest resistance in chicken (55%) and lowest in camel (25%), while all produce isolates remained susceptible (Table 3).

Tetracycline resistance was moderate to high across all groups, highest in chicken (60%) and fresh produce (60% for fruit cuts; 55.6% for vegetable cuts). Trimethoprim/sulfamethoxazole resistance showed a gradient level variation, with resistance at 320 μg/mL observed in 32.1% of beef, 35.3% of sheep, and 37.5% of camel isolates. In contrast, only 5% of chicken isolates and none from fruit or vegetable samples reached this high-level resistance toward trimethoprim/sulfamethoxazole (Table 3).

The distribution of MDR among MRSA isolates varied notably across food types (Figure 2). Overall, 69 of 87 isolates (79.3%) were classified as MDR, exhibiting resistance to three or more antimicrobial classes. The highest proportion of extensive MDR was observed in beef and camel meat, where 65.4% and 75.0% of isolates were resistant to four or more classes (Figure 2). In contrast, fruit and vegetable cuts exclusively harbored isolates with resistance to only three classes. Chicken meat and sheep meat displayed intermediate patterns, with 17.7% and 15.4% of isolates, respectively, resistant to five antimicrobial classes (Figure 2). Notably, a small subset of chicken meat isolates (5.8%) exhibited resistance to seven classes, the highest observed in this study.

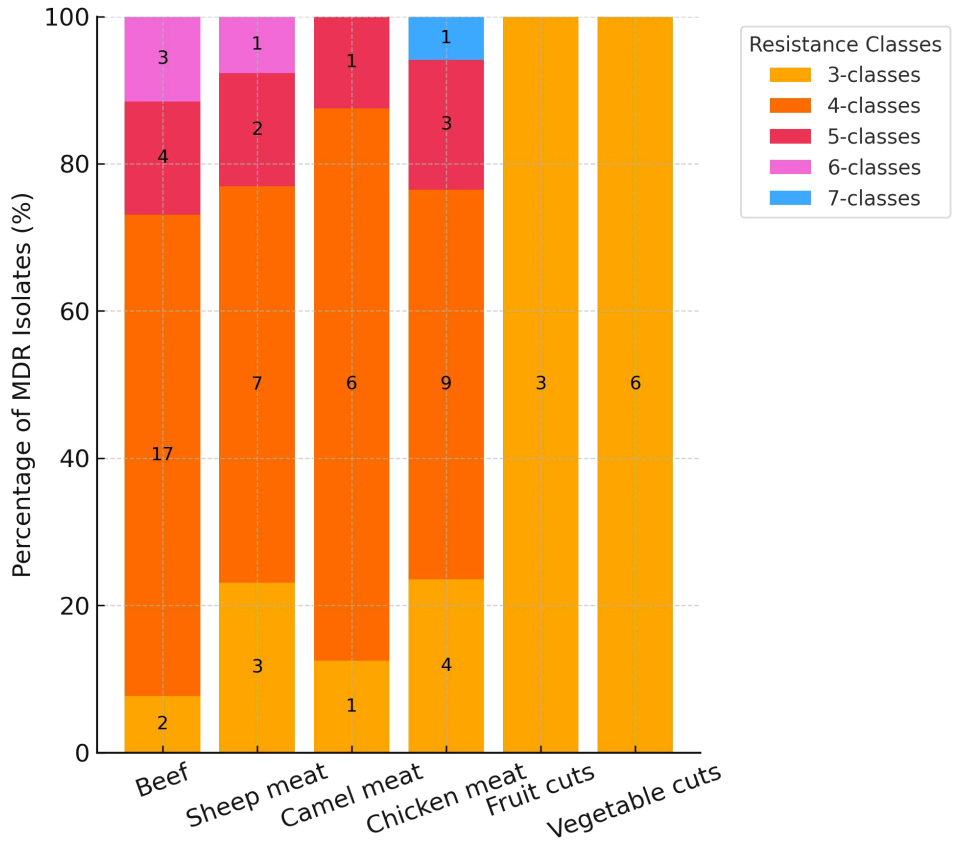

FIGURE 2
Distribution of multidrug resistance (MDR) among methicillin-resistant *Staphylococcus aureus* isolates (n = 87) by food type and number of antimicrobial classes.

3.4 Toxin gene screening among MRSA isolates

To assess the distribution of toxin genes among MRSA isolates (n = 87) from different food types, chi-square tests were performed for each gene. The *eta* gene showed a statistically significant variation across food categories (χ^2 = 16.61, *df* = 5, *p* = 0.005), indicating that its presence was not uniformly distributed. Further pairwise comparisons using Fisher's exact test revealed that the prevalence of the *eta* gene was significantly higher in isolates from vegetable cuts compared to those from beef (*p* = 0.010). No other pairwise comparisons reached statistical significance. In contrast, the *sea, seb*, and *sec* genes did not differ significantly between food types (all *p* > 0.20) (Figure 3). Importantly, none of the isolates carried the *sed*, *see*, or *etb* genes. Overall *sea* gene was the most frequently amplified across 29.1% of all characterized MRSA isolates (Figure 3). A small number of MRSA isolates (n = 4 (4.6%)) were found to harbor dual toxin genes. Among beef isolates, one carried *seb* and *sec*, while another harbored *sea* and *seb*. A sheep meat isolate also carried the *seb* and *sec* combination. Notably, a single isolate from fruit cuts carried *sea* and *eta*.

4 Discussion

Our study provides the first comprehensive data evaluating the prevalence and characteristics of MRSA in retail foods of animal and plant origin in the UAE. This work addresses a significant data gap in the region and highlights the potential of MRSA as a foodborne pathogen. By investigating multiple food types, our findings contribute valuable baseline information to inform national food safety surveillance and One Health initiatives in the UAE.

Our findings show a relatively high overall MRSA prevalence of 47.7% in retail meat and produce samples in the UAE. Our concluded prevalence in chicken meat (75.0%) notably exceeds values reported from several regions. For instance, MRSA was detected in only 1.7% of fresh chicken meat samples in a study from China (Wang et al., 2013), whereas a prevalence of 56.3% was reported in whole chicken carcasses examined in Egypt (Elshebrawy et al., 2025). A study by Bernier-Lachance et al. (2020) in Canada found a prevalence of just 1.2%. Given that the enrichment method applied in this study was also used in comparable investigations cited herein, the higher MRSA prevalence observed in retail chicken meat samples is unlikely to be due to methodological artifacts.

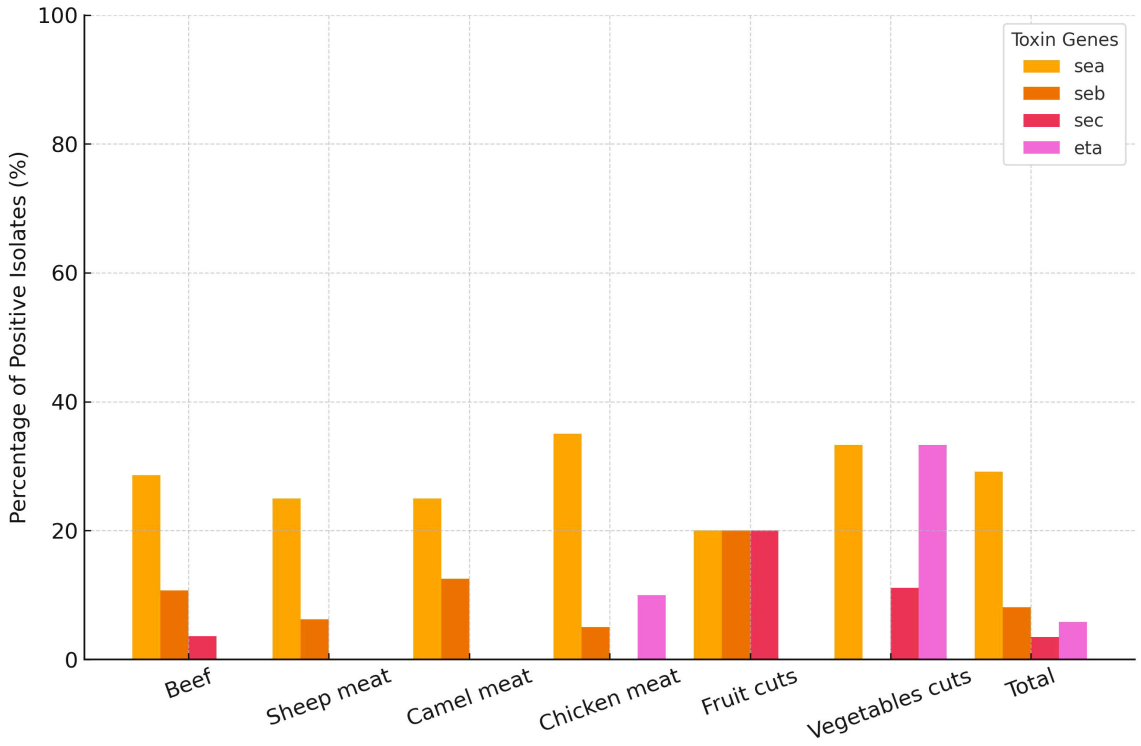

FIGURE 3
Frequency distribution of methicillin-resistant *Staphylococcus aureus* isolates (n = 87) carrying toxin genes (*sea, seb, sec*, and *eta*) across different food types sampled at retail level in Dubai, United Arab Emirates.

Instead, such variation may reflect differences in regional production systems, antimicrobial usage patterns, and biosecurity measures influencing MRSA contamination along the poultry supply chain.

Regarding beef and sheep meat, our observed MRSA prevalence of 45.7% and 44.0% is higher than some reported rates elsewhere. Studies from Canada and the United States have generally reported lower prevalence — for example, Bhargava et al. (2011) observed just 1.3% in beef, and Weese et al. (2010) found 5.6%. A report from Egypt found a rate of 4% among MRSA from beef (Hasanpour Dehkordi et al., 2017). In terms of sheep meat, our results (24% prevalence) are higher than reported in Iran (Hasanpour Dehkordi et al., 2017), and higher than the 0–5% levels reported in some European studies (González-Machado et al., 2024).

Data on camel meat MRSA prevalence is scarce globally, hence, our study strengthens the global data pool by providing novel insights into the occurrence of MRSA in camel meat, a culturally and economically important commodity in the Middle East. Compared to our finding, a Jordanian study by Quddoumi et al. (2006) found MRSA in 12.5% of camel meat samples, significantly lower than the 55% prevalence we observed. Consistent with our findings, Raji et al. (2016) and Alkuraythi et al. (2023) reported that camel meat exhibited the highest MRSA contamination rate among tested red meat types in Saudi Arabia. This suggests potential emerging risks in niche meat products in the UAE, possibly due to under-regulated handling or niche processing channels.

The logistic regression analysis strongly implicates product form as a driver of MRSA contamination in beef. Minced beef had a significantly higher prevalence (78.5%) than boneless or bone–in pieces (Table 2). Mincing disrupts the natural surface barrier, exposes fat and connective tissues rich in water activity, and vastly enlarges the surface area on which MRSA can adhere and multiply. It also funnels meat from multiple carcasses through common grinders and conveyors, multiplying opportunities for cross–contamination, especially if sanitation or temperature control is sub–optimal (Nastasijevic et al., 2023). Although the camel–meat regression model did not reach statistical significance (p = 0.087) (Table 2), the point estimate mirrors the beef pattern, suggesting that trimming boneless cuts could lower the bacterial load by removing surface tissue, whereas bone–in portions, which are often exposed to saw–blade aerosols, remain highly contaminated (72.7%). Given the cultural importance of camel meat in the region (Mohamed et al., 2024), this apparent reduction should not be dismissed; additional, adequately powered studies are warranted to refine the risk estimate. In contrast, chicken showed uniformly high MRSA prevalence in both whole carcasses and parts (~75%), with no difference between forms. This likely reflects the dominance of automated cutting lines in modern poultry abattoirs, where equipment surfaces, scalding tanks, and chilling baths create homogenous contamination pressure. Consequently, interventions for poultry should focus on upstream processing hygiene and equipment sanitation rather than product form only, whereas beef

10.3389/fcimb.2025.1628036

TABLE 3 Antimicrobial resistance patterns of methicillin-resistant *Staphylococcus aureus* isolates (n = 87) from different food types sampled at the retail level in Dubai, United Arab Emirates.

Antimicrobial	Resistance status*	Percentage (%) of resistance per each food type					
		Beef (n = 28)	Sheep meat (n = 17)	Camel meat (n = 8)	Chicken (n = 20)	Fruit cuts (n = 5)	Vegetable cuts (n = 9)
Cefoxitin screen test	Positive	100%	100%	100%	100%	100%	100%
Benzylpenicillin	R (>=0.5)	100%	100%	100%	95%	100%	100%
	S (0.25)	—	—	—	5%	—	—
Oxacillin	R (>=4)	100%	100%	87.5%	100%	100%	100%
	S (=2)	—	—	12.5%	—	—	—
Gentamicin	R (>=16)	32.1%	11.8%	50%	15%	—	—
	I	3.6%	—	—	—	—	11.1%
	S	64.3%	88.2%	50%	85%	100%	88.9%
Ciprofloxacin	R (>=8)	78.6%	58.8%	87.5%	40%	40%	33.3%
	I	—	—	—	—	—	11.1%
	S	21.4%	41.2%	12.5%	60%	60%	55.6%
Moxifloxacin	R (>=8)	—	—	—	5%	—	—
	I	14.3%	5.9%	—	10%	—	—
	S	85.7%	94.1%	100%	85%	100%	100%
Inducible Clindamycin resistance	Negative	46.4%	58.8%	75%	80%	100%	100%
	Positive	53.6%	41.2%	20%	20%	—	—
Erythromycin	R (>=8)	67.9%	64.7%	25%	85%	—	—
	I	—	—	12.5%	—	—	—
	S	32.1%	35.3%	62.5%	15%	100%	100%
Clindamycin	R (<=0.25)	53.6%	41.2%	25%	55%	—	—
	R (>=8)	—	5.8%	—	20%	—	—
	I	—	—	—	—	—	—
	S	46.4%	53%	75%	25%	100%	100%
Linezolid	S	100%	100%	100%	100%	100%	100%
Teicoplanin	S	100%	100%	100%	100%	100%	100%
Vancomycin	S	100%	100%	100%	100%	100%	100%
Tetracycline	R (>=16)	25%	29.4%	25%	60%	60%	55.6%
	S	75%	70.6%	75%	40%	40%	44.4%
Tigecycline	S	100%	100%	100%	100%	100%	100%
Rifampicin	R (>=32)	—	5.9%	—	—	—	—
	S	—	94.1%	—	—	—	—
Trimethoprim/Sulfa	R (80)	3.6%	5.9%	12.5%	—	—	—
	R (160)	14.3%	—	37.5%	—	20%	33.3%
	R (>=320)	32.1%	35.3%	37.5%	5%	40%	33.3%
	S	50%	58.8%	12.5%	95%	40%	33.3%

*R, Resistant; S, Susceptible; I, Intermediate. The numerical values in brackets indicate resistance cut-off in μg/ml.

—and potentially camel—require distinct control points for minced versus intact cuts to mitigate consumer exposure.

Our study detected MRSA at comparatively lower rates in retail vegetable (30.0%) and fruit cut (16.7%) samples in the UAE. These findings are consistent with international reports confirming the presence of MRSA in fresh produce, albeit at varying prevalence rates. For instance, a Malaysian study found MRSA in 21.4% of leafy vegetables (González-Machado et al., 2024). A study from China also supports the potential for MRSA contamination in fresh produce, with a reported prevalence of 1.0% in vegetables and 20.5% in fresh-cut fruits and vegetables (Wang et al., 2017). In North America, MRSA was identified in 28.2% of vegetable samples in a U.S. study (Yigrem et al., 2022) and 1.4% of plant-based imports in Canada (Jung and Rubin, 2020). Although the UAE results drawn from the present study fall within this global range, detecting MRSA in raw produce remains a public health concern, especially since some of these products are consumed without cooking, bypassing a critical control point for pathogen inactivation. The findings highlight the need for enhanced hygiene practices during post-harvest handling, slicing, and retail display, as well as strengthening surveillance programs to monitor emerging trends and protect consumer health.

MRSA resistance patterns in UAE retail foods reflect concerning variation. The notably high resistance to gentamicin (50%) and ciprofloxacin (up to 88%) in camel and beef isolates suggests selective pressure from the use of aminoglycosides in camel pastoral systems and fluoroquinolones in intensive cattle farming (Nastasijevic et al., 2023; Mohamed et al., 2024). This aligns with findings from various settings, such as ciprofloxacin resistance rates of 80–100% in MRSA isolated from retail beef in Louisiana (USA) and camel meat in Riyadh (KSA) (González-Machado et al., 2024; Khalifa et al., 2025). In contrast, chicken isolates showed the highest levels of resistance to macrolides and lincosamides—particularly erythromycin (85%) and clindamycin (55%)—a pattern consistent with data from a longitudinal study in Algeria (Belhout et al., 2022), and likely driven by the historical use of these antimicrobials in poultry production. Importantly, inducible clindamycin resistance (ICR) was detected only in meat-derived isolates, particularly from beef (53.6%) and sheep (41.2%), supporting previous evidence that ICR is primarily associated with livestock sources and rarely found in plant-based foods (Endale et al., 2023). These findings highlight the importance of implementing targeted, commodity-specific antimicrobial resistance surveillance in the UAE, aligned with a One Health approach that recognizes the interconnectedness of human, animal, and environmental health.

Our findings underscore the high prevalence of MDR among foodborne MRSA isolates, with nearly 80% of isolates characterized in the present study were resistant to three or more antimicrobial classes. The presence of such broadly drug-resistant MRSA in the food chain is a significant public health concern, as it compromises treatment options for potential infections. Comparable high MDR rates in food-associated MRSA have been reported in other regions, including neighboring Saudi Arabia and beyond. For instance, a study in Riyadh found that most MRSA isolates from retail processed foods were MDR, with a notable proportion even carrying vancomycin-resistance genes (Alghizzi et al., 2021). Likewise, in Nigeria over 80% of poultry meat MRSA isolates were MDR, and a few were resistant to all tested antibiotics (Igbinosa et al., 2023). The emergence of MDR-MRSA in diverse food products has also been documented (Mohammed et al., 2025), underscoring the global nature of this threat. Collectively, these findings highlight a need for strict antibiotic stewardship in agriculture and improved food hygiene measures to curb the spread of MDR pathogens from farm to fork and protect public health.

In addition to being found in foods, enterotoxigenic MRSA strains have also been isolated from individual patients and involved in a few reported foodborne outbreaks (Sergelidis and Angelidis, 2017). Around 95% of SFP cases are linked to the classical enterotoxins *sea* to *see* (Oliveira et al., 2022). Therefore, our study focused on screening *S. aureus* isolates for these five major SE genes. In the present study, the *sea* gene was the most commonly detected in 29.1% of all characterized MRSA isolates. This aligns with findings reported in China (29.7%) (Wang et al., 2017), Malaysia (30.8%) (Puah et al., 2016) and the USA (25.8%) (Ge et al., 2017). The high prevalence of the *sea* gene in MRSA isolates from retail food in the present study is notable, given that *sea* is the most commonly linked enterotoxin in SFP cases worldwide (Sergelidis and Angelidis, 2017; Shalaby et al., 2024). On the other hand, the detection of MRSA harboring the *eta* gene—that encodes for exfoliative toxin A (ETA) which is classically associated with staphylococcal skin infections—in retail fruit– and vegetable–cut samples is epidemiologically noteworthy; *eta* –positive strains are uncommon in the wider *S. aureus* population (≈5%) but are disproportionately of human origin (Linz et al., 2023), reflecting a possible nasal or cutaneous carriage in food handlers rather than primary contamination on the farm. To minimize the dissemination of MDR and toxigenic MRSA through the food value chain, preventive measures should focus on strengthening on-farm biosecurity and enforcing prudent antimicrobial use in food animal production. In addition, strict adherence to hygiene standards during slaughter, processing, and retail handling, combined with consumer education on safe food practices, is essential to reduce the risk of transmission to humans.

MRSA isolates co-harboring MDR and toxigenic determinants have indeed been reported in various regions. For example, in Cameroon, all MRSA isolates in one study were MDR and over half carried the PVL toxin gene (Mohamadou et al., 2022). Similarly, a Pakistani study found that around 69% of *S. aureus* isolates harbored the *mecA* resistance gene while also carrying various toxin genes (e.g., the enterotoxin gene *sea* in 53.2% of isolates and the toxic shock syndrome toxin gene *tst* in 24.2%), with 42 of 62 isolates co-occurring *mecA* and multiple virulence factors (Tasneem et al., 2022). Likewise, in Egypt, the majority of MRSA isolates were reported to be MDR and simultaneously positive for toxin genes such as *sea* and PVL (Abd El-Hamid et al., 2022). The co-occurrence of MDR and toxigenic genes is alarming because it produces strains that are not only difficult to treat but also highly virulent, thereby greatly increasing the public health risk by enabling the spread of staphylococcal infections that pose significant challenges to current therapeutic strategies.

Overall, this study provides valuable insights into MRSA's AMR profiles and toxin gene distribution in retail foods of animal and plant origin in the UAE. As one of the first efforts within a One Health framework to align MRSA surveillance across food sources in Dubai, the study contributes important baseline data to inform national risk assessments and public health interventions. Nonetheless, several limitations should be acknowledged. First, we did not collect nasal swabs or hand wash samples from food handlers at the sampling sites. While such data would have helped establish a clearer link between food contamination and food handler's carriage, this aspect was outside the scope of the study, which focused on retail food matrices. Future studies are recommended to incorporate human sampling to better trace contamination pathways. Second, the study was geographically limited to Dubai, so it was chosen as a case study due to its diversity and relevance within the UAE and as part of an integrated ongoing One Health investigation across food, clinical, animal, and environmental sectors. While Dubai offers a rich sampling environment, extending surveillance to other emirates is important for enhancing the representativeness and generalizability of findings. Sampling from other emirates or regions where camel meat is more accessible will also ensure broader coverage of this culturally significant food item. There is also a need to conduct WGS characterization of MRSA isolates to assess their relatedness to community-acquired strains and better understand their public health significance.

5 Conclusion

The findings reveal a high overall prevalence of MRSA, particularly in chicken, beef, and camel meat, and to a lesser extent in fruit and vegetable cuts. The detection of key virulence genes, such as *sea* and *eta*, alongside notable resistance to antimicrobials, raises concerns about the potential role of MRSA as a foodborne pathogen and the risk of transmission through the food chain. Future research should expand geographically, include food handlers in sampling protocols, and continue exploring culturally relevant food items to better inform national food safety strategies and antimicrobial resistance mitigation plans. Although this study is regionally focused on Dubai, its findings have broader significance. The high prevalence of multidrug-resistant and toxigenic MRSA in retail foods underscores foodborne transmission risks relevant to global supply chains. Key lessons, including the need for One Health surveillance, better food hygiene, and prudent antimicrobial use, apply to other regions and support coordinated international strategies to reduce the public health threat of MRSA.

Data availability statement

The original contributions presented in the study are included in the article/supplementary material. Further inquiries can be directed to the corresponding authors.

Ethics statement

This study did not involve human participants or animal subjects, and hence, no specific ethical approval was required according to United Arab Emirates University institutional guidelines and regulations. All procedures, methods, and analyses were carried out in compliance with relevant standards.

Author contributions

IH: Conceptualization, Formal Analysis, Investigation, Methodology, Resources, Visualization, Writing – original draft, Writing – review & editing. M-YM: Data curation, Formal Analysis, Investigation, Writing – review & editing. GL: Data curation, Formal Analysis, Investigation, Writing – review & editing. FA: Data curation, Formal Analysis, Investigation, Writing – review & editing. RG: Conceptualization, Funding acquisition, Methodology, Project administration, Validation, Writing – review & editing. MK: Conceptualization, Funding acquisition, Methodology, Project administration, Validation, Writing – review & editing. AS: Conceptualization, Funding acquisition, Methodology, Project administration, Validation, Writing – review & editing.

Funding

The author(s) declare financial support was received for the research and/or publication of this article. This research was funded by the United Arab Emirates (UAE)- the United States of America National Institute of Health (NH) Collaborative Awards (Grant #: AJF-NIH-1-MBRU).

Acknowledgments

Mohamed-Yousif Ibrahim Mohamed and Glindya Bhagya Lakshmi are indebted to the post-doctoral fellowship supported by the ASPIRE Research Institute for Food Security in the Drylands (ARIFSID) project (Subtheme 4.1—One Health and Antimicrobial Resistance). ASPIRE is a Research and Development Funding Organization in the United Arab Emirates that works as the technology transition pillar of Abu Dhabi's Advanced Technology Research Council (ATRC). We thank Ms. Afra Abdalla for her technical assistance in the laboratory.

Conflict of interest

The authors declare that the research was conducted in the absence of any commercial or financial relationships that could be construed as a potential conflict of interest.

The author(s) declared that they were an editorial board member of Frontiers, at the time of submission. This had no impact on the peer review process and the final decision.

Generative AI statement

The author(s) declare that Generative AI was used in the creation of this manuscript. The authors affirm that during the preparation of this manuscript, generative AI tools were used to support language refinement and clarity. Specifically, ChatGPT (OpenAI) was utilized to improve phrasing and grammar, and Grammarly was employed to assist with proofreading and grammatical corrections. All intellectual content, interpretation of results, and scientific conclusions were developed and critically reviewed by the authors without reliance on AI tools. The final manuscript was carefully edited and approved by all authors to ensure accuracy and integrity.

Any alternative text (alt text) provided alongside figures in this article has been generated by Frontiers with the support of artificial intelligence and reasonable efforts have been made to ensure accuracy, including review by the authors wherever possible. If you identify any issues, please contact us.

Publisher's note

References

Abd El-Hamid, M. I., Sewid, A. H., Samir, M., Hegazy, W. A. H., Bahnass, M. M., Mosbah, R. A., et al. (2022). Clonal diversity and epidemiological characteristics of ST239-MRSA strains. *Front. Cell Infect. Microbiol.* 12. doi: 10.3389/fcimb.2022.782045

Alghizzi, M. J., Alansari, M., and Shami, A. (2021). The prevalence of *Staphylococcus aureus* and methicillin-resistant *S. aureus* in processed food samples in Riyadh, Saudi Arabia. *J. Pure Appl. Microbiol.* 15, 91–99. doi: 10.22207/JPAM.15.1.03

Alkuraythi, D. M., Alkhulaifi, M. M., Binjomah, A. Z., Alarwi, M., Aldakhil, H. M., Mujallad, M. I., et al. (2023). Clonal flux and spread of *Staphylococcus aureus* isolated from meat and its genetic relatedness to *Staphylococcus aureus* isolated from patients in Saudi Arabia. *Microorganisms* 11, 2926. doi: 10.3390/microorganisms11122926

Belhout, C., Elgroud, R., and Butaye, P. (2022). Methicillin-Resistant *Staphylococcus aureus* (MRSA) and other methicillin-resistant *Staphylococci* and *Mammaliicoccus* (MRNaS) associated with animals and food products in Arab countries: A review. *Vet. Sci.* 9, 317. doi: 10.3390/vetsci9070317

Bernier-Lachance, J., Arsenault, J., Usongo, V., Parent, É., Labrie, J., Jacques, M., et al. (2020). Prevalence and characteristics of Livestock-Associated Methicillin-Resistant *Staphylococcus aureus* (LA-MRSA) isolated from chicken meat in the province of Quebec, Canada. *PloS One* 15, e0227183. doi: 10.1371/journal.pone.0227183

Bhargava, K., Wang, X., Donabedian, S., Zervos, M., da Rocha, L., and Zhang, Y. (2011). Methicillin-Resistant *Staphylococcus aureus* in retail meat, Detroit, Michigan, USA. *Emerg. Infect. Dis.* 17, 1135–1137. doi: 10.3201/eid1706.101095

Diederen, B., van Duijn, I., van Belkum, A., Willemse, P., van Keulen, P., and Kluytmans, J. (2005). Performance of CHROMagar MRSA medium for detection of methicillin-resistant *Staphylococcus aureus*. *J. Clin. Microbiol.* 43, 1925–1927. doi: 10.1128/JCM.43.4.1925-1927.2005

Elshebrawy, H. A., Kasem, N. G., and Sallam, K. I. (2025). Methicillin- and vancomycin-resistant *Staphylococcus aureus* in chicken carcasses, ready-to-eat chicken meat sandwiches, and buffalo milk. *Int. J. Food Microbiol.* 427, 110968. doi: 10.1016/j.ijfoodmicro.2024.110968

Endale, H., Mathewos, M., and Abdeta, D. (2023). Potential causes of spread of antimicrobial resistance and preventive measures in one health perspective-a review. *Infect. Drug Resist.* 16, 7515–7545. doi: 10.2147/IDR.S428837

Enright, M. C., Robinson, D. A., Randle, G., Feil, E. J., Grundmann, H., and Spratt, B. G. (2002). The evolutionary history of methicillin-resistant *Staphylococcus aureus* (MRSA). *Proc. Natl. Acad. Sci.* 99, 7687–7692. doi: 10.1073/pnas.122108599

Ge, B., Mukherjee, S., Hsu, C.-H., Davis, J. A., Tran, T. T. T., Yang, Q., et al. (2017). MRSA and multidrug-resistant Staphylococcus aureus in U.S. retail meats 2010–2011.*Food Microbiol.* 62, 289–297. doi: 10.1016/j.fm.2016.10.029

González-Machado, C., Alonso-Calleja, C., and Capita, R. (2024). Prevalence and types of methicillin-resistant *Staphylococcus aureus* (MRSA) in meat and meat products from retail outlets and in samples of animal origin collected in farms, slaughterhouses and meat processing facilities. A review. *Food Microbiol.* 123, 104580. doi: 10.1016/j.fm.2024.104580

Habib, I., Lakshmi, G. B., Mohamed, M.-Y. I., Ghazawi, A., Khan, M., Al-Rifai, R. H., et al. (2024). *Staphylococcus* spp. in salad vegetables: Biodiversity, antimicrobial resistance, and first identification of methicillin-resistant strains in the United Arab Emirates food supply. *Foods* 13, 2439. doi: 10.3390/foods13152439

Hasanpour Dehkordi, A., Khaji, L., Sakhaei Shahreza, M. H., Mashak, Z., Safarpoor Dehkordi, F., Safaee, Y., et al. (2017). One-year prevalence of antimicrobial susceptibility pattern of methicillin-resistant *Staphylococcus aureus* recovered from raw meat. *Trop. BioMed.* 34, 396–404. Available online at: http://msptm.org/files/Vol34No2/396-404-Hasanpour-Dehkordi-A.pdf.

Igbinosa, E. O., Beshiru, A., Igbinosa, I. H., Ogofure, A. G., Ekundayo, T. C., and Okoh, A. I. (2023). Prevalence, multiple antibiotic resistance and virulence profile of MRSA in retail poultry meat from Edo, Nigeria. *Front. Cell. Infect. Microbiol.* 13, 1122059. doi: 10.3389/fcimb.2023.1122059

Jung, D., and Rubin, J. E. (2020). Identification of antimicrobial resistant bacteria from plant-based food products imported into Canada. *Int. J. Food Microbiol.* 319, 108509. doi: 10.1016/j.ijfoodmicro.2020.108509

Kadariya, J., Smith, T. C., and Thapaliya, D. (2014). *Staphylococcus aureus* and *Staphylococcal* food-borne disease: An ongoing challenge in public health. *BioMed. Res. Int.* 2014, 1–9. doi: 10.1155/2014/827965

Khalifa, H. O., Abdelhamid, M. A. A., Oreiby, A., Mohamed, M.-Y. I., Ramadan, H., Elfadadny, A., et al. (2025). Fire under the ashes: A descriptive review on the prevalence of methicillin-resistant *Staphylococcus aureus* in the food supply chain. *J. Agric. Food Res.* 19, 101606. doi: 10.1016/j.jafr.2024.101606

Léguillier, V., Pinamonti, D., Chang, C.-M., Gunjan,, Mukherjee, R., Himanshu,, et al. (2024). A review and meta-analysis of *Staphylococcus aureus* prevalence in foods. *Microbe* 4, 100131. doi: 10.1016/j.microb.2024.100131

Leke, A., Goudjil, S., Mullie, C., Grognet, S., and Biendo, M. (2017). PCR detection of *Staphylococcal* enterotoxin genes and exfoliative toxin genes in methicillin-resistant and methicillin-susceptible *Staphylococcus aureus* strains from raw human breast milk. *Clin. Nutr. Exp.* 14, 26–35. doi: 10.1016/j.yclnex.2017.05.001

Linz, M. S., Mattappallil, A., Finkel, D., and Parker, D. (2023). Clinical impact of *Staphylococcus aureus* skin and soft tissue infections. *Antibiotics* 12, 557. doi: 10.3390/antibiotics12030557

Maes, N., Magdalena, J., Rottiers, S., De Gheldre, Y., and Struelens, M. J. (2002). Evaluation of a triplex PCR assay To discriminate *Staphylococcus aureus* from coagulase-negative *Staphylococci* and determine methicillin resistance from blood cultures. *J. Clin. Microbiol.* 40, 1514–1517. doi: 10.1128/JCM.40.4.1514-1517.2002

Magiorakos, A.-P., Srinivasan, A., Carey, R. B., Carmeli, Y., Falagas, M. E., Giske, C. G., et al. (2012). Multidrug-resistant, extensively drug-resistant and pandrug-resistant bacteria: an international expert proposal for interim standard definitions for acquired resistance. *Clin. Microbiol. Infect.* 18, 268–281. doi: 10.1111/j.1469-0691.2011.03570.x

Mohamadou, M., Essama, S. R., Ngonde Essome, M. C., Akwah, L., Nadeem, N., Gonsu Kamga, H., et al. (2022). High prevalence of Panton–Valentine leukocidin positive, multidrug resistant, Methicillin-resistant *Staphylococcus aureus* strains circulating among clinical setups in Adamawa and Far North regions of Cameroon. *PloS One* 17, e0265118. doi: 10.1371/journal.pone.0265118

Mohamed, M.-Y. I., Lakshmi, G. B., Sodagari, H., and Habib, I. (2024). A one health perspective on camel meat hygiene and zoonoses: Insights from a decade of research in the Middle East. *Vet. Sci.* 11, 344. doi: 10.3390/vetsci11080344

Mohammed, R., Nader, S. M., Hamza, D. A., and Sabry, M. A. (2025).). Public health implications of multidrug-resistant and methicillin-resistant Staphylococcus aureus in retail oysters.*Sci. Rep.* 15, 4496. doi: 10.1038/s41598-025-88743-5

Moradigaravand, D., Senok, A., Al-Dabal, L., Khansaheb, H. H., Habous, M., Alsuwaidi, H., et al. (2023). Unveiling the dynamics of antimicrobial utilization and resistance in a large hospital network over five years: Insights from health record data analysis. *PloS Digit Health* 2, e0000424. doi: 10.1371/journal.pdig.0000424

Nastasijevic, I., Proscia, F., Jurica, K., and Veskovic-Moracanin, S. (2023). Tracking antimicrobial resistance along the meat chain: One health context. *Food Rev. Int.* 1–35. doi: 10.1080/87559129.2023.2279590

Oliveira, R., Pinho, E., Almeida, G., Azevedo, N. F., and Almeida, C. (2022). Prevalence and diversity of *Staphylococcus aureus* and *Staphylococcal* enterotoxins in raw milk from northern Portugal. *Front. Microbiol.* 13. doi: 10.3389/fmicb.2022.846653

Puah, S., Chua, K., and Tan, J. (2016). Virulence factors and antibiotic susceptibility of *Staphylococcus aureus* isolates in ready-to-eat foods: Detection of *S. aureus* contamination and a high prevalence of virulence genes. *Int. J. Environ. Res. Public Health* 13, 199. doi: 10.3390/ijerph13020199

Quddoumi, S. S., Bdour, S. M., and Mahasneh, A. M. (2006). Isolation and characterization of methicillin-resistant *Staphylococcus aureus* from livestock and poultry meat. *Ann. Microbiol.* 56, 155–161. doi: 10.1007/BF03174998

Raji, M. A., Garaween, G., Ehricht, R., Monecke, S., Shibl, A. M., and Senok, A. (2016). Genetic characterization of *Staphylococcus aureus* isolated from retail meat in Riyadh, Saudi Arabia. *Front. Microbiol.* 7. doi: 10.3389/fmicb.2016.00911

Roy, M. C., Chowdhury, T., Hossain, M. T., Hassan, M. M., Zahran, E., Rahman, M. M., et al. (2024). Zoonotic linkage and environmental contamination of Methicillin-resistant *Staphylococcus aureus* (MRSA) in dairy farms: A one health perspective. *One Health* 18, 100680. doi: 10.1016/j.onehlt.2024.100680

Sergelidis, D., and Angelidis, A. S. (2017). Methicillin-resistant *Staphylococcus aureus*: a controversial food-borne pathogen. *Lett. Appl. Microbiol.* 64, 409–418. doi: 10.1111/lam.12735

Shalaby, M., Reboud, J., Forde, T., Zadoks, R. N., and Busin, V. (2024). Distribution and prevalence of enterotoxigenic *Staphylococcus aureus* and *Staphylococcal* enterotoxins in raw ruminants' milk: A systematic review. *Food Microbiol.* 118, 104405. doi: 10.1016/j.fm.2023.104405

Tasneem, U., Majid, M., Mehmood, K., Redaina,, Rehman, F. U., Andleeb, S., et al. (2022). Co-occurrence of antibiotic resistance and virulence genes in *Methicillin Resistant Staphylococcus aureus* (MRSA) isolates from Pakistan. *Afr. Health Sci.* 22, 486–495. doi: 10.4314/ahs.v22i1.57

Thomsen, J., Abdulrazzaq, N. M., Menezes, G. A., Ayoub Moubareck, C., Everett, D. B., and Senok, A. (2023). Methicillin resistant *Staphylococcus aureus* in the United Arab Emirates: a 12-year retrospective analysis of evolving trends. *Front. Public Health* 11. doi: 10.3389/fpubh.2023.1244351

Wang, W., Baloch, Z., Jiang, T., Zhang, C., Peng, Z., Li, F., et al. (2017). Enterotoxigenicity and antimicrobial resistance of *Staphylococcus aureus* isolated from retail food in China. *Front. Microbiol.* 8. doi: 10.3389/fmicb.2017.02256

Wang, X., Tao, X., Xia, X., Yang, B., Xi, M., Meng, J., et al. (2013). *Staphylococcus aureus* and methicillin-resistant *Staphylococcus aureus* in retail raw chicken in China. *Food Contr* 29, 103–106. doi: 10.1016/j.foodcont.2012.06.002

Weese, J. S., Avery, B. P., and Reid-Smith, R. J. (2010). Detection and quantification of methicillin-resistant *Staphylococcus aureus* (MRSA) clones in retail meat products. *Lett. Appl. Microbiol.* 51, 338–342. doi: 10.1111/j.1472-765X.2010.02901.x

Yigrem, C., Eribo, B., and Sangre, K. (2022). Incidence of antibiotic-resistant *Staphylococcus aureus* in leafy greens and clinical sources. *J. Microbiol. Res. (Rosemead Calif)* 12, 13–23. doi: 10.5923/j.microbiology.20221201.02

frontiers | Frontiers in Cellular and Infection Microbiology

TYPE Original Research
PUBLISHED 07 October 2025
DOI 10.3389/fcimb.2025.1667196

OPEN ACCESS

EDITED BY
Mattia Pirolo,
University of Copenhagen, Denmark

REVIEWED BY
Marie Louise Guadalupe Attwood,
North Bristol NHS Trust, United Kingdom
Riccardo Polani,
Sapienza University of Rome, Italy

*CORRESPONDENCE
Jiubiao Guo
jbguo@stu.edu.cn
Feifei Yin
yinfeifeiff@163.com
Dachuan Lin
lindachaun@muhn.edu.cn

†These authors have contributed equally to this work

RECEIVED 16 July 2025
ACCEPTED 15 September 2025
PUBLISHED 07 October 2025

CITATION
Peng R, Liang P, Jiang W, Li Z, Wang L, Huang Y, Zhang X, Guo Y, Wang Y, Wang J, Guo J, Yin F and Lin D (2025) Community gut colonization by *tet*(X4)-positive multidrug-resistant *Escherichia coli* in healthy individuals from urban residents in Shenzhen, China. *Front. Cell. Infect. Microbiol.* 15:1667196. doi: 10.3389/fcimb.2025.1667196

Community gut colonization by *tet*(X4)-positive multidrug-resistant *Escherichia coli* in healthy individuals from urban residents in Shenzhen, China

Ruoyan Peng[1†], Pei Liang[1†], Wenxiao Jiang[2†], Zhaodong Li[3], Li Wang[4], Yi Huang[1], Xianfang Zhang[1], Yijia Guo[1], Ying Wang[1], Jing Wang[5], Jiubiao Guo[6*], Feifei Yin[1*] and Dachuan Lin[1*]

[1]Hainan Medical University–The University of Hong Kong Joint Laboratory of Tropical Infectious Diseases & Key Laboratory of Tropical Translational Medicine of Ministry of Education, College of Basic Medical Sciences, Hainan Medical University, Haikou, China, [2]Department of Nutrition and Food Hygiene, School of Public Health, Shenzhen University, Shenzhen, China, [3]Institute of Clinical Medicine, The Second Affiliated Hospital of Hainan Medical University, Haikou, China, [4]The University of Hong Kong, Shenzhen, China, [5]School of Public Health, Xinjiang Medical University, Urumqi, China, [6]Clinical Research Center, The First Affiliated Hospital of Shantou University Medical College, Shantou, China

Background: Tigecycline remains a last-resort antibiotic for treating multidrug-resistant (MDR) Gram-negative pathogens. The emergence of *tet*(X4)-mediated high-level tigecycline resistance in *Escherichia coli* has raised global concern, yet its prevalence in healthy human populations remains limited.

Methods: We conducted a community-based surveillance study involving 245 fecal samples from healthy individuals in three urban communities in Shenzhen, China. Tigecycine-resistant strains were isolated using MacConkey agar supplemented with 2 mg/L tigecycline and confirmed by PCR detection of *tet*(X). Antimicrobial susceptibility testing, whole-genome sequencing (WGS), and phylogenetic analysis were performed.

Results: Tigecycline-resistant *E. coli* were detected in 1.6% (4/245) of samples. All isolates carried *tet*(X4) and exhibited an MDR phenotype. WGS revealed that *tet*(X4) was located on IncY (n=1) and IncFIA8-IncHI1/ST17 plasmids (n=3), which closely resembled previously described plasmids and co-harbored additional resistance genes. The core *tet*(X4)-carrying region in all four plasmids, associated with IS*CR2*, was highly similar to that of p47EC—the first *tet*(X4)-bearing plasmid identified in porcine *E. coli* in China. Notably, the three IncFIA-IncHI1/ST17 plasmids shared an identical 12,536-bp region structured as IS*1*–*catD*–*tet*(X4)–IS*CR2*–ΔIS*CR2*–*floR*–ΔIS*CR2*. Virulence-associated genes involved in adhesion, iron acquisition, biofilm formation, and secretion systems were also identified in four *tet*(X4)-positive isolates. The four isolates belonged to globally distributed sequence types ST10, ST201, ST877, and ST1308. Phylogenomic analysis demonstrated close genetic relatedness between these community isolates and strains from diverse geographical regions and hosts.

Conclusions: This study reveals silent intestinal colonization by *tet*(X4)-positive MDR *E. coli* among healthy urban residents, highlighting the role of community reservoirs in the dissemination of last-resort antibiotic resistance. These findings underscore the urgent need for One Health-oriented antimicrobial resistance surveillance and intervention strategies that extend beyond clinical settings.

KEYWORDS

community, healthy carriers, tigecycline resistance, *E. coli*, plasmids

Introduction

Tigecycline, a 9-t-butylglycylamido derivative of minocycline, is a glycylcycline antibiotic that inhibits bacterial protein synthesis by binding to the 30S ribosomal subunit (Yaghoubi et al., 2021). This mechanism allows tigecycline to evade traditional tetracycline resistance determinants, making it as a last-resort therapeutic agent for infections caused by multidrug-resistant (MDR) pathogens (Yaghoubi et al., 2021). However, the increasing emergence of tigecycline resistance is compromising its clinical utility.

Of particular concern is the *tet*(X) family of flavin-dependent monooxygenase genes, which inactivate tigecycline through enzymatic degradation (Aminov, 2021). Among them, the plasmid-mediated *tet*(X4), first identified in *Escherichia coli* from swine, confers high-level tigecycline resistance and facilitates horizontal gene transfer across diverse bacterial hosts and ecological inches (He et al., 2019). The widespread detection of *tet*(X4) in both clinical and agricultural settings, particularly among *E. coli* strains, underscores its growing public health threat (Li et al., 2023).

Although *tet*(X4)-positive *E. coli* has been increasingly reported in food-producing animals—a trend linked to the historical and extensive use of tetracyclines in agriculture—as well as in food products, and human patients (Aminov, 2021; Li et al., 2023), data on its carriage in healthy human populations, especially in community settings, remain limited (Ding et al., 2020, 2024; Dong et al., 2021). The human gut microbiota serves as a significant but underexplored reservoir for antimicrobial resistance genes (ARGs) (Carlet, 2012; Donskey, 2004). Within this niche, horizontal gene transfer can facilitate the dissemination of resistance determinants across environmental, zoonotic, and clinical bacterial populations (McInnes et al., 2020). While antimicrobial misuse and overuse are known drivers of resistance emergence (Allcock et al., 2017; Ferrara et al., 2024), it remains unclear whether AGRs, such as *tet*(X4), can persist or evolve in community-dwelling individuals without direct antibiotic exposure. This uncertainty is particularly relevant given that tetracyclines are poorly metabolized and can persist in the environment, potentially exerting low-level selective pressure through dietary or environmental exposure, even in the absence of clinical antibiotic use (Allcock et al., 2017).

Given the potential role of asymptomatic carriers in the silent spread of tigecycline resistance, enhanced surveillance of *tet*(X4) in healthy populations is urgently needed. In this study, we investigated tigecycline-resistant *E. coli* isolated from fecal samples of 245 asymptomatic adults residing in three urban communities in Shenzhen, China. Our objectives were to assess the prevalence of tigecycline resistance, characterize the genetic and plasmid features of *tet*(X4)-positive strains, and explore potential epidemiological links to clinical and agricultural sources. These findings offer important insight into the community-level dissemination of tigecycline resistance and highlight the need to broaden antimicrobial resistance (AMR) surveillance beyond clinical settings.

Materials and methods

Bacterial isolation and detection of the *tet*(X) gene

In October 2022, 245 fecal samples were obtained from healthy individuals aged 16 to 79 years, who had no self-reported symptoms of acute infection (e.g., diarrhea, fever, respiratory or urinary tract infections), no history of hospitalization or surgery in the past three months, and no antibiotic use within the preceding three months, across three residential communities in Shenzhen to investigate the prevalence of tigecycline-resistant *Enterobacteriaceae* (Supplementary Table S1). Samples were directly inoculated into LB broth and incubated at 37°C for 12–18 h for enrichment. Enriched cultures were then streaked onto LB agar plates containing 2 μg/mL tigecycline and incubated at 37°C for 12–18 h. Presumptive colonies were purified by subculturing, and bacterial species were identified using the VITEK-2 automated microbial identification system (bioMérieux, Lyon, France). The presence of the *tet*(X) gene was screened by PCR and Sanger sequencing using universal primers *tet*(X)-F (5′-CCGTTGGACTGACTATGGC-3′) and *tet*(X)-R (5′-TCAACTTGCGTGTCGGTAA-3′), as previously described (Wang et al., 2019).

Antimicrobial susceptibility testing

Antimicrobial susceptibility profiles were determined using the broth microdilution or the agar dilution method according to the

guidelines of the Clinical and Laboratory Standards Institute (CLSI). Minimum inhibitory concentrations (MICs) were assessed for 14 antibiotics: ampicillin, cefotaxime, meropenem, gentamicin, amikacin, streptomycin, tetracycline, tigecycline, chloramphenicol, nalidixic acid, ciprofloxacin, colistin, fosfomycin, and sulfamethoxazole-trimethoprim. MIC breakpoints for streptomycin and tigecycline were interpreted based on the European Committee on Antimicrobial Susceptibility Testing (EUCAST) criteria (https://www.eucast.org/), while those for other agents followed the 33rd edition of the CLSI document M100 (CLSI, 2023). *E. coli* ATCC 25922 was used as the quality control strain.

Conjugation assay

To assess the horizontal transferability of the *tet*(X4) gene, conjugation experiments were performed using *tet*(X)-positive isolates as donor strains and a high-level streptomycin-resistant *E. coli* strain C600 as the recipient. Briefly, donor and recipient strains were separately cultured in 2 mL LB broth at 37 with shaking (180 rpm) for 4 h, mixed at a 1:4 (v/v) ratio and incubated statically for 24 h. The cultures were then centrifuged at 5,000 × g for 5 min, the supernatant discarded, and the pellet resuspended in sterile PBS. Appropriate dilutions (100 µL) were plated on selective agar containing tigecycline (2 mg/mL) and streptomycin (3000 mg/mL) to select for transconjugants. Colonies were incubated at 37°C for 16–24 h and confirmed as transconjugants by PCR detection of the *tet*(X) gene as described above. All experiments were performed in triplicate.

Whole-genome sequencing and bioinformatics analysis

The same DNA extraction protocol was applied to both Illumina and Nanopore sequencing to ensure data consistency and comparability. Genomic DNA was extracted from *E. coli* isolates using the PureLink Genomic DNA Mini Kit (Invitrogen, USA). Short-read sequencing libraries were prepared using the Illumina NovoSeq PE150 platform (2×150 bp paired-end), while long-read sequencing was performed using the Oxford Nanopore MinION platform (Oxford Nanopore Technologies, UK). Hybrid genome assemblies were generated using Unicycler (v 0.5.0) (Wick et al., 2017) and subsequently corrected with Pilon (v 1.24) (Walker et al., 2014). Plasmid replicon types were identified using PlasmidFinder (Carattoli et al., 2014), and antibiotic resistance genes, including chromosomal mutations mediating resistance, were annotated using ResFinder (Bortolaia et al., 2020) and PointFinder (Zankari et al., 2017). Multilocus sequence typing (MLST) were assigned via MLST analysis (Larsen et al., 2012). Virulence factors were identified using ABRicate v0.8 with the VFDB database (updated October 2020). Comparative analysis of *tet*(X)-carrying plasmids and related plasmids was performed and visualized using BRIG (Alikhan et al., 2011).

A phylogenetic tree based on core genome single nucleotide polymorphism (cgSNP) was constructed using Parsnp v1.5.4 (https://github.com/marbl/parsnp) and visualized with iTOL (https://itol.embl.de/index.shtml). Our *tet*(X4)-positive *E. coli* isolate served as the reference genome for phylogenetic tree construction. To identify relevant strains, we retrieved *E. coli* isolates of the same ST from the NCBI database. cgSNP distances between the isolates sharing the same ST were calculated using Snippy v4.6.0 (https://github.com/tseemann/snippy), and only those with ≤200 SNPs relative to the reference were included in the final phylogenetic analysis.

Nucleotide sequence accession number

The whole-genome sequences of the four *tet*(X4)-positive isolates have been deposited in GenBank under accession number: PRJNA1288486.

Results

Prevalence of tigecycline-resistant *E. coli* isolates in healthy individuals

Tigecycline-resistant Enterobacteriaceae were identified in 4 out of 245 fecal samples collected from healthy individuals, yielding a prevalence rate of 1.63%. All isolates were confirmed as *E. coli* by both the VITEK2 automated identification system. PCR amplification and Sanger sequencing verified the presence of the *tet*(X4) gene in all four isolates. Notably, three isolates (SZ22HTE1, SZ22HTE2, and SZ22HTE3) were recovered from individuals residing in the same community (Dawang), whereas the fourth isolate (SZ22HTE4) originated from a separate community (Fenghua).

Phenotypic and genotypic characterization of antimicrobial resistance

All four *E. coli* isolates exhibited resistance to tigecycline, with MICs ranging from 8 to 32 mg/L (Supplementary Table S2). They also displayed resistance to multiple antibiotics, including ampicillin, streptomycin, tetracycline, and chloramphenicol (Table 1). Additionally, three isolates (SZ22HTE1–SZ22HTE3) were resistant to sulfamethoxazole/trimethoprim, whereas SZ22HTE4 remained susceptible. In contrast, all isolates were susceptible to cefotaxime, meropenem, gentamicin, amikacin, nalidixic acid, ciprofloxacin, colistin, and fosfomycin (Supplementary Table S2). According to the standard definition—resistance to at least one agent in three or more antimicrobial classes—all isolates were classified as multidrug-resistant (MDR).

WGS identified resistance genes that largely correlated with phenotypic profiles (Table 1). The presence of *tet*(X4), previously confirmed by PCR and Sanger sequencing, was further validated by WGS, explaining the observed tigecycline resistance. Additional tetracycline resistance genes, including *tet*(A), *tet*(B), and *tet*(M), were variably present and matched the tetracycline-resistant

10.3389/fcimb.2025.1667196

phenotypes. All isolates carried bla_{TEM-1B}, consistent with ampicillin resistance, and aminoglycoside resistance genes (*aadA1*, *aadA2*, *aadA22*, and *strA*/*strB*) aligned with streptomycin resistance. Resistance to chloramphenicol was associated with *cmlA1* and/or *floR*.

The plasmid-mediated quinolone resistance gene *qnrS1* was identified in all isolates, but no chromosomal mutations were found within the quinolone resistance-determining region, consistent with their susceptibility to fluoroquinolones. Sulfonamide resistance genes (*sul2*, *sul3*) and the trimethoprim resistance gene *dfrA12* were found only in SZ22HTE1–SZ22HTE3, in agreement with their resistance to sulfamethoxazole/trimethoprim. Additionally, all isolates harbored macrolide-lincosamide resistance genes *lnu*(G) and/or *erm*(42).

Virulence gene profiles of *tet*(X4)-positive *E. coli* isolates

All four *E. coli* isolates harbored multiple virulence-associated genes involved in adhesion, iron acquisition, biofilm formation, motility, and secretion systems, which are critical for bacterial colonization and pathogenicity (Table 2). Adhesion genes such as *fimH*, *ehaB*, *upaG*/*ehaG*, *csgG*, and *cgsF* were variably distributed among the isolates, supporting host cell attachment. Iron acquisition genes, including *entE*, *fepD*, *entC*, *fepG*, *fepC*, and *entB*, were also detected in a strain-specific manner, enabling iron scavenging essential for survival in host environments. The toxin gene *hlyE*/*clyA*, identified only in SZ22HTE1, may contribute to host cell lysis and tissue damage.

Gene associated with biofilm formation (*agn43*, *cah*, and *cgsG*) were detected in SZ22HTE1 to SZ22HTE3 and may enhance persistence and immune evasion. Motility-related genes (*flhA*, *flhB*, and *fliA*) were present in the same three isolates, likely facilitating bacterial movement and invasion. Secretion system genes (*aec27*/*clpV*, *aec15*, *tssM*, *espX4*, *espX1*, and *espX5*) were identified in various combinations across all four isolates and may facilitate the delivery of virulence factors into host cells (Table 2). Although the specific virulence gene profiles varied among isolates, each strain possessed multiple functional categories of virulence factors, underscoring their potential to cause clinically relevant infections.

Characterization of the *tet*(X4)-carrying plasmid in *E. coli* strains

All four isolates carried multiple plasmids with diverse replicon types and antimicrobial resistance genes (Supplementary Table S3). In strain SZ22HTE1, the *tet*(X4) gene was located on the largest plasmid, pSZ22HT1-1 (IncY, 106,177 bp), which also harbored 11 additional resistance genes bla_{TEM-1B}, *aadA1*, *aadA2*, *tet*(A), *tet*(M), *cmlA1*, *floR*, *sul2*, *sul3*, *dfrA12*, and *erm*(42). The *tet*(X4)-carrying IncY plasmid pSZ22HT1–1 exhibited high sequence similarity (>99.9%) to plasmid p803Rt_IncX1 (CP080067) isolated from a human-derived *E. coli* strain in Shenzhen, China with 94%

TABLE 1 Characterization of tigecycline-resistant *Escherichia coli* isolates in this study.

Strain	ST	Resistance patterns	Resistance genes	Location of tet(X4)
SZ22HTE1	201	AMP/STR/TET/TIL/CHL/SXT	bla_{TEM-1B}, *aadA1*, *aadA2*, *tet*(X4), *tet*(A), *tet*(M), *cmlA1*, *floR*, *qnrS1*, *sul2*, *sul3*, *dfrA12*, *erm*(42)	pSZ22HTE1-1 (IncY, 106,177 bp)
SZ22HTE2	877	AMP/STR/TET/TIL/CHL/SXT	bla_{TEM-1B}, *aadA1*, *aadA2*, *aadA22*, *strA*, *strB*, *tet*(X4), *tet*(B), *cmlA1*, *floR*, *qnrS1*, *sul3*, *dfrA12*, *lnu*(G)	pSZ22HTE2-1 (IncFIA8-IncHI1/ST17, 190,711 bp)
SZ22HTE3	10	AMP/STR/TET/TIL/CHL/SXT	bla_{TEM-1B}, *aadA2*, *aadA22*, *tet*(X4), *tet*(A), *floR*, *qnrS1*, *sul3*, *dfrA12*, *lnu*(G)	pSZ22HTE3-1 (IncFIA8-IncHI1/ST17, 201,009 bp)
SZ22HTE4	1308	AMP/STR/TET/TIL/CHL	bla_{TEM-1B}, *aadA22*, *tet*(X4), *tet*(A), *tet*(M), *floR*, *qnrS1*, *lnu*(G), *erm*(42)	pSZ22HTE4-1 (IncFIA8-IncHI1/ST17, 192,057 bp)

AMP, Ampicillin; STR, Streptomycin; TET, Tetracycline; TIL, Tigecycline; CHL, Chloramphenicol; SXT, Trimethoprim-sulfamethoxazole.

TABLE 2 Virulence genes of tigecycline-resistant *Escherichia coli* isolates in this study.

Strain	Adhesion	Iron Acquisition	Toxins	Biofilm	Motility	Secretion System
SZ22HTE1	*fimH*	*entE*, *fepD*	*hlyE*/*clyA*	*agn43*, *cah*	*flhA*, *ta*	*aec27*/*clpV*, *aec15*, *tssM*
SZ22HTE2	*ehaB*, *upaG*/*ehaG*	*entC*, *fepG*, *fepC*	–	*cgsG*	*flhB*	*clpV*, *espX4*
SZ22HTE3	*upaG*/*ehaG*, *csgG*, *cgsF*	*entB*	–	*cgsG*	*fliA*	*clpV*, *espX1*
SZ22HTE4	*upaG*/*ehaG*	*entE*, *entC*	–	–	–	*aec27*/*clpV*, *tssM*, *espX5*

coverage, and plasmid p13Q15 (ON934549) from an *E. coli* strain in Guangdong, China with 53% coverage (Figure 1A).

The remaining three isolates (SZ22HTE2, SZ22HTE3, and SZ22HTE4) each carried a *tet*(X4)-positive hybrid IncFIA8-IncHI1/ST17 plasmid, designated pSZ22HT2-1 (190,711 bp), pSZ22HT3-1 (201,009 bp), and pSZ22HT4-1 (192,057 bp), respectively. These plasmids also carried resistance genes $bla_{\text{TEM-1B}}$, *aadA22*, *qnrS1*, and *floR*. Comparative genomic analysis revealed that the *tet*(X4)-bearing IncFIA8-IncHI1/ST17 plasmids from SZ22HTE2, SZ22HTE3, and SZ22HTE4 were closely related to multiple plasmids, including *tet*(X4)-carrying plasmids p812A1-tetX4-193K (CP116047, *E. coli*, China), pYUGZP1-tetX (pig, *E. coli*, China) from pig source, and pTetX4_FZT33 (CP132725, *E. coli*, China) from hospital sewage (Figure 1B).

However, conjugation assays using *E. coli* C600 as the recipient strain failed to produce transconjugants under the tested conditions, indicating that these *tet*(X4)-bearing plasmids were either non-conjugative or required specific conditions or helper plasmids for mobilization.

Variation in the genetic environment of *tet*(X4)

As shown in Figure 2, the *tet*(X4) gene in the three IncFIA-IncHI1/ST17 plasmids (pSZ22HT2-1, pSZ22HT3-1, and pSZ22HT4-1) was embedded in an identical 12,536-bp region organized as IS*1*–*catD*–*tet*(X4)–IS*CR2*–ΔIS*CR2*–*floR*–ΔIS*CR2*. While the core *tet*(X4)-containing structure closely resembled that of p47EC, the first reported *tet*(X4)-bearing plasmid isolated from *E. coli* of porcine origin in China (He et al., 2019), several notable differences were observed. Most prominently, IS*CR2* replaced the upstream IS*1* element in p47EC. Furthermore, the chloramphenicol resistance gene *floR*, associated with an incomplete IS*CR2*, was located downstream of the *tet*(X4) structure in our plasmids, in contrast to its upstream position in p47EC.

Plasmid pSZ22HTE1–1 exhibited a different but related arrangement. It retained the conserved IS*CR2*–*catD*–*tet*(X4)–IS*CR2* structure found in p47EC, but its upstream region contained an additional resistance module carrying both *floR* and *erm*(42). In comparison, p47EC carried the ΔIS*CR2*-*erm*(42)-IS*Pa99* segment upstream of the *tet*(X4) conserved segment, but in the opposite orientation. These structural variations underscore the genetic plasticity of *tet*(X4)-associated regions and their potential for mobilization and dissemination across diverse plasmid backgrounds driven by mobile genetic elements.

Phylogenomic analysis of *tet*(X4)-positive *E. coli* strains

Four *tet*(X4)-positive *E. coli* isolates in this study were assigned to four sequence types (STs): ST10, ST201, ST877, and ST1308. To investigate the genetic relatedness between these *E. coli* isolates and publicly available *E. coli* strains of the same ST, we conducted a phylogenomic analysis based on cgSNPs. The resulting phylogeny revealed that our community-derived isolates were closely related to *E. coli* strains from diverse geographical regions and hosts (Figure 3).

Our *tet*(X4)-positive ST201 isolate (SZ22HTE1) exhibited high genetic similarity to three human clinical ST201 isolates from China (GCA_023516055.1, GCA_019880025.1, and GCA_030325125.1), differing by only 14–25 SNPs and carrying identical or similar antimicrobial resistance genes, suggesting a potential epidemiological link (Figure 3A). SZ22HTE1 also showed relatively limited divergence (105 and 136 SNPs) from *E. coli* strains of porcine (GCA_037105215.1, Spain), food (GCA_037106035.1, Thailand), and clinical (GCA_028636665.1, China) origin (Figure 3A), further indicating potential inter-host and inter-regional transmission.

Our ST10 *tet*(X4)-positive isolate, SZ22HTE3, clustered with nine ST10 *E. coli* isolates from diverse countries and sources. It was most closely related (41 SNPs) to an environmental isolate from South Africa. In contrast, it differed from the remaining eight isolates by 142–199 SNPs, suggesting a certain level of genomic divergence among ST10 isolates (Figure 3B). For ST1308, five isolates, including our community-derived strain SZ22HTE4, formed a tight phylogenetic cluster with minimal genetic SNP differences of only 58 or 63, suggesting recent common ancestry or possible transmission events. Among the four closely related isolates, three were isolated from swine in China (GCA_022538875.1, GCA_022538895.1, GCA_022538855.1), and one had an unreported source (GCA_023272775.1) (Figure 3C). By comparison, the ST877 lineage exhibited greater genetic heterogeneity. Compared with our *tet*(X4)-positive ST877 isolate (SZ22HTE2), the other 16 ST877 *E. coli* isolates displayed broader genomic divergence, with SNP differences ranging from 100 to 200, highlighting higher diversity within this ST (Figure 3D).

Discussion

Since its approval by the U.S. Food and Drug Administration in 2005, tigecycline has served a last-resort antibiotic for the treatment of severe infections caused by MDR bacteria, particularly carbapenem-resistant *Enterobacteriaceae* (Yaghoubi et al., 2021).

10.3389/fcimb.2025.1667196

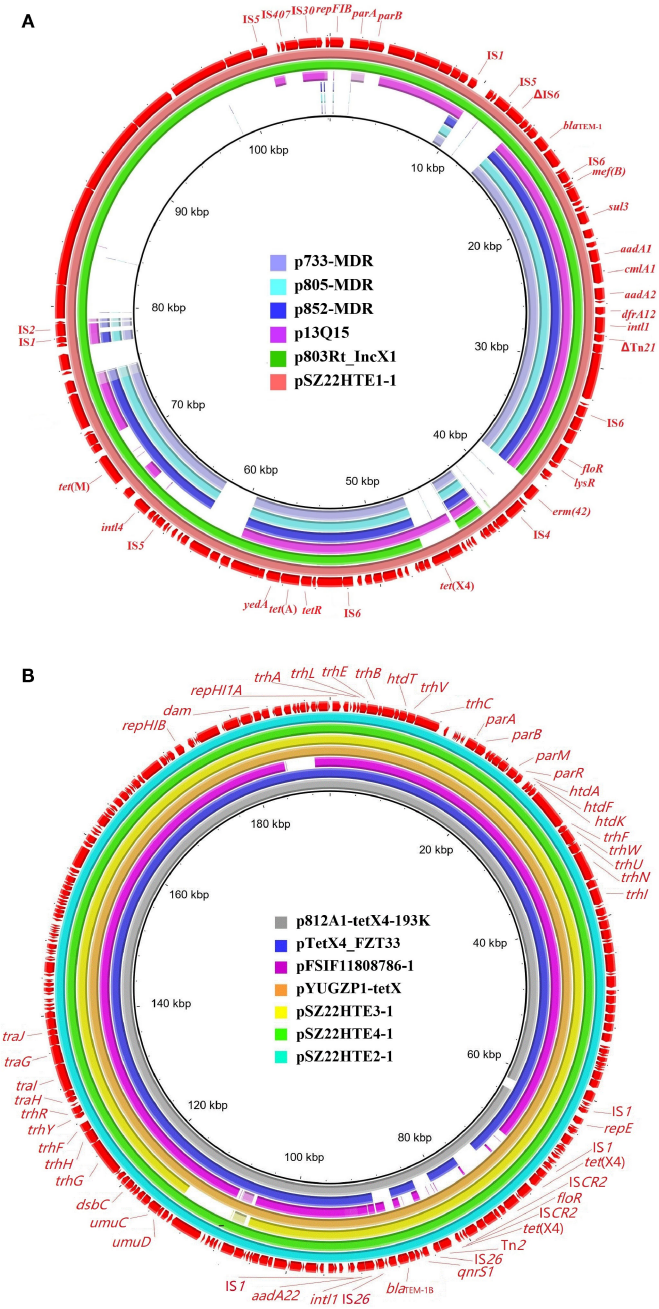

FIGURE 1
Sequence comparison of *tet*(X4)-bearing plasmids in this study with other similar plasmids using BRIG. **(A)** IncY plasmid pSZ22HTE1-1; **(B)** IncFIA8-IncHI1/ST17 plasmids pSZ22HTE2-1, pSZ22HTE3-1, and pSZ22HTE4-1. The outer circles in red with annotation are the reference plasmids pSZ22HTE1–1 and pSZ22HTE2-1, respectively.

However, the growing prevalence of tigecycline resistance has become a significant clinical and public health concern. Among the known resistance mechanisms, the plasmid-mediated *tet*(X4) gene has gained particular attention due to its ability to confer high-level tigecycline resistance and its rapid dissemination across bacterial species and ecological niches through horizontal gene transfer (Dong et al., 2021; He et al., 2019; Li et al., 2023).

Globally, *tet*(X4)-carrying *E. coli* strains have been detected in clinical, animal, food, and environmental settings (Li et al., 2023). However, their presence in healthy human populations, particularly in urban communities, remains insufficiently characterized. Our study identified a *tet*(X4)-positive *E. coli* colonization rate of 1.6% (4/245) in fecal samples from healthy individuals in Shenzhen, a densely populated metropolitan area. Although this prevalence is considerably lower than that observed in animal-derived (18.24%) and food-derived (20.6%) *E. coli* isolates, it exceeds the rates reported in clinical patients (0.07–0.1%) (Bai et al., 2019; He et al., 2019; Li et al., 2021), suggesting that the human gut may serve as a previously

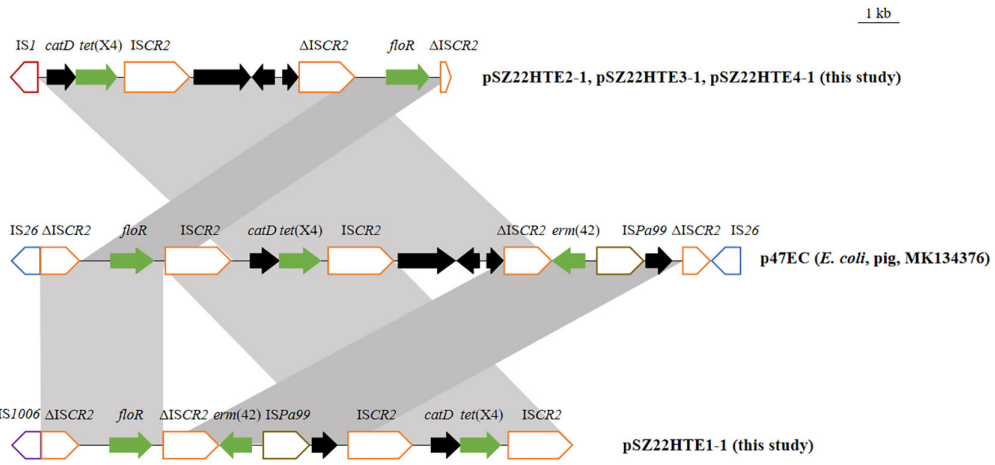

FIGURE 2
Genetic structures of the *tet*(X4) gene in this study and comparison with p47EC (MK134376). The extent and directions of genes are indicated by arrows. Antibiotic resistance genes are shown in red. Truncated mobile elements are marked with a "Δ" symbol. Insertion sequences (ISs) are represented as boxes labeled with their names. Regions with >99% identity are shaded in gray.

underappreciated reservoir for plasmid-mediated tigecycline resistance. These findings highlight the necessity of enhanced AMR surveillance in non-clinical community populations to detect early signs of resistance dissemination.

AMR is an escalating global health crisis, contributing to an estimated 30,000 deaths annually in the EU and nearly 5 million worldwide in 2019 (Cassini et al., 2019; Ho et al., 2025). The human gastrointestinal tract, comprising a dense and diverse microbial community (~10^{14} cells across approximately 1, 000 bacterial species), is a hotspot for the acquisition, persistence, and horizontal transfer of ARGs (Despotovic et al., 2023; Lynch and Pedersen, 2016). The gut microbiome not only reflects the local AMR burden but also influences patient outcomes, particularly in critically ill individuals with gut barrier dysfunction or acute gastrointestinal injury, where microbiome disruption and elevated ARG levels are associated with worse clinical outcomes (Bai et al., 2025). Notably, *E. coli*, a core member of the intestinal microbiota and a widely used sentinel organism in AMR surveillance, readily acquires ARGs from food, animal, and environmental sources, and can transfer them to pathogenic bacteria such as *Shigella* and *Klebsiella* through plasmids or other mobile genetic elements (Thanh Duy et al., 2020). In our study, three isolates (SZ22HTE2, SZ22HTE3, and SZ22HTE4) harbored the epidemic IncFIA8-IncHI1/ST17 plasmid carrying *tet*(X4), suggesting early-stage horizontal dissemination of tigecycline resistance within the community gut microbiota of an urban community. These plasmids co-harbored additional resistance genes, resulting in MDR phenotypes and enabling co-selection and persistence in diverse hosts (Lu et al., 2018; Yan et al., 2024). Notably, the epidemic IncFIA8-IncHI1/ST17 plasmid identified in this study shows high homology to pRDZ41 (CP139495.1) from *Klebsiella pneumoniae*, providing direct evidence for its potential to disseminate *tet*(X4) into this high-risk pathogen.

Importantly, these *E. coli* isolates possessed a range of virulence-associated genes related to adhesion (e.g., *fimH*, *ehaB*, *upaG*/*ehaG*), iron acquisition (e.g., *entE*, *fepD*), biofilm formation (e.g., *agn43*, *cah*), motility (e.g., *flhA*, *fliA*), and secretion systems (e.g., *aec27*/*clpV*, *tssM*). The coexistence of virulence factors and resistance determinants in community-derived *E. coli* is particularly alarming, as it increases the risk of difficult-to-treat infections and facilitates ARG dissemination into high-risk clinical pathogens.

Although the healthy human gut microbiota may provide colonization resistance against invasive AMR bacteria—potentially via mechanisms such as microbiome-mediated nutrient depletion (Isaac et al., 2022; Le Guern et al., 2021)—our findings underscore the vulnerability of even healthy individuals to colonization by plasmid-mediated tigecycline-resistant *E. coli* strains. This silent carriage may act as a hidden conduit for ARG dissemination between community and healthcare environments, presenting significant challenges for infection prevention and control.

WGS further revealed that our *tet*(X4)-positive isolates belonged to globally prevalent *E. coli* STs, e.g., ST10, ST877, and ST1308, frequently associated with MDR phenotypes and detected in both human and animal hosts (Elias et al., 2019; García et al., 2018; Liu et al., 2024). The detection of these epidemic STs in healthy individuals, along with their close genetic relatedness to isolates from clinical, food, animal, and the environmental sources, reinforces a One Health perspective. Phylogenomic analysis demonstrated close genetic relatedness between our community isolates and strains from diverse geographic regions and hosts (e.g., swine, food, environment), reinforcing the role of cross-sectoral transmission in the spread of *tet*(X4). This underscores the interconnectedness of AMR reservoirs across ecosystems and highlights the urgent need for integrated, cross-sectoral genomic surveillance.

Despite the valuable insights provided, this study has several limitations. Only three urban communities were sampled, and the number of *tet*(X4)-positive isolates was relatively small, limiting the generalizability of our findings. Additionally, although the plasmid

FIGURE 3
Core-genome SNP phylogeny of four *tet*(X4)-positive *E. coli* isolates (in red) with the same ST strains with ≤200 SNPs. **(A)** ST201; **(B)** ST10; **(C)** ST1308; **(D)** ST877. Branch lengths indicate SNP distances; key ARGs are annotated.

structures were well-characterized, functional studies such as assessing plasmid transfer under different conditions or colonization capacity *in vivo* were not performed. The observed lack of successful conjugation *in vitro* highlights the need for further investigation into the mobility mechanisms of *tet*(X4)-bearing plasmids. Further studies should explore whether these plasmids can successfully conjugate by employing diverse recipient strains, co-introducing helper plasmids, or optimizing mating conditions (e.g., modifying incubation temperature, adjusting donor-to-recipient ratios, or using filter mating assays) under alternative experimental settings. Importantly, future investigations should include larger-scale, longitudinal surveillance, and mechanistic assessments to better understand the dynamics and risks of *tet* (X4)-positive *E. coli* colonization in healthy populations.

Conclusion

In summary, our findings highlight the emergence of *tet*(X4)-positive MDR *E. coli* in the intestinal microbiota of healthy

individuals from urban communities. These isolates co-harbored multiple ARGs and virulence determinants, highlighting their potential to cause difficult-to-treat infections and to act as reservoirs for further resistance dissemination. The detection of globally circulating high-risk clones such as ST10 and ST201 in asymptomatic carriers underscores the silent spread of tigecycline resistance in non-clinical settings. These findings call for urgent and coordinated surveillance strategies beyond hospital environments, in alignment with One Health principles, to contain the spread of last-resort antibiotic resistance and safeguard public health.

Data availability statement

The datasets presented in this study can be found in online repositories. The names of the repository/repositories and accession number(s) can be found in the article/Supplementary Material.

Ethics statement

Ethical approval for human sample collection was obtained from the Shenzhen University Ethics Committee (Reference No. PN-202400026), in compliance with guidelines approved by an independent ethics board comprising non-institutional legal representatives and community stakeholders. The studies were conducted in accordance with the local legislation and institutional requirements. Written informed consent for participation was not required from the participants or the participants' legal guardians/next of kin. Regarding informed consent to participate, this study exclusively utilized anonymized residual pathogen samples obtained from routine clinical diagnostics. These samples were irreversibly de-identified prior to research use, with all personal identifiers (including but not limited to patient names, demographic data, medical records, and clinical history) removed. Only numerical laboratory tracking codes were retained. This research qualified for exemption from informed consent requirements under Clause [Specify Clause Number/Type, e.g., Article 39] of the Ethical Review Measures for Biomedical Research Involving Human Subjects (中国涉及人的生物医学研究伦理审查办法 https://www.gov.cn/zhengce/2016-10/12/content_5713806.htm), as it meets all criteria for exemption: 1. Non-linkability: Samples were completely unlinked from any identifiable individuals; 2.No Additional Risk: The research posed no additional physical, psychological, or social risks to the original providers; The study protocol and this exemption were formally reviewed and approved by the Medical Ethics Committee of Shenzhen University Health Science Center (SUHSC-MEC), with approval number PN-202400026. The committee confirmed that the secondary use of these irreversibly anonymized specimens falls under exempt ethical review categories. We have revised the manuscript's "Ethics approval and consent to participate" section to clearly state: "Informed consent to participate was not required for this study as it exclusively utilized irreversibly anonymized residual pathogen samples obtained from routine clinical diagnostics. These samples contained no personally identifiable information. This exemption complies with the Ethical Review Measures for Biomedical Research Involving Human Subjects [Reference Number] and was approved by the Medical Ethics Committee of Shenzhen University Health Science Center (PN-202400026).".

Author contributions

RP: Validation, Data curation, Investigation, Writing – review & editing. PL: Conceptualization, Investigation, Writing – review & editing. WJ: Writing – review & editing, Methodology, Data curation. ZL: Validation, Writing – review & editing, Visualization. LW: Data curation, Writing – review & editing, Resources. YH: Writing – review & editing, Visualization. XZ: Writing – review & editing, Investigation. YG: Writing – review & editing, Validation. YW: Software, Writing – review & editing. JW: Writing – review & editing. JG: Validation, Writing – review & editing, Supervision. FY: Data curation, Conceptualization, Project administration, Writing – review & editing, Supervision. DL: Conceptualization, Writing – original draft, Methodology, Funding acquisition.

Funding

The author(s) declare financial support was received for the research and/or publication of this article. This study was supported in part by Guangdong Basic and Applied Basic Research Foundation (2024A1515030195, No. 2023A1515012152 and No. 2022A1515110369), Hainan Provincial International Science and Technology Cooperation Research and Development Project (GHYF2024021), the National Natural Science Foundation of China (82060378), Major Project of Guangzhou National Laboratory (GZNL2023A01001).

Conflict of interest

The authors declare that the research was conducted in the absence of any commercial or financial relationships that could be construed as a potential conflict of interest.

Generative AI statement

The author(s) declare that Generative AI was used in the creation of this manuscript. The authors verify and take full responsibility for the limited use of generative AI in the preparation of this manuscript. Generative AI tools were used exclusively for grammatical refinement and sentence structure optimization to enhance clarity. All scientific content, data interpretation, conclusions, and writing remain the original work of the authors. No AI was used to generate results, analysis, or critical intellectual contributions.

Any alternative text (alt text) provided alongside figures in this article has been generated by Frontiers with the support of artificial intelligence and reasonable efforts have been made to ensure accuracy, including review by the authors wherever possible. If you identify any issues, please contact us.

Publisher's note

All claims expressed in this article are solely those of the authors and do not necessarily represent those of their affiliated organizations, or those of the publisher, the editors and the reviewers. Any product that may be evaluated in this article, or claim that may be made by its manufacturer, is not guaranteed or endorsed by the publisher.

Supplementary material

The Supplementary Material for this article can be found online at: https://www.frontiersin.org/articles/10.3389/fcimb.2025.1667196/full#supplementary-material

References

Alikhan, N. F., Petty, N. K., Ben Zakour, N. L., and Beatson, S. A. (2011). BLAST Ring Image Generator (BRIG): simple prokaryote genome comparisons. *BMC Genomics* 12, 402. doi: 10.1186/1471-2164-12-402

Allcock, S., Young, E. H., Holmes, M., Gurdasani, D., Dougan, G., Sandhu, M. S., et al. (2017). Antimicrobial resistance in human populations: challenges and opportunities. *Glob. Health Epidemiol. Genom.* 2, e4. doi: 10.1017/gheg.2017.4

Aminov, R. (2021). Acquisition and spread of antimicrobial resistance: A *tet*(X) case study. *Int. J. Mol. Sci.* 22, 3905. doi: 10.3390/ijms22083905

Bai, L., Du, P., Du, Y., Sun, H., Zhang, P., Wan, Y., et al. (2019). Detection of plasmid-mediated tigecycline-resistant gene *tet*(X4) in *Escherichia coli* from pork, Sichuan and Shandong Provinces, China, February 2019. *Euro Surveill.* 24, 1900340. doi: 10.2807/1560-7917.ES.2019.24.25.1900340

Bai, Y., Hu, Y., Chen, X., Hu, L., Wu, K., Liang, S., et al. (2025). Comparative metagenome-associated analysis of gut microbiota and antibiotic resistance genes in acute gastrointestinal injury patients with the risk of in-hospital mortality. *mSystems* 10, e0144424. doi: 10.1128/msystems.01444-24

Bortolaia, V., Kaas, R. S., Ruppe, E., Roberts, M. C., Schwarz, S., Cattoir, V., et al. (2020). ResFinder 4.0 for predictions of phenotypes from genotypes. *J. Antimicrob. Chemother.* 75, 3491–3500. doi: 10.1093/jac/dkaa345

Carattoli, A., Zankari, E., García-Fernández, A., Voldby Larsen, M., Lund, O., Villa, L., et al. (2014). In silico detection and typing of plasmids using PlasmidFinder and plasmid multilocus sequence typing. *Antimicrob. Agents Chemother.* 58, 3895–3903. doi: 10.1128/AAC.02412-14

Carlet, J. (2012). The gut is the epicentre of antibiotic resistance. *Antimicrob. Resist. Infect. Control* 1, 39. doi: 10.1186/2047-2994-1-39

Cassini, A., Högberg, L. D., Plachouras, D., Quattrocchi, A., Hoxha, A., Simonsen, G. S., et al. (2019). Attributable deaths and disability-adjusted life-years caused by infections with antibiotic-resistant bacteria in the EU and the European Economic Area in 2015: a population-level modelling analysis. *Lancet Infect. Dis.* 19, 56–66. doi: 10.1016/S1473-3099(18)30605-4

CLSI (2023). *Performance Standards for Antimicrobial Susceptibility Testing. CLSI Supplement M100. 33rd Edn* (Wayne, PA: CLSI).

Despotovic, M., de Nies, L., Busi, S. B., and Wilmes, P. (2023). Reservoirs of antimicrobial resistance in the context of One Health. *Curr. Opin. Microbiol.* 73, 102291. doi: 10.1016/j.mib.2023.102291

Ding, Y., Er, S., Tan, A., Gounot, J.-S., Saw, W.-Y., Tan, L., et al. (2024). Comparison of *tet*(X4)-containing contigs assembled from metagenomic sequencing data with plasmid sequences of isolates from a cohort of healthy subjects. *Microbiol. Spectr.* 12, e0396923. doi: 10.1128/spectrum.03969-23

Ding, Y., Saw, W. Y., Tan, L. W. L., Moong, D. K. N., Nagarajan, N., Teo, Y. Y., et al. (2020). Emergence of tigecycline- and eravacycline-resistant Tet(X4)-producing Enterobacteriaceae in the gut microbiota of healthy Singaporeans. *J. Antimicrob. Chemother.* 75, 3480–3484. doi: 10.1093/jac/dkaa372

Dong, N., Zeng, Y., Cai, C., Sun, C., Lu, J., Liu, C., et al. (2021). Prevalence, transmission, and molecular epidemiology of *tet*(X)-positive bacteria among humans, animals, and environmental niches in China: An epidemiological, and genomic-based study. *Sci. Total Environ.* 818, 151767. doi: 10.1016/j.scitotenv.2021.151767

Donskey, C. J. (2004). The role of the intestinal tract as a reservoir and source for transmission of nosocomial pathogens. *Clin. Infect. Dis.* 39, 219–226. doi: 10.1086/422002

Elias, L., Gillis, D. C., Gurrola-Rodriguez, T., Jeon, J. H., Lee, J. H., Kim, T. Y., et al. (2019). The occurrence and characterization of extended-spectrum-beta-lactamase-producing *Escherichia coli* isolated from clinical diagnostic specimens of equine origin. *Animals* 10, 28. doi: 10.3390/ani10010028

Ferrara, F., Castagna, T., Pantolini, B., Campanardi, M. C., Roperti, M., Grotto, A., et al. (2024). The challenge of antimicrobial resistance (AMR): current status and future prospects. *Naunyn Schmiedebergs Arch. Pharmacol.* 397, 9603–9615. doi: 10.1007/s00210-024-03318-x

García, V., García-Meniño, I., Mora, A., Flament-Simon, S. C., Díaz-Jiménez, D., Blanco, J. E., et al. (2018). Co-occurrence of *mcr-1*, *mcr-4* and *mcr-5* genes in multidrug-resistant ST10 enterotoxigenic and shiga toxin-producing *Escherichia coli* in Spain, (2006-2017). *Int. J. Antimicrob. Agents* 52, 104–108. doi: 10.1016/j.ijantimicag.2018.03.022

He, T., Wang, R., Liu, D., Walsh, T. R., Zhang, R., Lv, Y., et al. (2019). Emergence of plasmid-mediated high-level tigecycline resistance genes in animals and humans. *Nat. Microbiol.* 4, 1450–1456. doi: 10.1038/s41564-019-0445-2

Ho, C. S., Wong, C. T. H., Aung, T. T., Lakshminarayanan, R., Mehta, J. S., Rauz, S., et al. (2025). Antimicrobial resistance: a concise update. *Lancet Microbe* 6, 100947. doi: 10.1016/j.lanmic.2024.07.010

Isaac, S., Flor-Duro, A., Carruana, G., PuChades-Carrasco, L., Quirant, A., Lopez-Nogueroles, M., et al. (2022). Microbiome-mediated fructose depletion restricts murine gut colonization by vancomycin-resistant *Enterococcus*. *Nat. Commun.* 13, 7718. doi: 10.1038/s41467-022-35380-5

Larsen, M. V., Cosentino, S., Rasmussen, S., Friis, C., Hasman, H., Marvig, R. L., et al. (2012). Multilocus sequence typing of total-genome-sequenced bacteria. *J. Clin. Microbiol.* 50, 1355–1361. doi: 10.1128/JCM.06094-11

Le Guern, R., Stabler, S., Gosset, P., Pichavant, M., Grandjean, T., Faure, E., et al. (2021). Colonization resistance against multi-drug-resistant bacteria: a narrative review. *J. Hosp Infect.* 118, 48–58. doi: 10.1016/j.jhin.2021.09.001

Li, Y., Sun, X., Xiao, X., Wang, Z., and Li, R. (2023). Global distribution and genomic characteristics of *tet*(X)-positive *Escherichia coli* among humans, animals, and the environment. *Sci. Total Environ.* 887, 164148. doi: 10.1016/j.scitotenv.2023.164148

Li, Y., Wang, Q., Peng, K., Liu, Y., Xiao, X., Mohsin, M., et al. (2021). Distribution and genomic characterization of tigecycline-resistant *tet*(X4)-positive *Escherichia coli* of swine farm origin. *Microb. Genom.* 7, 667. doi: 10.1099/mgen.0.000667

Liu, Y. Y., Lu, L., Yue, C., Gao, X., Chen, J., Gao, G., et al. (2024). Emergence of plasmid-mediated high-level tigecycline resistance gene *tet*(X4) in *Enterobacterales* from retail aquatic products. *Food Res. Int.* 178, 113952. doi: 10.1016/j.foodres.2024.113952

Lu, J., Zhang, J., Xu, L., Liu, Y., Li, P., Zhu, T., et al. (2018). Spread of the florfenicol resistance *floR* gene among clinical *Klebsiella pneumoniae* isolates in China. *Antimicrob. Resist. Infect. Control* 7, 127. doi: 10.1186/s13756-018-0415-0

Lynch, S. V., and Pedersen, O. (2016). The human intestinal microbiome in health and disease. *N. Engl. J. Med.* 375, 2369–2379. doi: 10.1056/NEJMra1600266

McInnes, R. S., McCallum, G. E., Lamberte, L. E., and van Schaik, W. (2020). Horizontal transfer of antibiotic resistance genes in the human gut microbiome. *Curr. Opin. Microbiol.* 53, 35–43. doi: 10.1016/j.mib.2020.02.002

Thanh Duy, P., Thi Nguyen, T. N., Vu Thuy, D., Chung The, H., Alcock, F., Boinett, C., et al. (2020). Commensal *Escherichia coli* are a reservoir for the transfer of XDR plasmids into epidemic fluoroquinolone-resistant *Shigella sonnei*. *Nat. Microbiol.* 5, 256–264. doi: 10.1038/s41564-019-0645-9

Walker, B. J., Abeel, T., Shea, T., Priest, M., Abouelliel, A., Sakthikumar, S., et al. (2014). Pilon: an integrated tool for comprehensive microbial variant detection and genome assembly improvement. *PloS One* 9, e112963. doi: 10.1371/journal.pone.0112963

Wang, L., Liu, D., Lv, Y., Cui, L., Li, Y., Li, T., et al. (2019). Novel plasmid-mediated *tet*(X5) gene conferring resistance to tigecycline, eravacycline, and omadacycline in a clinical *Acinetobacter baumannii* isolate. *Antimicrob. Agents Chemother.* 64, e01326–e01319. doi: 10.1128/AAC.01326-19

Wick, R. R., Judd, L. M., Gorrie, C. L., and Holt, K. E. (2017). Unicycler: Resolving bacterial genome assemblies from short and long sequencing reads. *PloS Comput. Biol.* 13, e1005595. doi: 10.1371/journal.pcbi.1005595

Yaghoubi, S., Zekiy, A. O., Krutova, M., Gholami, M., Kouhsari, E., Sholeh, M., et al. (2021). Tigecycline antibacterial activity, clinical effectiveness, and mechanisms and epidemiology of resistance: narrative review. *Eur. J. Clin. Microbiol. Infect. Dis.* 5, 1–20. doi: 10.1007/s10096-020-04121-1

Yan, Z., Li, Y., Ni, Y., Xia, X., Zhang, Y., Wu, Y., et al. (2024). Plasmid-borne tigecycline resistance gene *tet*(X4) in *Salmonella enterica* and *Escherichia coli* isolates from a pediatric patient with diarrhea. *Drug Resist. Updat.* 77, 101145. doi: 10.1016/j.drup.2024.101145

Zankari, E., Allesøe, R., Joensen, K. G., Cavaco, L. M., Lund, O., and Aarestrup, F. M. (2017). PointFinder: a novel web tool for WGS-based detection of antimicrobial resistance associated with chromosomal point mutations in bacterial pathogens. *J. Antimicrob. Chemother.* 72, 2764–2768. doi: 10.1093/jac/dkx217

frontiers | Frontiers in Cellular and Infection Microbiology

TYPE Original Research
PUBLISHED 16 October 2025
DOI 10.3389/fcimb.2025.1672468

OPEN ACCESS

EDITED BY
Valerio Baldelli,
University of Milan, Italy

REVIEWED BY
Verónica Mixão,
National Health Institute Doutor Ricardo Jorge (INSA), Portugal
Sonia Aracil-Gisbert,
Instituto Ramón y Cajal de Investigación Sanitaria (IRYCIS), Spain

*CORRESPONDENCE
Wentao Zhu
wentaozhu@126.com
Li Gu
didcm2006@mail.ccmu.edu.cn

RECEIVED 24 July 2025
ACCEPTED 11 September 2025
PUBLISHED 16 October 2025

CITATION
Zhu W, Chen X, Shen H, Wei M, Yang C and Gu L (2025) Genomic diversity, antimicrobial resistance and dissemination of *Serratia marcescens complex* in patients admitted to ICUs.
Front. Cell. Infect. Microbiol. 15:1672468.
doi: 10.3389/fcimb.2025.1672468

Genomic diversity, antimicrobial resistance and dissemination of *Serratia marcescens complex* in patients admitted to ICUs

Wentao Zhu*, Xi Chen, Hong Shen, Ming Wei, Chunxia Yang and Li Gu*

Department of Infectious Diseases and Clinical Microbiology, Beijing Institute of Respiratory Medicine and Beijing Chao-Yang Hospital, Capital Medical University, Beijing, China

Background: *Serratia* spp. is an important nosocomial pathogen, with increasing threat of antimicrobial resistance. We aimed to describe the population structure, antimicrobial resistance and dissemination of *Serratia* isolates in ICUs of China.
Methods: *Serratia* spp. were isolated from patients admitted to ICUs of a large hospital between January 2014 and December 2024. Whole-genome and clinical data were collected to identify their epidemiological and evolutionary characteristics.
Results: 106 *Serratia* isolates was divided into five species based on phylogenomic and ANI analyses, namely *S. sarumanii*, *S. ureilytica*, *S. marcescens*, *S. bockelmannii*, and *S. nevei*. The predominant ST was ST595 (12.3%), followed by ST525 (10.4%) and ST428 (4.7%), all of which belonged to *S. sarumanii*. Based on a 16 SNPs threshold, 15 distinct clusters and 44 singleton strains were identified, with the largest cluster circulating in five different ICUs over the past 11 years. Notably, most grouped isolates within each cluster were isolated from different ICUs, indicative of potential inter-ICU transmission. The unique genes significantly enriched within each species contributed to their niche adaptation and plasticity. Various beta-lactamase genes, such as $bla_{\text{CTX-M}}$ and bla_{OXA}, were detected, along with carbapenemase genes including $bla_{\text{KPC-2}}$ and $bla_{\text{NDM-5}}$ in nine isolates.
Conclusion: These results contribute to understanding the population structure and dissemination of *Serratia* spp. in ICUs, highlighting their ongoing evolution towards increasing resistance and outbreak potential.

KEYWORDS

***Serratia*, genomic surveillance, dissemination, antimicrobial resistance, ICU - intensive care unit**

Introduction

Serratia is a genus of Gram-negative, rod-shaped bacteria belonging to the family *Yersiniaceae* in the order Enterobacteriales (Adeolu et al., 2016). *Serratia* is considered to be

ubiquitous in diverse environments, including water, soil, plants, and insects (Ono et al., 2022). However, it is not a common component of the human fecal microbiome (Bush and Vazquez-Pertejo, 2024). *Serratia* isolates can cause a range of nosocomial infections, including pneumonia, urinary tract infections, bacteremia, meningitis and endocarditis, particularly in immunocompromised patients (Mahlen, 2011). These infections account for about 1% to 2% of hospital-acquired infections (HAIs) and can lead to outbreaks with high morbidity and mortality rates, especially in pediatric or intensive care unit (ICU) wards (Mahlen, 2011; Aracil-Gisbert et al., 2024).

Taxonomically, the genus *Serratia* comprises twenty-four species (https://lpsn.dsmz.de/genus/serratia). *S. marcescens*, the most prevalent opportunistic human pathogen in this genus, frequently causes outbreaks of hospital-associated infections (Khanna et al., 2013; Van Goethem et al., 2024). Other members, such as *S. rubidaea* and *S. liquefaciens*, have also been reported to cause hospital-acquired infections, although less frequently (Dubouix et al., 2005; Karkey et al., 2018). Recently, a new species, *S. sarumanii*, was isolated from a wound swab (Klages et al., 2024). The transmission of some human-associated *Serratia* species via contaminated medical devices, such as nebulizers and catheters, is well known (Mahlen, 2011). However, most studies consist of individual case reports (Williams et al., 2022).

Clinical *Serratia* isolates are typically identified using MALDI-TOF MS (Aracil-Gisbert et al., 2024; Pérez-Viso et al., 2024; Van Goethem et al., 2024; Zhang et al., 2024). However, MALDI-TOF MS struggles to distinguish the species within *Serratia marcescens* complex (SMC), including *S. marcescens*, *S. ureilytica*, *S. bockelmannii* and *S. nematodiphila* (Harch et al., 2025). Furthermore, newly proposed species, such as *S. montpellierensis* (Blackburn et al., 2024) and *S. sarumanii* (Klages et al., 2024), may be sufficiently distinct at the molecular level, yet are not represented in current MALDI-TOF MS databases. Therefore, MALDI-TOF MS cannot reliably differentiate species within the SMC and should be complemented by whole genome sequencing (WGS) for species identification (Harch et al., 2025).

In this work, we aimed to provide a comprehensive understanding of *Serratia marcescens* complex in the ICUs of our hospital over an 11-year period (2014–2024). Based on WGS, we conducted a large-scale precision epidemiology analysis to decipher the evolution of clinical *Serratia marcescens* complex. Additionally, we compared the genomic features, in-hospital transmission patterns, antimicrobial resistance, and clinical characteristics of *Serratia marcescens* complex across different species.

Materials and methods

Study design and bacterial isolates

This retrospective study investigated inpatients infected with *Serratia marcescens* complex at Beijing Chao-Yang Hospital of Capital Medical University, a 2,500-bed public teaching hospital located in the capital of China that receives approximately four million patients per year. The study enrolled *Serratia marcescens* complex isolated from inpatients admitted to the ICUs from January 2014 to December 2024. Firstly, samples from patients suspected of having a bacterial infection were collected and send to the clinical microbiology laboratory for pathogen isolation and identification. The clinical samples included sputum, bronchoalveolar lavage fluid (BLAF), urine, drainage, body fluid, and wound. Suspected isolates that were cultured on China blue agar plates (Product code: HBPM6233, Thermo, USA) were initially identified using MALDI-TOF MS. Secondly, initial inclusion criteria varied across sample types. For non-sterile samples, such as sputum and BLAF, inclusion was only considered when the number of *Serratia marcescens* complex in the sample accounted for the vast majority. For sterile samples, inclusion was only considered when the number of *Serratia marcescens* complex in the sample was higher than 10^5 CFU/mL. Thirdly, the final inclusion criteria required that the patients received the appropriate treatment for the *Serratia marcescens* complex infection, as determined based on their electronic medical records. In total, non-duplicate isolates were mainly recovered from sputum (n = 89), followed by BLAF (n = 6), urine (n = 5), ascites (n = 3), drainage (n = 2), and wound (n = 1).

Antimicrobial susceptibility testing

Antimicrobial susceptibility testing of the bacterial isolates was investigated using the VITEK 2 system (bioMérieux, France) with GN09 cards following the guidelines provided by the Clinical and Laboratory Standards Institute (CLSI, 2025). In addition, the susceptibility of several antimicrobial agents, such as meropenem and imipenem, were determined or confirmed using the Kirby-Bauer method. *Escherichia coli* ATCC 8739 was used as the reference strain for quality control in all procedures. A total of 17 antimicrobial agents were tested, including amikacin (AK), aztreonam (ATM), ceftazidime (CAZ), Ciprofloxacin (CIP), gentamicin (CN), ceftriaxone (CRO), cefepime (FEP), imipenem (IPM), levofloxacin (LEV), meropenem (MEM), minocycline (MH), piperacillin (PRL), cefperazone-sulbactam (SCF), sulfamethoxazole-trimethoprim (SXT), tigecycline (TGC), tobramycin (TOB), and piperacillin-tazobactam (TZP).

Whole-genome sequencing and annotation

The genomic DNA of all bacterial isolates was extracted using Wizard Genomic DNA extraction kits (Promega, Wisconsin, USA) and stored at −80 °C until shipment to the Shanghai Majorbio Biopharm Technology Co., Ltd for whole genome sequencing on an Illumina HiSeq 2500 platform, resulting in a 2×150 bp paired-end library for each isolate. The quality control of raw sequenced reads was conducted as previously reported (Liu et al., 2025), which was used to eliminate sequences with low-quality (Q ≤ 20) and adapters. The clean data obtained was *de novo* assembled to generate draft contigs using SPAdes v4.1.0 (Prjibelski et al., 2020). The gaps of draft contigs were further filled using gapclose v1.12, resulting in

draft genomes (Xu et al., 2020). Whole genome annotation, such as potential open reading frames and their functions, was investigated using Prokka pipeline v1.14.5 (Seemann, 2014). Taxonomic classification was determined using the GTDB Toolkit, which was based on the Genome Database Taxonomy (GTDB) (https://gtdb.ecogenomic.org/). The reference genomes for *S. marcescens*, *S. ureilytica*, *S. nevei*, *S. bockelmannii*, and *S. sarumanii* in the GTDB were GCF_017299535.1, GCF_013375155.1, GCF_008364245.1, GCF_008011855.1, and GCF_001537005.1, respectively. The species of sequenced genome was also identified using the rMLST scheme as previously proposed (Aracil-Gisbert et al., 2024; Harch et al., 2025), which is available at https://pubmlst.org/species-id.

Comparative genomic analysis

The sequence type (ST) of genomes was determined using PubMLST 7-loci schema (https://pubmlst.org/organisms/serratia-spp). Unassigned allele sequences were extracted and submitted to BIGSdb (Jolley and Maiden, 2010), and obtained 47 new STs. The whole-genome average nucleotide identity (ANI) was calculated as previously described (Bonnin et al., 2025), with intra-species strains displaying > 95% ANI. Antimicrobial resistance genes were identified using abricate v1.0.0 based on the NCBI AMRFinderPlus database (Feldgarden et al., 2019). The intrinsic genes were determined according to a previous report (Sandner-Miranda et al., 2018). The identified antimicrobial resistance genes were further classified into drug class based on the Comprehensive Antibiotic Resistance Database (CARD) (Alcock et al., 2020). Virulence genes were screened using abricate v1.0.0 based on virulence factor database (VFDB) with 80% coverage and 80% identity (Chen et al., 2016; Liu and Zhu, 2025; Zhu et al., 2025). The GFF3 format of each genome was obtained from Prokka annoation result and used to conduct core-pan genome analysis using the Roary pipeline v3.12.0 (Page et al., 2015). The *Serratia* core genome was defined by sequences present in ≥ 95% of these genomes as previously reported (Näpflin et al., 2025; Zhu et al., 2025).

Phylogenetic analysis

Single nucleotide polymorphism (SNP) analysis was conducted using Snippy v4.6.0 with default parameters (https://github.com/tseemann/snippy), utilizing the first identified genome (CY27690) from this study as the reference. The core genome alignment was then refined to eliminate elevated densities of base substitutions and recombination events using Gubbins v3.4 (Croucher et al., 2015). The core genome SNP (cgSNP) distance matrix of all paired genomes was calculated using snp-dists (https://github.com/tseemann/snp-dists). Paired genomes differing by no more than 16 SNPs were categorized as possible outbreaks (cluster groups) in the hospital, according to the previously recommended threshold (Chng et al., 2020), and were visualized using Standard Neighbour Joining algorithm of GrapeTree of (https://github.com/achtman-lab/GrapeTree). The maximum likelihood tree, based on core genome alignment, was built using IQtree v2.0.6 (https://github.com/Cibiv/IQ-TREE) and visualized using the Interactive Tree of Life (iTOL) web server (https://itol.embl.de/).

Statistical analysis

The clinical symptoms and demographic data were retrospectively extracted from the electronic medical record system. Categorical variables, such as age groups, were compared using the median and interquartile range (IQR). Violin plots were obtained using ggplot2 package. P values of < 0.05 indicated statistical significance. All statistics analyses were performed using R software package v4.3.3 (https://www.r-project.org/).

Results

Spatiotemporal distribution of *Serratia marcescens* complex in the ICUs

From January 2014 to December 2024, a total of 874 *Serratia* strains were isolated from all departments. The prevalence of *S. marcescens* complex in all bacterial strains isolated from the whole hospital ranged from 0.40% to 3.54% per year, with the highest prevalence occurring in 2014 (Supplementary Figure S1A). Among all the *Serratia* strains, the prevalence of these *S. marcescens* complex isolated from the ICUs was 4.6% to 30.4% per year, with the highest prevalence seen in 2024 (Supplementary Figure S1B). This suggested that the prevalence trend of *S. marcescens* complex in all bacterial strains was the opposite of that of *S. marcescens* complex from the ICU in *Serratia* strains per year (Supplementary Figure S1). In total, 106 non-repetitive *Serratia* spp. were included for further analysis (Supplementary Data Sheet 0), with isolation coming from five different ICUs: cardiac ICU (CICU, n = 8), emergency ICU (EICU, n = 18), neurology ICU (NICU, n = 30), respiratory ICU (RICU, n = 23), surgical ICU (SICU, n = 27).

Population structure of *Serratia marcescens* complex in the ICU

All the 106 *Serratia* spp. were initially identified as *S. marcescens* by the standard method in clinical labs (MALDI-TOF MS). To further confirm their species classification and genetic diversity, the whole genomes of these isolates were sequenced. The core genome among these isolates revealed a total of 469,717 core SNPs that were shared. Phylogenomic analysis based on core genome alignment indicated that the 106 *Serratia* isolates were clustered into five groups (Figure 1). ANI analysis of these 106 *Serratia* isolates also showed a diverse population structure, forming five groups (Supplementary Figure S2). The ANI values between different groups were all below the generally accepted 95-96% ANI threshold, suggesting that the five groups belonged to five

different species, including *S. sarumanii* (n = 62), *S. ureilytica* (n = 17), *S. marcescens* (n = 13), *S. bockelmannii* (n = 11), and *S. nevei* (n = 3).

The *in silico* MLST analysis was performed utilizing the established *Serratia* spp. scheme. In total, these *Serratia* strains were categorized into 62 STs, with 43 STs represented by only one isolate each. The most prevalent ST was ST595 (12.3%, 13/106), followed by ST525 (10.4%, 11/106), ST428 (4.7%, 5/106), ST362 (2.8%, 3/106), ST554 (2.8%, 3/106), and ST842 (2.8%, 3/106). The ST diversity of *Serratia* strains from inpatients admitted to the SICU was more pronounced (Supplementary Figure S3). Notably, over a quarter of the isolates from patients in the NICU and RICU belonged to ST525 (26.7%) and ST595 (26.1%), respectively. Furthermore, all ST525 and ST595 isolates belonged to *S. sarumanii* (Figure 1). Interestingly, the STs of all the isolates from the CICU were different.

Genomic diversity of *Serratia marcescens* complex in the ICUs

The pairwise SNP distance matrix was estimated based on the core genome mentioned above, and used to construct a minimum spanning tree (MST). The isolates belonged to separate lineages that were identical to the species classification (Figure 2). The number of pairwise SNPs among the analyzed *Serratia* isolates ranged from 0 to 17723, with all isolates sharing a median of 3300 (IQR 3,197-14,535) SNPs with the first isolated strain (CY27690). Based on the threshold of 16 SNPs, these 106 isolates were assigned to 15 distinct genetic clusters (GCs) and 44 singleton strains. The majority of GCs were comprised of only two isolates (IQR 2-3). The largest GC was cluster 4, which included thirteen ST595 isolates and one ST839 (new ST identified in this study) isolate (CY83385) (Figure 3). These strains from cluster 4 circulated in five different ICUs over the past 11 years (Figure 3). Cluster 11, the second largest transmission chain, contained ten isolates from ST525, which were mainly prevalent in NICU between 2020 and 2021 before spreading to SICU in 2021 and RICU in 2024. Cluster 5 contained six isolates from three different STs (ST428, ST490, and ST525), spreading among four ICUs between 2014 and 2020. Cluster 6 had only five isolates from two ICUs, which belonged to two STs, including two from ST368 and three from ST362. Of particular interest was that isolates in each cluster were collected over a span of at least two different years (Supplementary Figure S4), suggesting the duration for which the strains had been circulating. Overall, most clustered isolates in each cluster were isolated from different ICUs, indicating of potential outbreaks and transmission.

Analysis of accessory genome

Accessory genes were analyzed to determine the presence of adaptive traits across different species. As the number of genomes

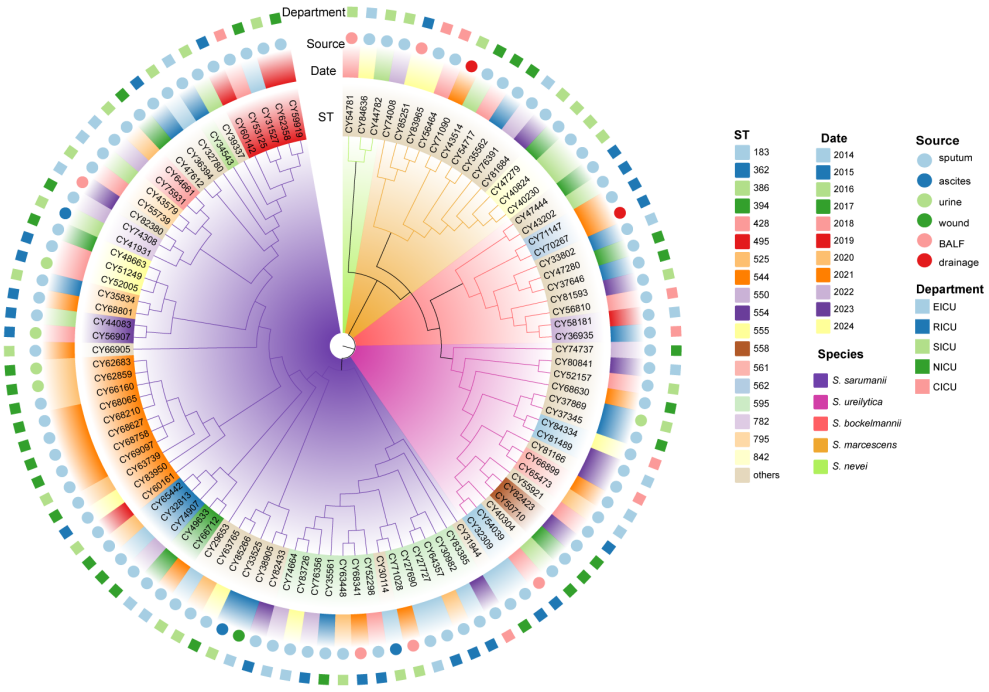

FIGURE 1
Phylogenetic analysis of *Serratia* clinical isolates based on core genome. The maximum-likelihood phylogenetic tree was constructed using 3151 core genes that were presented in ≥ 99% of genomes. The branch colors are labeled with corresponding species. The colored rings, from the inside out, represent the ST, collection date, source, and department of the strains isolated, respectively. BALF, bronchoalveolar lavage fluid; CICU, cardiac ICU; EICU, emergency ICU; NICU, neurology ICU; RICU, respiratory ICU; SICU, surgical ICU.

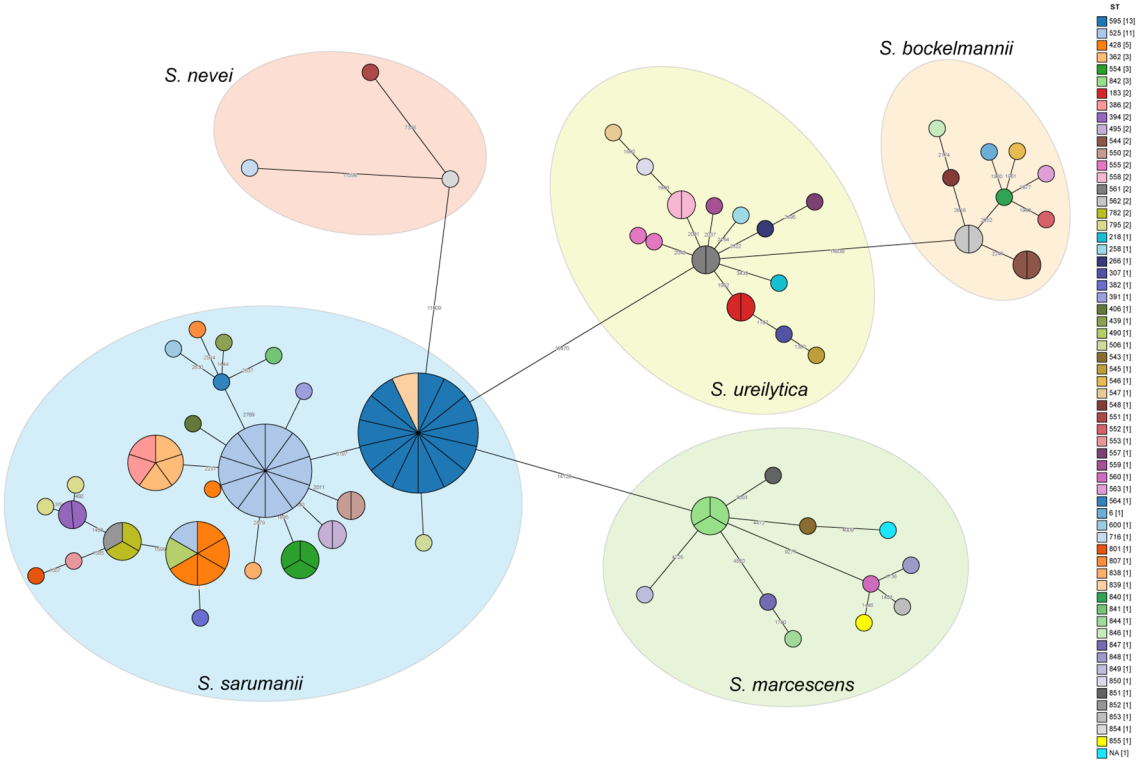

FIGURE 2
Minimum spanning trees showing the SNP difference among *Serratia* clinical isolates. Strains are grouped together based on having less than 16 SNPs. Each circle or section of the pie chart represents an individual strain, with the color indicating its ST. The number of SNPs between strains are showed on the connecting lines. The numbers in brackets in the legend indicate the number of strains in each ST.

examined increased, the number of core genes remained relatively stable, while the number of accessory genes showed an increasing trend (Supplementary Figure S5). Among 14242 (80.6%) accessory genes identified, less than 95% were shared across all *Serratia* spp. The average number of accessory genes per isolate within each species was determined (Figure 4A; Supplementary Data Sheets 2–5), with the highest number found in isolates of *S. sarumanii* ($P < 0.05$). Unique genes were notably enriched in isolates of *S. sarumanii* (n = 1075), the most represented species in the study, followed by *S. ureilytica* (n = 1063) (Figure 4B). Of particular interest within all *S. marcescens* isolates were the enrichment of *adh3*, coding for alcohol dehydrogenase, and *fosB2*, which imparts resistance to the antibiotic Fosfomycin. Moreover, isolates of *S. sarumanii* were enriched in various proteins, including hemolysin transporter protein ShlB, macrolide export ATP-binding/permease protein MacB, toxic protein HokC that required for toxin and drug export, as well as proteins associated with type II secretion system like type II secretion system protein E J, and L.

Antimicrobial susceptibility and resistance phenotypes

The antimicrobial susceptible testing revealed that a total of 76 (71.7%) isolates were susceptibility to all 17 antimicrobial agents tested (Supplementary Data Sheet 1). The resistance of the remaining 30 strains ranged from 1 and 13 antimicrobial agents per isolate, with a median of 5 (IQR 3-9) (Figure 5). Among these *Serratia* spp., the most common resistance was observed against CRO (24.5%, 26/106), followed by PRL (23.6%, 25/106), ATM (21.7%, 23/106), CIP (14.1%, 15/106), LEV (11.3%, 12/106), CN (10.4%, 11/106), and FEP (9.4%, 10/106). Notably, nine isolates were resistant to IPM (8.5%, 9/106), indicating the emergence of carbapenem-resistant *S. marcescens* complex. The prevalence of other resistance phenotypes was all less than 10% (< 9 isolates). The most prevalent resistant profile included resistance to CRO, PRL, and ATM simultaneously. The resistant profile of most antimicrobial resistant isolates was unique among *Serratia* spp. in this study. Furthermore, isolates demonstrating antimicrobial resistance to the tested agents were primarily presented in *S. sarumanii* (83.3%, 25/30) and *S. bockelmannii* (10.0%, 3/30).

Patterns of antimicrobial resistance and virulence genes

To investigate their resistome, genomes were screened for the presence of antimicrobial resistance (AMR) genes (Figure 6). A total of 52 AMR genes were identified from the 106 *Serratia* isolates, which were classified into 14 drug classes. The number of AMR genes varied

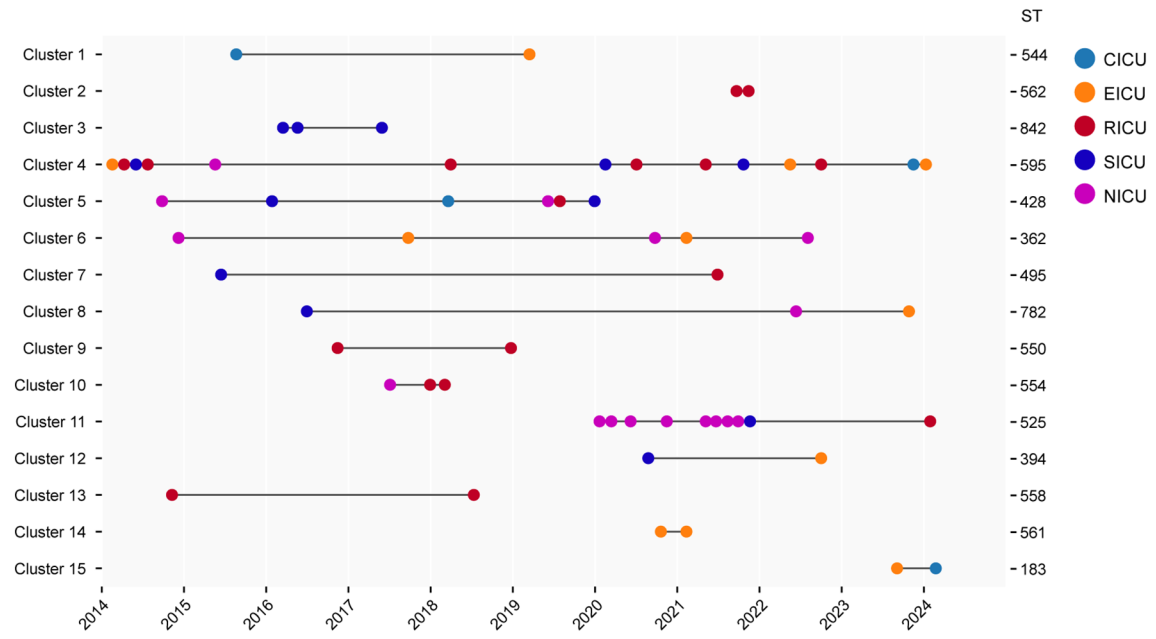

FIGURE 3
Timeline of detected cases in each cluster. The left Y axis is labeled with the name of each cluster, and the right Y axis is labeled with the ST of corresponding cluster. The X axis is labeled with collection year. CICU, cardiac ICU; EICU, emergency ICU; NICU, neurology ICU; RICU, respiratory ICU; SICU, surgical ICU.

across isolates, ranging from 3 to 21, with a median of 4 (IQR 3-4). The most prevalent AMR gene was intrinsic *aac(6')_Serra* gene (97/106), which was prevalent in all five species. However, the second most prevalent AMR gene, intrinsic *oqxB9* gene (70/106), was absent in isolates belonging to *S. bockelmannii* and *S. ureilytica*, and present in several isolates of *S. marcescens*. The strains carrying AMR genes associated with cephalosporin, aminoglycoside, and antibiotic efflux were distributed in all isolates. Among 12 beta-lactamase genes conferring resistance to cephalosporin, intrinsic bla_{SRT} gene was the most prevalent (56/106). Additionally, three acquired $bla_{CTX\text{-}M}$ genes, including $bla_{CTX\text{-}M\text{-}14}$ (n = 12), $bla_{CTX\text{-}M\text{-}3}$ (n = 12), and $bla_{CTX\text{-}M\text{-}15}$ (n = 2), were prevalent in 26 isolates, which was consistent with the results of the CRO resistance genotypes. In addition, acquired carbapenemase genes were detected in nine *Serratia* isolates (8.5%, 9/106), including five $bla_{KPC\text{-}2}$ (4.7%, 5/106) and four $bla_{NDM\text{-}5}$ (3.8%, 4/106), which aligned with the results of the IPM resistance phenotypes.

The potential pathogenicity of *Serratia* spp. in the ICUs were determined based on the distribution of virulence genes (Figure 6). The most common virulence-related genes were intrinsic *fliG* and *fliM* genes, which were prevalent in all isolates. And, the intrinsic *cheY* gene, involved in the transmission of sensory signals to the flagellar motors, was the second common virulence-related gene (64.2%, 68/106), followed by intrinsic *fliP* gene (43.4%, 46/106), which were sporadically distributed across species. It is noteworthy that three isolates contained a high-pathogenicity island comprised of *fyuA*, *irp1*, *irp2*, *ybtA*, *ybtE*, *ybtP*, *ybtQ*, *ybtS*, *ybtT*, *ybtU*, *ybtX*. Furthermore, there was a significant difference in the number of virulence genes between several species (Supplementary Figure S6), as well as between isolates of several clusters (Supplementary Figure S7).

Clinical manifestations of *Serratia marcescens* complex in the ICU

To evaluate the differences in clinical manifestations, we retrieved the electronic medical records of inpatients infected with *Serratia* spp. The median age of all cases was 69 years (IQR 60-79), with 68.9% of them being male (73/106). We proceeded to compare the clinical manifestations caused by the four main species (Supplementary Table S1). Although the proportion of male patients infected with *S. ureilytica* seems to be similar to that of female patients, a larger proportion of males were infected with the remaining three species, with a significant difference noted in *S. sarumanii* (P = 0.0001). The median age of patients diagnosed with *Serratia* infection showed a significant difference among four species ($P < 0.05$), with the median age of patients diagnosed with *S. bockelmannii* being the youngest. Individuals infected with *S. sarumanii*, *S. ureilytica* and *S. marcescens* tended to be older. The clinical symptoms including fever (median 38° C, IQR 37.6-38.8°C) and cough had a higher prevalence. The incidence of severe pneumonia ranged from 16.7-28.6%. Dyspnea and chill were only observed in patients infected with *S. sarumanii* and *S. ureilytica*. The abnormality rate of clinical examination varied, with the highest WBC count observed in cases of *S. marcescens* and *S. bockelmannii*, neutrophilic granulocyte percentage in *S. marcescens*, and hemoglobin in *S. sarumanii*.

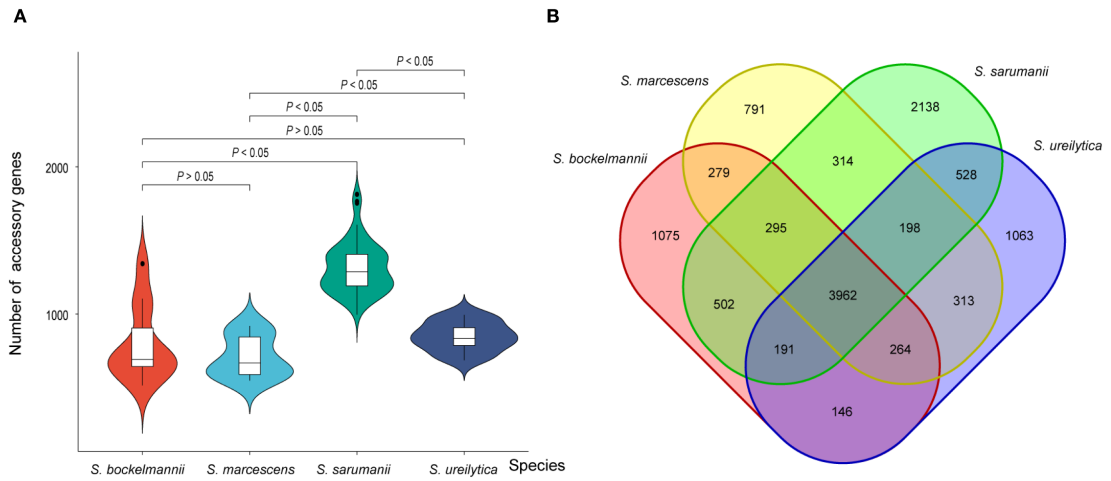

FIGURE 4
(A) Violin plot displaying the number of accessory genes for each species **(A)**. The horizontal line within each box plot represents the median number of accessory genes for each species. Significance values are labeled on the top of plot. **(B)** Venn plot illustrating the shared accessory genes among each species.

Discussion

Although a wide variety of species have been proposed in the genus *Serratia*, most of the understanding of *Serratia* has focused on the type species, *S. marcescens* (Williams et al., 2022). This study retrospectively investigated the *Serratia* species isolated from multiple sources, revealing the wide genomic diversity of human-associated *Serratia* within five ICU wards over the past 11 years. These *Serratia* spp. were genomically classified into five species, with the majority of them being *S. sarumanii*, which was identified as a novel species in the genus *Serratia* in 2024 (Klages et al., 2024). The findings of this study indicated that there were multiple species of *Serratia* can infected humans, and similar species may not be accurately distinguished by MALDI-TOF MS, but could be differentiated by conserved genomic regions.

Analysis of closely clustered isolates using cgSNP distance matrix with a threshold of 16 SNPs (David et al., 2019) revealed a high incidence of clonal dissemination of *Serratia* spp. Our study also showed that the largest cluster had spread over 11 years, including inter-ICU transmission, which exceeded previous

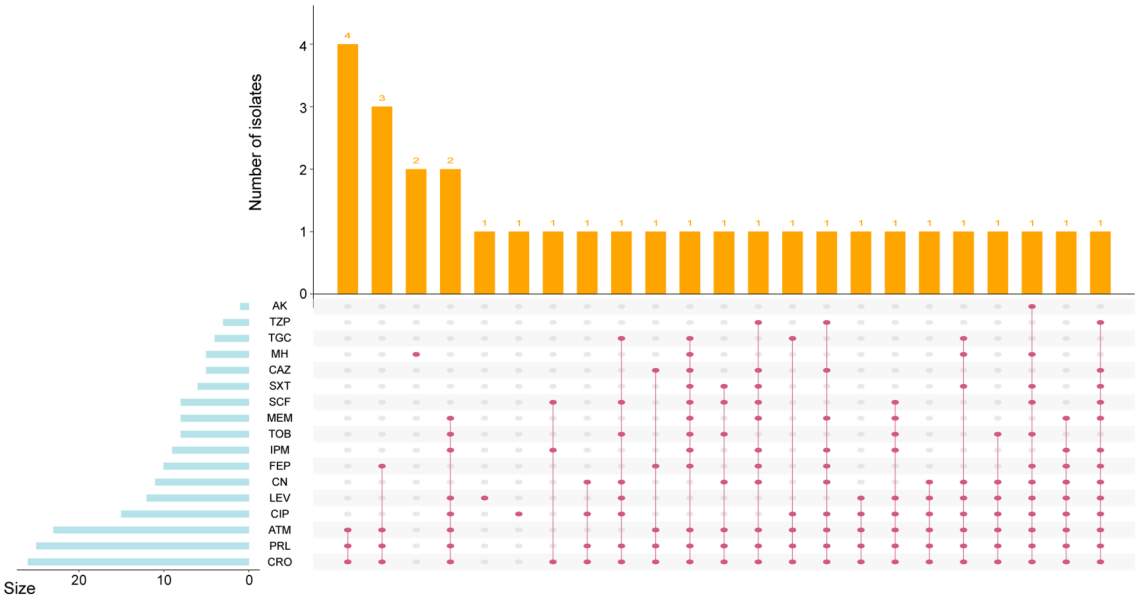

FIGURE 5
UpSetR plot showing the resistance phenotype of *Serratia* clinical isolates. The left histogram indicates the number of isolates with each antimicrobial resistance. The top histogram reveals the distribution of isolates by type. The phenotypic results indicate resistance as defined by the Clinical and Laboratory Standards Institute guidelines.

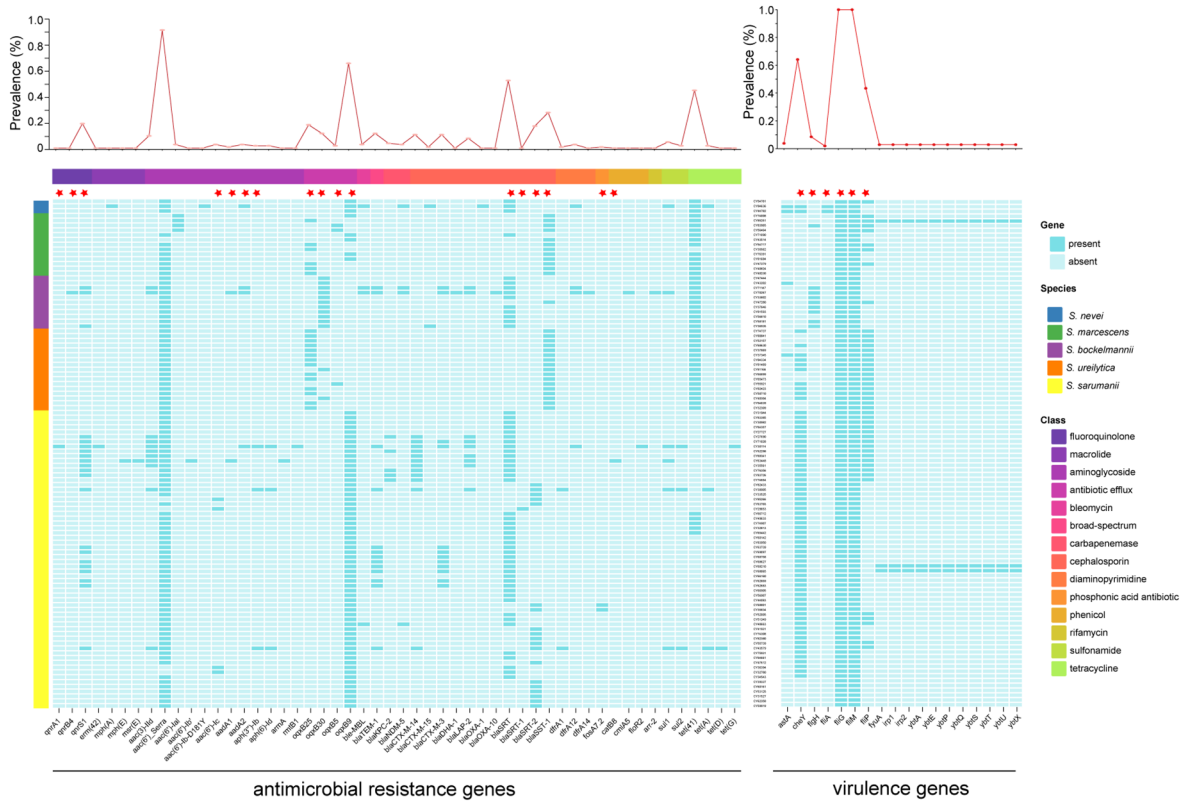

FIGURE 6
Distributions of antimicrobial resistance genes and virulence genes. The line chart at the top showed the incidence of each gene. The color of left rectangle represents the corresponding species, while the color of top rectangle is labeled with the corresponding drug class of antimicrobial resistance genes. The intrinsic antimicrobial resistance and virulence genes were labeled with red five-pointed stars.

reports (Zhang et al., 2024). Multiple simultaneous transmission chains were identified within the same ICU, raising concerns about ongoing dissemination. However, the full extent of *Serratia* spp. dissemination may be underestimated as not all isolates collected from 2014 to 2025 were included, nor those obtained prior to 2014. The exact routes of transmission remain unclear, but potential sources could include contact with caregivers, cleaning workers, shared bathrooms, and changes in hospital departments during a patient's stay. In addition, more than 11,500 SNPs were identified between one isolate and the other two isolates within *S. nevei*, indicating the potential existence of a sixth group.

Both intrinsic and acquired AMR genes contributed to antibiotic resistance across *Serratia* species. The chromosomal AmpC-type β-lactamase genes, including bla_{SRT}, bla_{SRT-1},and bla_{SRT-2}, were present in all isolates, with each isolate having a resistance gene, consistent with previous research (Matteoli et al., 2021). The acquired β-lactamase genes in this study, such as bla_{CTX-M} and bla_{OXA}, were found primarily in *S. sarumanii* species. Notably, carbapenemase-producing *Serratia* spp. were detected, with bla_{KPC-2} found exclusively in *S. sarumanii*. Additionally, the carbapenemase gene, bla_{NDM-5}, was prevalent in three *Serratia* species. Although previous reports have described the presence of bla_{KPC-2}, bla_{VIM-1}, and bla_{OXA-48} in *Serratia* spp (Matteoli et al., 2021; Pérez-Viso et al., 2024; Tang et al., 2024; Zhang et al., 2024), NDM-5-producing *Serratia* isolates have been rarely reported in China or elsewhere (Matteoli et al., 2021; Nakanishi et al., 2022; Pérez-Viso et al., 2024). Fortunately, none of these carbapenemase-producing *S. marcescens* complex caused clonal outbreaks in the hospital.

Analysis of the virulome of *S. marcescens* complex revealed a narrower range of features, with virulence genes related to flagella being the most common (Pérez-Viso et al., 2024). The intrinsic *cheY* gene, encoding proteins of chemotaxis, was present in most isolates, potentially delivering secondary signals to flagellar motors (Paul et al., 2010; Lazzaro, 2019). Furthermore, the *Yersinia* high-pathogenicity island, comprising genes related to the synthesis of the siderophore yersiniabactin (Carniel, 2001), was identified in *S. sarumanii* and *S. marcescens* in this study, and had previously been found in *S. liquefaciens* (Olsson et al., 2003). The transmission and exact virulence level of all these genes in *Serratia* spp. remain poorly understanded and require further investigation. Additionally, individual species contained unique genes compared with other three species, such as type II secretion system only presented in *S. sarumanii*.

In conclusion, we provided important insights into the population structure of *S. marcescens* complex were provided based on 106 isolates collected from ICUs in a single center over the past 11 years, representing five different species. Investigation into the potential transmissions of these *Serratia* isolates revealed that the majority of them were clonal related. Antimicrobial resistance analysis

showed that while the overall incidence of resistance was not severe, carbapenemase-producing *S. marcescens* complex had emerged as early as 2014. To prevent the dissemination of these emergent and future clones, further research is needed to understand the transmission mechanisms and routes associated with these clinically significant *Serratia* clones.

Data availability statement

The original contributions presented in the study are publicly available. This data can be found here: BioProject accession number PRJNA1191627, with genome accession numbers JBMIOK000000000, JBMIOL000000000, and JBJNLA000000000 to JBJNOZ000000000.

Ethics statement

This study was approved by the Ethics Committee of Beijing Chaoyang Hospital, Capital Medical University (2024-ke-381).

Author contributions

WZ: Conceptualization, Funding acquisition, Project administration, Writing – original draft, Writing – review & editing. XC: Formal analysis, Resources, Writing – original draft. HS: Formal analysis, Resources, Writing – original draft. MW: Resources, Writing – original draft. CY: Resources, Writing – review & editing. LG: Project administration, Writing – review & editing.

Funding

The author(s) declare financial support was received for the research and/or publication of this article. This work was supported by the National Natural Science Foundation of China (82502766), and the Beijing Chao-Yang Hospital Golden Seeds Fundation (CYJZ202220). The funders had no role in study design, data collection and analysis, decision to publish, or preparation of the manuscript.

Acknowledgments

We would like to thank all of staff from the Department of Infectious Diseases and Clinical Microbiology at Beijing Chao-Yang Hospital for their contribution to this work.

Conflict of interest

The authors declare that the research was conducted in the absence of any commercial or financial relationships that could be construed as a potential conflict of interest.

Generative AI statement

The author(s) declare that no Generative AI was used in the creation of this manuscript.

Any alternative text (alt text) provided alongside figures in this article has been generated by Frontiers with the support of artificial intelligence and reasonable efforts have been made to ensure accuracy, including review by the authors wherever possible. If you identify any issues, please contact us.

Publisher's note

Supplementary material

The Supplementary Material for this article can be found online at: https://www.frontiersin.org/articles/10.3389/fcimb.2025.1672468/full#supplementary-material

References

Adeolu, M., Alnajar, S., Naushad, S., and Gupta, R. S. (2016). Genome-based phylogeny and taxonomy of the 'enterobacteriales': Proposal for enterobacterales ord. Nov. Divided into the families enterobacteriaceae, erwiniaceae fam. Nov., pectobacteriaceae fam. Nov., yersiniaceae fam. Nov., hafniaceae fam. Nov., morganellaceae fam. Nov., and budviciaceae fam. Nov. *Int. J. Syst. Evol. Microbiol.* 66, 5575–5599. doi: 10.1099/ijsem.0.001485

Alcock, B. P., Raphenya, A. R., Lau, T. T. Y., Tsang, K. K., Bouchard, M., Edalatmand, A., et al. (2020). Card 2020: Antibiotic resistome surveillance with the comprehensive antibiotic resistance database. *Nucleic Acids Res.* 48, D517–d525. doi: 10.1093/nar/gkz935

Aracil-Gisbert, S., Fernández-De-Bobadilla, M. D., Guerra-Pinto, N., Serrano-Calleja, S., Pérez-Cobas, A. E., Soriano, C., et al. (2024). The ICU environment contributes to the endemicity of the "serratia marcescens complex" in the hospital setting. *mBio* 15, e0305423. doi: 10.1128/mbio.03054-23

Blackburn, M. B., Tannières, M., Sparks, M. E., Gundersen-Rindal, D. E., and Bon, M. C. (2024). Serratia montpellierensis sp. Nov., isolated from laboratory-reared parasitic wasps psyttalia lounsburyii silvestri and psyttalia ponerophaga silvestri (hymenoptera: Braconidae). *Curr. Microbiol.* 81, 146. doi: 10.1007/s00284-024-03666-0

Bonnin, R. A., Naas, T., and Dortet, L. (2025). Diversity of β-lactamase resistance and genome of morganella spp clinical isolates in China-authors' reply. *Lancet Microbe* 6, 101004. doi: 10.1016/j.lanmic.2024.101004

Bush, L., and Vazquez-Pertejo, M. (2024). *Klebsiella, enterobacter, and serratia infections* (Merck Manual). Available online at: https://www.merckmanuals.com/professional/infectious-diseases/gram-negative-bacilli/klebsiella-enterobacter-and-serratia-infections.

Carniel, E. (2001). The yersinia high-pathogenicity island: An iron-uptake island. *Microbes Infect.* 3, 561–569. doi: 10.1016/S1286-4579(01)01412-5

Chen, L., Zheng, D., Liu, B., Yang, J., and Jin, Q. (2016). Vfdb 2016: Hierarchical and refined dataset for big data analysis–10 years on. *Nucleic Acids Res.* 44, D694–D697. doi: 10.1093/nar/gkv1239

Chng, K. R., Li, C., Bertrand, D., Ng, A. H. Q., Kwah, J. S., Low, H. M., et al. (2020). Cartography of opportunistic pathogens and antibiotic resistance genes in a tertiary hospital environment. *Nat. Med.* 26, 941–951. doi: 10.1038/s41591-020-0894-4

CLSI (2025). *Performance standards for antimicrobial susceptibility testing. 35th ed*Clsi supplement m100 (Wayne, PA: Clinical and Laboratory Standards Institute).

Croucher, N. J., Page, A. J., Connor, T. R., Delaney, A. J., Keane, J. A., Bentley, S. D., et al. (2015). Rapid phylogenetic analysis of large samples of recombinant bacterial whole genome sequences using gubbins. *Nucleic Acids Res.* 43, e15. doi: 10.1093/nar/gku1196

David, S., Reuter, S., Harris, S. R., Glasner, C., Feltwell, T., Argimon, S., et al. (2019). Epidemic of carbapenem-resistant klebsiella pneumoniae in europe is driven by nosocomial spread. *Nat. Microbiol.* 4, 1919–1929. doi: 10.1038/s41564-019-0492-8

Dubouix, A., Roques, C., Segonds, C., Jeannot, M. J., Malavaud, S., Daude, S., et al. (2005). Epidemiological investigation of a serratia liquefaciens outbreak in a neurosurgery department. *J. Hosp Infect.* 60, 8–13. doi: 10.1016/j.jhin.2004.09.029

Feldgarden, M., Brover, V., Haft, D. H., Prasad, A. B., Slotta, D. J., Tolstoy, I., et al. (2019). Validating the amrfinder tool and resistance gene database by using antimicrobial resistance genotype-phenotype correlations in a collection of isolates. *Antimicrob. Agents Chemother.* 63 (11), e00483-19. doi: 10.1128/AAC.00483-19

Harch, S. A. J., Jenkins, F., Farhat, R., and van Hal, S. J. (2025). Complexities in species identification for serratia marcescens complex for the modern microbiology laboratory. *Microbiol. Spectr.* 13, e0136124. doi: 10.1128/spectrum.01361-24

Jolley, K. A., and Maiden, M. C. (2010). BIGSdb: Scalable analysis of bacterial genome variation at the population level. *BMC Bioinf.* 11, 595. doi: 10.1186/1471-2105-11-595

Karkey, A., Joshi, N., Chalise, S., Joshi, S., Shrestha, S., Thi Nguyen, T. N., et al. (2018). Outbreaks of serratia marcescens and serratia rubidaea bacteremia in a central kathmandu hospital following the 2015 earthquakes. *Trans. R Soc. Trop. Med. Hyg* 112, 467–472. doi: 10.1093/trstmh/try077

Khanna, A., Khanna, M., and Aggarwal, A. (2013). Serratia marcescens- a rare opportunistic nosocomial pathogen and measures to limit its spread in hospitalized patients. *J. Clin. Diagn. Res.* 7, 243–246. doi: 10.7860/JCDR/2013/5010.2737

Klages, L. J., Kaup, O., Busche, T., Kalinowski, J., and Rückert-Reed, C. (2024). Classification of a novel serratia species, isolated from a wound swab in north rhine-westphalia: Proposal of serratia sarumanii sp. nov. *Syst. Appl. Microbiol.* 47, 126527. doi: 10.1016/j.syapm.2024.126527

Lazzaro, M. (2019). Factores de virulencia de serratia marcescens.

Liu, Q., Shen, H., Wei, M., Chen, X., Gu, L., and Zhu, W. (2025). Global phylogeography and antibiotic resistance characteristics of morganella: An epidemiological, spatial, comparative genomic study. *Drug Resist. Update* 78, 101180. doi: 10.1016/j.drup.2024.101180

Liu, Q., and Zhu, W. (2025). Diversity of β-lactamase resistance and genome of morganella clinical isolates in China. *Lancet Microbe* 6, 101003. doi: 10.1016/j.lanmic.2024.101003

Mahlen, S. D. (2011). Serratia infections: From military experiments to current practice. *Clin. Microbiol. Rev.* 24, 755–791. doi: 10.1128/CMR.00017-11

Matteoli, F. P., Pedrosa-Silva, F., Dutra-Silva, L., and Giachini, A. J. (2021). The global population structure and beta-lactamase repertoire of the opportunistic pathogen serratia marcescens. *Genomics* 113, 3523–3532. doi: 10.1016/j.ygeno.2021.08.009

Nakanishi, N., Komatsu, S., Iwamoto, T., and Nomoto, R. (2022). Characterization of a novel plasmid in serratia marcescens harbouring bla(ges-5) isolated from a nosocomial outbreak in Japan. *J. Hosp Infect.* 121, 128–131. doi: 10.1016/j.jhin.2021.11.022

Näpflin, N., Schubert, C., Malfertheiner, L., Hardt, W. D., and von Mering, C. (2025). Gene-level analysis of core carbohydrate metabolism across the enterobacteriaceae pan-genome. *Commun. Biol.* 8, 1241. doi: 10.1038/s42003-025-08640-5

Olsson, C., Olofsson, T., Ahrné, S., and Molin, G. (2003). The yersinia hpi is present in serratia liquefaciens isolated from meat. *Lett. Appl. Microbiol.* 37, 275–280. doi: 10.1046/j.1472-765X.2003.01387.x

Ono, T., Taniguchi, I., Nakamura, K., Nagano, D. S., Nishida, R., Gotoh, Y., et al. (2022). Global population structure of the serratia marcescens complex and identification of hospital-adapted lineages in the complex. *Microb. Genom* 8 (3), 000793. doi: 10.1099/mgen.0.000793

Page, A. J., Cummins, C. A., Hunt, M., Wong, V. K., Reuter, S., Holden, M. T., et al. (2015). Roary: Rapid large-scale prokaryote pan genome analysis. *Bioinformatics* 31, 3691–3693. doi: 10.1093/bioinformatics/btv421

Paul, K., Nieto, V., Carlquist, W. C., Blair, D. F., and Harshey, R. M. (2010). The c-di-GMP binding protein YcgR controls flagellar motor direction and speed to affect chemotaxis by a "backstop brake" mechanism. *Mol. Cell* 38, 128–139. doi: 10.1016/j.molcel.2010.03.001

Pérez-Viso, B., Hernández-García, M., Rodríguez, C. M., Fernández-de-Bobadilla, M. D., Serrano-Tomás, M. I., Sánchez-Díaz, A. M., et al. (2024). A long-term survey of serratia spp. Bloodstream infections revealed an increase of antimicrobial resistance involving adult population. *Microbiol. Spectr.* 12, e0276223. doi: 10.1128/spectrum.02762-23

Prjibelski, A., Antipov, D., Meleshko, D., Lapidus, A., and Korobeynikov, A. (2020). Using spades *de novo* assembler. *Curr. Protoc. Bioinf.* 70, e102. doi: 10.1002/cpbi.102

Sandner-Miranda, L., Vinuesa, P., Cravioto, A., and Morales-Espinosa, R. (2018). The genomic basis of intrinsic and acquired antibiotic resistance in the genus serratia. *Front. Microbiol.* 9, 828. doi: 10.3389/fmicb.2018.00828

Seemann, T. (2014). Prokka: Rapid prokaryotic genome annotation. *Bioinformatics* 30, 2068–2069. doi: 10.1093/bioinformatics/btu153

Tang, B., Zhao, H., Li, J., Liu, N., Huang, Y., Wang, J., et al. (2024). Detection of clinical serratia marcescens isolates carrying bla(kpc-2) in a hospital in China. *Heliyon* 10, e29702. doi: 10.1016/j.heliyon.2024.e29702

Van Goethem, S., Xavier, B. B., Glupczynski, Y., Berkell, M., Willems, P., Van Herendael, B., et al. (2024). Genomic epidemiological analysis of a single-centre polyclonal outbreak of serratia marcescens, Belgium 2022 to 2023. *Euro Surveill* 29 (48), 2400144. doi: 10.2807/1560-7917.ES.2024.29.48.2400144

Williams, D. J., Grimont, P. A. D., Cazares, A., Grimont, F., Ageron, E., Pettigrew, K. A., et al. (2022). The genus serratia revisited by genomics. *Nat. Commun.* 13, 5195. doi: 10.1038/s41467-022-32929-2

Xu, M., Guo, L., Gu, S., Wang, O., Zhang, R., Peters, B. A., et al. (2020). TGS-gapcloser: A fast and accurate gap closer for large genomes with low coverage of error-prone long reads. *Gigascience* 9 (9), giaa094. doi: 10.1093/gigascience/giaa094

Zhang, F., Li, Z., Liu, X., Li, Z., Lei, Z., Zhao, J., et al. (2024). In-host intra- and inter-species transfer of bla(KPC-2) and bla(NDM-1) in serratia marcescens and its local and global epidemiology. *Int. J. Antimicrob. Agents* 64, 107327. doi: 10.1016/j.ijantimicag.2024.107327

Zhu, W., Chen, X., Shen, H., Wei, M., Gu, L., and Liu, Q. (2025). Genomic evolution, antimicrobial resistance, and dissemination of global serratia spp. Unveil increasing species diversity and carbapenemae–resistance: A retrospective and genomic epidemiology study. *Curr. Res. Microbial Sci.* 9, 100456. doi: 10.1016/j.crmicr.2025.100456

Zhu, W., Liu, Q., Liu, J., Wang, Y., Shen, H., Wei, M., et al. (2025). Genomic epidemiology and antimicrobial resistance of morganella clinical isolates between 2016 and 2023. *Front. Cell. Infect. Microbiol.* 14. doi: 10.3389/fcimb.2024.1464736

Frontiers in
Cellular and Infection Microbiology

Investigates how microorganisms interact with their hosts

Explores bacteria, fungi, parasites, viruses, endosymbionts, prions and all microbial pathogens as well as the microbiota and its effect on health and disease in various hosts.

Discover the latest Research Topics

See more →

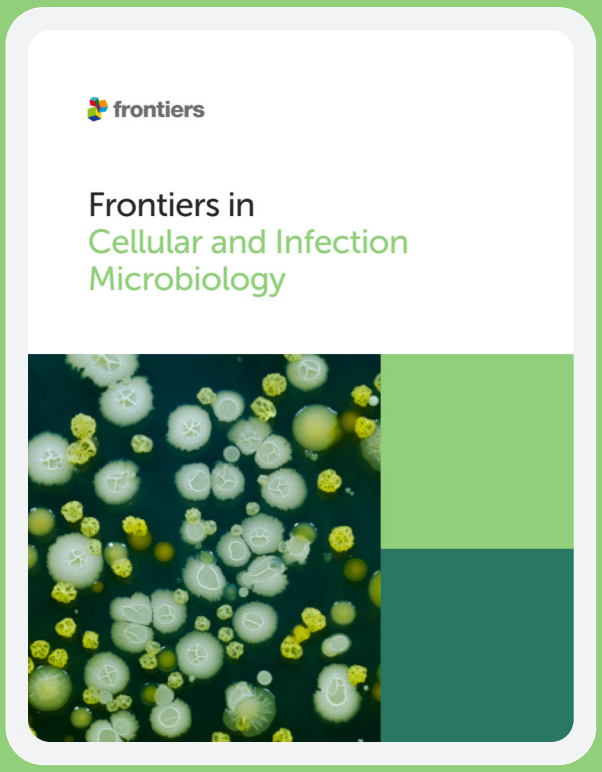

Frontiers

Avenue du Tribunal-Fédéral 34
1005 Lausanne, Switzerland
frontiersin.org

Contact us

+41 (0)21 510 17 00
frontiersin.org/about/contact